Late Cenozoic Uplift of Southeastern Tibet

by

Marin Kristen Clark

A.B., Cornell University (1995)

Submitted to the Department of Earth, Atmospheric, and Planetary Sciences
in partial fulfillment of the requirements for the degree of

Doctor of Philosophy

at the

MASSACHUSETTS INSTITUTE OF TECHNOLOGY

May 2003

Author . .....
Department of Earth, Atmospheric, and Planetary Sciences
February 28, 2003

Certified by .....
Dr. Leigh H. Royden
Professor
Thesis Supervisor

Accepted by .....
Dr. Ronald G. Prinn
Chairman, Department of Earth, Atmospheric, and Planetary Sciences

Acknowledgments

The number of people who have contributed to this work in some fashion is overwhelming, my apologies in advance if I have forgotten to recognize them all.

First, I would like to extend a thank you to my committee members for their time and efforts: Wiki Royden, Clark Burchfiel, Kelin Whipple, Martha House, and Kip Hodges. Thank you to Wiki Royden for being the best advisor I could have ever asked for. I am grateful to her for giving me the freedom to work independently and to pursue my own ideas at the same time providing the encouragement, mentoring, and advice (scientific and otherwise!) needed to develop those ideas into solid scientific projects. Her grasp of the bigger picture will never cease to amaze me. But most of all, she has been a lot of fun to work with and I hope to have the chance to work with her again someday. Thank you to Clark Burchfiel for providing valuable advice, encouragement and helping to tie together the geomorphology and crustal dynamics with the fathomless, complicated geologic record of eastern Tibet. It has been a remarkable experience to work in the field (and in the lab over maps!) with Clark. Thank you to Kelin Whipple for pushing me to provide as many quantitative details as possible in order to ground my qualitative, arm-waving ideas about landscape development. His input has been essential for trying to bring together a big-picture tectonic view with the quantitative side of geomorphology to make a much more solid piece of work. Thank you to Martha House for her work on the helium project, her advice, encouragement and instruction. I am very glad she joined us in the field in 2001, it was an incredibly productive trip and a lot of fun. I learned a ton from her from analytical lab work to petrology, her breadth of knowledge is incredible.

This work would not have been possible without the expertise, knowledge and hard work of our Chinese colleagues, including: Xuan-Yang Zhang, Wenqing Tang, Zhiliang Chen, Dong Peng, drivers and staff (Chengdu Institute of Geology and Mineral Resources); Liangzhong Chen (Yunnan Institute of Geological Sciences); and Erchie Wang (Academica Sinica). I hope we have a chance to work again together in the future. I also would like to thank Katra Andreini and Michael Stewart for their hard work in the field and contributions to these projects in 1998 and 2002 respectively. Thank you to John Bush (MIT) for working with me on the dynamic topography project, it has been an exciting project and a lot of fun to work on. Thank you to Peter Clift (WHOI) for his input and interest in tying the on-shore erosional record with off-shore sediment budgets of the South Asian continental margin. I'm looking forward to where this work might lead. Thank you to Ken Farley (Caltech) for his generosity and openness to allow me to work in his (U-Th)/He lab with Martha, I learned a great deal from being involved in the lab work.

Thank you to Ray and Margaret Donelick (Apatite to Zircon, Inc.) for work on the heavy mineral separates for the (U-Th)/He analyses and for performing the apatite fission-track analyses, Lindsay Hedges (Caltech) for her patience and instruction in teaching me to prepare apatites for (U-Th)/He analysis. A huge thank you to Linda Meineke especially (MIT) and Kai Mc Bride for their computer system support. I am grateful to Roberta Bennett-Calorio (MIT) for so very many things, such as, being the floor-mom, cook, counsellor, mediator, advisor, party-organizer, travel agent, and an all-and-out general resource on all sorts of necessary life things. Thank you to Karen Garofalo (MIT) Cindy Haines (MIT) for their hard work on travel plans to Tibet and for dealing with samples and invoices, and for Karen's thoughtful cards and parties for all her students. A big thank you to the education office, Carol Sprague and Vicki Mc Kenna, for their advice, support and lenience. They do such a great job. Great librarians have been essential, thank you to Kathy Keefe (MIT), Joe Hankins (MIT), Michael Noga (MIT), Jim O'Donnell (Caltech), Dr. Flavia Lanini (archives library at ETH-Bibliothek, Zurich) for your expertise. As well, thank you to Prof. Jean-Pierre Burg and Gerold Zeilinger (ETH, Zurich) and Prof. Jacques Malavieille (Univ. of Montpellier II) for your

hospitality and valuable input while I was researching the work of Arnold Heim and the group led by Jacques Malavieille at Gonga Shan.

Thank you to several other professors here at MIT who have given input to this thesis, including: Sam Bowring, John Grotzinger, John Southard, David Mohrig, Brad Hager, Rob van der Hilst, and Bob King. I would also like to thank several student with whom I've worked closely with in China: Lindsay Schoenbohm, for her input and work on the river reconstruction project in particular and all other things geomorphic, Eric Kirby for his advice and often lively conversations, Sinan Akciz for his friendship and his expertise on the pre-early Miocene history of eastern Tibet, and Chris Studnicki-Gizbert for keeping me on my toes whether from down the hall or by email from a dusty internet cafe half a world away. I've gained a lot from conversations with the new group of students working on the eastern Tibet project, specially Will Ouimet and also Alison Cohen and Chang Li. I look forward to seeing their work! Thank you to Julie Kunselman for all of her hard work on the CORONA images used in this thesis. As well, I cannot imagine a more cohesive and supportive graduate student community, and it is true that you often learn the most from the fellow students around you, for me these people include: Simon Brocklehurst, Noah Snyder, Jose Hurtado, Arthur White, Julie Baldwin, Karen Viskupic, Lindy Elkins, Jenny Piontek-Matzel, Cam Wobus, Ben Crosby, Joel Johnson, Wes Watters, David Fike, Anke Friedrich, Amy Draut, John Thurmond, Steve DiBenedetto, Odin Smith, Mousumi Roy, Jeremy Boyce, Blair Schoene, and Becky Flowers.

Graduate school and this thesis would not have been possible without the terrific professors and advisors I had as an undergraduate at Cornell University, in particular: Larry Brown (Cornell Univ.), Doug Nelson (Syr. Univ), Jack Bird (Cornell Univ.), Jack Oliver (Cornell Univ.). It brings me sadness that Doug is not here to see the completion of this work for I know we would have had a great long debate about it! I am particularly grateful to Larry Brown and the Cornell Tradition Fellowship (Sue Hitchcock, Director) for giving me an opportunity to work in Tibet with Project INDEPTH and to the group of graduate students with whom I worked with on that project: Doug Alsdorf, Michael Hauck, Michael Edwards, Yizhaq Makovsky, Michael Cogan, and Thomas Finkbeiner.

A special thank you on a professional, as well as personal, note to Nathan Niemi for his support and guidence, lively scientific debate, great feedback on papers, general resourcefulness in all matters, and for sticking through my decision to come to MIT for graduate school.

Finishing a thesis is an academic achievement, but also a personal one. I am grateful for the support and guidence of my family and friends. Thank you to my family: my mother and father, Vincent and Marti Clark (the greatest sister-dog sitter-chauffeur-cheerleader around), Timmy Gannon, Angie and John Bertano, Edith Dado, Dennis Dado, Bill Morey and Sally Miller, Anna and Clark Morey, Mary and Carl Moreland, Krista Moreland, Donna and Chris Nicholas, Courtney, Dana and Christopher Nicholas. I am so sorry my father and godfather are not here to see this thesis finished, they had so much to do with my education. My soon-to-be family: Ruth Anne and Chuck Niemi, Neil and Julianna Niemi for all their help and support, especially the last several months. Thank you to my close friends for providing support both here in Boston, and from far away: Nico and Kendra Larco, Silvia and Jorge Larco, Jennifer Young, Meghan Hayes, Jenny Middleton, Elizabeth Fitzsimons, Chris Schmidt, Susan, Abby, and Siobhan Murray, and Kat Tibbitts.

Thank you to Chiu-Mi Lai for introducing me to the work of the Medieval Chinese Poet, Li Po and his work entitled, 'the Dangers of the Szechuan Road'. This poem just sums it all up!

The work in this thesis was supported by a NSF graduate fellowship, NSF grant #EAR-9614970 (Burchfiel, Royden and Whipple), #EAR-0003571 (Royden, Burchfiel, Whipple, King, Van der Hilst, and Hodges); and #EAR-9814303 (Royden and Hager); NASA grant #NAG5-6062 (Whipple and Burchfiel).

for my parents

Thomas and Mary Clark

Contents

List of Figures

List of Tables

The Dangers of the Szechuan Road

Aah!
Aah!
What terrors!
How perilous, how steep!
It is harder to walk the Szechuan road than to climb the blue sky!
Since Ts'an Ts'ung and Yü Fu
Shaped a kingdom in those formless wastes
Forty-eight thousand years have gone by,
Yet from thence to the frontiers of Ch'in
    there is no human dwelling.
Only westward, from the Great White Mountain,
    was a bird-way,
Cutting through the Omei ranges,
But the earth crumbled, rocks crashed down,
    and strong men perished.
Afterwards they set sky-ladders and hanging bridges, linked together.
Above are the peaks where six dragons turn back the sun;
Below, the churning streams that clash and burst into foam.
The yellow cranes' flight cannot reach across,
And the monkeys, trying to clamber over, gibber piteously.
How the road coils in the Pass of Green Mud!
With nine turns in a hundred steps,
    it twists past crag and chasm.
Reaching for Orion, passing the Well star,
    I look up and gasp for breath,
Then beating my breast, I sit and heave a long sigh...

Oh if you travel westward, friend, when would you return?
Dangerous is the way and the rocks cannot be scaled!
You shall see only sad birds, chirping on ancient trees,
The male fluttering after the female,
    back and forth through the woods.
You shall hear no voice but the cuckoo's
    calling to the moon at evening
Weary of the empty mountains.
It is harder to walk to Szechuan road
    than to climb the blue sky:
The mere tale of it will drain the colour from youth's cheeks.
Between sky and mountain tops, there is not a foot's space;
Withered pines hang headlong over precipitous cliffs;
Flying cataracts and rushing torrents mingle their din –
They smash on the cliffs and boil among the rocks,

like thunder in ten thousand valleys.
How fearful is this place!
Alas, traveller from afar,
What brings you here?
Sword Ledge is a lofty rugged spot:
If one man kept the Pass,
Ten thousand could not break through.
The guardians of the Pass are strangers to you –
They may act like wolves and jackals.

By daylight, one flees from savage tigers,
At night, from long serpents
Who grind their fangs and suck blood
And raven on men like hemp.
Men say the Brocade City is a place for pleasure,
But it would be better to hurry home,
For it is harder to walk the Szechuan road than to
climb the blue sky.
I turn and look to the west
and heave a long sigh...

Li Po (from *The three hundred T'ang poems*, translated by Innes Herdan)

Chapter 1

Introduction

Orogenic plateaus are excellent settings in which to examine regional-scale deformation in the continents and the underlying rheologic controls on the tectonic style and spatial distribution of that deformation. Created by the early Eocene Indo-Asian continent-continent collision, the Tibetan Plateau stands at an average elevation of nearly 5 kilometers over an area that is roughly the size of the eastern United States (see recent review by *Rowley*, [1996]). The unusually large extent and relatively young geologic history of the Tibetan Plateau make it a good location to study processes of continental deformation. Furthermore, it has been proposed that global climate has been affected by the uplift of Tibet, due to increased rates of silicate weathering and the presence of a laterally extensive high landmass, thus making the study of the geologic history of the plateau of broad interest to both solid earth and atmospheric scientists.

The major controversies over the tectonic history and topographic evolution of Tibet have important implications for understanding the mechanical and dynamic behavior of the crust during orogenesis. A principle controversy revolves around the question: how does the lithosphere accommodate the $\sim$ 2000 km of post-collisional convergence between India and Eurasia? Geologic data support a range of mechanisms including the underthrusting of Indian lithosphere beneath Eurasia, the penetrative deformation of the Eurasian lithosphere, and the lateral extrusion of Eurasian lithosphere [e.g. *Barazangi and Ni*, 1982; *Tapponnier et al.*, 1982; *Dewey et al.*, 1988; *Houseman and England*, 1993; *Hauck et al.*, 1998]. However, the relative importance of these mechanisms is widely disputed. The topographic and

deformation history of eastern Tibet offers the opportunity to explore end-member scenarios of accomodation to continental convergence by assessing the relative contributions of eastward extrusion of intact lithospheric blocks and the distributed deformation of the crust or lithosphere. These end-member views of deformation in the continental crust and lithosphere each have been constructed to explain some key aspects of observational data from Tibet.

Stuctural observations that describe large offsets (>500 km) on major strike-slip faults (several hundred kilometers in length) in eastern Tibet support the idea that as much as 830,000 km^2 of post-collisional $\sim$ N-S convergence between India and Eurasia could be accommodated by eastward extrusion of lithospheric fragments [e.g. *Tapponnier et al.*, 1982; *Avouac and Tapponnier*, 1993; *Leloup, et al.*, 1995; *Leloup et al.*, 2001]. Large magnitude displacements apply mainly to an early history (Oligocene - early Miocene) of strike-slip faulting while post late-Miocene strike-slip offsets are limited to less than 100 km [e.g. *Scharer et al.*, 1990; *Allen et al.*, 1991; *Harrison et al.*, 1992; *Leloup et al.*, 1995; *Wang et al.*, 1998; *Replumaz et al.*, 2001]. In this interpretation, plate-like behavior may dominate the deformational style in eastern Tibet where lithospheric fragments do not internally deform but rather are subject to large lateral translations and or rotations [e.g. *Avouac and Tapponnier*, 1993]. In this conception, lithospheric fragments are bounded by strike-slip faults, which penetrate the mantle lithosphere, and thus require a mechanically competent lower crust and mantle lithosphere such that stresses are efficiently transmitted from the mantle lithosphere through the crust and strain is localized on discrete structures [e.g. *Leloup et al.*, 1995]. The interpretation that strike-slip faults in eastern Tibet may accommodate N-S convergence of India and Eurasia by lateral (eastward) extrusion was originally motivated by analogue plasticine experiments, which assume 2D plane strain [*Tapponnier et al.*, 1982] and latter explored by kinematic models of slip-line theory [*Avouac and Tapponnier*, 1993]. Thus, lateral extrusion is limited in its ability to explain the evolution of Tibet because it does not address how the topography of Tibet has evolved and does not consider the role of buoyancy forces (related to the variations in crustal thickness) that may control or affect deformation.

In contrast, models that view the tectonic history of Tibet as the deformation of a vis-

cous material do not address the large magnitude lateral displacements on strike-slip faults, but rather predict distributed deformation within the continent (e.g. *England and Houseman*, 1988; *Houseman and England*, 1993; *Royden*, 1996; *Shen et al.*, 2001] . These models are largely motivated by the topography of Tibet and predict the morphologic development of the plateau in response to the continuing northward penetration of the rigid Indian craton into the less-competent Eurasian lithosphere or crust. Thin-sheet approximations, which consider the entire lithosphere with a depth-averaged viscosity, succeed at producing the first-order morphologic features of the plateau [e.g. *England and Houseman*, 1988; *Houseman and England*, 1993], but fail to explain several salient features of the topographic history and deformation patterns.

While thin-sheet models only consider a depth-averaged rheology and do not allow for vertical variations in horizontal velocity, viscous models which consider a depth-dependent rheology permit the development of an extremely weak layer in the middle to lower crust, where temperatures in a thick crust are predicted to be high [*Royden*, 1996; *Shen et al.*, 2001]. These models suggest that this weak crustal layer may deform by rapid flow in response to lateral pressure gradients due to variations in crustal thickness . This phenomenon is critically distinct from thin-sheet models because it is able to describe the modern morphology of the plateau, the topographic evolution, as well as the strain distribution observed in the geologic record and in geodetic data. The development of a weak lower crust suggests that the style and distribution of deformation is highly sensitive to lateral pressure gradients due to variations in crustal thickness and results in the decoupling of the crust and mantle lithosphere due to the large differential (horizontal) strains experienced by the deep crust. Furthermore, models with a depth-dependent rheology with a weak lower crust preclude lithospheric scale strike-slip faults, such as the offsets proposed in eastern Tibet during Oligocene - early Miocene time. However, these models may be consistent with the lesser magnitude offsets along the post-Miocene structures, provided that these shallow structures sole into horizontal shear zones at mid-crustal depths.

The uplift history of southeastern Tibet offers an opportunity to explore the mechanisms by which northward convergence of India with Eurasia is accommodated. This bears directly on the relationship between plateau uplift, structural history and the role of the

deep crust during orogenesis. The motivating questions central to this thesis are: 1) What is the spatial pattern of surface uplift in southeastern Tibet?, 2) When did it develop?, and 3) How do the spatial and temporal patterns of topographic development elucidate the deformation mechanisms and crustal dynamics involved in plateau formation?. Together the chapters in this thesis summarize the late Cenozoic uplift history of the southeastern Tibet and implications for the rheologic control on crustal deformation.

Unlike its southern counterpart, the Himalaya, where major thrust faulting has played an integral part in crustal thickening, the $\sim$ 5 km high eastern plateau has developed without evidence for major upper crustal shortening during late Cenozoic time [*Dirks et al.*, 1994; *Burchfiel et al.*, 1995; *King et al.*, 1997; *Wang et al.*, 1998; *Chen et al.*, 2000]. Consequently, the geomorphic history (i.e. the landscape evolution) contains critical information for understanding the surface uplift history in eastern Tibet. Chapters 2, 3, and 4 deal with a description of the geomorphology in eastern Tibet and the relative and absolute chronology of the landscape evolution that can be determined from field observation and low-temperature thermochronology.

A regionally continuous low-relief landscape forms a carapace to the gently dipping southeastern plateau margin, suggesting that a relict (i.e. pre- modern plateau) landscape of low-relief and low elevations existed across southeastern Tibet prior to uplift of the modern plateau margin (Chapter 2). Therefore the modern altitude of the relict landscape can be used as a datum to measure surface uplift in response to plateau development and suggests that uplift has occurred over long wavelengths ($>$1000 km).

Analyses of drainage patterns from digital topographic data and field observations has given insight into the spatial and, potentially, temporal patterns of surface uplift along the eastern margin of the plateau (Chapter 3). There is abundant evidence that river capture, river reversal, and drainage reorganization play prominent roles in the geomorphic history of eastern Tibet. Compilation of field data, digital data, and published geomorphic observations yields constraints on the broad wavelength of surface uplift of the southeastern plateau margin and provides a means by which the geometry of the drainage reorganization can be used to establish a lower bound on the timing and amount of surface uplift.

The modern major river courses that cross the southeastern plateau have cut substantial

bedrock river gorges (up to 3.5 km) into the uplifted relict landscape, however, this deep fluvial dissection has not yet progressed entirely through the landscape. Consequently, perched (elevated) remnants of the relict landscape are still preserved and are locally mantled by early Tertiary sediment suggesting that little exhumation of the relict landscape surface has occurred since the initiation of major bedrock river incision. We suggest that the onset of this major river incision can be related to the initiation of uplift along the eastern plateau margin. Using the relict landscape surface as an erosional datum, we collected elevation transects across remnant surfaces and in deep river gorges for low-temperature thermochronology in order to determine the absolute chronology of landscape evolution in eastern Tibet and relate it to the uplift history of the plateau margin (Chapter 4).

Chapters 5 and 6 address the theoretical implications of the data put forward in the preceding chapters, with a particular emphasis on the role of the deep crust in dictating the style and distribution of deformation related to plateau development. The long-wavelength uplift and lack of major shortening structures in the upper crust suggests that the middle to lower crust has been preferentially thickened during plateau development. Therefore, the regional scale gradients of the eastern plateau margin may directly reflect the rheologic heterogeneity of the mid to lower crust in the plateau foreland. Geodynamic modeling of viscous flow in a channel geometry allow us to derive estimates of lower crustal viscosity based on these regional topographic slopes (Chapter 5).

Sub-regional areas of anomalously high topography and extreme relief associated with young low-temperature thermochronometric ages, extensional detachment-style faulting, and late-Miocene crustal anatexis [*Roger et al.*, 1995] are spatially associated with convexities (in plan view) of steep plateau margins. These convexities develop in areas where we interpret weak lower crust from beneath the central plateau to be flowing around strong regions in the plateau foreland beneath which lower crustal flow is absent. Geodynamic modelling suggests that the geologic observations may be consistent with dynamically maintained topography produced by lower crustal flow around a rigid obstacle (Chapter 6). The results from this study also provide estimates of crustal viscosity and flow velocity that are consistent with 2D flux models of plateau margin development presented in Chapter 5.

Development of the regional geomorphic history has been critical for understanding and relating data from many sub-disciplines in order to investigate the driving mechanisms of uplift in eastern Tibet. The assembly of geomorphic data with structural histories, thermochronologic studies, and geophysical observations direct the development of theoretical models that further our understanding of the physical processes and parameters that govern crustal behavior during tectonic deformation. This approach requires a combination of field work, digital analyses of topographic and imagery data using Geographic Information Systems (GIS), acquiring and interpreting structural data, low-temperature thermochronometric analyses and the development of quantitative models.

1.1 References

Avouac, J. P. and P. Tapponnier, Kinematic model of active deformation in Central Asia, *Geophys. Res. Lett., 20*, 895–898, 1993.

Barazangi, M., and J. Ni, Velocities and propagation characteristics of *Pn* and *Sn* beneath the Himalayan arc and Tibetan Plateau: Possible evidence for underthrusting of Indian continental lithosphere beneath Tibet, *Geology, 10*, 179–185, 1982.

Burchfiel, B. C., Z. Chen, Y. Liu, and L. H. Royden, Tectonics of the Longman Shan and adjacent regions, central China, *Int. Geol. Rev., 37*, 661–735, 1995.

Chen, Z., B. C. Burchfiel, Y. Liu, R. W. King, L. H. Royden, W. Tang, E. Wang, J. Zhao, and X. Zhang, GPS measurements from eastern Tibet and their implications for India/Eurasia intercontinental deformation, *J. Geophys. Res., 105*, 16,215–16,227, 2000.

Dewey, J., R. M. Shackleton, C. Chang, and Y. Sun, The tectonic evolution of the Tibetan Plateau, *Philos. Trans. R. Soc. London, Ser. A, 327*, 379–413.

Dirks, P. H. G. M., C. J. L. Wilson, S. Chen, Z. Luo, S. Liu, Tectonic evolution of the NE margin of the Tibetan Plateau; evidence from the central Longman Mountains, Sichuan Province, China, *J. Southeast Asian Earth Sci., 9(1-2)*, 181–192, 1994.

England, P. C. and G. A. Houseman, The mechanics of the Tibetan Plateau, *Philos. Trans. of the Royal Soc. of London A, 326*, 301–320, 1988.

Harrison, T. M., W. Chen, P. H. Leloup, F. J. Ryerson, P. Tapponnier, An early Miocene transition in deformation regime within the Red River fault zone, Yunnan, and its significance for Indo-Asian tectonics, *J. Geophys. Res., 97*, 7159–7182, 1992.

Hauck, M. L., K. D. Nelson, L. D. Brown, W. Zhao, and A. R. Ross, Crustal structure of the Himalaya orogen at ~90 ° east longtitude from project INDEPTH deep reflection profiles, *Tectonics, 17*, 481–500, 1998.

Houseman, G., and P. England, Crustal thickening versus lateral expulsion in the Indian-Asian continental collision, *J. Geophys. Res., 98*, 12,233–12,249, 1993.

King, R. W., F. Shen, B. C. Burchfiel, L. H. Royden, E. Wang, Z. Chen, Y. Liu, X. Zhang, J. Zhao, and Y. Li, Geodetic measurement of crustal motion in southwest China, *Geology, 25*, 179–182, 1997.

Leloup, P. H., T. M. Harrison, F. J. Ryerson,, W. Chen, Q. Li, P. Tapponnier, R. Lacassin, Structural, petrological and thermal evolution of a Tertiary ductile strike-slip shear zone, Diancang Shan, Yunnan, *J. Geophys. Res, 98*, 6,715–6,743, 1993.

Leloup, P. H., R. Lacassin, P. Tapponnier, U. Schäerer, D. Zhong, S. Lui, L. Zhang, S. Ji, and P. T. Trinh, The Ailao Shan-Red River shear zone (Yunnan, China), Tertiary transform boundary of Indochina, *Tectonophysics, 251*, 3–84, 1995.

Replumaz, A., R. Lacassin, P. Tapponnier, P. H. Leloup, Large river offsets and Plio-Quaternary dextral slip rate on the Red River Fault (Yunnan, China), *J. of Geophys. Res., 106*, 819–836, 2001.

Roger, F., S. Calassou, J. Lancelot, J. Malavieille, M. Mattauer, Z. Xu, Z. Hao, and L. Hou, 1995, Miocene emplacement and deformation of the Konga Shan granite (Xianshui He fault zone, west Sichuan, China): Geodynamic implications, *Earth Planet. Sci., Lett., 130*, 201–216.

Rowley, D. B., Age of initiation of collision between India and Asia: A review of stratigraphic data, *Earth Planet. Sci. Lett., 145*, 1–13, 1996.

Royden, L. H., Coupling and decoupling of crust and mantle in convergent orogens: Implications for strain partitioning in the crust, *J. Geophys. Res., 101*, 17,679– 17,705.

Royden, L., B. C. Burchfiel, R. W. King, E. Wang, Z. Chen, F. Shen, and Y. Liu, Surface deformation and lower crustal flow in eastern Tibet, *Science, 276*, 788–790, 1997.

Schäerer, U., P. Tapponnier, R. Lacassin, P. H. Leloup, D. Zhong, and S. Ji, Intraplate tectonics in Asia: a precise age for large-scale Miocene movement along the Aliao Shan-Red River shear zone, China, *Earth Planet. Sci. Lett., 97*, 65–77, 1990.

Shen, F., L. H. Royden, and B. C. Burchfiel, Large-scale crustal deformation of the Tibetan Plateau, *J. Geophys. Res., 106*, 6793–6816, 2001.

Tapponnier, P., G. Peltzer, A. Y. Le Dain, R. Armijo, P. Cobbold, Propagating extrusion tectonics in Asia; new insights from simple experiments with plasticine, *Geology, 10*, 611–616, 1982.

Wang, E., B. C. Burchfiel, L. H. Royden, L. Chen, J. Chen, and W. Li, Late Cenozoic Xianshuihe-Xiaojiang, Red River, and Dali fault systems of southwestern Sichuan and central Yunnan, China, *Geol. Soc. Am. Spec. Paper, 327*, 1998.

Chapter 2

Deformation of a regional low-relief relict landscape (erosion surface) in eastern Tibet

Abstract

Recent field work and DEM analysis show that remnant, local areas of a low-relief landscape (or "erosion surface") are geographically continuous across the southeastern Tibetan Plateau margin and can be correlated in order to define the maximum envelope of topography of the margin itself. This observation contradicts earlier notions that the low-gradient plateau margin slope (i.e. the maximum elevation of the margin) is a product of landscape dissection and reduction by fluvial incision due to the presence of major rivers which drain this portion of the plateau and plateau margins. Although initial development of the erosion surface is likely diachronous, we propose that a continuous low-relief landscape existed at low elevations prior to uplift and long-wavelength tilt of the southeastern plateau margin.

The modern altitude of the erosion surface provides an excellent datum for constraining the total amount of surface uplift of the southeastern plateau margin. The long-wavelength tilt of the surface across the plateau margin without major disruption mirrors the low-gradient decrease in crustal thickness across the plateau margin, which suggests that crustal

thickening has occurred in a distributed manner. Because large-magnitude compressional structures of late Cenozoic-age are lacking, we propose that crustal thickening beneath the southeastern plateau margin has largely been accomplished by preferential thickening the lower crust.

Perched, relict landscape remnants that reflect slow erosion, low initial elevations and slow uplift rates contrast sharply with the rapidly eroding modern river gorges that incise the surface, indicating that the modern landscape is not in equilibrium. Surface remnants are preserved because incision of the fluvial system has been largely limited to major rivers and principle tributaries, and has not yet progressed throughout the entire fluvial network. This "transient condition" of the landscape in southeastern Tibet reflects the initiation of rapid bedrock incision into a developing plateau margin, and the altitude of the remnant erosion surface can also be used as a datum by which to measure the total amount of erosion since the beginning of plateau uplift.

2.1 Introduction

The continent-continent collision between India and Eurasia is largely responsible for creating the Tibetan Plateau, the most extensive region of elevated topography on Earth [Figure 2.1]. The development of such an anomalously high landmass has been of interest to scientists in a broad range of disciplines ranging from lithospheric dynamics to the interaction between tectonics, climate and surface processes. Studies of the Tibetan Plateau have raised several first-order questions such as: 1) how is plate convergence accommodated in the continents and what are the relative contributions of continental subduction, uniform or differential shortening in the upper and lower crust, and lateral extrusion of rigid lithospheric blocks?; 2) how do spatial (or temporal) variations in crust and mantle rheology partition deformation throughout the orogen?; 3) does the convective removal of the mantle lithosphere contribute to surface uplift and high plateau elevation?; and 4) how do elevated mountain chains and laterally extensive plateaus affect global and regional climate patterns?

All of these questions depend critically on evaluating the relationship between topo-

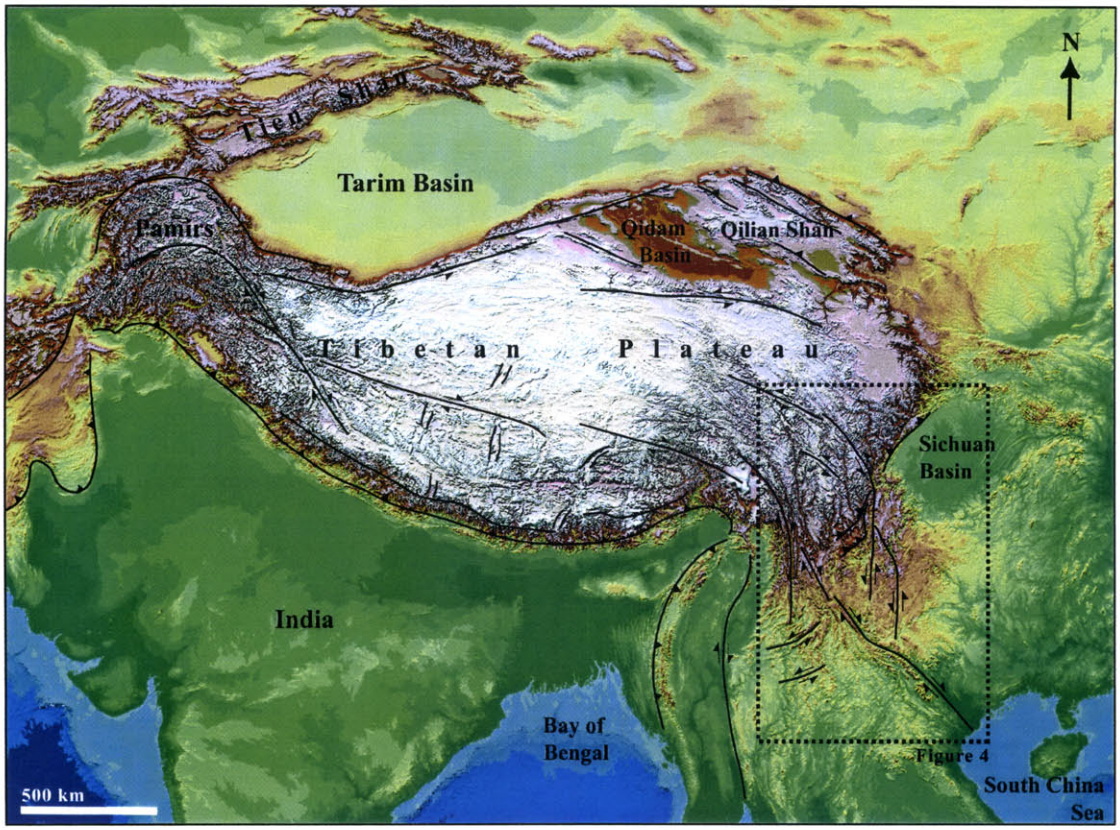

Figure 2.1: Topographic map of Tibet and major geologic structures of Cenozoic age. Topography derived from publicly available $\sim$ 1 km resolution GTOPO30 topography data [*U.S.G.S.*, 1993]. Inset box shows location of Figure 2.3

graphic evolution and the structural, erosional and climatic history of the plateau and surrounding regions. However, these relationships remain poorly understood largely because paleoaltitude is difficult to measure directly. Therefore surface uplift is difficult to quantify and must be inferred from a wide variety of geologic, geomorphic and paleontological methods. Studies that have attempted to link these data to surface uplift history have suggested that plateau development at a sub-regional scale is complex and varies substantially across the orogen [e.g. *Argand*, 1924; *Molnar and Tapponnier*, 1975; *Rowley*, 1996; *Chung et al.*, 1998; *Murphy et al.*, 1997; *Zheng, et al.*, 2000; *Kapp et al.*, in press].

Eastern Tibet offers an excellent opportunity to investigate the relationship between large-scale surface uplift and crustal thickening (i.e. plateau development) in order to address fundamental questions regarding: 1) the role of the deep crust and the importance

of rheologic heterogeneity in partitioning deformation, 2) the role of strike-slip systems in accommodating lateral (eastward) extrusion, and 3) the opportunity to address the geometry and timing of lateral growth of the Tibetan Plateau. The continuity, spatial extent, and the magnitude of Cenozoic surface shortening structures are inadequate to account for the amount of crustal thickening observed across eastern Tibet [e.g. *Burchfiel et al.*, 1995; *Royden et al.*, 1997], emphasizing the role of the deep crust which must preferentially thicken during plateau development. The near absence of surface shortening structures of late Cenozoic age also emphasizes the importance of the using the geomorphic record to delineate the history of surface uplift.

In this paper we focus on the relationships between the geomorphic and tectonic record on a regional scale in order to use landscape evolution as an indicator of "pre-existing" topography (i.e. prior to the Indo-Asian collision) and to define the spatial pattern of surface uplift. We describe the preservation of a regional, low-relief relict landscape which defines the surface of the topographically high eastern plateau and the low-gradient slope of the southeastern plateau margin. Preservation of this relict landscape surface, potentially provides an excellent datum for constraining the total amount of surface uplift. Because fluvial systems are particularly sensitive to baselevel changes, uplift rate and climate conditions, we also disscuss the implications of the initiation of significant river incision across eastern Tibet into this relict landscape.

2.2 Modern topography and models of crustal deformation

Models that describe plateau formation differ most significantly in their predictions for the tectonic evolution of eastern Tibet, defined geographically as the area east of the drainage divide separating the major rivers that flow into the south and east Asian seas from the internally-drained west-central plateau [Figure 2.2]. Significant differences in these models arise from questions of whether deformation is best described by the extrusion of large, rigid crustal (or lithospheric) blocks along major strike-slip faults [*Tapponnier et al.*, 1982;

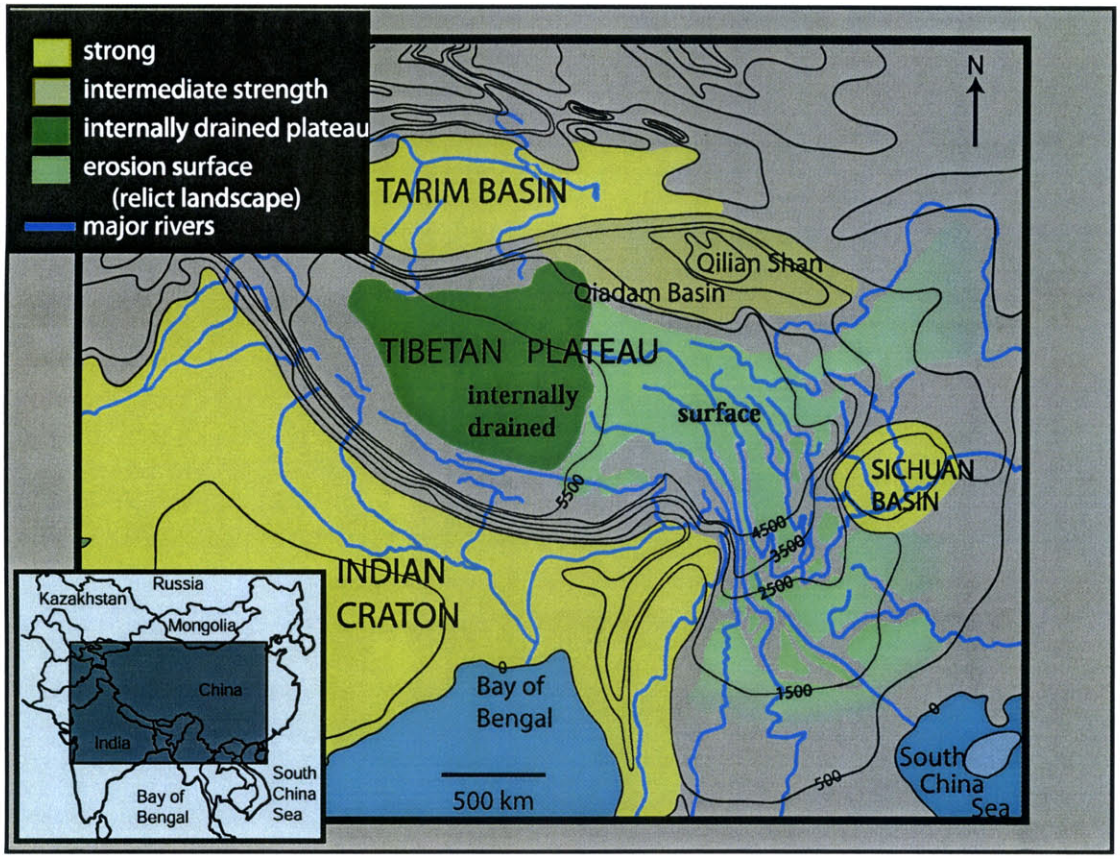

Figure 2.2: Geomorphic map of Tibet. Elevation is shown by smoothed contours (1000 m interval). The dark green region outlines the internally-drained west-central plateau. The general extent of the low-relief relict landscape in eastern Tibet is shown in light green. Low-lying areas cratonic areas that have experienced relatively minor Cenozoic deformation are highlighted in yellow.

Tapponnier et al., 1986], or as a viscous material by either uniform shortening of the lithosphere or by enhanced flow within a weak lower crustal layer [*England and Houseman*, 1986; *Royden*, 1996; *Clark and Royden*, 2000; *Shen et al.*, 2001].

Abundant evidence exists for major movements on strike-slip faults in Oligocene - Middle(?) Miocene time, although the magnitude of displacement of these structures (between a few 100 km to 1000 km total offset) and the degree of internal deformation within individual crustal blocks are the subject of much debate [*Leloup, et al.*, 1995; *Leloup et al.*, 2001; *Wang and Burchfiel*, 1997]. The late Miocene to present day surface deformation in eastern Tibet is also dominated by strike-slip faulting, but these younger faults have offsets

of only a few 10's of kilometers [*Replumaz, et al.*, 2001; *Wang et al.*, 1998]. Substantial crustal thickening across eastern Tibet [*Li and Mooney*, 1998] has also occurred since Early Cenozoic time and kinematic descriptions of strike-slip faulting alone fail to address this fundamental aspect of the tectonic evolution of eastern Tibet.

The modern topography generally mirrors the pattern of crustal thickness across the eastern plateau and plateau margins [*Li and Mooney*, 1998], suggesting that the spatial development of elevated topography and the pattern of surface uplift has generally paralleled patterns of crustal thickening through time (we restrict the following discussions to the region of eastern Tibet to be south of the Qilian Shan/Qiadam Basin region). The area of highest elevation in eastern Tibet covers a region of approximately the size of France, stands at an average elevation between 4500-5000 m. However the morphology and topographic gradients vary considerably along strike of the plateau margins [*Clark and Royden*, 2000] [Figure 2.2]. The Longmen Shan, adjacent to the Sichuan Basin, is the only portion of the eastern plateau margin where a topographically steep escarpment has developed ($\sim$4.5 km elevation gain over a distance of $\sim$50 km) and the areas north and south of the Sichuan basin are characterized by broad, low-gradient plateau margins ($\sim$4.5 km elevation gain over distances of $\sim$1500-2000 km).

The preservation of relict, low-relief landscape remnants that define the maximum envelope of topography across the southeastern plateau margin contradicts earlier notions that the low-gradient plateau margin slope is a product of landscape dissection and reduction by fluvial incision due to the presence of major rivers which drain this portion of the plateau and plateau margins [Figure 2.2]. The regularity and long-wavelength of the topographic surface over the southeastern and northeastern plateau margins are unusual for orogenic systems and suggest that crustal thickening occurred in a broadly distributed fashion for a considerable distance away from the high plateau interior extending into the eastern foreland.

2.3 Use of a landscape "surface" as a reference datum

In areas of active tectonism, the pre-uplift landscape is often rapidly destroyed due to increased erosion rates associated with an increase in topographic slope. However, geomorphic relationships observed in eastern Tibet suggest that landscapes formed prior to Cenozoic uplift are preserved discontinuously across the eastern plateau and plateau margins as high elevation remnants of low-relief "surfaces", not yet destroyed by the active intense fluvial incision affecting the high altitudes of eastern Tibet [Figure 2.3]. We propose that these remnant, isolated surfaces are the oldest landscape features in eastern Tibet and can be spatially reconstructed as the relict landscape prior to Cenozoic uplift and can be used as paleo sub-horizontal datum for quantifying surface uplift related crustal thickening.

There are many inherent problems with using a landscape surface as a datum, especially at regional scales, and it is therefore necessary to discuss our reasoning and approach to establishing the landscape evolution in eastern Tibet. The history of landscape evolution and the identification of relict, low-relief landscapes stems from the original Davisian concept of the "peneplain", the product of the final stage of landscape evolution when a landscape is graded by fluvial erosion to sea level [*Davis*, 1899]. Thus, these ancient (static) planar features recognized in the modern landscape could be identified and correlated to represent an absolute horizontal datum recording deformation or uplift with respect to sea level. Later derivatives of the peneplain concept also focused on a genetic description for low-relief landforms (i.e. peneplains, pediplains, etchplains, etc.), each providing a newly recognized mechanism for generating a landscape of low-relief.

In the past hundred years since Davis' original conception of the peneplain, we have recognized several problems: 1) The final stage of landscape evolution resulting in a peneplain (i.e. a static landform), is predicated on the concept of the "life-cycle" of a landscape where landscapes evolve predictably to intermittent, instantaneous pulses of tectonic uplift. However, geomorphic research over the past fifty years has demonstrated that landscapes are dynamic systems responding to a continuum of spatial and temporal tectonic and climatic conditions, and demonstrate differential erosional responses to lithologic variations [see *Merritts and Ellis*, [1994] for a review]. Furthermore, quantification of erosion rates

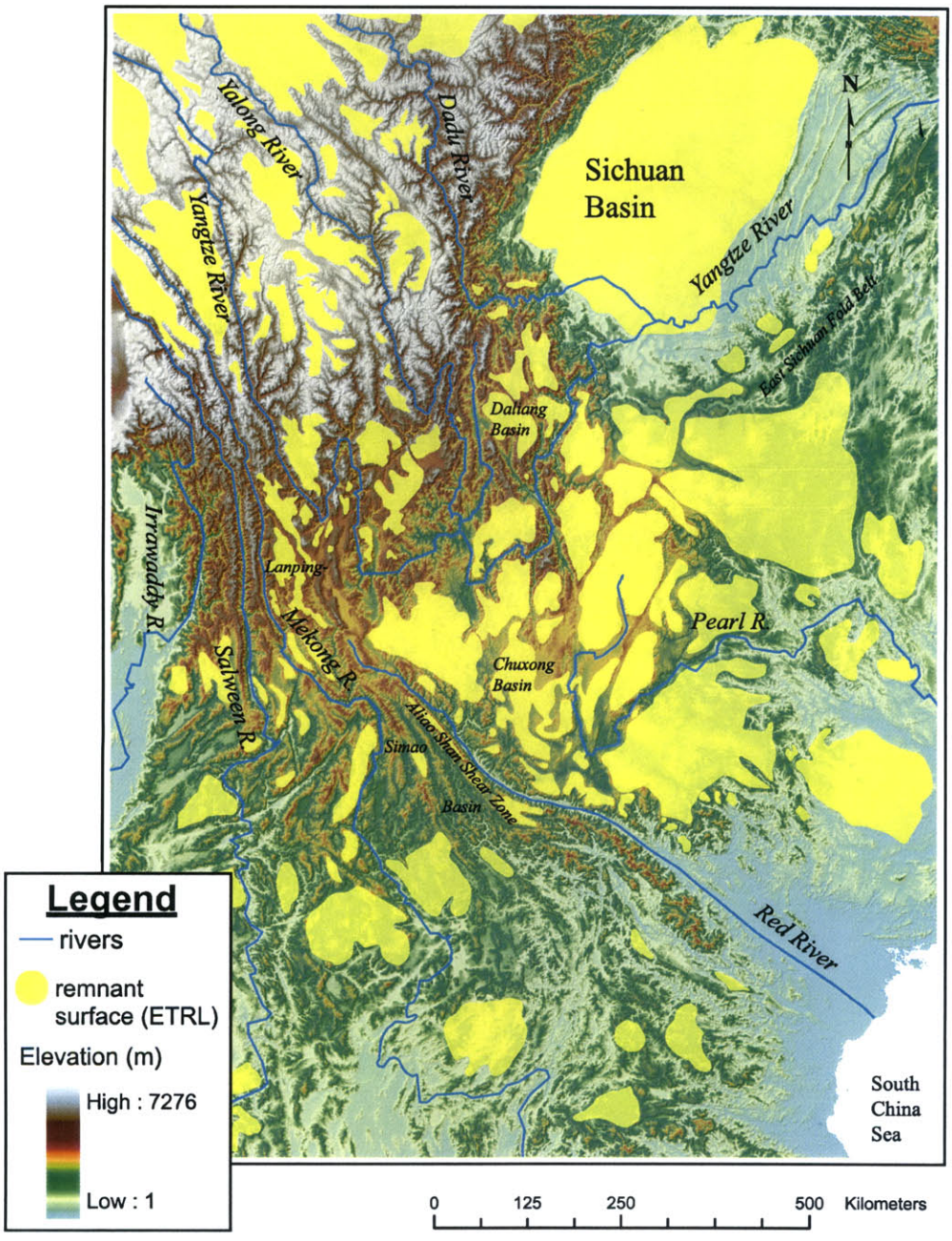

Figure 2.3: Detailed map of the low-relief, relict landscape (or erosion surface) of eastern Tibet. Surface is shown in yellow over a base map of digital topography derived from publicly available $\sim$ 1 km resolution GTOPO30 topography data [*U.S.G.S.*, 1993].

has challenged the concept of a "static" ancient landform, even under extremely slow erosion rates (< 0.01 mm/yr), and questions the meaning of an "age" of a landscape. 2) Low-relief surfaces or landscapes can grade to a local baselevel that may be at any elevation. Therefore, planar, low-relief landscapes need not imply an original elevation near sea level. 3) Landscapes are polygenetic, and often form through the superposition of genetically unrelated surface processes. Moreover, continuous low-relief landscapes need not be strictly erosional. We commonly observe in the modern landscape the juxtaposition of low-relief erosional landscapes and adjacent depositional (or formerly depositional) ones.

The problems encountered with the peneplain concept has limited the geomorphic and geologic communities to studies of smaller-scale "erosion surfaces", where well identified, time-correlative, and often genetically related erosional horizons are used to define offsets across recent or active tectonic structures [e.g. *Spotila and Sieh*, 2000; *Schoenbohm et al.*, 2001] or are used to limit the age of tectonic deformation by cross-cutting relationships [e.g. *Gubbels et al.*, 1993]. However, the temporal and genetic relationships required for such studies necessitates a local scale study and severely limits, if not precludes, the utility of landscape evolution over much larger extents as the surface expression of crust and mantle dynamics.

In order to identify the paleolandscape of eastern Tibet associated with the pre-plateau uplift conditions, we seek a new definition for a revised concept of the "peneplain" (e.g. *Davis*, 1899). We wish to identify a relict landscape that may incorporate a collection of landforms of different origins and different ages and which accounts for the polygenetic, dynamic nature of landscape evolution at regional scales. In this paper we use a paleosurface description similar to that proposed by *Widdowson* [1997] where our reconstruction of the relict low-relief landscape of eastern Tibet is accomplished by the spatial correlation of "remnant surfaces" defined as "*a remnant of a regionally significant paleo-landscape with a low-relief topographic surface, of initially erosional and/or depositional origin, that is associated with a protracted period of erosion*". The application of this term "*remnant surface*" will be used in the following section to describe the individual areas where we map relict landscape features and discuss their relationship to the geology, stratigraphy and topography. Our ultimate goal is to correlate these individual remnant surfaces across eastern

Tibet in order to define the paleolandscape prior to Cenozoic uplift.

2.4 "Active" vs. "Relict" landscapes in eastern Tibet

The general contrast in the morphology of the landscape of eastern Tibet from low-relief high elevation "surfaces" to low elevation, deeply dissected landscapes of the major river valleys is obvious to even the casual observer. However, in order to identify remnant surfaces in eastern Tibet as a part of a relict, pre- plateau uplift landscape of eastern Tibet, we establish specific criteria that describe the contrast in morphology and erosional history/conditions that allow us to distinguish a relict landscape remnant from the active landscape. In this section, we describe the "active" landscape, and the transition from the remnant surfaces to the active landscape. The following section describes how remnant surfaces were identified and mapped across eastern Tibet.

The "active" landscape in eastern Tibet is dominated by bedrock river erosion and deep steep-walled canyons. The eastern Tibetan Plateau is drained by several of the world's largest and longest rivers. In eastern (southeastern) Tibet these include the Salween, Mekong, Yangtze (and major tributaries), Red and Pearl rivers. The Salween, Mekong, and Yangtze rivers have their headwaters in central Tibet, immediately east of the Yadong-Gulu rift system. These rivers have carved impressive river canyons that are a maximum of 3 - 3.5 km deep where the rivers cross from the high eastern plateau into the southeastern plateau margin [Figure 2.4, 2.5, 2.6].

We assume that the kilometers of incision observed on these major rivers and principle tributaties has occurred in response to the uplift of the plateau to its modern elevation and favorable climate conditions. We define the "active" landscape as areas that are responding (by increased fluvial incision rates, mass-wasting, etc.) to the deep incision of the major rivers and principle tributaries. The characteristics of these large rivers include bedrock terraces (up to $\sim$1 km above the modern river valleys) that are common within the river valleys on the Yangtze, Yalong and Dadu Rivers [Figure 2.7]. Thin mantles of alluvium or mass-wasting debris are also common on bedrock valley floors, as are occasional flights of alluvial terraces. Sediment storage in the river valleys is short-term and likely related

to mass-wasting events caused by seismicity or short-term climate fluxuations. Some alluvial terraces are associated with lake deposits and have been linked to earthquake triggered landslides that temporarily dam a river (i.e. the Xigada Formation [*Bureau of Geology and Mineral Resources, Sichuan*, 1990; X. Zhang (pers. comm.)]). Sediment commonly accumulates in the river valley floor behind active strike-slip faults, such as the Jianchuan Fault near the First Bend in the Yangtze River, but the total volume of this ponded sediment is small [Figure 2.6]. In areas of erosionally less-resistant lithologies, such as late Mesozoic - early Tertiary sedimentary basins, wider, more open valleys have developed with alluviated valley floors.

Surface remnants are not isolated from the rest of the fluvial network. The headwaters of many tributary systems originate on surface remnants as alluvial systems and transition down stream to steep bedrock rivers where they join the deeply incised major rivers. The transition of the fluvial system from remnant surfaces to the active landscape suggests that the landscape is responding to changing uplift conditions and that high elevation surface remnants are portions of the landscape that have not yet adjusted to their modern altitude and regional topographic slope.

Figure 2.8 and 2.9 show an example of this transition along a tributary river that originates on a surface remnant and eventually joins the Yalong River (a major tributary of the Yangtze River) over a total distance of $\sim$200 km. Figure 2.8 shows a map view of the tributary taken from a CORONA image and compared with a longitudinal river profile. The moderately-high albedo area in the image (outlined in yellow) shows the extent of the preserved remnant surface. Where the river crosses this surface it is a braided alluvial stream with approximately 500 m of fluvial relief over a distance of about 100 km. The longitudinal profile shows a change in concavity which is coincident with a change in the river morphology from a wide valley with a braided alluvial river and flights of alluvial terraces to a more narrow river valley with exposed bedrock walls and a single, armored river bed. Further downstream, an abrupt knickpoint (abrupt change in slope of the river channel) is observed just $\sim$10 km before entering the main river and is associated with a steep channel slope and narrow channel and valley width. The low steepness values and alluvial character of the tributary where it crosses the surface suggest that erosion rates are

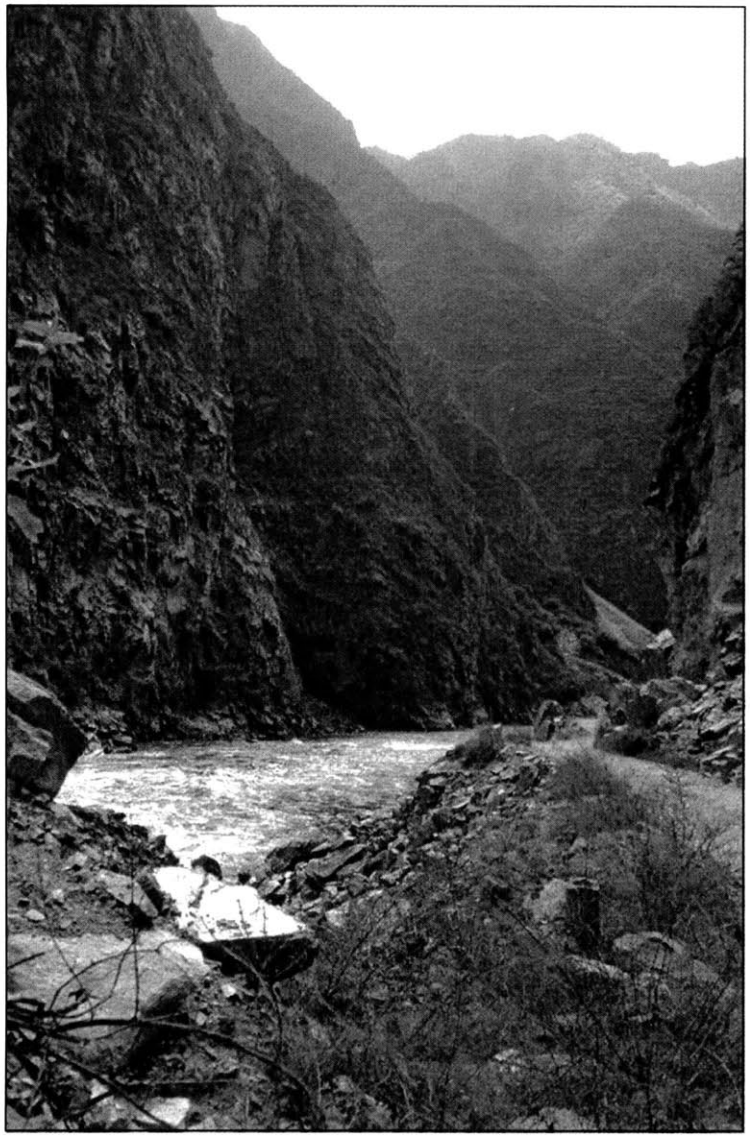

Figure 2.4: Middle Dadu river gorge, elevation 2000 m.

slow, especially compared to the steep bedrock river valleys downstream [Figure 2.9]. Unmetamorphosed early Tertiary sediment and Eocene through Cretaceous low-temperature thermochronology ages [*Clark et al.*, 2002; *Xu and Kamp*, 2000; *Bureau of Geology and Mineral Resources, Sichuan*, 1990] suggest that little material has been eroded from this surface since at least Eocene time [Figure 2.8 d-e].

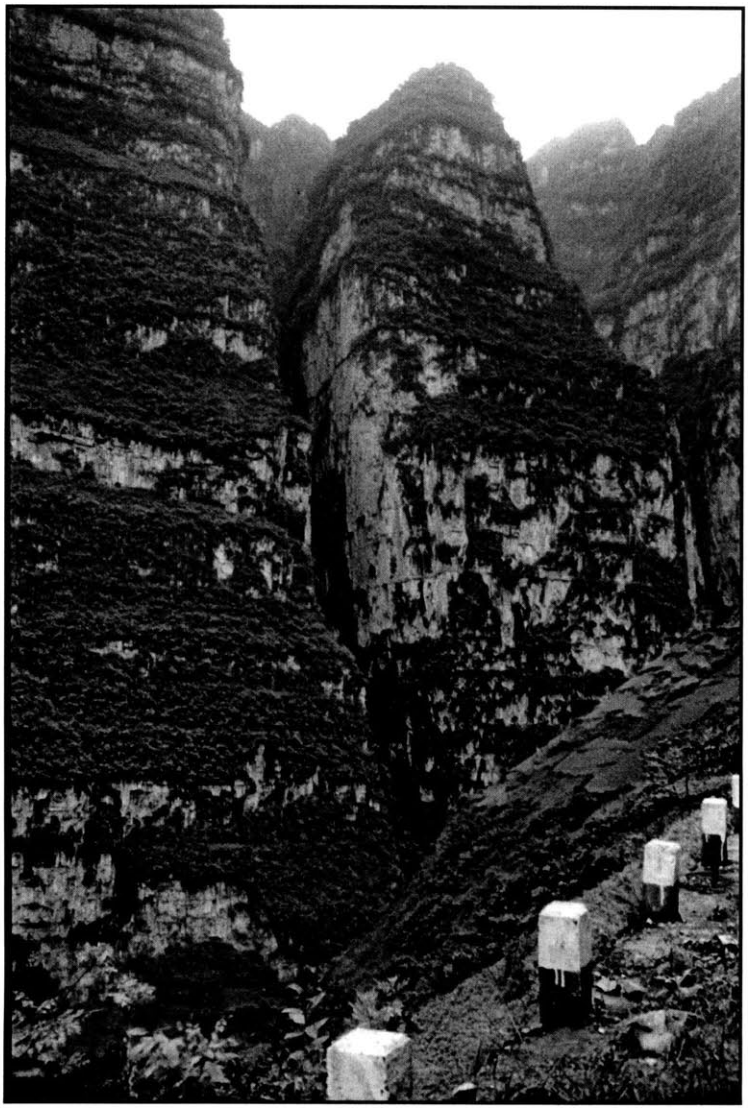

Figure 2.5: Lower Dadu River gorge, elevation 800 m.

2.5 Mapping and characterizing relict landscape (surface) remnants

In this section, we propose a protocol for identifying (mapping) surface remnants through an evaluation of topography, slope and relief maps, CORONA imagery, 1:200,000 scale geologic maps [*Bureau of Geology and Mineral Resources, Sichuan*, 1991; *Bureau of Geology and Mineral Resources, Yunnan*, 1990], and field observations. The next section

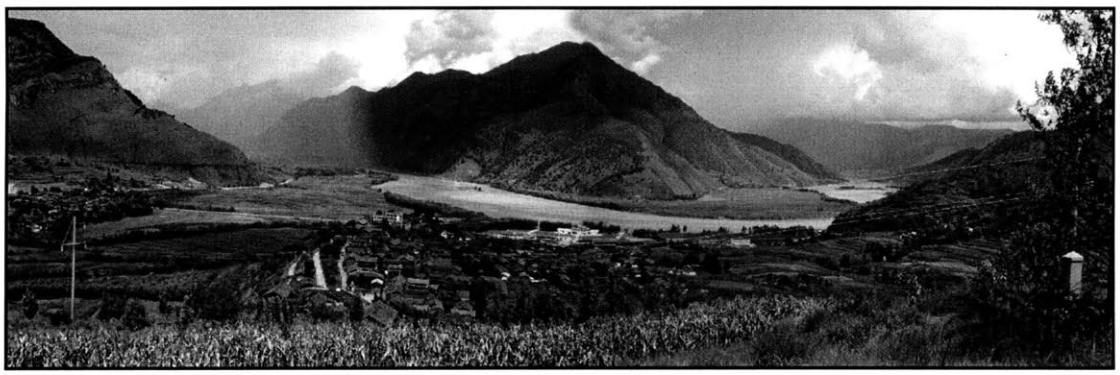

Figure 2.6: Yangtze River "First-Bend", elevation 1600 m.

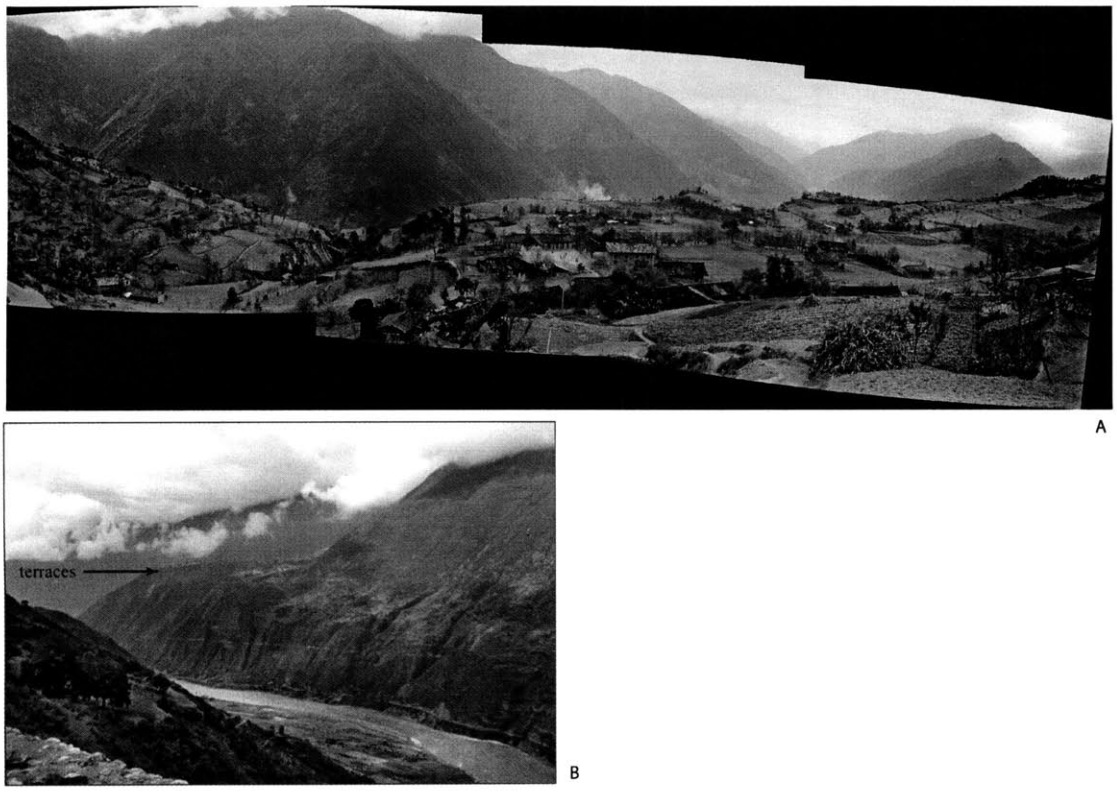

Figure 2.7: Luding river terraces (Dadu River), elevation 1400 m. Bedrock terraces are $\sim$ 800 m above the river valley.

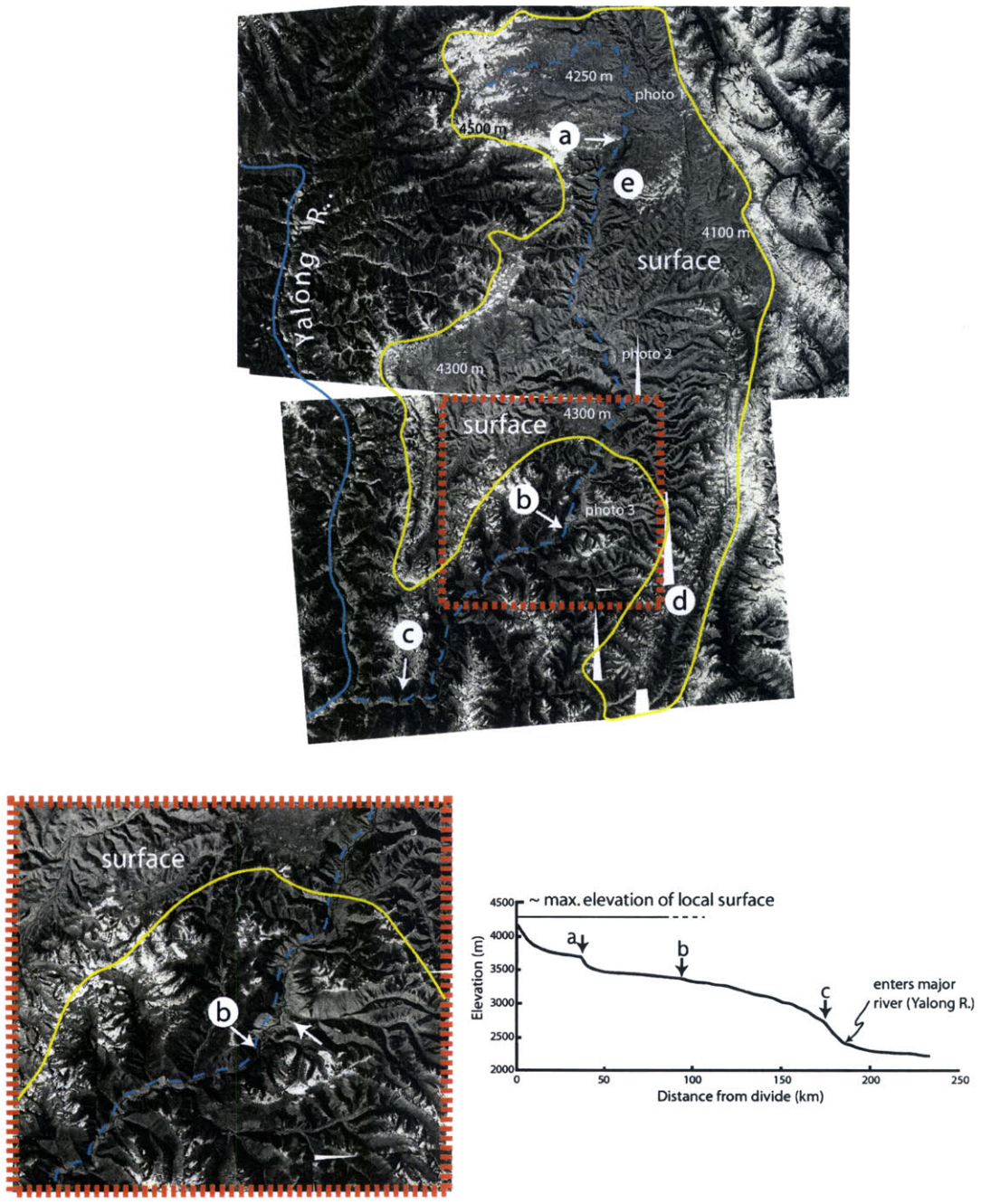

Figure 2.8: Example of river transition. Mapped positions on the CORONA image (a-c) correspond to knickpoints (abrupt changes in river slope) on the river profile: (a) likely reflects crossing a more resistant lithology (granite) compared to the surrounding Triassic sediments; (b) is associated with an abrupt change from a wide, alluvial (transport-limited) river system to a bedrock (detachment-limited) or mixed channel; and (c) is associated with an abrupt steepening of the channel just before entering the main Yalong gorge. (d and e) represent locations of early Tertiary sediment and thermochronology data respectively. Photos refer to Figure 2.9.

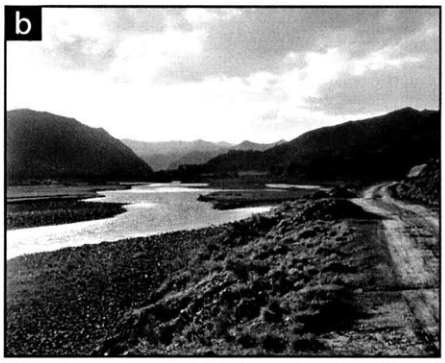

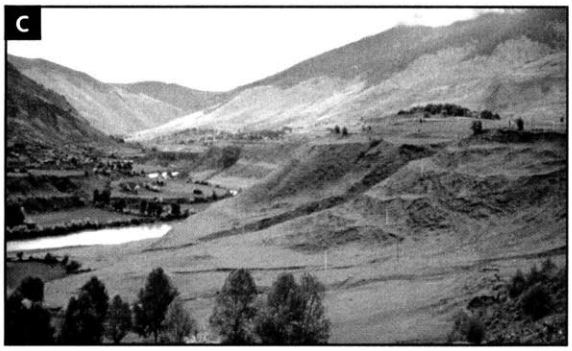

Figure 2.9: Example of river transition from relict surface to steep river gorge, field photos. Figures A-C show a gradational change in the alluvial portion of the tributary as it crosses the relict surface shown in Figure 2.8 referred to as photos 1-3 respectively. Figure C is 500 m below the maximum elevation of the surface. Figure D shows the bedrock portion of an adjacent tributary just before entering the main Yalong River gorge, equivalent to a position below point C on Figure 2.8.

discusses the relationships between the surface remnants, topography, and the structural history.

Identification of the geographical extent of surface remnants in detail is an iterative process that requires the evaluation of multiple datasets in concert with field observations. Mapping surfaces can be approached by considering the landscape in a piecewise manner across local areas (i.e. 200 x 200 km^2). In each local area we assess whether the highest elevation portion of the landscape contrasts with the active landscape. In some areas there is no contrast, and a high elevation relict landscape cannot be identified. We use a number of criteria to identify contrasting landscape elements (relict vs. active), these include: elevation, local slope, local relief, tectonic history, active structures, and erosional processes. A summary of the general criteria used to identify remnant surfaces are found in Table 2.1. Specific characteristics that best describe a contrast in the landscape vary as a function of lithology, structural history, altitude and latitude and these details are discussed in the next section.

Local relief and slope are key features of the remnant surfaces in eastern Tibet. A local relief map of the general region immediately shows the contrast in relief between the major river valleys ($\sim$1000 – 4200) compared to the high-elevation surfaces ($<$ 600 m) [Figure 2.10]. Figure 2.11 shows a relief map for just the high elevation surfaces and demonstrates the continuity of low-relief areas across the plateau margin.

Figure 2.12 and 2.13 show an example of how different datasets were compared in order to determine the extent of remnant surfaces. In Figure 2.12 we outline (in black) the areas that fit the high-elevation, low-slope and low-relief criteria outlined in Table 2.1. The combined topography/slope map uses the slope values as shading for the topography, allowing high elevation, low-slope areas to be identified by a smooth texture. This type of map was a useful illustration and guide for mapping surface remnants.

Figure 2.13 shows an example from CORONA imagery in the same area. The surface extent is mapped by identifying the contrast in albedo from the moderately high values on the surface to low values in the deep river canyons (this contrast was most easily seen on images with low sun angles). From CORONA images and field work we observe that hillslope creep, alluvial (transport limited) rivers, and chemical weathering dominate the

erosional processes across these high elevation surfaces. Low values calculated for river steepness indicies [*Kirby and Whipple*, 2001] and knickpoints separating alluvial rivers on high surfaces from bedrock reaches further downstream were also used to distinguish the high surfaces from the active landscape [Figure 2.8 and 2.9]. and Geologic maps show limited and local early Tertiary, Neogene and Quaternary sedimentary deposits [*Bureau of Geology and Mineral Resources, Sichuan*, 1991]. Extent and continuity of surface remnants were also evaluated from viewing 3D topography images [Figure 2.14]. By combining all these criteria, we map the extent of the surface remnants shown by the yellow polygons in Figure 2.13.

We also consider the potential contribution of glacial erosion to forming the high elevation surface landscape. Evidence of glaciation is observed locally, particularly where the surface elevation is in excess of 5000-5500 m elevation. However, we do not think that high-elevation glacial surfaces formed by "altiplanation" could have contributed significantly to formation of remnant surfaces in eastern Tibet. These types of glacial processes typically act on narrow ridges (i.e. creating "concordant" summit surfaces) and cannot explain the formation of a low-relief landscape over areas of 100 km^2 or more.

2.6 Modern topography, erosion and structural evolution of eastern Tibet

The local morphology of surface remnants in eastern Tibet is strongly influenced by underlying lithology, structure, altitude and latitude and the geographical continuity (or lack there of) between individual surfaces is a function of the intensity of Cenozoic deformation and degree of fluvial dissection by the modern major rivers [Figure 2.2 and 2.3]. Reconstruction of the relict pre-plateau landscape depends critically on this integration of the structural, sedimentological and geomorphic record. Here we discuss the surface and other relevant geomorphic features and geology in each of five sub-provinces. The specific characteristics that distinguish remnant surfaces from the active landscape are discussed in each section.

Table 2.1: Criteria for identification of remnant surfaces.

Data type	Criteria
Topography	Locally, highest elevation in landscape.
Longitudinal river profiles	Channel segments with low steepness indices and knickpoints separating upstream alluviated channel reaches from bedrock channels downstream.
Slope	Moderately low slopes (between 1.2 - 10 degrees).
Relief	Low relief (< 600 m)[†].
Geologic maps	Lack of late Cenozoic active sedimentation and limited (few to several hundred meters of mid to early Cenozoic sedimentation.
Field observations	Identification of slow weathering processes (i.e. hillslope creep and transport-limited (alluvial) rivers, periglacial or chemical weathering processes; saprolite/thick weathering profiles [*Schoenbohm et al.*, 2002]) that contrast with the active landscape (detachment-limited (bedrock) river erosion, mass wasting, and debris flows).
CORONA imagery	Moderately high albedo contrast with low albedo active bedrock channels for images with low sun angles. Images are also used to evaluate relative elevation, slope/relief, and identify active erosional processes and change in fluvial morphology.

[†] Some averaging of the active landscape occurs across edges of remnant surfaces. In these areas local relief can be as high as 1 km.

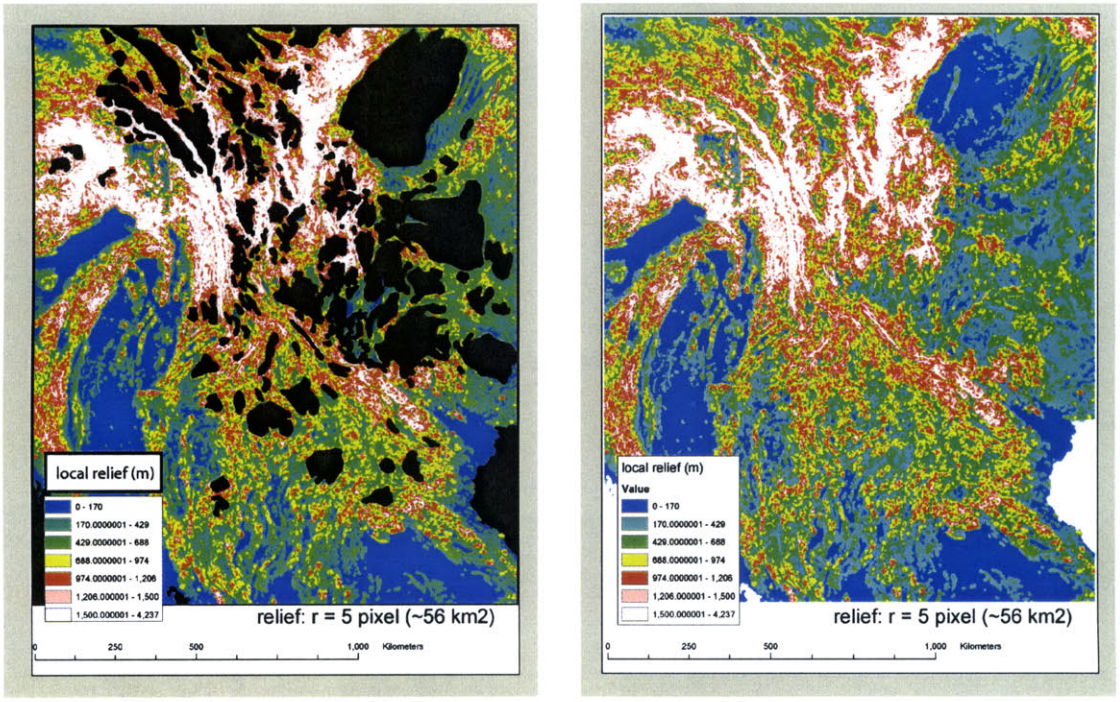

Figure 2.10: Relief maps derived from $\sim$ 1 km resolution digital topography calculated for a circular domain (56 km^2). (A) Relief for only the active landscape, excluding remnant surfaces and (B) relief values for the entire landscape. Areas of intense fluvial incision are characterized high relief values ($\sim$1000-4200 m).

Pre- Indo-Asian collision deformation (i.e. before 45 Ma), Paleozoic/Proterozoic paleo-passive margin boundaries, and Paleozoic/Mesozoic suture zones control much of the present-day heterogeneity in eastern Tibet. Yet despite the complex tectonic history of eastern Tibet, the topographic boundaries of the modern plateau largely ignore pre-existing structural features, with a few important exceptions. In general, the area affected by late Cenozoic uplift can be subdivided into five distinct provinces: 1) the Songpan - Garze terrane, 2) Longmen Shan and Yalong thrust belts, 3) the Sichuan Basin, 4) the South China Fold Belts, and 5) the Three Rivers fold and thrust belts, discussed individually in the following sections [Figure 2.15]. (For a more detailed treatment of the structural history of this area, the reader is urged to the consult the following reviews: *Burchfiel et al.*, [1995]; *Leloup, et al.*, [1995]; *Wang and Burchfiel*, [1997]; *Wang et al.*, [1998]; *Leloup, et al.*, [2001]).

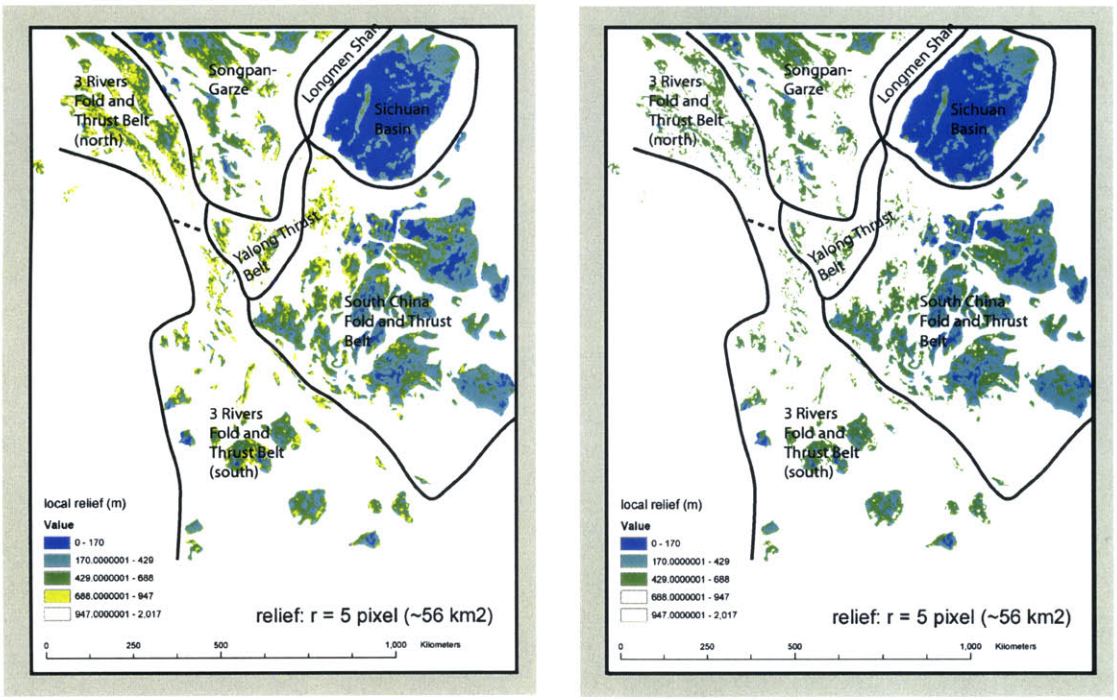

Figure 2.11: Relief maps derived from $\sim$ 1 km resolution digital topography calculated for a circular domain (56 km^2). (A) Relief calculated only for surface remnants limited to less than 947 m and (B) and less than 688 m. Some averaging of relief occurs between the edges of surface remnants and tributaries that have incised in response the the downcutting of major rivers. This results in higher relief values between $\sim$600 - 1000 m.

2.6.1 Songpan-Garze terrane

Rocks of the Songpan-Garze terrane make up much of the high flat plateau region of eastern Tibet and consist predominately of early to middle Triassic flysch with a depositional(?) thickness of more than 10 kilometers [Figure 2.15]. These rocks were deposited in a broad basin that separated the North China Block from the Yangtze platform to the south [*Bureau of Geology and Mineral Resources, Sichuan*, 1991; *Mattauer et al.*, 1992; *Burchfiel et al.*, 1995]. Subsequently these rocks were extensively folded, separated from their underlying metamorphic and possibly oceanic basement across a major decollement, and subjected to widespread post-orogenic plutonism of latest Triassic to Jurassic age [*Mattauer et al., 1992*; *Roger et al.*, 1994; *Burchfiel et al.*, 1995]. These plutons remain largely undeformed and limit significant deformation of the Songpan-Garze terrane to late Triassic time.

Post-Triassic rocks are rare in the Songpan-Garze terrane except near its boundaries

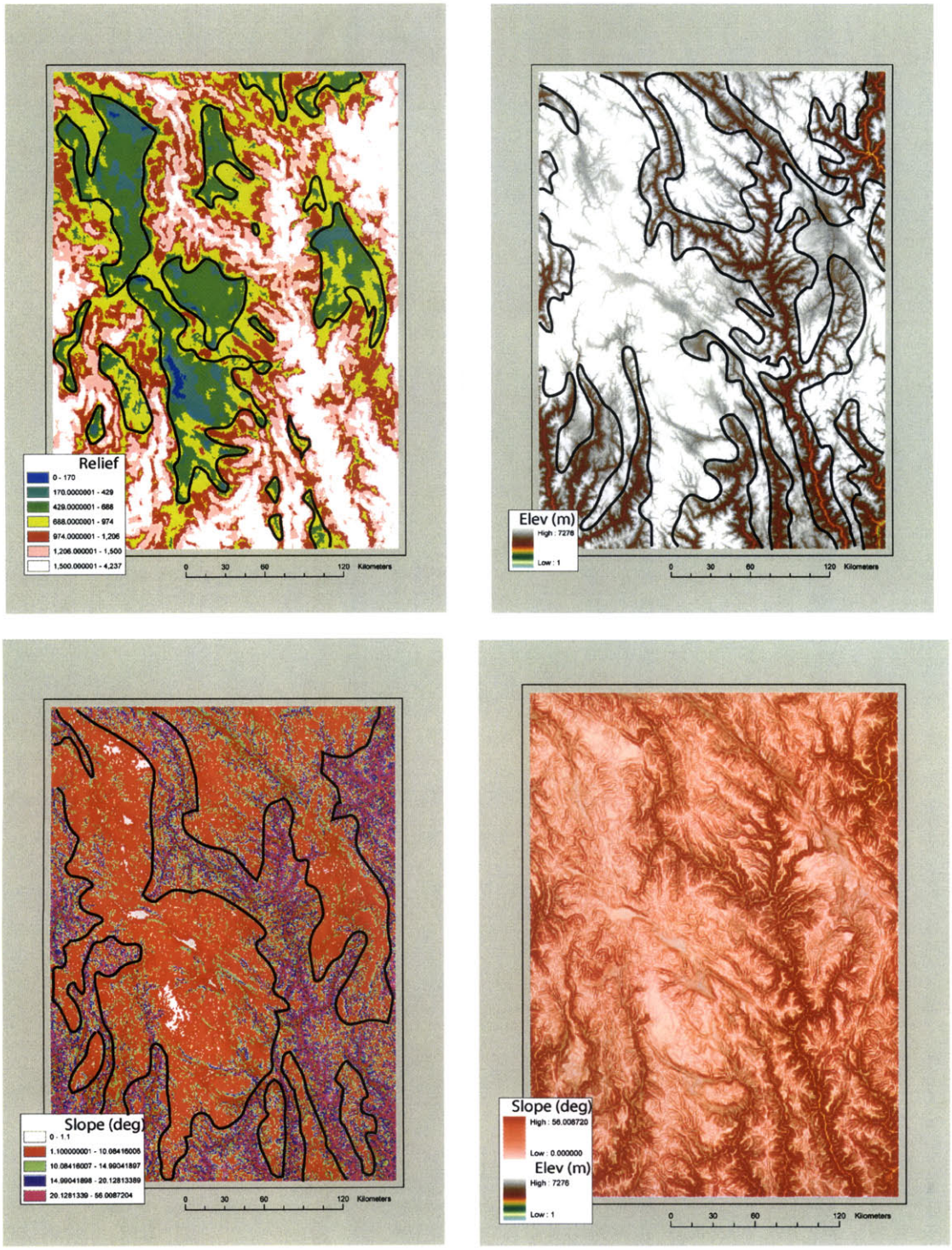

Figure 2.12: Example of surface characterization and identification from topography, slope, relief, and combined topography/slope maps. Black outlines the extent of the criteria outlined in Table 2.1.

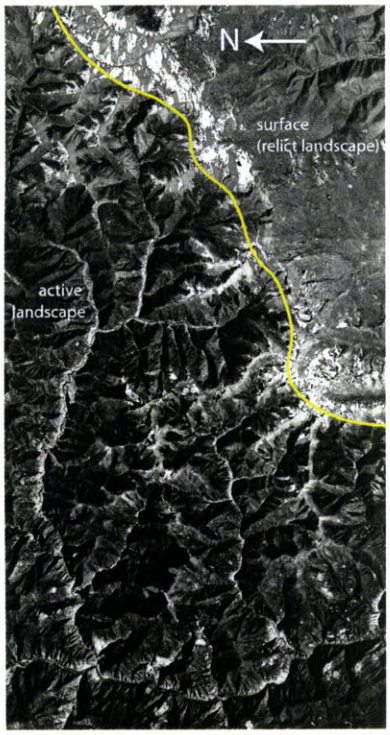

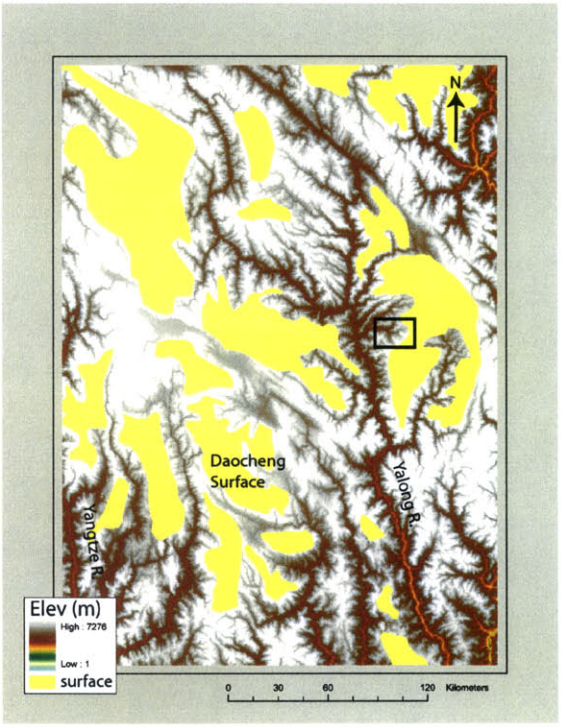

Figure 2.13: Example of surface characterization and identification from CORONA imagery. Black inset box shows extent of CORONA image. Yellow polygons outline our mapping of the extent of relict surface that we derived from the combination of topography, slope and relief criteria, imagery, geologic and field observations.

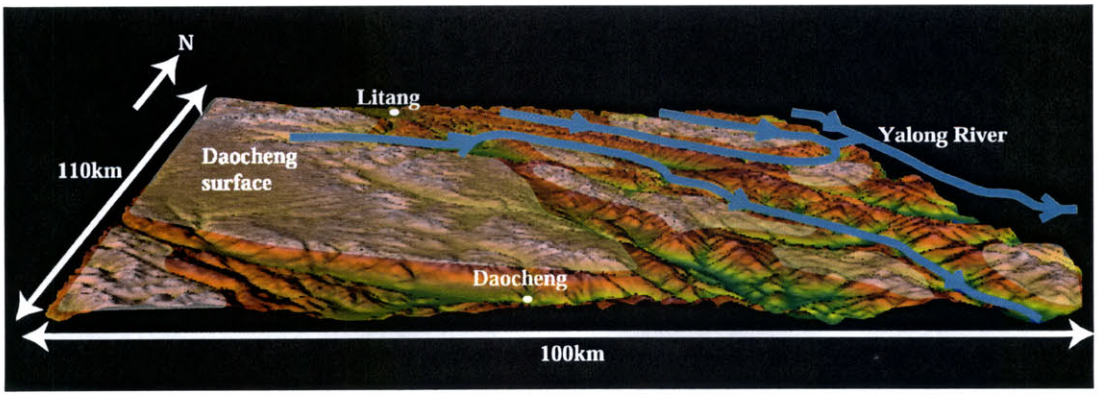

Figure 2.14: Example of 3-D image of digital topography, view north. Remnant surfaces areas are outlined in white and make up the topographically highest portion of the landscape. These surface remnants are being actively destroyed by bedrock incision of the Yalong River.

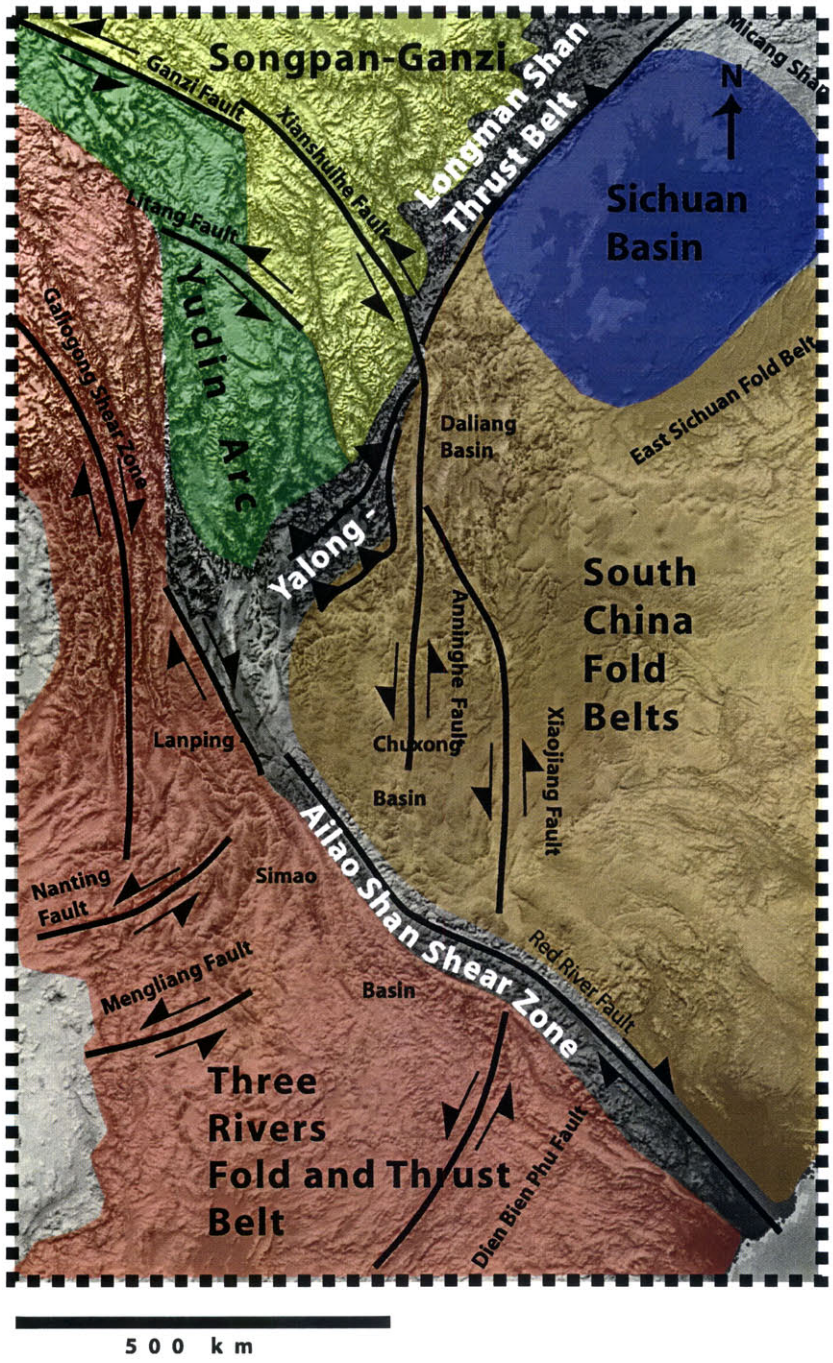

Figure 2.15: Major tectonic terranes and Cenozoic geologic features for eastern Tibet.

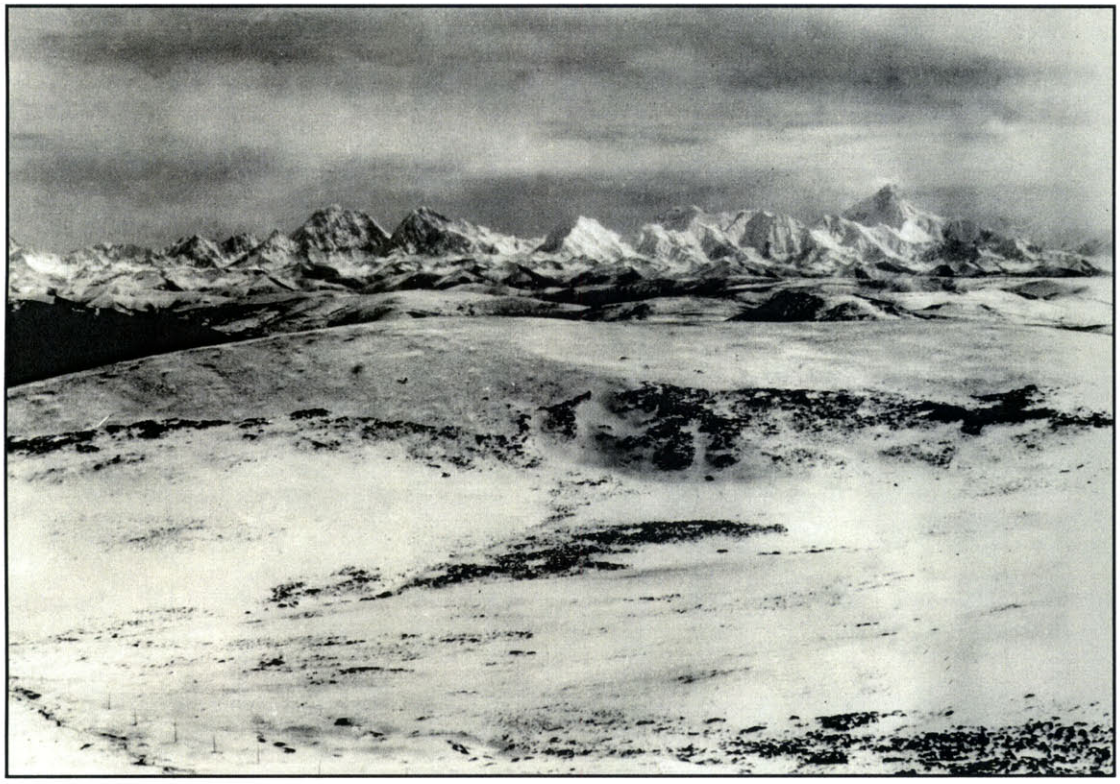

Figure 2.16: View across relict landscape at > 4000 m to the east. High-relief topography in the background is the Gonga Shan massif (elevations between 5000-7756 m). Photo courtesy of the archives of Prof. Arnold Heim, ETH, Zürich, 1930-1.

with adjacent geologic terranes [*Bureau of Geology and Mineral Resources, Sichuan*, 1991]. Early Tertiary coarse clastic sedimentary rocks crop out in narrow fault-bounded basins near the southern and southwestern extent of the Songpan-Garze terrane. These rocks are depositionally unconformable on an originally low-relief surface, deformed and subsequently beveled by erosion to low relief, conformable with the elevation of the surrounding area. Both deformed and undeformed granites of middle Miocene age are present between the Longmen Shan and Yalong thrust belts, in an area of local active tectonism near Gonga Shan [*Mattauer et al.*, 1992; *Roger et al.*, 1995] that is also associated with anomalously high local relief and elevations [Figure 2.16].

Much of the Songpan-Garze terrane forms a high elevation landscape with low-local relief (generally less than 600 m of relief at 4000-5000 m elevation) [Figure 2.17 and 2.11]. This high altitude landscape is preserved as a series of surface remnants that appear to

A

B

Figure 2.17: Remnant surface at 4500 m elevation, Songpan-Garze terrane. View north.

Figure 2.18: Remnant surface at 4700 m elevation, Songpan-Garze terrane, view south.

have formed an originally continuous landscape, subsequently incised by major rivers to form deep river gorges. Remnant surfaces bevel deformed Triassic flysch and cross-cutting undeformed plutons as well as deformed early Tertiary sediments and in places remnant surfaces are preserved over extensive tracts of more than 10,000 km^2 [e.g. *Burchfiel et al.*, 1995; *Wang et al.*, 1998; *Kirby et al.*, 2002] [Figure 2.3]. Active river channels are alluvial within the relict landscape and transition into steep, intensely incised bedrock canyons downstream as they join a major river or principle tributary.

Neogene and Quaternary sediments locally mantle surface remnants and are generally

associated with active faults or are local fluvial and glacial deposits. There is little vertical displacement of the surface, or adjacent surface patches, across the major active strike-slip faults of eastern Tibet (e.g. the Xianshuihe, Garze and Litang Faults) despite horizontal displacements of up to 60 km. The remnant landscape is locally disrupted by active normal faults that bound small graben and appear to transfer motion between strike-slip faults (e.g. the Litang and Garze basins, *Wang et al.*, [1998]).

At elevations in excess of ~4500 m, extremely low-relief (planar) surfaces (< a few hundred meters) are present across some of the granite plutons [Figure 2.10] and 2.14]. The formation of these more planar surfaces may be a combination of periglacial weathering processes acting on surfaces at high altitudes and the high susceptibility of particular granite compositions to chemical weathering [Figure 2.18]. We interpret these types of weathering processes as the reduction of an initially low-relief landscape to a more planar surface, and not as the initial stages of development of this low-relief landscape. Alpine glaciation is locally observed, however the sedimentary and geomorphic record does not support the presence of widespread glacial erosion that may have significantly modified surface remnants [*Bureau of Geology and Mineral Resources, Sichuan*, 1991].

Geologic and thermochronometric data suggest that the remnant landscape surfaces of the Songpan-Garze terrane sustained a protracted period of slow erosion. The shallow emplacement depth of the Songpan-Garze plutons at 2.5 to 3 kbars and preservation of Triassic shallow basin sediments in the western Songpan-Garze terrane, limit the total post-Triassic - Jurassic erosion to less than about 10 km [*Mattauer et al.*, 1992; *Roger*, 1994; *Burchfiel et al.*, 1995; *Kirby et al.*, 2002]. Granite plutons immediately west of the Longmen Shan have experienced slow cooling at less than ~3 °C/km from Jurassic time until the Late Miocene [*Kirby et al.*, 2002]. Apatite and zircon fission-track measurements on elevation transects within 1 kilometer of the surface are also consistent with slow exhumation rates (< 0.01 mm/yr) since Cretaceous time [*Xu and Kamp*, 2000]. However the western Songpan-Garze terrane probably existed as a gently east-dipping, low-relief highland prior to Cenozoic time because has served as a source of sediment supplied to the Sichuan Basin since Jurassic time [*Burchfiel, et al.*, 1995]. High elevations related to the modern Longmen Shan margin did not develop until late Cenozoic time and are most likely related to

the development of the eastern Tibetan Plateau [*Kriby et al.*, 2002].

2.6.2 Longmen Shan and Yalong Thrust Belts

The Longmen Shan and Yalong thrust belts define the southeastern boundary of the Songpan-Garze terrane and are primarily comprised of Paleozoic and Proterozoic passive margin sediments thrust eastward in late Triassic - early Jurassic time [*Bureau of Geology and Mineral Resources, Sichuan*, 1991; *Bureau of Geology and Mineral Resources, Yunnan*, 1990; *Mattauer et al.*, 1992; *Dirks et al.*, 1994; *Burchfiel et al.*, 1995; *Wang et al.*, 1998] [Figure 2.15]. Late Triassic - Cretaceous sedimentation southeast of the thrust belts probably reflects deposition in an adjacent foreland basin [*Burchfiel et al.*, 1995]. The thrust belt was reactivated in Cenozoic time as indicated by the involvement of Oligocene sedimentary rocks in the deformation [*Burchfiel et al.*, 1995]. Cenozoic shortening was limited to a few tens of kilometers, perhaps explaining the lack of Cenozoic foredeep basin sediments in the Sichuan Basin [*Dirks et al.*, 1994; *Burchfiel et al.*, 1995].

The average elevation of the Longmen Shan is 4500 m, although individual peaks reach as high as 6500 m within less than 100 km from the low-lying Sichuan Basin, which has an average elevation of about 500 m. No erosion surface remnants are preserved across this high-relief ($\sim$1000 – 4200 m), intensely dissected landscape where valley to ridge relief can exceed 3000 m [*Kirby et al.*, 2002] and alpine glacial erosion is active at elevations in excess of $\sim$6000 m. [Figure 2.10].

The Longmen Shan thrust belt coincides with the trend of the steep plateau margin adjacent to the Sichuan Basin. *Kirby et al.* [2002] have suggested that the age of the steep topographic escarpment observed across the Longmen Shan is between $\sim$12 - 5 Ma, however the correlation between the timing of escarpment development and Cenozoic structural activity in the thrust belt remains unclear. The Longmen Shan thrust belt is truncated to the southwest by the active left-lateral Xianshuihe Fault, and it appears to be displaced $\sim$60 km to the southeast, where it emerges as the east-vergent Yalong (or Jinhe-Qinhe) thrust belt [*Wang et al.*, 1998] [Figure 2.15]. The Yalong thrust belt trends sub-parallel to elevation contours that cross the low-gradient slope of the southeastern plateau margin. Cenozoic

Figure 2.19: Remnant surface at 3000 m elevation, Yanyuan Basin.

rocks are not involved in the Yalong thrust belt, therefore Cenozoic reactivation is speculative and based on correlation with the Longmen Shan thrusts. The Yalong thrust belt appears to end to the southwest in a complex region of active faulting [*Wang et al.*, 1998].

Remnants of an erosion surface or relict landscape are well-preserved across the northern Yalong thrust belt and between its northern and southern splays [Figure 2.3 and Figure 2.19]. These remnants are disrupted by the southern splay of the Yalong thrust belt along its northeastern and central segments, but are not disrupted along is southwestern segment. The surface remnants are locally offset by active faults but generally not by more than a few hundred meters and surfaces are well preserved within individual fault blocks.

Some parts of the Yalong thrust belt have experienced intense fluvial incision, especially along the Yalong River and its principle tributaries where relief between the plateau surface and the major river gorges can be greater than 3 kilometers [Figure 2.20]. Alluvial rivers with gentle-gradients dominate the active erosion of remnant surfaces and transition downstream to become steep, narrow bedrock river gorges that eventually drain into the Yalong and Yangtze rivers. Locally, although glacial erosion is recognized at high elevations across the northern splay of the Yalong thrust belt but geologic maps and imagery data suggest that glaciation has not contributed significantly to the erosion that has occurred in this area.

The relationship between the Cenozoic sediments and the polygenetic history of the

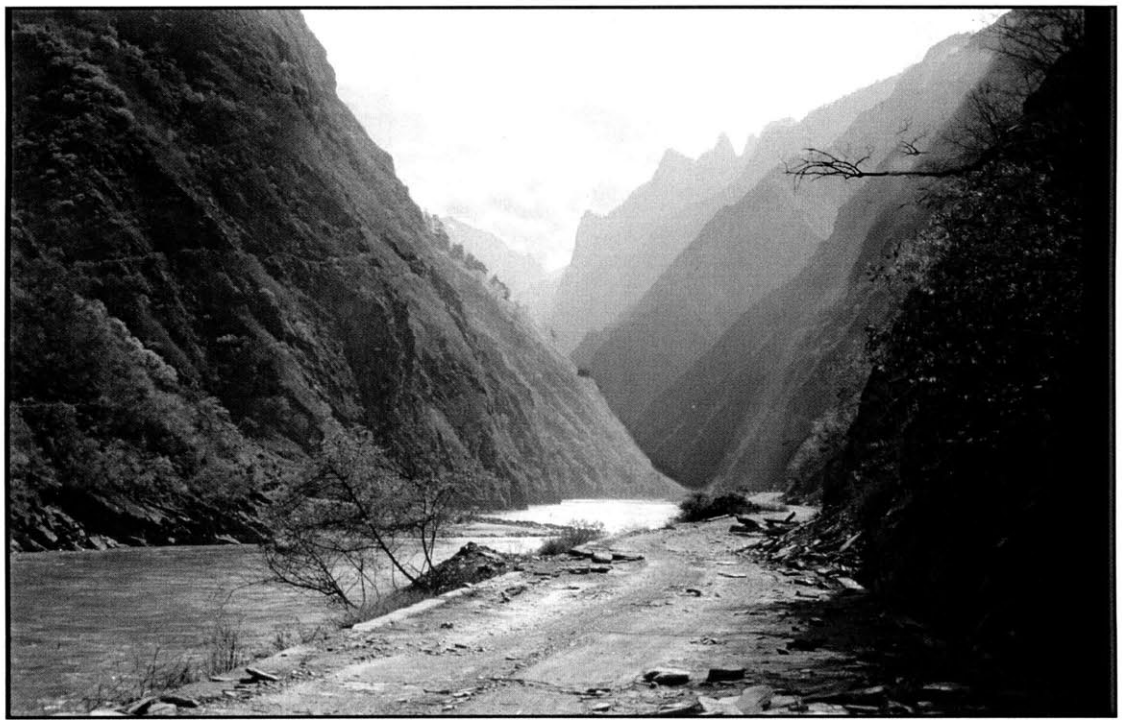

Figure 2.20: Yalong River gorge, elevation 1600 m.

erosion surface underscores an important point about the dynamic evolution of the low-relief landscapes of eastern Tibet. A discontinuous, northeast-trending belt of Cenozoic sediment is preserved along strike between the northern and southern splays of the Yalong thrust belt [*Bureau of Geology, Yunnan*, 1990; *Bureau of Geology, Sichuan*, 1991]. Excluding the Jianchuan Basin proper, the oldest sediments are mapped as Eocene - Oligocene(?) (pre-Pliocene sediments in this belt do not have strict age control and their age designations should be considered as estimates). These Eocene - Oligocene sediments generally consist of coarse clastic material (fluvial sandstones, conglomerates and debris flows) and are flat-lying to moderately folded or tilted. These sedimentary sequences, which are up to several hundred meters thick, are not contained in fault bounded basins but rather are distributed across and mantle an older low-relief landscape, constraining the age of surface remnants in this area to be of Eocene - Oligocene(?) or older [*Bureau of Geology, Sichuan*, 1991; *Bureau of Geology, Yunnan*, 1990] [Figure 2.21]. This sedimentary sequence occasionally contains multiple erosional angular unconformities and has subsequently been

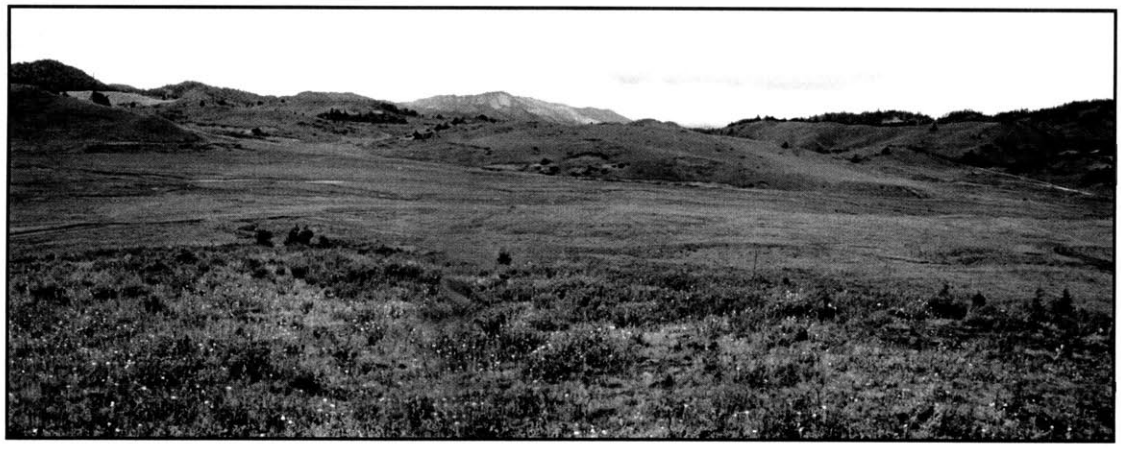

Figure 2.21: Remnant surface at 4000 m elevation, between Mekong and Yangtze rivers.

erosionally beveled to low-relief at an elevation conformable with the surrounding area prior to onlapping undeformed coal-bearing Pliocene sediments [*Bureau of Geology and Mineral Resources, Sichuan*, 1991; *Bureau of Geology and Mineral Resources, Yunnan*, 1990].

A prime example of the typical relationship between erosion, early- mid(?) Cenozoic sedimentation and deformation, subsequent erosion, and further tectonic disruption by more recent active faulting occurs in the Yanyuan Basin, a Pliocene-Quaternary basin that is bounded to the south and west by active normal faults. Eocene - Oligocene(?) conglomerates, fluvial sandstones, volcaniclastics rocks and tuffs are deposited on an undulating karstic surface formed above the underlying Triassic sequences at the north end of the basin. These sediments are mapped as correlative with sandstones and conglomerates that crop out southwest of the basin. These basal units to the Tertiary section appear to have been tilted and capped by flat-lying conglomerates of a similar lithology. The structurally highest sedimentary units have been eroded to low-relief [Figure 2.19]. In the southern Yanyuan basin, well dated coal-bearing, flat-lying Pliocene sediments are deposited on an erosional surface of low-relief, limiting the latest age of erosional planation to pre-Pliocene time. Active normal faults that bound the west and southern edge of the basin offset the surface remnant within the Yanyuan Basin by 300 m relative to a remnant surface capped by correlative, relatively undeformed Eocene - Oligocene(?) sediments to the southwest.

The complexity and detail observed in the sedimentary, erosional and tectonic record in Yanyuan illustrate the intricacies of a dynamic landscape, which we generalize in the identification of a "remnant surface".

2.6.3 Sichuan Basin

The physiographic expression of the Sichuan Basin represents a small residual, relatively undeformed part of the Yangtze platform that has largely escaped tectonic activity of different ages that have affected the surrounding regions [Figure 2.2 and 2.15]. Sediments exposed in the Sichuan Basin are primarily Late Triassic to Cretaceous foredeep sediments deposited in response to Mesozoic tectonism in the Longmen Shan [*Burchfiel et al.*, 1995]. Isolated outcrops of Paleocene rocks, conformable with the underlying Cretaceous sequences, are present in the southwest corner of the basin and the adjacent foothills and are involved in northeast trending folds that are erosionally beveled and capped by thin, locally-deposited Neogene sediments [*Burchfiel et al.*, 1995] [Figure 2.3]. Some evidence exists for growing anticlines beneath blind-thrusts in the western portion of the basin, but the rates of shortening are slow [*Burchfiel et al.*, 1995]. Pre-Neogene rocks within the Sichuan Basin are stratigraphically continuous with deposits to the east and south outside the basin, that have been uplifted as a part of the southeastern plateau margin. Only a thin veneer of $<$200 m of alluvial Quaternary sediment is preserved along the northwest margin representing minor Cenozoic sedimentary deposition on an otherwise erosionally-floored "bedrock" basin [*Bureau of Geology and Mineral Resources, Sichuan*, 1991], indicating the absence of flexural loading in response to Cenozoic crustal thickening beneath the adjacent Longmen Shan [*Burchfiel et al.*, 1995; *Royden et al.*, 1997].

Recent seismic tomography indicate that the Sichuan Basin is underlain by a fast seismic anomaly, extending at least to 250 km depth, suggesting that the lack of deformation of the Sichuan Basin may be attributed or related to the presence of a thick, cold mantle root [*Lebedev and Nolet*, 2003]. Also, the area beneath the high eastern plateau and the southeastern plateau margins are underlain by an anomalously slow seismic anomaly. The Sichuan Basin also has relatively low heat flow (40 - 70 mW/m^2) compared to the adjacent

elevated region of the southeastern plateau margin (60 - 100 mW/m^2) [*Hu et al.*, 2000].

The steep plateau margin of the Longmen Shan is the western topographic boundary of the low elevation Sichuan Basin ($\sim$ 500m). The low-gradient southeastern and northeastern plateau margins "wrap-around" the Sichuan Basin, forming its northern, southern, and eastern topographic boundaries [Figure 2.2]. The topographic boundaries to the east and north are defined by areas that were affected by Mesozoic age deformation in the Eastern Sichuan Fold Belt and Micang Shan respectively, however, the much steeper boundaries to the west and south (the Longmen Shan and the Daliang Shan respectively) suggest Cenozoic reactivation or superposition over earlier Mesozoic deformation. The topography of the southern margin of the basin (part of the southeastern plateau margin) obliquely cuts the southwest trending Mesozoic foredeep sequences and is bounded by steeply dipping reverse faults of Cenozoic age [*Bureau of Geology and Mineral Resources, Sichuan*, 1990].

The planar local relief (mostly less than 200 m) of the Sichuan Basin cannot be attributed to significant Cenozoic sediment deposition [Figure 2.10]. Steep and deeply incised bedrock rivers that drain the steep topography to the west and south become braided, alluvial rivers when they reach the Sichuan Basin, however the sediment of these rivers bypasses the basin and is carried to the southeast to the Yangtze River and probably has done so throughout the Cenozoic. Detrital apatite fission-track ages from Mesozoic sedimentary rocks are near their depositional age, indicating that limited erosion has occurred since deposition ($<$ 4 km) [*Arne et al.*, 1997] and further suggesting that the extremely low-relief character of the Sichuan Basin may be inherited from the depositional surface of the Mesozoic foredeep basin. The lack of both significant Cenozoic deposition and erosion suggest that the low-elevation and low-relief morphology of the Sichuan Basin may be long-lived since at least early Mesozoic time. Eocene to Cretaceous apatite and zircon fission-track ages from high elevations within the Songpan-Garze terrane west of the Longmen Shan [*Xu and Kamp*, 2000] suggest that the low-relief landscape of the Sichuan Basin may have been broadly continuous with erosion surface remnants preserved across the Songpan-Garze, and we suggest that it may also have been continuous with erosion surface remnants preserved to the south across the Daliang Shan (South China Fold Belts, see below) which are topographically offset by the uplift of the southeastern plateau margin

relative to the Sichuan Basin.

2.6.4 South China Fold Belts

We define the South China Fold Belts as the area south of the Sichuan Basin and Yalong Thrust Belt and northeast of the Three Rivers Belt, which includes the southern portion of the Yangtze Platform (senso-stricto) which has experienced contractional deformation during Mesozoic and Cenozoic time [Figure 2.15]. Rocks of this region primarily consist of Proterozoic and Paleozoic sediments and volcanics in the east which underlie the thick Mesozoic through locally Paleocene - Eocene sedimentary basins exposed to the west (the Chuxiong Basin and the Daliang Basin) [*Bureau of Geology and Mineral Resources, Sichuan*, 1990; *Bureau of Geology and Mineral Resources, Yunnan*, 1991]. These sediments are interrupted by rocks of the north-south trending "Kundian High" that consists of Proterozoic basement (chiefly granite) and existed as a paleo-topographic highland during Paleozoic and Mesozoic time [*Burchfiel et al.*, 1995].

Northeast trending folds affect much of the South China Fold Belt and undeformed Cretaceous plutons in the south and overlying unfolded upper Cretaceous sediments in the north, limit this deformation to late Jurassic - Cretaceous time [*Wang et al.*, 1998]. In southern Yunnan, flat-lying Eocene sediments overlie folded Triassic, Paleozoic and Precambrian rocks over a karst surface of low relief, however, the timing of this folding is not well-constrained but may be contemporaneous with late Jurassic - Cretaceous folding further north [*Wang et al.*, 1998].

Post-Eocene folding affects much of the western region of the South China Fold Belt and is probably contemporaneous with northeast trending folds in the southwestern Sichuan Basin that parallels the Longmen Shan. North-northeast trending folds involving Paleozoic to Eocene rocks, rarely Oligocene, occur across the Chuxiong Basin and Daliang Basin [*Wang et al.*, 1998] and are overprinted or contemporaneous with north - northwest trending folds that are responsible for 20-25 km of post - Eocene (Oligocene?) shortening across the Chuxiong Basin [*Leloup et al.*, 1995; *Wang et al.*, 1998]. The northeast trending folds may be contemporaneous with Cenozoic reactivation of the Yalong Thrust Belt. Late

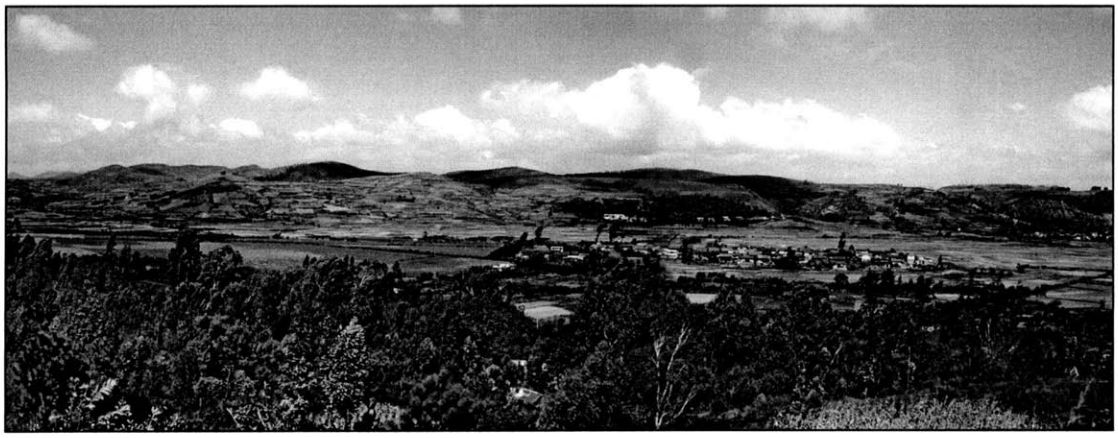

Figure 2.22: Remnant surface at 2000 m elevation, the South China Fold and Thrust Belt.

Oligocene - Miocene rocks are mostly absent and folds have been erosionally beveled and unconformably overlain by unfolded coal-bearing Pliocene and rarely uppermost Miocene - Pliocene sediments [*Wang et al.*, 1998].

Commonly referred to as the Yunnan Plateau, the region of the South China Fold Belt ranges in elevation from ~3km in the northwest to less than < 1 km in the southeast where the topography of surface remnants merge with low-relief, low elevation areas near the South China coastal margin [e.g. *Leloup et al.*, 1995; *Wang et al.*, 1998] [Figure 2.3, 2.22 and 2.10]. Remnant erosion surfaces are well preserved across most of the South China Fold Belts, and are disrupted only in areas of local active faulting [*Schoenbohm et al.*, 2001] and by limited fluvial incision. The South China Fold Belt experiences a more humid modern climate than areas to the north so that modern karst topography and the development of thick soils are common. The initial ages of remnant surfaces in the South China Fold Belts are diachronous across this region with generally older surfaces in the east and south and younger surfaces in the west. On the basis of onlapping unfolded Cretaceous sediments and unfolded Eocene sediments, the age of the surfaces can be limited to pre-Cretaceous and pre-Eocene respectively [*Wang et al.*, 1998]. Further, to the west where post-Eocene - Oligocene(?) sediments have been folded, the age of deformation and subsequent erosion is not well constrained and can only be suggested to be pre-Pliocene, however it could be as old as late-Oligocene [*Wang et al.*, 1998].

Surfaces of the South China Fold Belt are cut by deep river gorges only along the Yangtze, Pearl and Red Rivers, and much of the deep incision is limited to the main rivers and a limited number of principle tributaries. The lesser degree of fluvial incision in this area compared to the Yalong Thrust Belt and the Songpan-Garze terrane is probably due to the lower elevations and distal position on the plateau margin. Furthermore, the subdued relief of the western region of the South China Fold Belt may have been largely inherited from the depositional landscapes associated with basin filling of the Chuxong and Daliang Basins and has subsequently been modified by moderate deformation and limited erosion.

As in the Yalong Thrust Belt and the Songpan Garze terrane this morphology was distinct on slope maps, showing a sharp transition from the low slope areas of the remnant surfaces and the high slope areas that had been intensely fluvially dissected and created steep, narrow canyons. However, some tributaries to major river systems in the South China Fold Belt, as well as segments of the Yangtze River itself, narrow river canyon walls have not been maintained and rapidly incising rivers have developed broad river valleys, whose main lower channel becomes alluviated and the steep bedrock reaches are spatially limited to a short reaches where the river first flows across the edge of a remnant surface. This fluvial incision pattern is common in the areas of the Chuxong Basin and the Daliang Basin and is most likely related to the much higher erodability of the Mesozoic - Tertiary sediments in the western basins of the South China Fold Belt than the sediments to the east and the geologic terranes to the north. Much of the slope map of the South China Fold Belt shows low relief highlands that are characterized by moderately low slope values (1.2 - 10 degrees), and the wide alluviated river bottoms have very low slope values (less than 1.2 degrees), thus, the contrast in slope values used to identify surface remnants is reversed from areas to the north and remnant surfaces are difficult to discern from a slope map alone.

Pliocene - Quaternary graben vertically offset surface remnants, however the numerous strike - slip faults in this area do not, except along the Xianshuihe Fault in the northern Anning River valley. The vertical offset across this fault is $\sim$1 - 1.5 km near the headwaters of the Anning River and decreases to the south where there is no longer any offset of remnant surfaces across the fault. This surface offset occurs within an area of active uplift near the Gonga Shan massif.

2.6.5 Three Rivers Fold and Thrust Belt

The Three Rivers fold and thrust belt is a complex region of small, terranes accreted in late Paleozoic through Mesozoic time [Figure 2.15]. It is separated from the Songpan-Garze terrane in the north by the Permo-Triassic Yidun arc, and from the South China Fold Belt/Yangtze platform in the south by the metamorphic rocks of the Aliao Shan, Dian Chang Shan, and Xuelong Shan. Many of the Paleozoic and Mesozoic suture zones and tectonic boundaries in this region were reactivated during Cenozoic time as a result of the Indo-Asian collision. Cenozoic deformation in this region appears to have been accommodated by shortening and clockwise rotation of small crustal fragments in a complicated manner as the eastern Himalayan syntaxis has progressed northward in time [*Wang and Burchfiel*, 1997]. The left-lateral transpressional Aliao-Shan Shear Zone is the principle boundary separating the intensely rotated and deformed region of the Three Rivers fold and thrust belt to the southwest from the much less deformed areas of the South China Fold Belt to the northeast. Cooling ages from the shear zone suggest deformation occurred between 34 - 17 Ma [*Leloup, et al.*, 1995; *Leloup et al.*, 2001] and may be contemporaneous with thin-skinned folding and thrusting of Mesozoic- early Tertiary sediments of the Lanping-Simao Basin [*Wang and Burchfiel*, 1997].

The Three Rivers fold and thrust belt is the only north-south trending geologic terrane in eastern Tibet that occurs both on the topographically high flat plateau as well as throughout the entire southeastern plateau margin slope, and thus is oriented perpendicular to the southeastern plateau margin [Figure 2.15]. Despite its perpendicular orientation to the plateau margin, topography of the southeastern plateau is regular across the Three Rivers Fold and Thrust Belt and the adjacent tectonic boundaries [Figure 2.2].

Much of the region that was deformed in the Three Rivers fold belt has been eroded to low local relief, including the Oligocene- early Miocene Aliao Shan Shear Zone [*Schoenbohm et al.*, 2002]. Undeformed Pliocene sediments unconformably onlap remnant erosion surfaces that cut Post Early Tertiary deformation in the Lanping-Simao Belt [*Bureau of Geology and Mineral Resources, Yunnan*, 1990]. However, local relief observed on the remnant surfaces is greater than in the adjacent Chuxong Basin in the South China Fold

Belts. This probably reflects either more intense deformation or less erosion than in areas to the east, possibly due to a younger age of deformation. Preservation of remnant surfaces on top of fault blocks that have been rotated and/or vertically offset is common to the west and south of the Lanping-Simao Basin. Here, remnant surfaces are disrupted to a high degree and reflect the intensity of Cenozoic deformation relative to other areas.

No remnant surfaces are observed in the vicinity of the Three Rivers area between the Mekong, Salween and Irrawaddy rivers. This region of intensely dissected, high relief ($\sim$1000 - 4200m) topography covers an area roughly 100 km by 300 km and is a locus of intense strike-slip and compressional deformation related to the northward movement of India into Eurasia [*Akciz et al.*, 2001]. [Figure 2.10]. North of the Three Rivers Area, remnant landscape surfaces are well preserved in-between the Salween, Mekong and Yangtze rivers.

2.6.6 Late-Miocene to Recent tectonic activity

The recent geologic record (since 8 - 4 Ma) to the present day deformation field defined by GPS measurements show that deformation in eastern Tibet (south of the Xianshuihe Fault) is dominated by strike-slip faulting [Figure 2.1]. Graben-style normal faults are common and associated with the transfer of motion between individual strike-slip fault segments [*King et al.*, 1997; *Wang et al.*, 1998; *Chen et al.*, 2000]. This deformation pattern accommodates rotation of crustal fragments around the eastern Himalayan syntaxis without significant translation of upper crustal material toward the eastern foreland [*King et al.*, 1997; *Wang et al.*, 1998; *Chen et al.*, 2000]. Total Neogene - Quaternary offset along these faults is variable and reaches up to $\sim$60 km of left-lateral displacement on the Xianshuihe Fault in western Sichuan [*Wang et al.*, 1998]. GPS stations west of the Xianshuihe-Xiaojiang fault system define a crustal fragment rotating clockwise about the eastern Himalayan syntaxis at a velocity of $\sim$10 mm/yr with respect to South China [*Chen et al.*, 2000]. Taken together, these data along with the absence of late Miocene - Pliocene shortening structures suggest that surface shortening perpendicular to the topographic gradient has been minor since at least Miocene - Pliocene time.

GPS stations in the Longmen Shan show no shortening across the steep Longmen Shan plateau margin within the resolution of the data, less than 3 mm/yr [*Chen et al.*, 2000]. It is surprising to observe little horizontal deformation across such an impressive topographic escarpment but the geologic record also indicates that the magnitude of Cenozoic surface shortening in the Longmen Shan has been small [*Dirks et al.*, 1994; *Burchfiel et al.*, 1995; *Royden et al.*, 1997; *Chen et al.*, 2000; *Kirby et al.*, 2002].

2.7 Reconstruction of a relict, low-relief landscape across eastern Tibet from surface remnants.

The surface remnants described in the preceding section collectively comprise a low-relief carapace to the eastern Tibetan Plateau and southeastern plateau margin [Figure 2.23 and 2.24]. When areas affected by recent river incision are excluded, this low-relief landscape is continuous across all tectonic sub-provinces although its local morphology varies as a function of several factors, including bedrock lithology, the degree of Cenozoic deformation and relative latitude and altitude. Remnant surfaces have remarkable spatial continuity across the southeastern plateau margin from low-elevations ($<$ 1 km), where they merge with the coastal plain of the South Asia marginal seas to plateau elevations of $\sim$5 km over a lateral distance of $\sim$1500- 2000 km [Figure 2.23].

The amount of fluvial relief observed in alluvial river systems which cross remnant surfaces is consistent with river concavity and steepness values measured from their longitudinal profiles. This agreement suggests that the remnant surface landscape was formed under low-uplift conditions, arguing that the surface remnants represent portions of an originally continuous relict landscape. Across the plateau, we observe that the offset between remnant surfaces is within the amount of local relief observed across the surfaces [Figure 2.14]. This argues that the elevation of adjacent surfaces can be correlated with one another to reconstruct the paleo-landscape. As discussed in the previous section, the fluvial network in eastern Tibet is continuous from the remnant surfaces to the major river gorges. Although there is evidence for large-scale drainage reorganization by river capture

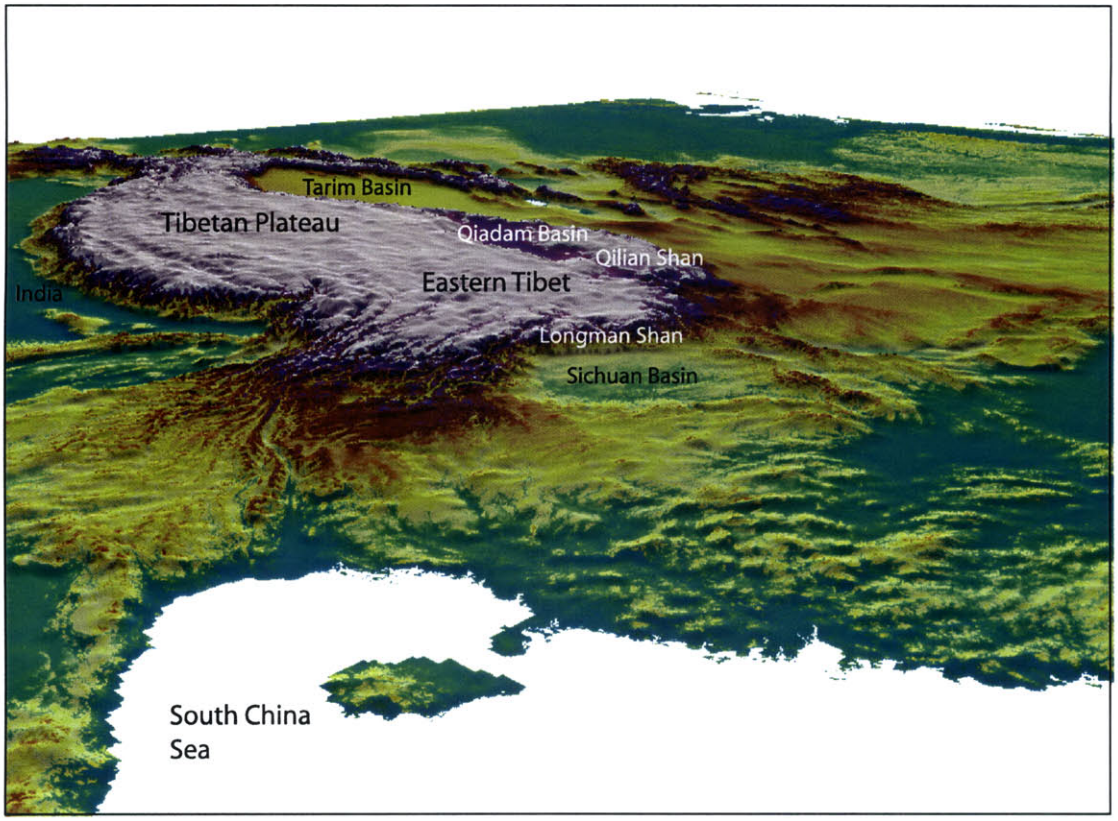

Figure 2.23: 3-D perspective of digital topography of Tibet, view west.

and reversal [*Clark et al.*, in press], this reorganization has not affected the continuity of the fluvial system across surface remnants. This continuity suggests that adjacent remnant surfaces were likely responding to the same baselevel conditions set by the major rivers and probably were eroded to similar elevations as one another prior to uplift of the plateau.

We suggest that these remnant surfaces across eastern Tibet collectively comprise preserved portions of the relict, low-relief landscape prior to plateau uplift. Although the relict landscape has been locally disrupted by active faulting, tectonic deformation has not played a significant role in the disruption or destruction of the eastern Tibet relict landscape except at the Longmen Shan escarpment. We use this surface as an originally sub-horizontal topographic datum that had an original regional southeast gradient of 10^{-3} - 10^{-4} set by the pre-uplift slope of the major rivers. From this datum we can measure the total surface uplift of eastern Tibet in Late Cenozoic time.

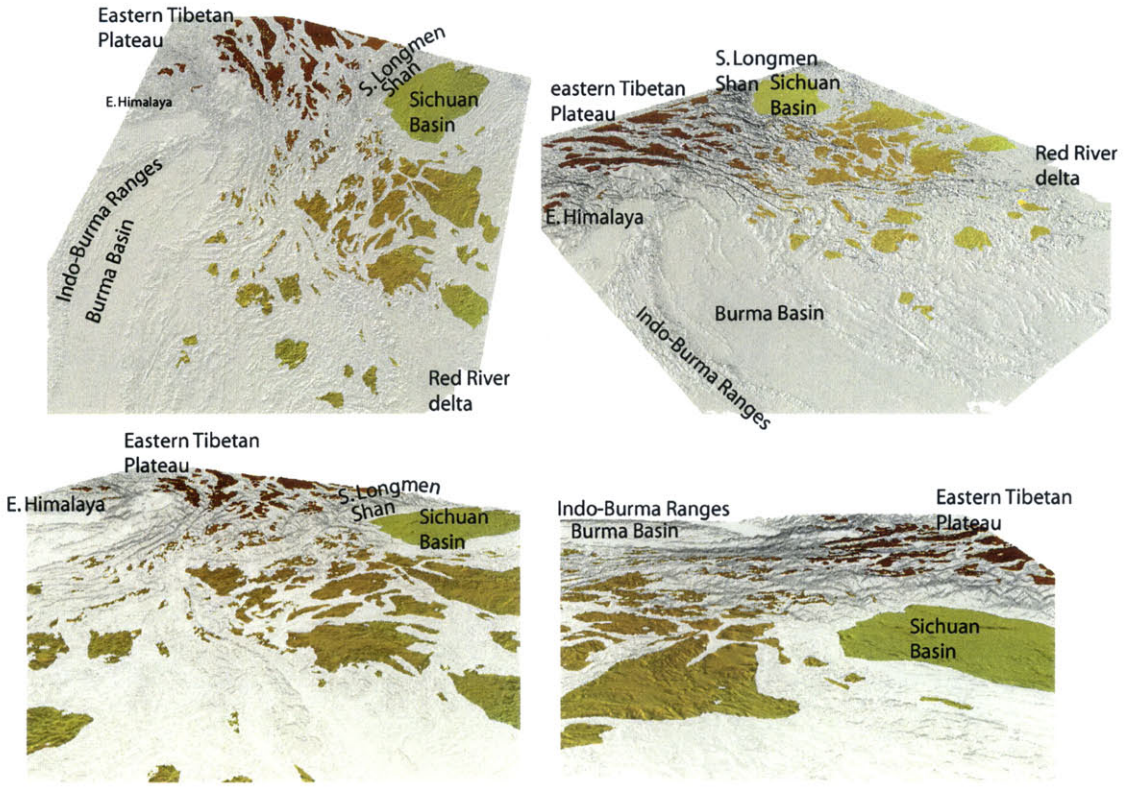

Figure 2.24: 3-D perspective view of surface remnants draped over a shaded relief map.

2.8 Age of east Tibetan relict landscape and major river gorges: Discussion of geomorphic evolution

Study of landscape evolution in eastern Tibet inherently leads to two questions: 1) what is the "age" of the landscape (relict and modern) and 2) how does this age reflect the tectonic history of the region? Although we have stressed that the relict landscape mantling the eastern Tibetan Plateau and its margins is a dynamic landform, there are several useful temporal determinations we can derive for this landscape. First is the timing of "formation"; when did the landscape first become low-relief? In some cases, the landscape may have developed at low-relief by deposition while in other cases the landscape may have experienced tectonic deformation resulting in moderate to high topographic relief, which was

subsequently beveled to low-relief by erosion. Second is the "duration" of the low-relief landscape. We define the duration as the time period during which the landscape remains at low-relief and experiences slow-erosion rates, although this stage does not preclude limited, local deposition. Finally, we can define the timing of "destruction" of the low-relief landscape by major tectonic disruption or regional-scale erosion. The timing of destruction of the relict, low-relief landscape in eastern Tibet reflects the formation of the modern, active landscape condition of erosion by rapid bedrock river incision. Thus destruction of the relict landscape in eastern Tibet indicates, at least in part, the initiation of uplift of the eastern Tibetan Plateau. It is plausible that the rapid incision of the major rivers could lag behind the onset of uplift, depending on the climate conditions. However, we suggest that the changes in topographic gradient related to uplift were probably sufficient enough such that river incision occurred within a few million years of initiation of uplift.

Correlation of individual landscape surfaces indicates that a low-relief landscape of regional extent existed across eastern Tibet prior to Late Cenozoic uplift. The diachronaeity of erosion and sedimentation processes that formed this relict landscape is evident in the sedimentary and geomorphic record across the plateau. Some elevated plateau areas have not experienced deformation or erosion since Eocene or Cretaceous time as indicated by low-relief unconformities covered by flat-lying sediments. Other areas have experienced Eocene - Oligocene(?) sedimentary deposition followed by deformation and subsequent erosion to an elevation conformable with the surrounding landscape. Locally, unconformities developed above the deformed rocks are onlapped by flat-lying Pliocene and, rarely, upper Miocene sediments. Thus the relict landscape is a dynamic feature with a complex history of development and maintenance of low-relief landscapes, punctuated by periods of deformation. Sedimentary and structural relationships suggest that this complex low-relief landscape history and modification of the landscape by deformation and subsequent erosion largely occurred prior to significant surface uplift of this now relict landscape in Late Cenozoic time.

Much of the regional low-relief character of the relict landscape of eastern Tibet was probably inherited from the initial depositional environments of the sedimentary rocks exposed throughout this region. Many Mesozoic to early Tertiary sedimentary basins occur

across eastern Tibet; these were deformed into broad fold belts without evidence for rapid erosion commonly associated with high, mountainous topography. Sedimentary basin formation, followed by moderate deformation that did not create steep topographic or laterally extensive high topography, suggests that this relict landscape did not require extensive early Cenozoic erosion to produce a regionally low-relief, low elevation landscape prior to Late Cenozoic uplift.

Across the southeastern plateau margin major disruption of the relict landscape in eastern Tibet by tectonic structures is minimal although portions of this relict landscape are locally offset by Late Miocene and younger faults. Differences in local preservation of the relict landscape in adjacent tectonic terranes reflects underlying lithologic variation as well as differences in the magnitude of Cenozoic deformation. Remnants of the relict landscape are preserved from elevations of $\sim$5 km on the plateau to less than 1 km elevation where it merges southeastward with the modern coastal plain. The continuity of the relict landscape with modern sea-level indicates that prior to uplift it existed at low elevation.

The modern altitude and continuity of the reconstructed relict landscape defines a spatial pattern of uplift that parallels the modern plateau slope. We use the measured channel steepness measurements for channel segments on remnant surfaces to estimate the gradient of the major river systems prior to uplift and estimate the paleo- regional gradient of this relict landscape to have been between 10^{-3} to 10^{-4} which is also consistent with regional, low-relief modern landscapes. This indicates that at least $\sim$4 km of surface uplift of the high eastern plateau has occurred in Late Cenozoic time. Surface uplift usually cannot be measured directly and must be inferred indirectly from rock uplift or exhumation patterns [e.g. *Molnar and England*, 1990], so that preservation of the relict landscape offers a rare opportunity to measure regional-scale surface uplift. This highlights the potential for using relict landscapes as sub-horizontal, low-elevation datum surfaces.

Uplifted remnants of the relict landscape are undergoing rapid destruction by bedrock erosion of major rivers that drain the eastern Tibetan Plateau. Data from apatite (U-Th)/He and fission-track thermochronology show that bedrock river incision along the topographically highest portion of the southeastern plateau margin began by 7-13 Ma [*Clark et al.*, in prep]. Erosion by bedrock river incision must follow the initiation of high topography be-

cause it would be impossible to form deep bedrock rivers within a low-elevation landscape. These data, by themselves, cannot determine if the commencement of bedrock incision was coeval with surface uplift. Because bedrock river incision requires that a critical shear stress acting on the base of the river must be exceeded, which is a function of river discharge and slope [e.g. *Howard and Kerby*, 1983; *Howard et al.*, 1994; *Whipple and Tucker*, 1999], a river crossing a region of long-wavelength uplift under arid climate conditions could remain at or near sub-critical shear stress levels. Under these extreme conditions a river could remain transport-limited without significant incision into the uplifting landscape. Thus if the climate was particularly arid when uplift began in eastern Tibet, bedrock incision may have lagged behind surface uplift until precipitation increased sufficiently (or the slope increased sufficiently) to allow rivers to exceed critical shear stress. However, we suggest that such a time lag could not have been greater than 1-2 M.y.. The contribution of climate change to the incision of major rivers is distinct from the climate/uplift conditions that controlled formation of the relict landscape. The regional gradient of the relict landscape suggests that this landscape formed during low uplift conditions irrespective of climate condition.

The most significant disruption of the relict landscape occurs across the Longmen Shan where extensive surface remnants are preserved across the Songpan-Garze (at $\sim$4.5 km elevation) and across the Sichuan Basin ($\sim$500 m elevation) and are vertically offset by 4 km across the narrow Longmen Shan escarpment. Slow exhumation rates determined from thermochronologic dating indicate that subdued topography existed across the Longmen Shan escarpment from Jurassic time to at least 12 Ma, because low denudation rates in the presence of extreme topographic gradients would require extremely non-erosive climate conditions that are unreasonable for central Asia in Miocene time [*Kirby et al.*, 2002]. These data indicate that rapid exhumation began between $\sim$12 and $\sim$5 Ma in the Longmen Shan and reflects the initiation of major surface uplift, irrespective of climatic conditions [*Kirby et al.*, 2002].

2.9 Implications for plateau development, crustal rheology and crustal dynamics

There are two distinct patterns in plateau margin development in eastern Tibet: the steep topographic front developed at the Longmen Shan margin and the gently-sloping topographic margin of southeastern and northeastern Tibet. Mesozoic and early Tertiary rocks and structures are continuous across the Longmen Shan and southeastern plateau margins but the Cenozoic history of these regions are distinctly different. Mesozoic foredeep deposits are preserved in the Sichuan Basin at low elevations (~500 m). Post-Oligocene thrust faulting occurs in the Longmen Shan, however it appears to be limited to a few tens of kilometers shortening and associated minor folding in the adjacent foreland. Cenozoic thrust faulting did not flexurally load the Sichuan Basin as indicated by the lack of significant Cenozoic sedimentary deposition in the basin [*Burchfiel et al.*, 1995; *Dirks et al.*, 1994]. Despite the absence of significant shortening structures, a steep topographic escarpment developed in the Longmen Shan by late Miocene - early Pliocene time [*Kirby et al.*, 2002].

To the southwest, counterparts to the rocks in the Longmen Shan thrust belt and its Mesozoic foredeep deposits in the Sichuan basin are preserved at 2 - 4 kilometers elevation along the southeastern plateau margin [*Burchfiel et al.*, 1995]. Here (in the Yalong Thrust Belt), Cenozoic reactivation of thrust faults is unconstrained and post Eocene - Oligocene(?) folding in the adjacent foreland is significantly greater than in the Sichuan Basin and has a magnitude similar to that of the Longmen Shan in Cenozoic time (*Leloup et al.*, [1995] estimate 25 - 30 km shortening across the Chuxong Basin).

The intersection of the two plateau margins is a complicated area of cross-folding of similar (if not contemporaneous) age [*Burchfiel et al.*, 1995]. High angle faults bound the topographic edge of the southeastern plateau margin against the Sichuan Basin, but these faults appear to have vertical displacements approximately equal to the 2 km height of the topographic step across this plateau edge and accommodate the vertical offset of the surface. There are no discrete (major) structures or tectonic boundaries that define the topographic boundary between the Sichuan Basin and the southeastern plateau margin. The

differing topographic expression of the Longmen Shan and the southeastern plateau margins is not related to preexisting (Mesozoic - early Tertiary) structure and crustal boundaries because both areas are underlain by the same tectonic terrane, the Yangtze Craton (composed of a Proterozoic basement overlain by Proterozoic to Paleozoic passive margin sequences and Mesozoic - early Tertiary terrestrial rocks). However, the Sichuan Basin corresponds to a part of the Yangtze Craton that has escaped earlier Mesozoic deformation that affected rocks surrounding the basin, suggesting a deep crustal and/or mantle control on strength as is consistent with the results of recent seismic tomography [*Lebedev and Nolet*, 2003].

The absence of major upper crustal shortening indicates that the lower crust has been preferentially thickened during plateau development in eastern Tibet. Differences in the plateau margin topography (steep plateau margins versus broad, low-gradient margins) reflect the differential spatial patterns of crustal thickening. In particular, the long wavelength uplift of the southeastern plateau margin suggests that distributed lower crustal thickening (over wavelengths of > 1000 km) has occurred since Late Cenozoic time. Because crustal thickening has occurred over long wavelengths in less than $\sim$10 Ma [*Clark et al.*, in prep], deformation appears to have been accomplished by thickening of very weak crustal rocks at depth without significant surface shortening [*Clark and Royden*, 2000]. The continuity of the relict landscape in eastern Tibet perpendicular to the plateau margin and the longevity of through going river drainage patterns that cross the plateau margin [*Clark et al.*, in press] suggest that no significant steep topographic front ever existed across the southeastern plateau.

The wavelength and magnitude of material flux through the lower crust of southeastern Tibet is probably very unusual and it is likely that many factors have contributed to this phenomenon. The rheologic strength of the deep crust is largely a function of lithology, temperature and the presence of aqueous fluids [*Brace and Kohlstedt*, 1980; *Kirby*, 1983]. Thermochronology data from apatite (U-Th)/He and apatite fission-track suggest that eastern Tibet has a high geothermal gradient of ~ 40 - 60 $^{\circ}$C/km. Potassic volcanism since the Oligocene in eastern Tibet and slow seismic velocities in the mantle lithosphere beneath southeastern Tibet also suggest the presence of a hot mantle lithosphere beneath eastern

Tibet that may be partially responsible for the elevated crustal geotherms. The crustal composition in southeastern Tibet is dominated by thick sedimentary sequences from Paleozoic to Cenozoic in age. These thick sedimentary sequences likely have high heat production due to the concentration of radioactive heat producing elements. The introduction of fluids, by the dehydration of muscovite in metasedimentary rocks, may introduce partial melt at elevated temperatures in the mid-crust, resulting in melt-induced weakening of the deep crust [e.g. *Rushmer*, 2001]. All of these factors may have contributed to the development of a weak crustal layer beneath southeastern Tibet.

Surface geology and GPS data suggest that southeastern Tibet is undergoing rotation around the eastern Himalayan syntaxis with little net translation toward the foreland since about 4-8 Ma (Wang, et al., 1998; Chen et al., 2000) while the pattern of surface uplift suggests the mobilization of deep crustal material to the southeast, independent of the pattern of strain recorded in the upper crust, since 7-13 Ma. The lack of correlation between the orientation, style and magnitude of structure in the upper crust and the pattern of crustal thickening determined from the topography suggests that the upper and lower crust in southeastern Tibet are decoupled. Therefore we propose that the strike-slip faults which dominate the surface strain record must sole into mid-crustal detachments since at least middle-late Miocene time and precludes any major tectonic extrusion of lithospheric fragments during this time. We suggest that a model of viscous deformation concentrated in the deep crust may explain the distributed pattern of surface uplift and crustal thickening in southeastern Tibet, which has occurred independently of the structural history of the upper crust in Late Cenozoic time.

2.10 References

Akciz, S., Burchfiel, B. C., Chen L., Yin J., 2001, Geometry, kinematics and regional significance of the Chong Shan shear zone, Yunnan, China, Abstracts with Programs - Geological Society of America, 33 (6), p. 395.

Arne, D., Worley, B., Wilson, C., Chen, S., Foster, D., Luo, Z., Liu, S., Dirks, P., 1997, Differential exhumation in response to episodic thrusting along the eastern margin of

the Tibetan Plateau, Tectonophysics, v. 280, p. 239 - 256.

Argand, E., 1924, La tectonique de l'Asia, Cong. Geol. Intern., Liege, 1922, p. 169 - 371.

Brace, W.F., and Kohlstedt, D.L., 1980, Limits on lithospheric stress imposed by laboratory experiments: Journal of Geophysical Research, v. 85, p. 6248-6252.

Burchfiel, B. C., Chen, Z., Liu, Y., Royden, L. H., 1995, Tectonics of the Longmen Shan and adjacent regions, Central China, International Geology Review, v. 37, pp. 661 - 735.

Bureau of Geology and Mineral Resources of Sichuan Province, 1991, in Regional Geology of Sichuan Province, Beijing, Geological Publishing House, 730 p.

Bureau of Geological and Mineral Resources of Yunnan Province, 1990, in Regional Geology of Yunnan Province, Beijing, Geological Publishing House, 728 p.

Chen, Z., Burchfiel, B. C., Liu, Y., King, R. W., Royden, L. H., Tang, W., Wang, E., Zhao, J., and Zhang, X., 2000, GPS measurements from eastern Tibet and their implications for India/Eurasia intercontinental deformation, J. Geophysics Research, v. 105, p. 16,215 - 16, 227.

Chung, S., Lo, C., Lee, T., Zhang, Y., Xie, Y., Li, X., Wang, K., Wang, P., 1998, Diachronous uplift of the Tibetan plateau starting 40 Myr ago, Nature, v. 394, p. 769 - 773.

Clark, M. K. and Royden, L. H., 2000, Topographic ooze: Building the eastern margin of Tibet by lower crustal flow, Geology, v. 28, n. 8, pp. 703 - 706.

Clark, M. K., Schoenbohm, L., Royden, L. H., Whipple, K. X., Burchfiel, B. C., X. Zhang, W. Tang, E. Wang, L. Chen, in press, Surface uplift, tectonics, and erosion of eastern Tibet as inferred from large-scale drainage patterns, Tectonics.

Clark, M. K., House, M. A., Royden, L. H., Burchfiel, B. C., Whipple, K. X., Zhang, X., Tang, W., in prep. for submission to J. Geophys. Res., Late Cenozoic uplift in eastern Tibet, Part 2: Timing of bedrock river erosion initiation from low-temperature thermochronology.

Davis, W. M., 1899, The Geographic Cycle, Geographical Journal, v. 14, p. 481 - 504.

Dirks, P. H. G. M., Wilson, C. J. L., Chen, S., Luo, Z. L., and Liu, S.,1994, Tectonic evolution of the NE margin of the Tibetan Plateau; evidence from the central Longmen

Mountains, Sichuan Province, China, Journal of Southeast Asian Earth Sciences, v. 9, no. 1-2, pp. 181 - 192.

England, P. and Houseman, G., 1986, Finite strain calculations of continental deformation, 2, Comparison with the India-Asia collision zone, J. Geophys. Res., 91, p. 3,664 - 3,676.

Gubbels, T. L., Isacks, B. L., and Farrar, E., 1993, High-level surfaces, plateau uplift, and foreland development, Bolivian Central Andes, Geology, v. 21, p. 695 - 698.

Heim, A., ETH-library, Zürich, Call no. Hs 494b:25 ♯290.

Howard, A. D. and Kerby, G., 1983, Channel changes in badlands, Geol. Soc. Am. Bull., v. 94, p. 739 - 752.

Howard, A. D., Seidl, M. A., Dietrich, W. E., 1994, Modeling fluvial erosion on regional to continental scales, J. Geophs. Res., v. 99, p. 13,971 - 13,986.

Hu, S., He, L., Wang, J., 2000, Heat flow in the continental area of China: a new data set, Earth and Planetary Science Letters, v. 179, pp. 407 - 419.

Kapp, P. , Murphy, M. A., Yin, A., Harrison, T. M., Ding, L., Guo, J., in press, Mesozoic and Cenozoic tectonic evolution of the Shiquanhe area of western Tibet.

King, R. W., Shen, F., Burchfiel, B. C., Royden, L. H., Wang, E., Chen, Z., Liu, Y., Zhang, X., Xhao, J., Li, Y., 1997, Geodetic measurement of crustal motion in Southwest China, Geology, v. 25, n. 2, pp. 179 - 182.

Kirby, E., Reiners, P. W., Krol, M. A., Whipple, K. X., Hodges, K. V., Farley, K. A., Tang, W., Chen, Z., 2002, Late Cenozoic evolution of the eastern margin of the Tibetan Plateau: Inferences from 40Ar/39Ar and (U-Th)/He thermochronology, Tectonics, 10.1029/2000TC001246.

Kirby, E. and K. X. Whipple, Quantifying differential rock-uplift rates via stream profile analysis, Geology, 29, 415–418, 2001.

Kirby, S.H., 1983, Rheology of the lithosphere: Reviews of Geophysics and Space Physics, v. 21, p. 1458-1487.

Lebedev, S. and Nolet, G., 2003, The upper mantle beneath SE Asia from S-velocity tomography, Journal of Geophysical Research, v. 108, 10.1029/2000JB000073.

Leloup, P. H., Harrison, T. M., Ryerson, F. J., Chen, W., Li, Q., Tapponnier, P., and La-

cassin, R., 1995, The Ailao Shan-Red River shear zone (Yunnan, China), Tertiary transform boundary of Indochina, Tectonophsyics, 251, p. 3 - 84.

Leloup, P. H., Arnaud, N., Lacassin, R., Kienast, J. R., Harrison, T. M., Phan Trong, T. T., Replumax, A., and Tapponnier, P., 2001, New constraints on the structure, thermochrnology, and timing of the Ailao Shan-Red River shear zone, SE Asia, Journal of Geophysical Research, v. 106, p. 6,683 - 6,732.

Li, S. and Mooney, W. D., 1998, Crustal structure of China from deep sounding profiles, Tectonophysics, v. 288, pp. 105 - 113.

Mattauer, M., Malavieille, J., Calassou, S., Lancelot, J., Roger, F., Hao, Z., Xu, Z., and Hou, L., 1992, La chane Triasique de Songpan-Garze (Ouest Sichuan et Est Tibet): une chane de plissement-dcollement sur marge passive, C. R. Acad. Sci. Paris, 314, p. 619 - 626.

Merritts, D. and Ellis, M., 1994, Introduction to Special Issue on Tectonics and Topography, in Ellis, M. and Merritts, D., eds., Tectonics and Topography, Special Section Part I, Journal of Geophysical Research, v. 99, p. 12,135 - 12,141.

Molnar, P. and England, P., 1990, Late Cenozoic uplift of mountain ranges and global climate change: chicken or egg?, Nature, v. 346, p. 29 - 34.

Molnar, P., and Tapponnier, P., 1975, Cenozoic tectonics of Asia: Effects of a continental collision: Science, v. 189, p. 419 - 426.

Murphy, M. A., Yin, A., Harrison, T. M., Drr, S. B., Chen, Z., Ryerson, F. J., Kidd, W. S. F. Wang X., Zhou, X., 1997, Did the Indo-Asian collision alone create the Tibetan plateau?, Geology, v. 25, p 719 - 722.

Raymo, M. E., Ruddiman, W. F., and Froelich, P. N., 1988, Influence of late Cenozoic mountain building on ocean geochemical cycles, Geology, V. 16, p 649 - 653.

Roger, F., 1994, Datation et tracage des granitodes associes a la chaine de Songpan-Garze (W Sichuan, Chine) par les methodes: U-Pb, Rb-Sr et Sm-Nd [PhD thesis], Universite Montpellier II, France.

Roger, F., Calassou, S., Lancelot, J., Malavieille, J., Mattauer, M., Xu, Z., Hao, Z., Hou, L., 1995, Miocene emplacement and deformation of the Konga Shan granite (Xianshui He fault zone, west Sichuan, China): Geodynamic implications, Earth Plan. Sci. Lett.,

v. 130, p. 201 - 216.

Replumaz, A., Lacassin, R., Tapponnier, P., Leloup, P. H., 2001, Large river offsets and Plio-Quaternary dextral slip rate on the Red River Fault (Yunnan, China), J. Geophys. Res., 106, p. 819 - 836.

Rowley, D. B., 1996, Age of initiation of collision between India and Asia: A review of stratigraphic data: Earth Planet. Sci. Lett., v. 145, p. 1 - 13.

Royden, L. H., 1996, Coupling and decoupling of crust and mantle in convergent orogens: Implications for strain partitioning in the crust, Journal of Geophysical Research, v. 101, n. B8, pp. 17,679 - 17,705.

Royden, L. H., Burchfiel, B. C., King, R. W., Wang, E., Chen, Z., Shen, F., and Yuping, L., 1997, Surface deformation and lower crustal flow in eastern Tibet, Science, v. 276, pp. 788 - 790.

Rushmer, T., 2001, Volume change during partial melting reactions; implications for melt extraction, melt geochemistry and crustal rheology, *in Partial melting of the crust and flow of orogens, C. Teyssier and O. Vanderhaeghe, eds., Tectonophysics, 342*, 389–405.

Schoenbohm, L., Whipple, K. X., Burchfiel, B. C., and Chen, L., 2002, Incision along the Red River, Yunnan Province, China: A transient response to regional surface uplift, EOS, Transactions, American Geophysical Union, Fall Meeting Suppl.

Shen, F., Royden, L. H., and Burchfiel, B. C., 2001, Large-scale crustal deformation of the Tibetan Plateau, Journal of Geophysical Research, v. 106, n. 4, pp. 6,793 - 6,816.

Spotila, J. A. and Sieh, K., 2000, Architecture of transpressional thrust faulting in the San Bernardino Mountains, southern California, from deformation of a deeply weathered surface, Tectonics, v. 19, n. 4, p. 589 - 615.

Tapponnier, P., Peltzer, G., Le Dain, A. Y., Armijo, R., and Cobbold, P., 1982, Propogating extrusion tectonics in Asia: New insights from simple experiments with plasticine: Geology, v. 10, p.611 - 616.

Tapponnier, P., Peltzer, G., and Armijo, R., 1986, On the mechanics of the collision between India and Asia , in Coward, M. P., and Ries, A. C., eds., Collision tectonics: London, Geol. Soc. Spec. Publ. No. 19, p. 115 - 157.

U.S. Geological Survey, 1993, Digital elevation models, data user guide, 5: Reston, Virginia, U.S. Geological Survey, p. 1-50.

Wang, E., Burchfiel, B. C., Royden, L. H., Chen, L., Chen, J., Li, W., Chen, Z., 1998, Late Cenozoic Xianshuihe-Xiaojiang, Red River, and Dali fault systems of southwestern Sichuan and central Yunnan, China, Geological Society of America Special Paper, v. 327, 108 p.

Wang, E. and Burchfiel, B. C., 1997, Interpretation of Cenozoic tectonics in the right-lateral accommodation zone between the Ailao Shan Shear Zone and the eastern Himalayan syntaxis: Int. Geol. Rev., v. 39, p. 191 - 219.

Whipple, K. X. and Tucker, G. E., 1999, Dynamics of the stream-power river incision model: Implications for height limits of mountain ranges, landscape response timescales and research needs, J. Geophs. Res, v. 104, p. 17,661 - 17,674.

Widdowson, M., 1997, The geomorphological and geological importance of palaeosurfaces, in Palaeosurfaces: Recognition, Reconstruction and Palaeoenvironmental Interpretation, Geol. Soc. Sp. Pub. No. 120, p. 1 - 12.

Xu, G. and Kamp, P., 2000, Tectonics and denudation adjacent to the Xianshuihe Fault, eastern Tibetan Plateau: Constraints from fission-track thermochronology, J. Geophys. Res., v. 105, p. 19,231 - 19,251.

Zheng, H., Powell, C. M., An, Z., Zhou, J., Dong, G., 2000, Pliocene uplift of the northern Tibetan Plateau, Geology, v. 28, p. 715 - 718.

Chapter 3

Surface Uplift, Tectonics, and Erosion of Eastern Tibet from Large-Scale Drainage Patterns[1]

M. K. Clark,[a] L. M. Schoenbohm,[a] L. H. Royden,[a] K. X. Whipple,[a] B. C. Burchfiel,[a] X. Zhang,[b] W. Tang,[b] E. Wang,[c] and L. Chen[d]

[a] *Department of Earth, Atmospheric, and Planetary Sciences, Massachusetts Institute of Technology 77 Massachusetts Avenue, Cambridge, Massachusetts* 02139, *USA.*
[b] *Chengdu Institute of Geology and Mineral Resources, Chengdu, China.*
[c] *Academica Sinica, Beijing, China.*
[d] *Yunnan Institute of Geological Sciences, Kunming, China.*

Abstract

A new regional compilation of the drainage history in southeastern Tibet suggests that the modern rivers draining the plateau margin were once tributaries to a single, southward-flowing system which drained into the South China Sea. Disruption of the paleo-drainage occurred by river capture and reversal prior to or coeval with the initiation of Miocene (?) uplift in eastern Tibet, including ~2000 m of surface uplift of the lower plateau margin since reversal of the flow direction of the Yangtze River. Despite lateral changes in course due to capture and reversal, the superposition of eastward and southward draining rivers that cross the southeastern plateau margin suggests that uplift has occurred over long-wavelengths (> 1000 km), mimicking the present low-gradient topographic slope.

[1] From Tectonics, Clark, M. K., Schoenbohm, L. M., Royden, L. H., Whipple, K. X., Burchfiel, B. C., Zhang, X., Tang, W., Wang, E., and Chen, L., in press.

Thus reorganization of drainage lines by capture and reversal events explains most of the peculiar patterns of the eastern plateau rivers, without having to appeal to large magnitude tectonic shear.

3.1 Introduction

In actively deforming regions, the geometry and evolution of fluvial systems are sensitive to surface uplift. Thus, the uplift and tectonic history of these regions may be partially contained in the geometry of the associated river systems, as recorded in the shapes of longitudinal and transverse river profiles and in the geometries of the drainage basins [e.g. *Howard*, 1967; *Seeber and Gornitz*, 1983; *Oberlander*, 1985; *Jackson and Leeder*, 1994, *Cox*, 1994]. Typically, tectonogeomorphic studies of fluvial systems have concentrated on the identification of active geologic structures and the relative rates of uplift across those structures using longitudinal river profiles [e.g. *Hack*, 1973; *Seeber and Gornitz*, 1983; *Merritts and Vincent*, 1989]. However, large scale drainage basin morphologies can also place important constraints on regional patterns of surface uplift and shear strain, thus providing critical information about the kinematics of crustal deformation [e.g. *Potter*, 1978; *Cox*, 1989; *Summerfield*, 1991; *Ollier and Pain*, 1997; *Brookfield*, 1998; *Hallet and Molnar*, 2001].

One area where analysis of river systems may be particularly useful as a guide to tectonism and surface uplift is in the region of the eastern Tibetan plateau, where much of the young surface uplift appears to have occured without the development of significant shortening structures at the surface [e.g. *Burchfiel et al.*, 1995; *Royden et al.*, 1997; *Wang and Burchfiel,* 2000]. Thus study of the river systems that traverse this portion of the plateau remains one of the few avenues for documenting the spatial and temporal pattern of uplift (Figure 3.1).

In southeastern Tibet, the very low-gradient plateau margin (5 km elevation gain over 1500 km in length), is defined by a regionally continuous, relict low-relief landscape which is now preserved over large aerial extents in the interfluves between deeply incised river gorges. Along the southeastern plateau margin, we interpret this erosion surface to repre-

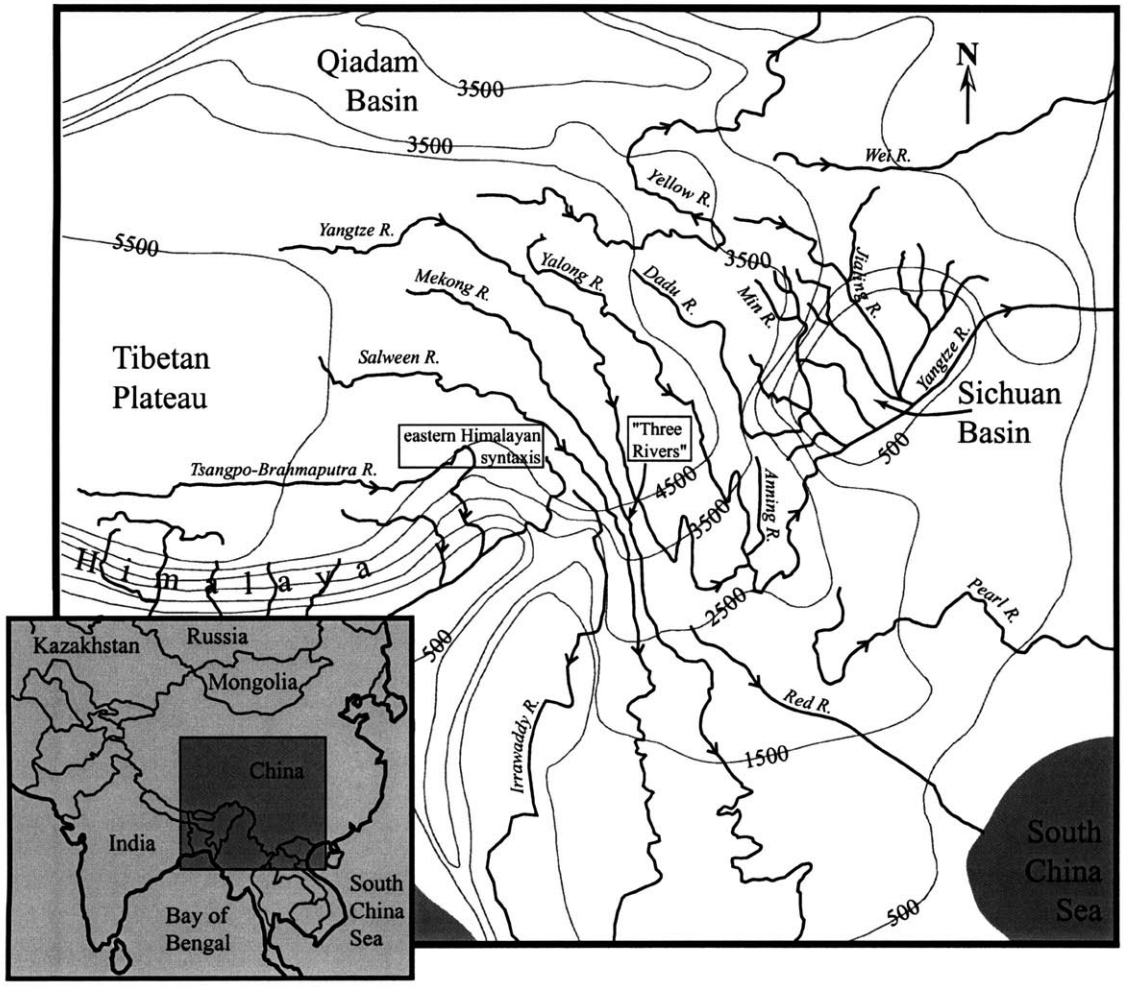

Figure 3.1: Major river courses of eastern Tibet superimposed on a smoothed elevation contour map derived from publicly available ~1 km resolution GTOPO30 topography data [*U.S.G.S.*, 1993]. Arrows represent modern flow direction. Dark shaded box in inset map shows location of the study area.

sent a remnant landscape that has not yet equilibrated to present day conditions (i.e. the uplift that has caused the incision of major river canyons) and the spatial continuity of this landscape argues for broad surface uplift and long wavelength tilt of the plateau margin during crustal thickening. Rapid erosion by continental scale rivers (the Salween, Mekong and Yangtze Rivers and tributaries) that run over thousands of kilometers in length, have incised deep bedrock gorges up to 2 to 3 km in depth along the steepest portion of the plateau margin (between the 3500 - 4500 contour inverval [Figure 3.1]). Thus it appears that the older, uplifted low-relief landscape that defines the plateau surface is currently

being destroyed by aggressive river incision, presumably in response to the uplift of the eastern plateau.

The major rivers of eastern Tibet have attracted considerable attention due in part to their peculiar drainage basin morphology. Early studies focused primarily on the history and geometry of individual rivers, emphasizing changes in river patterns due to river capture and drainage direction reversal [e.g. *Abendanon*, 1907; *Gregory and Gregory*, 1925; *Lee*, 1933; *Barbour*, 1936]. More recent studies have generally attempted to link the regional fluvial patterns to the rise of the Tibetan plateau and the continental collision between India and Eurasia [e.g. *Koons*, 1995; *Brookfield*, 1998; *Metivier* et al., 1999; *Hallet and Molnar*, 2001], though some of these recent studies also mention examples of individual river capture events as a partial explanation for one or more of the unusual drainage basin morphologies in southeastern Tibet. An end-member view considers the modern river courses as passive strain markers within the crust, concluding that the unusual drainage pattern in southeastern Tibet has resulted solely from deformation by horizontal shear of initially typical drainage basins during the Indo-Asian collision [*Brookfield*, 1998; *Hallet and Molnar*, 2001]. In this scenario, the central portions of the Salween, Mekong, and Yangtze drainage basins become highly attenuated due to large-scale, right-lateral shear caused by the northward progression of the eastern Himalayan syntaxis.

In this paper we assemble a number of separate geomorphic observations made by various authors, and our own field and digital elevation model (DEM) analyses, in order to assess the importance of river capture, to reconstruct the evolution of the drainage systems, and to examine the implications for uplift of the eastern Tibetan Plateau.

3.2 Drainage pattern analysis and geomorphology of southeastern Tibet

Drainage anomalies, defined as deviation from common regional patterns, can provide information on tectonic deformation, and styles of regional drainage patterns can be interpreted as the product of the regional relief on which they form [e.g. *Zernitz*, 1932; *Howard*,

1967]. For example, a 'dendritic' pattern describes a river system where branching tributaries enter the trunk stream at wide angles. Where this pattern is observed at a continental scale, this type of drainage pattern reflects erosion of horizontal sediments or beveled, uniformly resistant crystalline rocks and forms in areas of low regional relief. In particular, these drainage basins have predictable length to width ratios [*Potter*, 1978]. While the term 'dendritic' may be applied to any such branching system, it is commonly reserved to describe river patterns that occur without pronounced structural or slope control [*Zerniz*, 1932]. In contrast, more narrowly spaced tributary basins with narrow tributary angles are defined as a 'parallel' drainage pattern indicating strong (steep) slope control. 'Trellis' and 'rectangular' patterns have tributary junctions that form at right angles, often with regular spacing, which indicate geometric control by underlying structures or joint systems. Transitional drainage patterns that show a change from one basic type of system to another may reflect changes in exposure of underlying structural geometries, changes in uplift patterns or initiation of surface uplift, and possibly changes in climate by the onset of glaciation.

In Tibet, we attempt to correlate deviations from and changes to basic drainage patterns, with the regional slope and tectonic conditions by which they may have formed. The Longman Shan plateau margin (adjacent to the Sichuan Basin) and the Himalayan front are similar in morphologic character and are both very steep ($\sim$ 5 km elevation gain over 50-200 km). However, the Longmen Shan differs from the Himalayan front in that it has developed despite evidence for minimal upper crustal shortening of Tertiary age [*Dirks et al.*, 1994; *Burchfiel et al.*, 1995; *Royden et al.*, 1997]. Although modest shortening may be occuring along the Longman Shan ($<$ 3 mm/yr), it is almost an order of magnitude less than the rate of shortening along the Himalayan front [*Lave et al.*, 2000; *King et al.*, 1997; *Chen et al.*, 2000]. The drainage systems observed in the Himalaya and the Longmen Shan are typical of transverse or consequent drainage systems developed on steep mountain fronts (Figure 3.2a): the rivers are short, closely spaced (similar to a 'parallel' drainage pattern) with steep river gradients and have incised narrow deep canyons with high local relief [e.g. *Hovius*, 2000; *Kirby et al.*, in press]. The Brahmaputra and Dadu Rivers are exceptions where the river consists of a short, steep river segment transverse to the mountain range, and a longer, low-gradient river that flows parallel or behind the mountain range, a geometry

that is most likely the product of river capture, as described below.

Bedrock river incision is typically modeled as a power-law function of drainage area (as a proxy for discharge) and local channel gradient [e.g. *Howard and Kerby*, 1983; *Howard* et al., 1994; *Whipple and Tucker*, 1999]. By considering a constant relationship between slope and drainage area throughout a drainage basin, the contribution of drainage area can be 'corrected' or excluded so that the channel gradients of different rivers (or segments along a river) can be directly compared and used to reflect spatial variations in uplift rate (i.e. by 'channel steepness') [e.g. *Snyder et al.*, 2000; *Kirby and Whipple*, 2001; *Kirby et al.*, in press]. Analyses of channel steepness for bedrock river channels that cross the Longman Shan indicate a region of vertical rock uplift localized at the steep plateau margin [*Kirby et al.*, in press].

The southeastern and parts of the east-northeastern plateau margins have far lower regional topographic gradients than the Himalayan and Longmen Shan plateau margins [e.g. *Clark and Royden*, 2000]. In southeastern Tibet, the active tectonic regime is dominated by strike-slip deformation and associated normal faulting, which accommodate translation of crustal blocks around the eastern Himalayan syntaxis and the contribution of active or Cenozoic upper crustal shortening to the long-wavelength gradient in crustal thickness is also minimal [*Burchfiel et al.*, 1995; *Wang et al.*, 1998; *King et al.*, 1997; *Chen et al.*, 2000; *Wang and Burchfiel*, 2000; *Li and Mooney*, 1998]. Therefore it has been proposed that the bulk of the crustal thickening of these low-gradient plateau margins has taken place by preferential thickening of the lower crust during regional scale flow of lower crustal material [*Royden et al.*, 1997; *Clark and Royden*, 2000; *Shen et al.*, 2001] .

The rivers that drain the low-gradient southeast and northeast margins of the plateau have very long axial lengths and therefore much lower average longitudinal gradients than rivers crossing the steep plateau margins (Figure 3.2b). The scale of these eastern Tibet rivers are comparable to the world's longest and largest river basins but differ in significant ways. Most of the world's largest/longest river basins occur in areas of regionally low-relief, such as cratonic interiors (i.e. Amazon, Mississippi, Congo Rivers). These cratonic rivers have very low longitudinal river gradients (on the order of 10^{-4} or less, based on the averaged gradient of drainage basin relief divided by the trunk river length), are

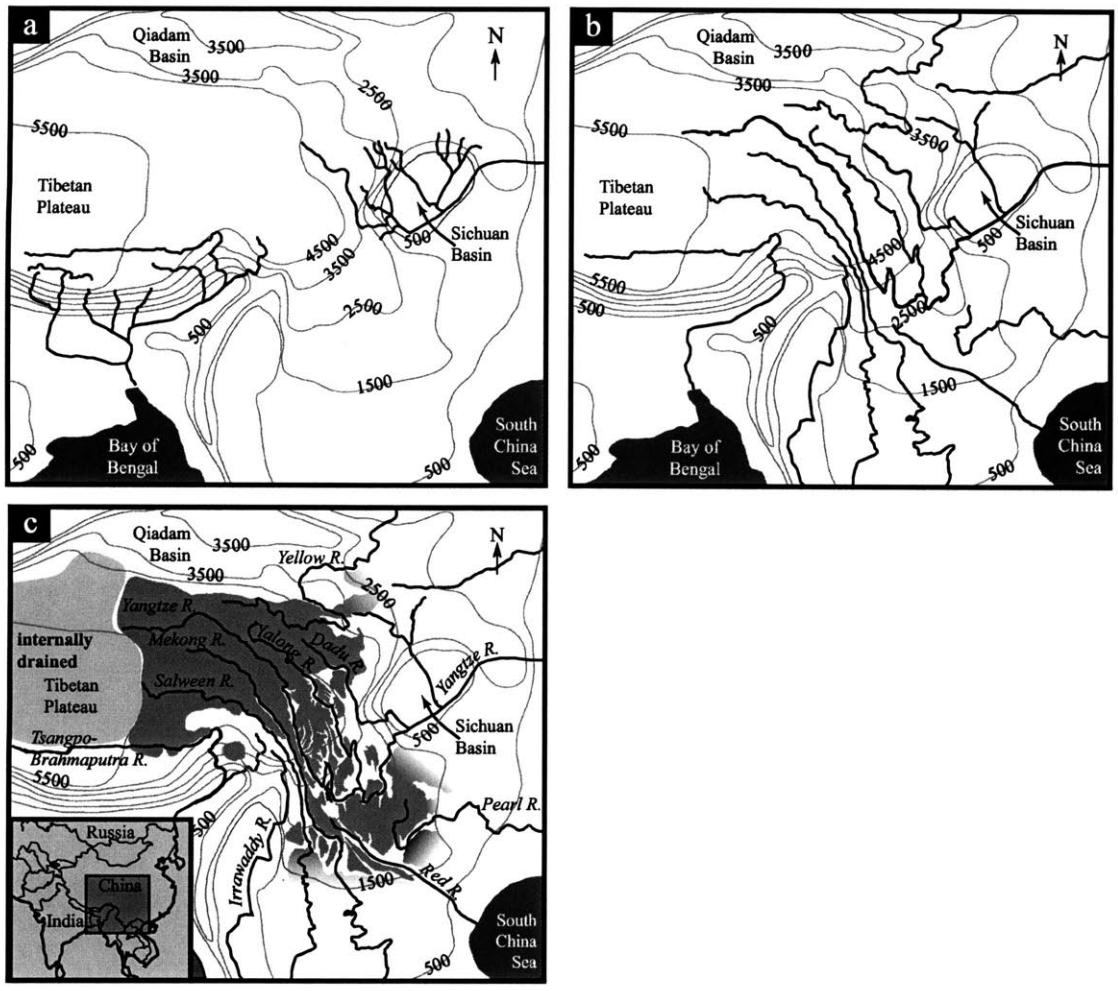

Figure 3.2: Major rivers of eastern Tibet plotted on topography (smoothed elevation contours in meters). a) Major rivers that are less that a few hundred kilometers in length and are characterized by steep river profile gradients (corrected for drainage area). b) Rivers that are more than one thousand kilometers in length and characterized by low-gradient profiles (corrected for drainage area). c) Generalized extent of regional erosion surface (preserved relict, low-relief landscape), shown in dark-grey shaded regions. Surface is defined from field observations and DEM analyses. At low elevations, this relict surface merges with an "active" or modern surface which has not experienced significant surface uplift (represented by gradational shading at the southeastern and northeastern extent of the surface). Light gray shading on high plateau represents the internally drained west-central high plateau.

transport-limited (alluvial) rivers, have highly predictable length/drainage area ratios, and have drainage basins that are typically tear-drop shaped - typical of regional-scale 'dendritic' drainages [*e.g. Zernitz*, 1932]. The major eastern Tibet rivers (the Yellow, Yangtze, Mekong and Salween Rivers) are comparable to other major world river basins in length; however, their drainage basins tend to be attenuated and irregularly shaped, they are dominantly detachment-limited (bedrock) rivers incised into narrow river gorges over much of their length, and they have average river gradients (10^{-3}) that are at least an order of magnitude higher than average cratonic, alluvial rivers, but still at least 1 to 2 orders of magnitude lower than their steep plateau margin equivalents (i.e. a trans-Himalayan river with an average gradient of $\sim 10^{-1} - 10^{-2}$).

The other notable characteristic of the major, long rivers that drain the southeastern margin of the Tibetan Plateau is that they are deeply incised into a regionally preserved erosion surface (Figure 3.2c). The low-gradient southeastern plateau margin is defined by a regionally continuous, relict, low-relief landscape preserved over large aerial extents in between these deeply incised river gorges. While we assume that initial local development of this erosion surface is diachronous, we propose that it existed as a regional surface at low elevations prior to uplift of the eastern plateau margin due to its spatial continuity. Therefore its present day elevation provides an excellent datum for constraining total surface uplift. While the major rivers of southeastern Tibet are deeply incised into narrow bedrock gorges, evidence for ancestral river courses exists in abandoned channels, fragments of abandoned channels (i.e. wind gaps with fluvial sediments) and alluvial capped bedrock terraces that occur up to a kilometer in elevation above the modern channel. Also barbed tributaries along sections of major rivers suggest that portions of these rivers have reversed their flow direction, probably in conjunction with a capture event. These geomorphic observations serve as evidence for a paleo-drainage pattern of southeastern Tibet that predates the most recent episode of rapid bedrock incision and in many places contrasts sharply with the pattern of the present day river courses. Detailed evidence regarding the drainage pattern evolution is outlined in the following section.

3.3 Reconstruction of Drainage Lines

Commonly-cited geomorphic evidence for changes in drainage systems include evidence of river capture, remnants of paleo-drainage systems, and drainage reversals. The location of a river capture is commonly indicated by a sharp change in the modern river course with the old river course marked by an abandoned river valley (or "wind gap") that contains fluvial sediments. Occasionally high fluvial terraces present along the drainage line upstream from the capture point may correlate with the wind gap and define a paleo-longitudinal river gradient prior to capture. Knickpoints (abrupt changes in stream gradient) are also commonly observed on the upstream portion of captured drainage lines. Correlated bedrock terraces, wind gaps, and abandoned river channels (or underfit river channels where the volume rate of flow in the river is smaller than expected for the width of the river valley) can also be used to identify paleo-river courses.

Barbed drainage patterns, where the tributary confluence angles are systematically greater than 90°, are diagnostic of drainage reversal [e.g. *Summerfield*, 1991]. For example, many cited cases of drainage reversal come from the East African Rift, where recent uplift at the rift axis has caused rivers to be defeated (lose their ability to maintain their course and drainage directions) and to reverse direction. It has been suggested that such reversal events only occur in areas of minimal relief with very low stream gradients [e.g. *Ollier*, 1981; *Summerfield*, 1991].

Proceeding from east to west, as summarized in Figure 3.3, we examine the evidence for river capture of major drainage lines in southeastern Tibet, as well as reversal of flow direction along portions of these drainages. The order in which these captures are discussed here is geographical, and in a later section we will suggest a chronology of capture/reversal events with implications for surface uplift of the southeastern plateau margin.

3.3.1 Dadu/Anning River capture

The Dadu River is a major tributary to the Yangtze River. It follows a north-south course east of the Longman Shan range, which forms the steep eastern plateau margin adjacent to the Sichuan Basin (Figure 3.3a). At its southern extent within the plateau, the Dadu River

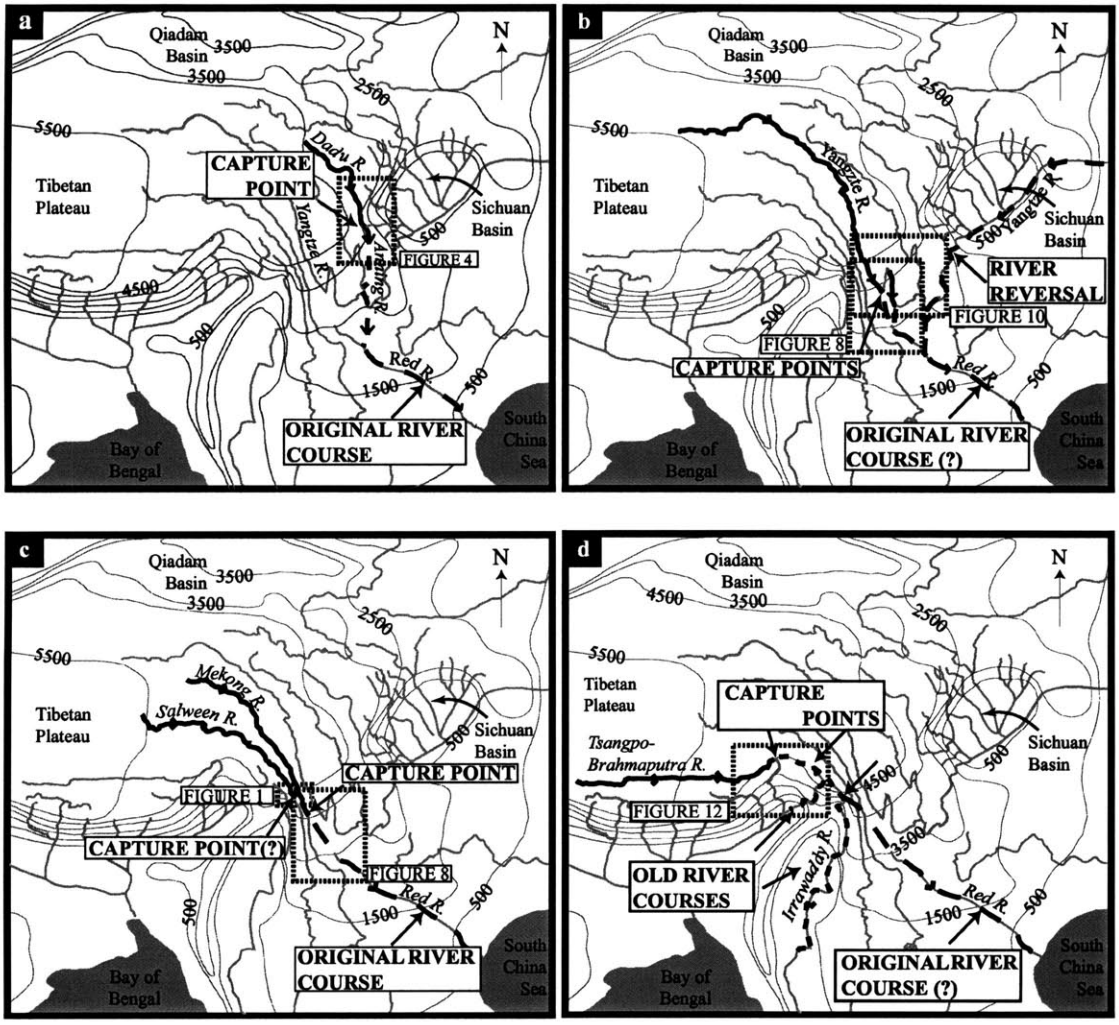

Figure 3.3: Summary of river captures for eastern Tibet. Small dashed boxes refer to more detailed figures for each capture event. a) Capture of the Anning River by the Dadu River. b) Reversal of the Middle of the Yangtze River and capture of the Upper Yangtze River from the paleo-Red River. c) Capture of the Upper Mekong and possible the Upper Salween Rivers from the paleo-Red River. d) Successive capture of the Tsangpo River from: possibly the paleo-Red River, the Irrawaddy R., Lhuit R. and most recently by the Brahmaputra River in the area of the eastern Himalayan syntaxis.

is incised into in a narrow deep gorge, makes an abrupt (90°) change in course and flows eastward into the southwestern Sichuan basin (Figure 3.4). The abrupt change in course occurs adjacent to a low, wide pass (a wind gap) that separates the north-south portion of the Dadu River from the headwaters of the north-south oriented Anning River, also a tributary to the Yangtze River. In contrast to the narrow, deeply incised inner gorges and steep river gradients along the lower Dadu River, the Anning River flows in a broad, alluviated valley with gentle river gradients close to its headwaters, and is presently underfit with respect to its modern drainage area (Figure 3.5). Fluvial sediments preserved in the wind gap are described as Pliocene(?) [1:200,000 map, *Bureau of Geology and Mineral Resources of Sichuan*, 1991], however, the age is constrained by neither paleontological nor magnetostratigraphic methods and therefore can only be tentatively assigned. The preserved fluvial gap sediments show a distinct southward-dipping slope, despite the modern drainage direction that flows north (Figure 3.6).

High alluvium-capped bedrock terraces are preserved nearly 800 meters above the modern Dadu River just north of the bend and appear to correlate broadly with the wind gap and the low river gradients on the Anning River (Figure 3.5c). The high terraces, sediment filled wind gap, and low longitudinal river gradients on the Anning River possibly define a paleo-longitudinal profile of the paleo-Dadu/Anning River, indicating that the originally south flowing Dadu/Anning river has been captured by an east flowing river that became the lower Dadu River [*Barbour*, 1936; *Wang et al.*, 1998](Figure 3.4c). In the uppermost part of its headwater region, the Anning River abruptly changes to a very steep river gradient leading up to the wind gap where fluvial sediments are preserved at a higher elevation than what would be predicted by simply projecting the upper Dadu River, above the knickpoint related to capture, across the gap (Figure 3.4c). The oversteepened gradients of the uppermost Anning River and the elevated wind gap lie within a broad region of uplift associated with the adjacent Gonga Shan massif, thus the apparent warping in the reconstructed profile is most likely related to uplift. The elevation difference between the bedrock terraces and the Anning River valley floor beneath the regional erosion surface suggests that 1-2 km of incision occurred prior to the capture event.

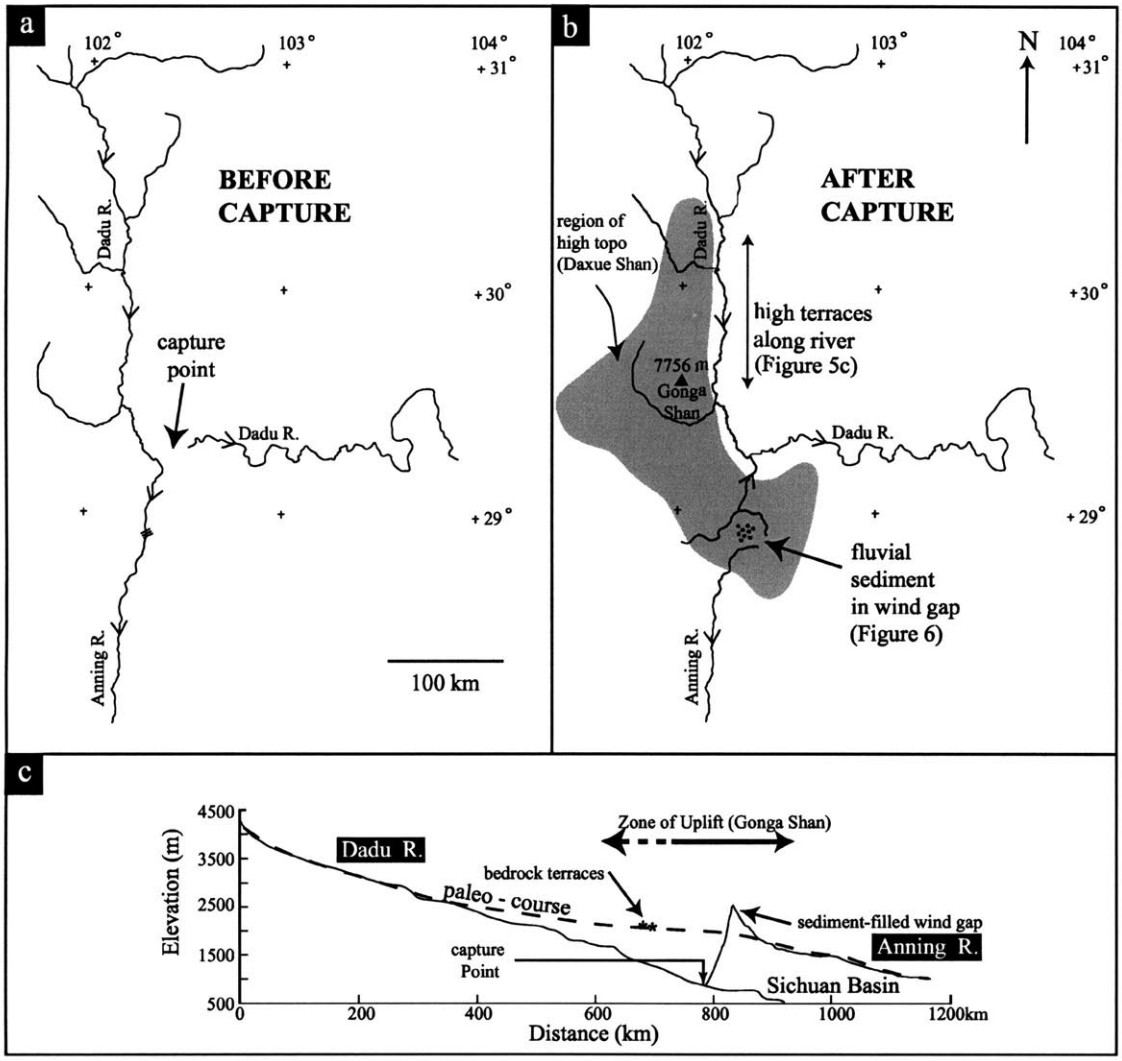

Figure 3.4: a) Detailed reconstruction of Dadu-Anning R. capture, where the paleo-Anning River flowed directly south. (b) After capture, the upper reaches of the paleo-Anning are redirected to the east out the Dadu River. Stranded fluvial sediments (shown by stippled pattern) are preserved in the paleo-river course (wind-gap), and high bedrock terraces are observed upstream of the capture. Triple line pattern (///) indicates position of restored river course. Capture occurs in the vicinity of anomalously high topography at and around Gonga Shan (7756 m). (c) Longitudinal river profile of the Dadu and Anning rivers, projected onto a north-south profile which is proposed as the reconstructed drainage path. Dashed line represents schematic reconstruction of paleo Dadu-Anning river profile prior to capture.

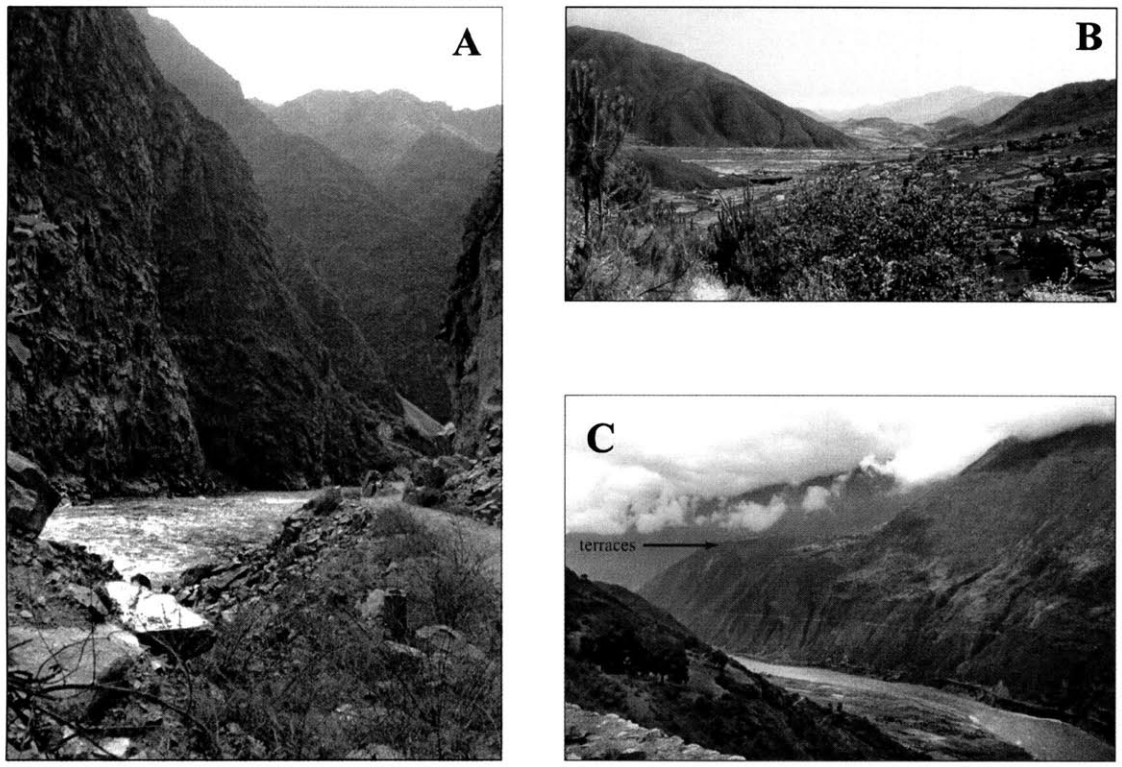

Figure 3.5: a) View north of the Dadu River gorge upstream of the capture point. b) View south of the Anning River valley, from near its headwaters. c) View southwest at high strath (bedrock) terraces near Luding on the Dadu River. Terraces are approximately 800 m above the modern river elevation.

3.3.2 Middle Yangtze River reversal

For the purposes of discussion, we divide the Yangtze River into three sections: the Upper Yangtze River, defined as the section from the headwaters to the first major bend in the river course ("First Bend"); the Middle Yangtze River defined from the "First Bend" to the Three Gorges area, east of the Sichuan Basin; and the Lower Yangtze River defined from the Three Gorges area to the East China Sea (Figure 3.7a). *Barbour,* [1936], first proposed a large-scale reversal of the Middle Yangtze River (including the Min and lower Dadu rivers, but not the Anning, Yalong or Upper Yangtze rivers [Figure 3.7c]), which rerouted the southwest flowing drainage of the Middle Yangtze to a northeasterly course into the Lower Yangtze. This event is supported by the large confluence angles of major tributaries along the Middle Yangtze River (barbed tributaries), reversed terraces, and drainage basin

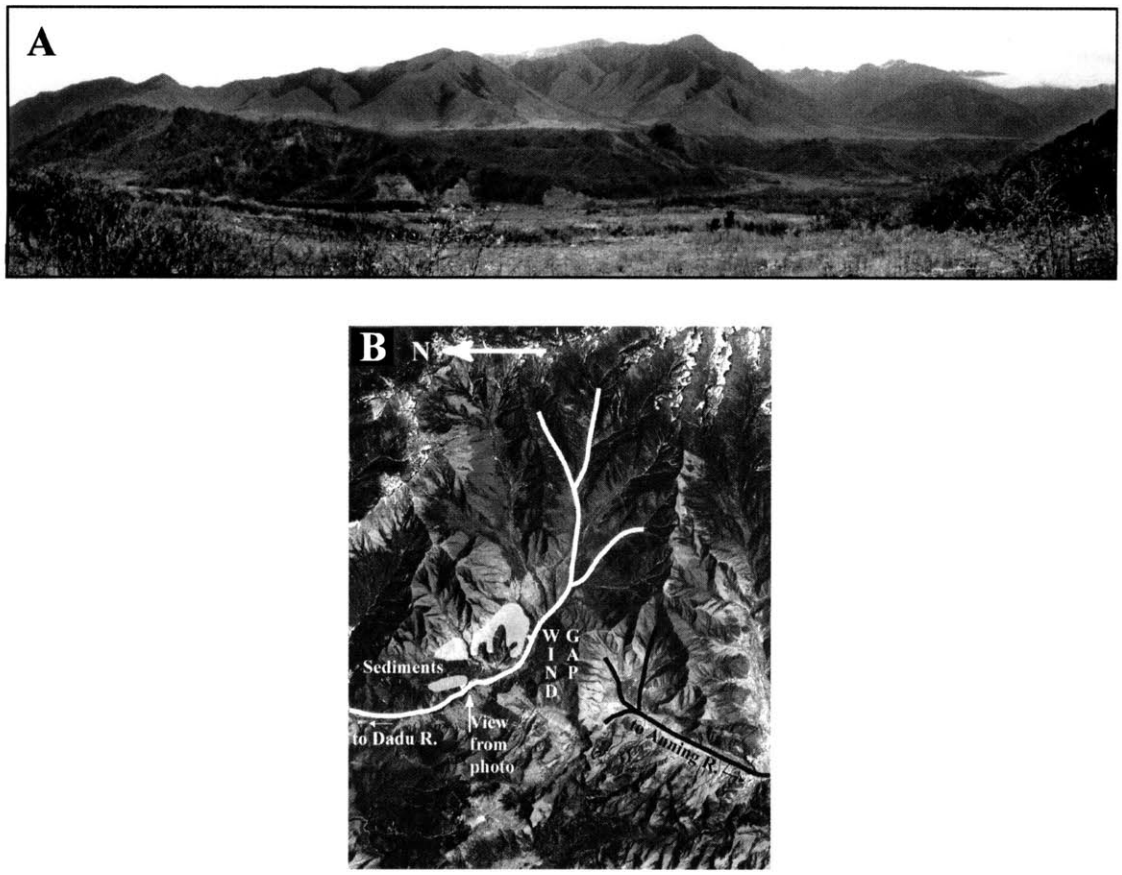

Figure 3.6: a) View east of wind gap sediments (mid-ground) located in the pass separating the headwaters of the Anning River with the Dadu River. Surface of sediment package dips south. b) CORNONA image of the wind gap, showing north directed drainage around south-sloping gap sediments.

morphology which all suggest that the Middle Yangtze River has reversed its flow direction [*Barbour*, 1936; *Zhao et al.*, 1997]. In this interpretation, the paleo-Yangtze River consisted only of the present Lower Yangtze River, flowing east to the East China Sea (Figure 3.7a), whereas the modern Middle and Upper Yangtze River are interpreted to have previously flowed south as tributaries to the Red River.

The northeasterly course of the Middle Yangtze River is oblique to the present regional topographic gradient over about 1000 km of its length. Similar to the Upper Yangtze, the Middle Yangtze River is deeply incised into bedrock gorges where the river flows across the southeast plateau margin. It becomes a wider, braided alluvial river when it flows off of the lower plateau margin and along the southeastern margin of the Sichuan Basin. Here

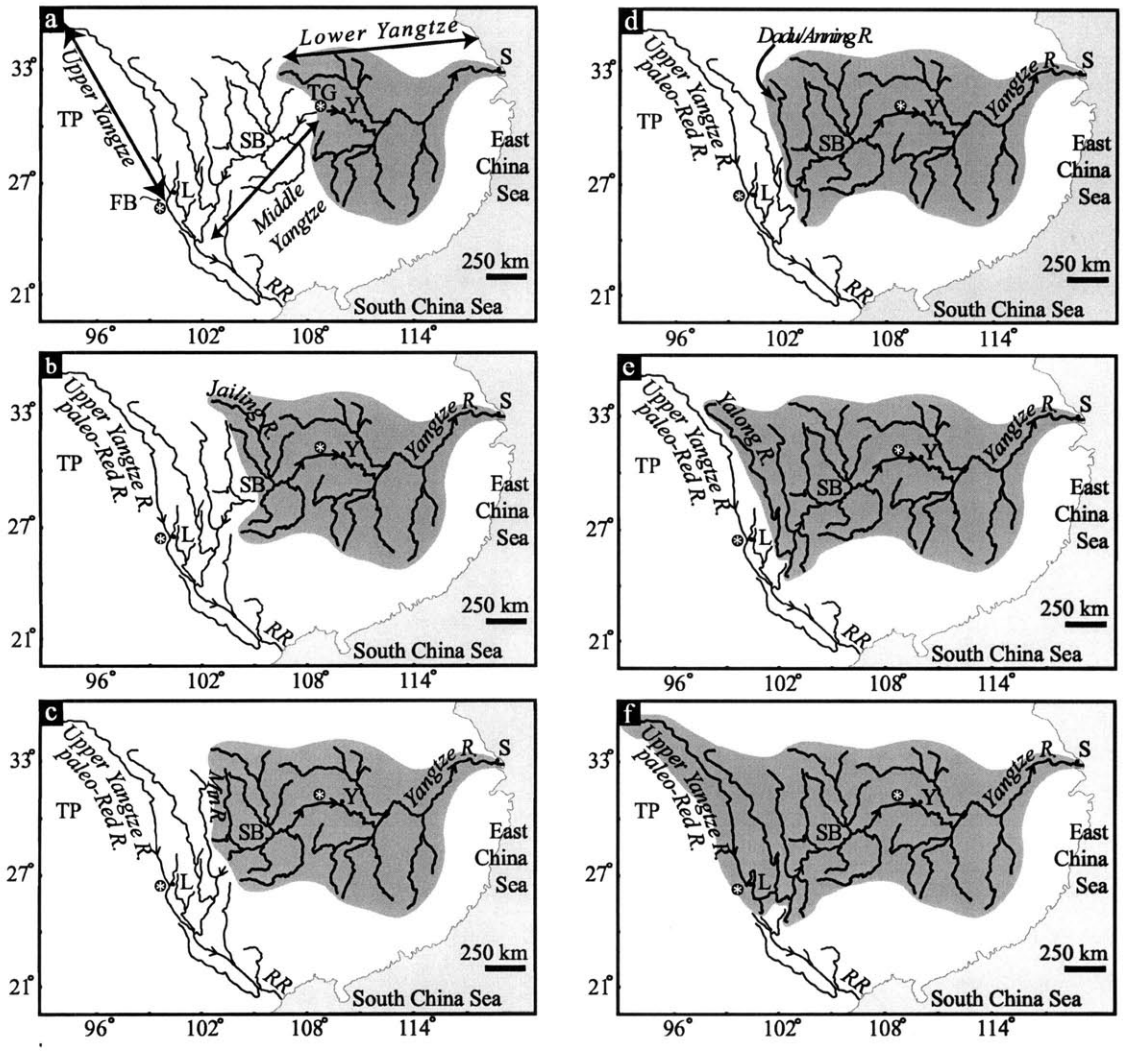

Figure 3.7: Reversal of Middle Yangtze River and sequential captures of major tributaries to the Middle Yangtze River. Grey outline delineates drainage basin development of the Yangtze River. Asterisk symbols (*) indicate segment of Middle Yangtze that reverses direction, from the "Three Gorges" to the "First Bend". Abbreviations are as follows: FB = First Bend of the Yangtze River, L = Lijiang, RR = Red River, S = Shanghai, SB = Sichuan Basin, TG = Three Gorges, Y = Yichang a) Interpreted original drainage basin of the Lower Yangtze River, where the headwaters of this basin are in the Three Gorges region. b) Reversal of the Middle Yangtze is initiated by the reversal of a small segment of river along the main course and the capture of the Jialing River to the east, into the Lower Yangtze River basin. c) Reversal progresses from east to west with the capture of the Min River, d) the Dadu/Anning River, e) Yalong River, and f) terminates with the capture of the Upper Yangtze River at the "First Bend", which results in the modern drainage basin morphology.

the river is moderately incised (a few hundred meters) into the South China Fold Belts with flights of Quaternary alluvial terraces occurring along the river [*Barbour*, 1936]. The river is more deeply incised into bedrock (several hundred meters) where it cuts across basement cored anticlines in the Three Gorges area [e.g. *Abendanon*, 1907; *Gregory*, 1929; *Barbour*, 1936]. By comparison, the Lower Yangtze River is of an entirely different character, flowing on a wide alluvial flood plain for its entire length [*Gregory*, 1929; *Barbour*, 1936].

Because instantaneous large scale reversal of a river over 1000 km seems unlikely, we propose that the reversal of the Middle Yangtze was accomplished piecemeal by successive reversals of small segments of river and consequent captures of major tributaries into the eastern basin (Figure 3.7). For example, the initial reversal/capture event was at the Jialing/Yangtze River confluence, where the short segment of Middle Yangtze River upstream from the confluence was reversed, and thus redirected (captured) flow of the Jialing River out to the east into the lower Yangtze River (Figure 3.7b). In this manner, the reversal of the Middle Yangtze river could have been accomplished by a sequence of river reversals over short segments leading to successive captures of large tributary basins. These captures must have progressed from east to west because reversed channel segments must be diverted away from the basin to the east and into the lower Yangtze River. Thus the eastern portions of the Middle Yangtze must have been diverted first. This proposal extends the original proposal of capture/reversal events by *Barbour* [1936] by including the Anning, Yalong and Upper Yangtze Rivers as well (Figure 3.7).

3.3.3 Upper Yangtze/ Red River capture

Geomorphology

The Upper Yangtze River flows from the central plateau through the southeastern plateau margin, where it radically alters its south-southeasterly course down the regional topographic gradient to an east/northeast course that trends obliquely across the plateau margin. Geographers as early as the 15^{th} century suggested that the Upper Yangtze River and similarly its major tributaries (e.g. the Yalong and Dadu-Anning rivers) originally drained

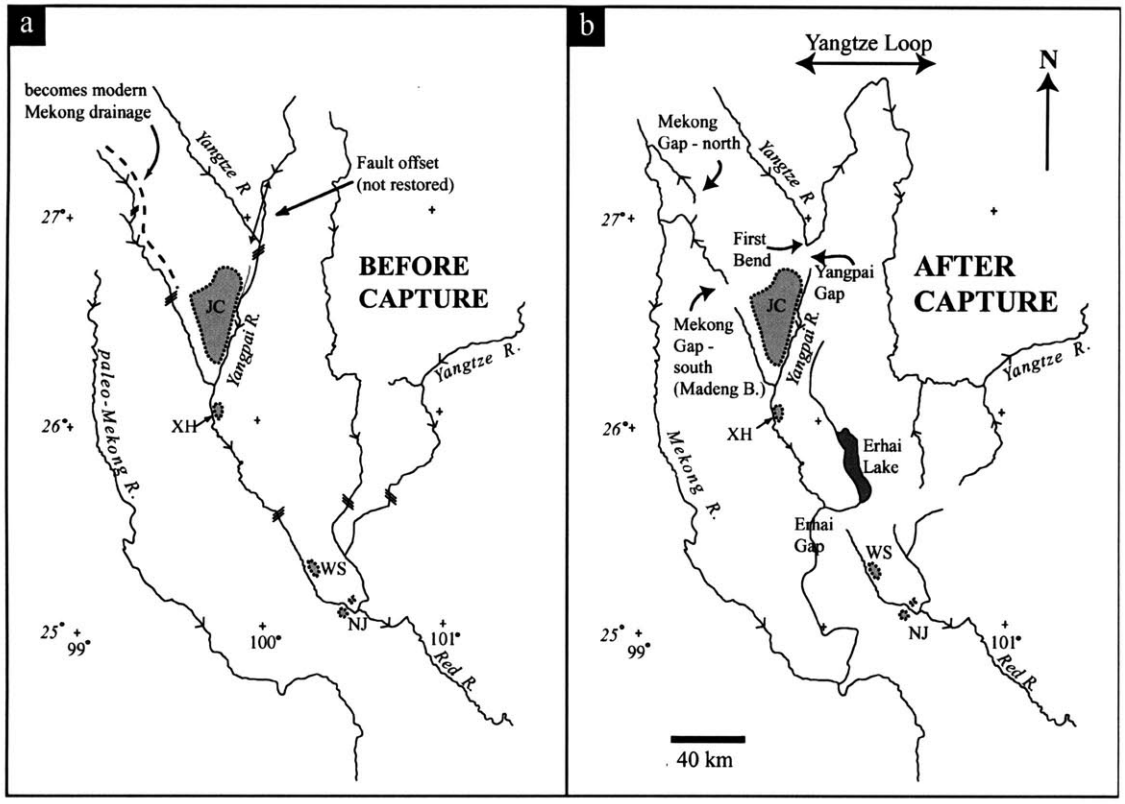

Figure 3.8: Detailed reconstruction of the Upper Yangtze and Upper Mekong river captures. a) Prior to capture, the Upper Mekong River and the Upper Yangtze River flowed into the paleo-Red River. b) After capture, the Upper Mekong is redirected into the (modern) Mekong River, and the Upper Yangtze is redirected to the east, through the Middle and Lower Yangtze River as a part of a sequence of river reversals and captures (Figure 3.7). Triple line pattern (///) indicates location of restored river course prior to capture. Light gray polygons show areas of preserved Tertiary fluvial sediments that may correlate with a paleo-river system prior to capture. Abbreviations are as follows: JC = Jianchuan, NJ = Nanjian, and WS = Weishan, and XH = Xiahou.

south into either the Mekong River or the Red River [e.g. (and references therein) *Lee*, 1933; *Barbour* et al., 1936; *Tregar*, 1965; *Brookfield*, 1998; *Metivier* et al., 1999] (Figure 3.8). The large amount of Cenozoic offshore sediment in the Gulf of Tonkin is difficult to explain by the modern drainage area and sediment supply of the Red River, suggesting that the drainage area of the modern Red River has been reduced by capture of its headwaters by the modern Yangtze and Mekong Rivers [*Metivier* et al., 1999].

It has been proposed that the upper Yangtze was probably a tributary to the Red River

and flowed through a wind gap at the southern terminus of the "First Bend" in the river (Yangpai Gap) and another low-lying wind gap (the Erhai Gap) into the modern headwaters of the Red River [e.g. *Gregory and Gregory*, 1925; *Ting*, 1933; *Lee*, 1933] (Figure 3.8a). However, based on recent field work, we propose that the 'Yangpai Gap' (as previously described) is not an abandoned river valley (or "wind gap"), but rather is a narrow structural valley most likely formed by the Jianchuan Fault which has also locally offset the Yangtze River at the First Bend [*Wang et al.*, 1998]. However, east of the Yangpai Gap *senso-stricto*, we observe a broad, smooth, extremely flat surface that continues across to the north-northwest side of the modern Yangtze River gorge, where the river is offset ~30 km by the Jianchuan Fault [*Wang et al.*, 1998] (Figure 3.8b). This local surface however, is at approximately the same elevation as the regional erosion surface which mantles this portion of the plateau margin. From field observations and CORONA imagery, the extremely smooth and flat nature of the surface observed along the reconstructed capture point of the Yangtze, suggests that it may represent the floor of a large alluvial paleo-river (i.e. the paleo-Yangtze-Red River) at approximately the elevation of the erosion surface. On a regional scale, the position of this interpreted valley floor requires only a subtle change in position for the capture of the Upper Yangtze from the Red River from previous reports, yet this change does affect the precise location of potentially recoverable sedimentary deposits that might be used to determine paleo-slope and scale of the river prior to capture (i.e. by methods outlined in *Paola and Mohrig* [1996]). This observation is also consistent with at least the lower portions of the paleo-Upper Yangtze having been a broad alluvial river developed on subdued, low-relief topography at the time of capture, which would allow a reversal/capture to occur.

Sedimentology

The most convincing evidence of river capture comes from relict fluvial sediment preserved in a wind-gap directly adjacent to the capture point. While we do not observe sediments in this ideal geometry, we present observations from four localities of preserved fluvial sequences from Jianchuan (40 km south of the proposed wind gap) to the headwater basins of the Red River that we tentatively propose to be remnants of a paleo-south flow-

ing Yangtze/Mekong-Red River system (Figure 3.8). The Tertiary sedimentary record in the region between the Yangtze "First-Bend" and the Red River can be divided into three distinct groups: 1) Folded Paleocene-Eocene clastic sediments that are conformable with underlying Jurassic and Cretaceous redbed basins (i.e. the Yangbi, Simao and Chuxiong basins), 2) early-mid(?) Tertiary debris-flow units, and 3) Miocene or Pliocene fine-grained silt, mud, and coal deposits [*Bureau of Geology and Mineral Resources of Yunnan,* 1990]. Thus, well-exposed fluvial sequences such as the ones described in the following section exposed along the reconstructed path of a paleo-Upper Yangtze/Mekong-Red River course are unidentified elsewhere in the Tertiary section of this area. However, the lack of index fossils and/or provenance indicators require that the correlation of these individual outcrops are made on their lithologic uniqueness alone.

West of the city of Jianchuan (40 km south of the "First Bend" of the Yangtze River) , up to ~800m of well-exposed middle(?)-Tertiary alluvial/fluvial sandstones are observed (Baoxiangshi and Lijiang formations, [*Bureau of Geology and Mineral Resources of Yunnan*, 1990]), most likely representing a structural depocenter. Interbedded cobble and sandstone beds in the lower part of the section are overlain by massive, well-sorted medium grained sandstones which comprise the middle part of the section (Figure 3.9a). Sandstone beds frequently contain mud rip-up clasts in the lower 10 cm of the beds and are often separated by thin mud drapes and thicker mud beds that occasionaly are bioturbaded and contain fossil leaf hash. Occasionally we observe irregularly interbedded sandstone and fine-grained siltstone (Figure 3.9b), and rarely observe preserved of cross-bedding and large channel scours (~5m). This sequence is undeformed to slightly tilted and lies unconformably on fossil-bearing Paleocene calcareous mudstone, shale and evaporites [*Bureau of Geology and Mineral Resources of Yunnan*, 1990]. We did not observe the top of the Baoxiangshi and Lijang Fm., however, Chinese maps indicate that the section is capped unconformably to the north of Jianchuan by a massive conglomerate sequence, and locally capped south of Jianchuan by a Miocene fossil-bearing, interbedded siltstone and coal sequence [*Bureau of Geology and Mineral Resources of Yunnan, 1990*]. The Baoxiangshi and Lijiang formations and the overlying conglomerate sequence do not contain distinctive index fossils, thus their age can only be constrained from the stratigraphic record to be in

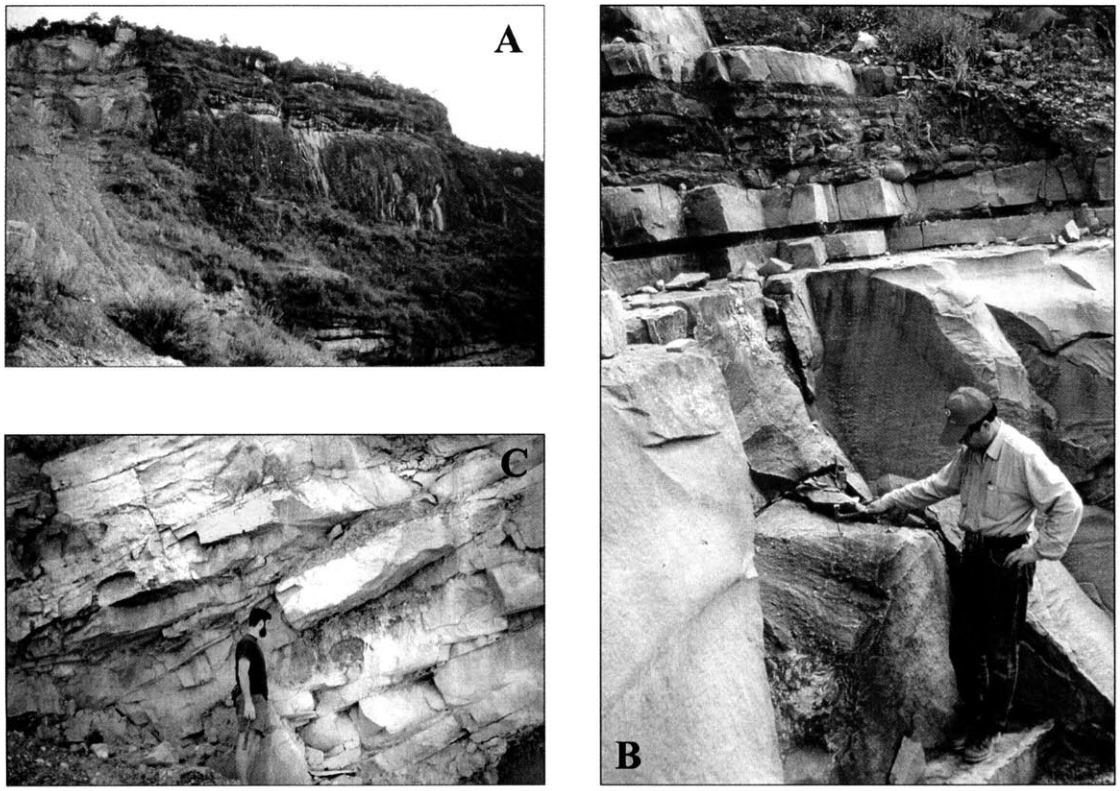

Figure 3.9: a) View east of the Baoxiangshi Fm. near Jianchuan. b) Close-up photograph of the Baoxiangshi Fm., massive sandstones with sections of interbedded mudstones and thin sandstone units. c) Close-up of thickly-bedded sandstone units at Nanjian.

between Paleocene and Miocene in age. This sandstone sequence lies within the Jianchuan basin complex, which is a complicated area of sediments that range from Paleocene to the Quaternary and are intruded by a series of sub-volcanic syenites and trachytes, that are in some locations as old as 22-35 Ma [*Schärer et al.*, 1990; *Schärer et al.*, 1994] and in places intrude sediments mapped as Pliocene [1:200,000 map, *Bureau of Geology and Mineral Resources of Yunnan, 1990*]. However, tight age constraints for the Baoxiangshi and Lijang formations are difficult to establish because of the poor exposure of direct cross-cutting relationships between these intrusives and the sedimentary sequence in the Jianchuan Basin.

Three additional isolated outcrops of less well-exposed fluvial sandstone sequences similar to the section at Jianchuan can be traced south along the Yangpai River and into the modern Red River drainage (Figure 3.8). These outcrops are characterized by massive, well-sorted medium to coarse-grained sandstone beds with occasional fine laminations, thin

mud-drapes, and occasional fossiliferous mud intervals (Figure 3.9c). Ripples and rip-up clasts are also common. The upper-most section of the northern-most locality (Xiahou) is capped by fossiliferous strata and grey clays. The sandstone beds at Nanjian (Figure 3.9c) contain cross-beds and are also irregularly interbedded with fine-grained siltstone. All of these sections rest unconformably on the Mesozoic-early Tertiary Yangbi redbed basin and are mapped as Pliocene, however no distinctive index fossils are present [*Bureau of Geology and Mineral Resources of Yunnan*, 1990]. Unlike the gently-warped sandstone units of the Baoxiangshi and Lijang formations, these three outcrops show tectonic tilting, most likely related to either extensional faulting bounding the Diancang Shan (Xiaho) or strike-slip faulting on strands of the Red River Fault (Weishan and Nanjian). Thermochronology in the Diancang Shan suggests that extensional exhumation began 4.7 Ma [*Leloup et al.*, 1993], thus constraining the age of sediments at Xiahou to be at least older than early Pliocene.

Role of Drainage Reversal in Capture Events

The capture of the Upper Yangtze River away from the Red River is not a typical capture event. At the location of the Yangpai Gap, the river makes an anomalous $\sim$150 km hairpin loop (Figure 3.8 and 10). From his sketch of the paleo-drainage of northwestern Yunnan *Lee* [1933], proposed that the bend geometry had resulted from a capture event between two originally south-flowing tributaries of the Yangtze River. This is supported by large, deeply incised, barbed tributaries of the north-flowing segment of the river loop that indicate a paleo-course that flowed to the south (Figure 3.10). The Yalong River has a similar geometry suggesting that the same coupled capture/reversal event has also determined the Yalong course (Figure 3.10). This combination of reversal/capture separates the wind-gap and the capture point along the channel. Thus in the case of both the Yangtze and the Yalong rivers, the wind gap is located at the southern terminus of the first bend, while the capture point is about $\sim$100-150 km to the north at the apex of the second bend in the river (Figure 3.10).

As discussed above, possible reversal/capture events along the east-west flowing section of the Middle Yangtze would have also diverted the originally south flowing tributaries

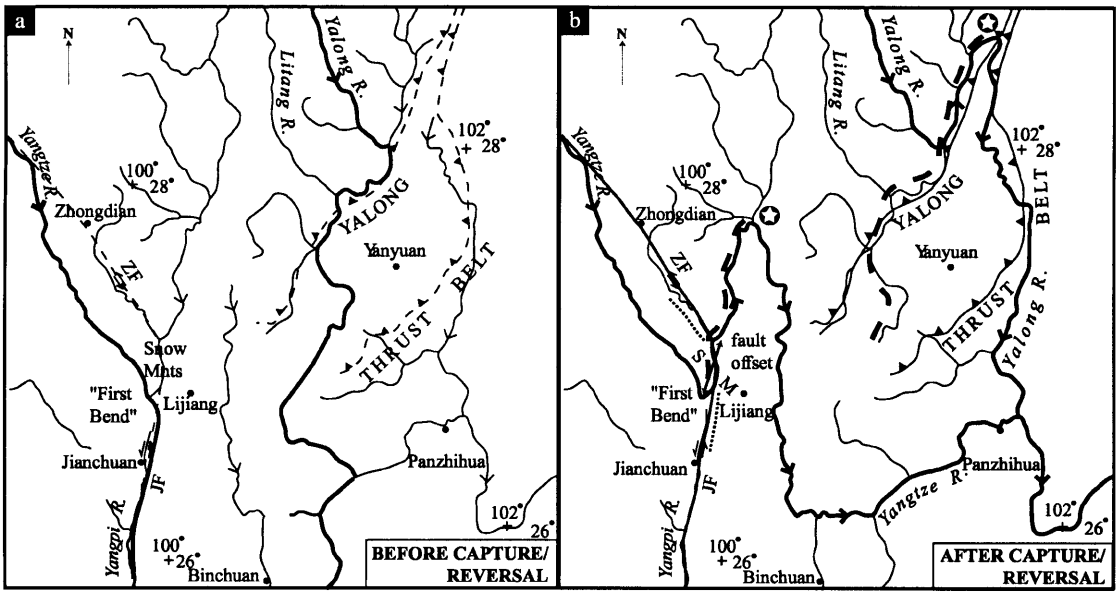

Figure 3.10: Reconstruction of Yalong and Yangtze River loops. a) Proposed reconstructed river pattern, prior to reversal and capture. Arrows represent direction of flow along main rivers. b) Modern river pattern, after proposed capture and reversal events. Heavy line indicates major river course of the main Yangtze and main Yalong Rivers, dashed heavy line indicates segment of river that reverses flow direction and star symbol marks the point of capture. Both Yangtze and Yalong River loops occur along strike of the Yalong Thrust Belt, which is suggested to have a few tens of kilometers of horizontal displacement in Oligo-Miocene time [*Burchfiel, et al.*, 1995]. Possibly uplift along the Yalong Thrust Belt, and its southward projection into the Yangtze River, induced backtilting and reversal of tributaries to the Yalong and Yangtze River, resulting in capture of the Upper Yangtze and Yalong rivers to the east. A small segment of the Yangtze loop can be attributed to offset along the Zhongdian/Jianchuan Fault [*Wang et al.*, 1998]. Thinly-dotted line represents location of possible pre-capture paleo-channel. Abbreviations are as follows: ZF = Zhongdian Fault and JF = Jianchuan Fault.

of the Red River (such as the Yalong and Dadu/Anning rivers) into the east flowing Yangtze [*Lee*, 1933; *Barbour*, 1936] (Figure 3.7). Determination of the paleo-drainage reconstruction of the secondary captures of the Yalong and Dadu/Anning Rivers are more elusive, because the principle paleo-drainage pattern runs parallel to active graben structures and paleo-river channel sediments can be difficult to distinguish from graben fill in active tectonic basins. Further field studies are needed to reconstruct the drainage pattern in this area in more detail, possibly from drill core and shallow seismic data that would be able to identify paleo-river sediments and sediment architecture in less well exposed areas.

3.3.4 Upper Mekong/ Red River capture

Just north of the first wind gap separating the Upper Yangtze River from the Red River, is the "Three Rivers" area where the Yangtze, Mekong and Salween are separated by narrow, closely spaced divides (Figure 3.1). In the "Three Rivers" area, there is a remnant surface preserved between the Mekong and Yangtze rivers with overlying flat-lying Eogene sediments [1:200,000 map, *Bureau of Geology and Mineral Resources of Yunnan*, 1990]. Near the northern extent of this "Three Rivers" area, along the Mekong River, there are two broad, low gradient barbed tributaries that flow north into the modern south-flowing Mekong River (Figure 3.8). Miocene, Pliocene and Quaternary sediment are preserved in both tributary valleys [1:200,000 map, *Bureau of Geology and Mineral Resources of Yunnan*, 1990; *Wang et al.*, 1998].

In the southern tributary basin (Madeng Basin), Mesozoic sediments from the Lanping-Simao tectonic unit extend across nearly the entire basin as isolated hills which suggests that the Neogene and Quaternary sediments in the basin are probably quite thin [*Wang et al.*, 1998] (Figure 3.8). The Tongdian Fault runs through the Madeng Basin, however the sense of offset and amount of Late Cenozoic activity is disputed [e.g. *Leloup et al.*, 1995; *Wang et al.*, 1998], and the resulting control on the morphology of the basin due to the tectonic activity is uncertain. Compared to the valley where the Jianchuan Fault is located (south of the Yangtze river bend), the Madeng Basin is a much broader, flat floored valley, suggesting either greater fluvial dissection or extensional fault activity.

From recent field work in the southern tributary valley (Madeng Basin), we observed: 1) deformed fine-grained, coal bearing sediments and clays at the north end of the valley, 2) faulted volcaniclastic sediments at the southeastern margin to the basin, and 3) dissected broad Pleistocene alluvial fans. None of these sediments cropping out in the basin could be linked to a through-flowing fluvial system, and therefore did not provide conclusive evidence for a paleo-river course of a southflowing Mekong river through this valley. However, the geographic position, geometry and morphology of the valley is suggestive of a wind-gap geometry between the Upper Mekong River and the Red River (Figure 3.8).

We propose that the original course of the Mekong River was through the northern and

southern wind gaps and then south along the Yangpai River where, in this reconstruction, it would have converged with the reconstructed course of the paleo-Upper Yangtze River before flowing through the Erhai gap to the Red River. Thus we propose that the Mekong River was a major tributary to the Red River system prior to the reorganization of drainage lines in southeastern Tibet. Likewise, the sediment in the catchments of the Upper Mekong River would have contributed to the deposition of the offshore sediment in the Gulf of Tonkin in the South China Sea [*Metivier et al.*, 1999].

3.3.5 Upper Salween/ Red River capture

Reconstruction of the Salween River is speculative because it has been affected by the young and active deformation and uplift of the region near the eastern Himalayan syntaxis that affects the "Three Rivers" area. The deformation in this area appears to have disrupted the topography of the area and obscured any potential paleo-river courses. Clearly some strike-slip shear must have occurred in the area where the modern Salween bends to the northwest around the eastern Himalayan syntaxis in the region of the Three Rivers area [e.g. *Hallet and Molnar*, 2001]. However, we suggest that the area of strike-slip shear is confined to the local region where the erosion surface has been strongly disrupted ("Three Rivers" area [Figure 3.1]). However, we propose that shear in the "Three Rivers" area must at least be limited to the area between the Mekong, Salween and upper Irrawaddy rivers, because of remnants of erosion surface are preserved between the Mekong and Yangtze rivers with flat lying Eogene sediments mantling the surface in this location [1:200,000 map, *Bureau of Geology and Mineral Resources of Yunnan*, 1990].

We could not distinguish the original course of the Salween River prior to uplift and deformation of the "Three Rivers" area: either the modern course of the Salween represents the original drainage line or the Upper Salween was captured away from the Red River in a manner similar to the Upper Mekong and Upper Yangtze Rivers. If the Upper Salween has been captured, we speculate that capture of the Salween River may have occurred over a relatively low divide at about 28° 30′ N, where a large tributary to the Salween makes an anomalous loop in the vicinity of a high peak, Mt. Moinigkawagarbo (6740 m) (Figure

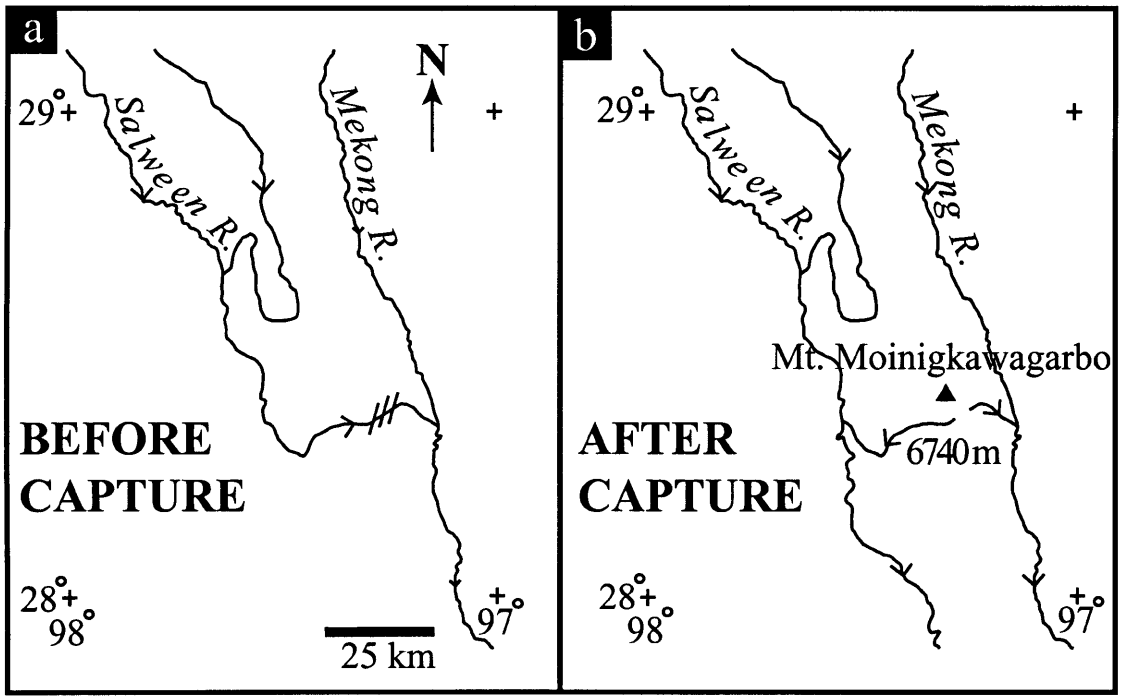

Figure 3.11: Speculative reconstruction of Salween River capture. a) Prior to river capture, the Upper Salween may have been a tributary to the Upper Mekong, and thus the paleo-Red River system. b) We propose that the course of the Salween may have been captured by a steeper river to the south (the modern Lower Salween River) aided by defeat of the original river course into the Mekong by uplift at Mt. Moinigkawagarbo. However, this reconstruction is highly speculative because localized deformation in this area near the eastern Himalayan syntaxis would have obscured any paleo-river courses if they existed.

3.11).

3.3.6 Tsangpo/Brahmaputra capture

In the vicinity of the eastern Himalayan syntaxis, the east-west flowing Tsangpo River makes an abrupt, tight loop, turning south through an extremely steep gorge into the north-south flowing Brahmaputra River, and eventually draining into the Bay of Bengal. Many authors have proposed that a river capture event is responsible for the unusual drainage pattern and deep incision near this bend in the river course, and assign the Tsangpo's original course through the Parlung River to the Lhuit or Irrawaddy rivers [e.g. *Burrard and Hayden*, 1907; *Seeber and Gorniz*, 1983; *Koons*, 1995; *Brookfield*, 1998; *Zeitler*, 2001].

The geometry of this river suggests that the paleo-Tsangpo River was originally similar in length and gradient to the other major rivers draining the southeastern plateau margin, but that it has recently been captured by one of the short, steep transverse Himalayan rivers (the Brahmaputra River). This drainage pattern/capture geometry is similar to that of the Dadu-Anning capture along the eastern plateau margin where a short, steep transverse river (Dadu River) has captured one of the large tributaries to the Yangtze River (the paleo-Anning River), making an abrupt change in river course at the point of capture.

Major barbed tributaries to the Parlung River indicate a southeastward paleo-flow direction [*Burchfiel et al.*, 2000]. The headwaters of the Parlung are separated from the Lhuit and then the Irrawaddy by low, wide passes in a wind-gap geometry (Figure 3.12). The proposed capture points of the paleo-Tsangpo-Parlung River lie in the region of the disputed border between India, China and Burma. Because of inaccessibility and limited available topographic data, we cannot evaluate the possibility of preserved of fluvial sediments in these passes. Tentatively, we propose that the paleo-Tsangpo drained through the Parlung River (flowing southeast) into the Irrawaddy River, and that the paleo-Tsangpo-Parlung-Irrawaddy River was first captured by a steep-gradient section of the upper Lhuit River, and most recently was captured by the Brahmaputra. It is possible that the Tsangpo was also a tributary to the Red River system (Figure 3.3). However, because deformation near the syntaxis must be taken into account, and because the morphology is highly disrupted and inaccessible, it is impossible to identify conclusively the original course for the Tsangpo without careful sediment provenance work in offshore basins.

3.3.7 Summary of drainage line and drainage basin reconstruction

Restoration of the capture events discussed in this paper yield a paleo-regional drainage pattern that resembles a large-scale dendritic network (Figure 3.13). Such abundant evidence for river capture suggests that some, if not all, of the peculiarity of the modern river drainage basin morphology is due to reorganization of drainage lines instead of shear deformation of the drainage basins by active tectonism as proposed by *Hallet and Molnar* [2001] .

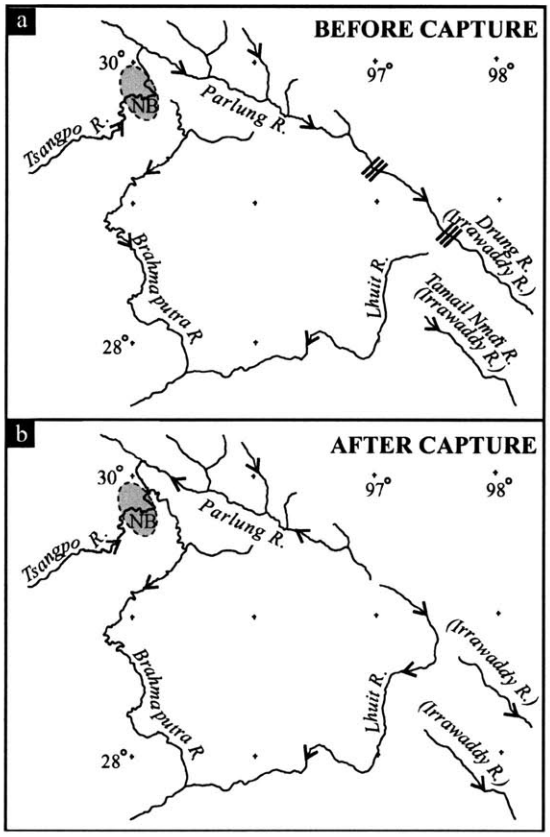

Figure 3.12: Reconstruction of Tsangpo-Brahmaputra River capture. a) Prior to capture, the paleo- Tsangpo River flowed into the Irrawaddy River. Shaded area represents the topographic expression of the Nambshebarwa massif (NB) b) The Tsangpo River was likely first captured by the Lhuit River then subsequently by the Brahmaputra River.

Examination of the geometries of the different capture events described here yield three different types of capture. The first type is where a longer, orogen parallel river (behind the range front) is captured by an aggressive, steep transverse river. This type of capture produces an identifiable right-angle bend (or very tight bend) in map view, at the terminus of a steep mountain range. The second type consists of the complicated coupled reversal/capture events that have taken place on the Yangtze River and major Yangtze tributaries. The third type, demonstrated by the Mekong River and possibly the Salween, can be described as a lateral capture, where the drainage direction of the original river course and the capturing river are close to parallel, as opposed to the first example of the transverse river capture, where the two rivers are orthogonal, and the captured river produces a sharp bend

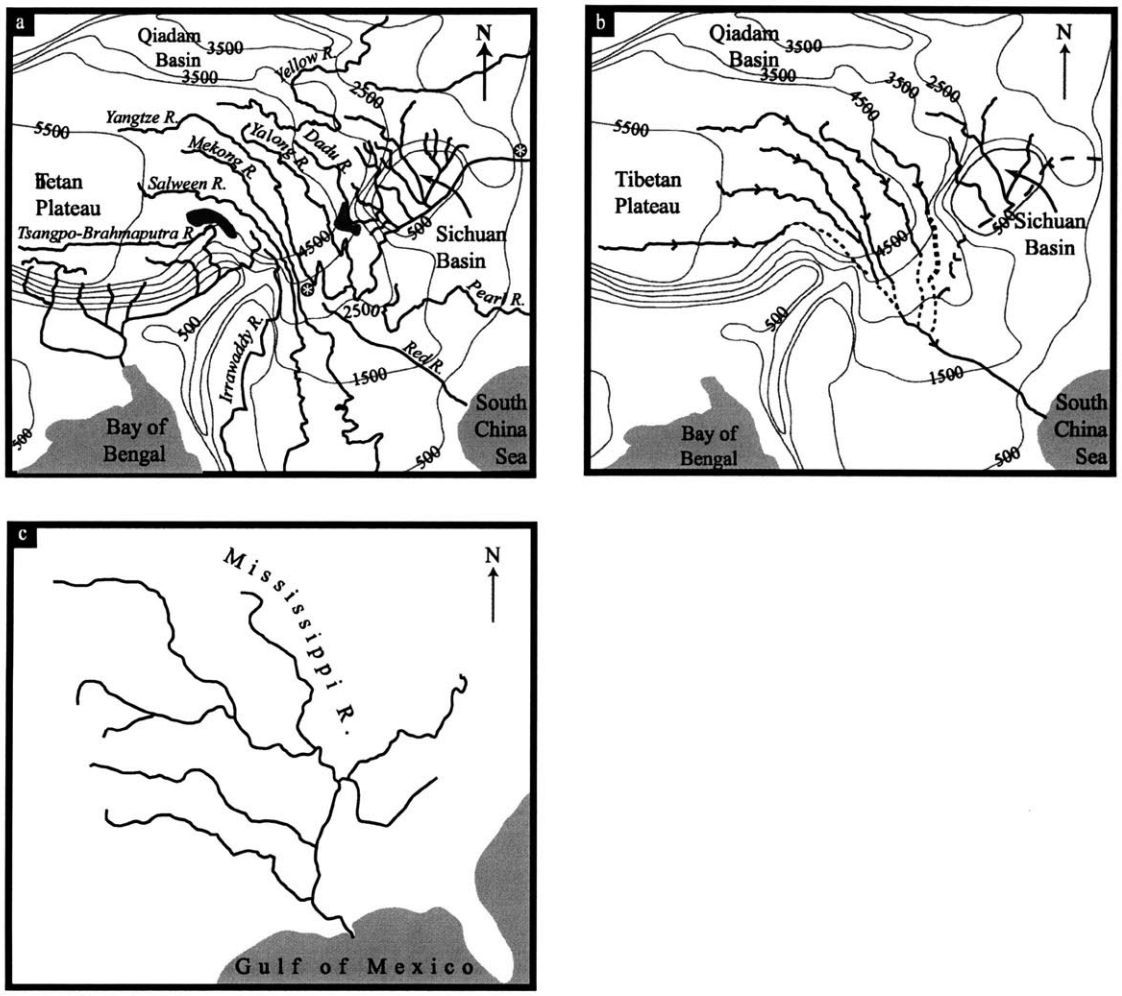

Figure 3.13: Reconstruction of major river captures in eastern Tibet. a) Modern major river courses in eastern Tibet. Solid grey areas represent the areas of sub-regional uplift of the Nyainqentanglha Shan and the Daxue Shan. Asterisk symbols mark segment of the Middle Yangtze River that reverses flow direction. b) Reconstructed river courses (direction and path) prior to major river capture and reversal events. c) Example of regional scale dendritic patterns of low-relief continental interiors: Mississippi R. of the U.S.A. [*U.S.G.S.*, 1993] at the same scale as the reconstruction in b).

in the course of the river.

Figure 3.14 (color) illustrates what happens to basin morphology when we restore the drainage lines according to the capture events described in the previous section. When all the drainage lines are restored, the original (Lower) Yangtze Basin is a large coastal basin draining to the East China Sea (Figure 3.7a). The Red River drains most of the continental interior to the south-southeast, while the Mekong, Salween and Irrawaddy are linear coastal basins draining to the south (Figure 3.14a [color]). After reversal and capture of the Upper Yangtze, and the major tributaries of the Middle Yangtze to the east, the former Lower Yangtze basin is enlarged, extended to the west, and now includes more than half of the original Red River drainage area (Figure 3.14b [color]). Capture of the Upper Mekong, Upper Salween, and Tsangpo Rivers into the Lower Mekong, Lower Salween and Irrawaddy basins, produces a "bottleneck" basin shape (Figure 3.14c [color]). The Tsangpo-Brahmaputra drainage looks like it was part of the bottleneck basin, but became decapitated, losing its headwaters to a steeper, more aggressive trans-Himalaya river (Figure 3.14d [color]).

Reconstruction of major river captures in eastern Tibet. a) Modern major river courses in eastern Tibet. Solid grey areas represent the areas of sub-regional uplift of the Nyainqentanglha Shan and the Daxue Shan. Asterisk symbols mark segment of the Middle Yangtze River that reverses flow direction. b) Reconstructed river courses (direction and path) prior to major river capture and reversal events. c) Example of regional scale dendritic patterns of low-relief continental interiors: Mississippi R. of the U.S.A. [*U.S.G.S.*, 1993] at the same scale as the reconstruction in b).

3.4 Timing of drainage reorganization and surface uplift rates

The timing and geometry of individual capture events and drainage reversals can be used to place constraints on the magnitude and rates of surface uplift. Although the timing constraints for these captures are not well known, in the following section we outline tentative

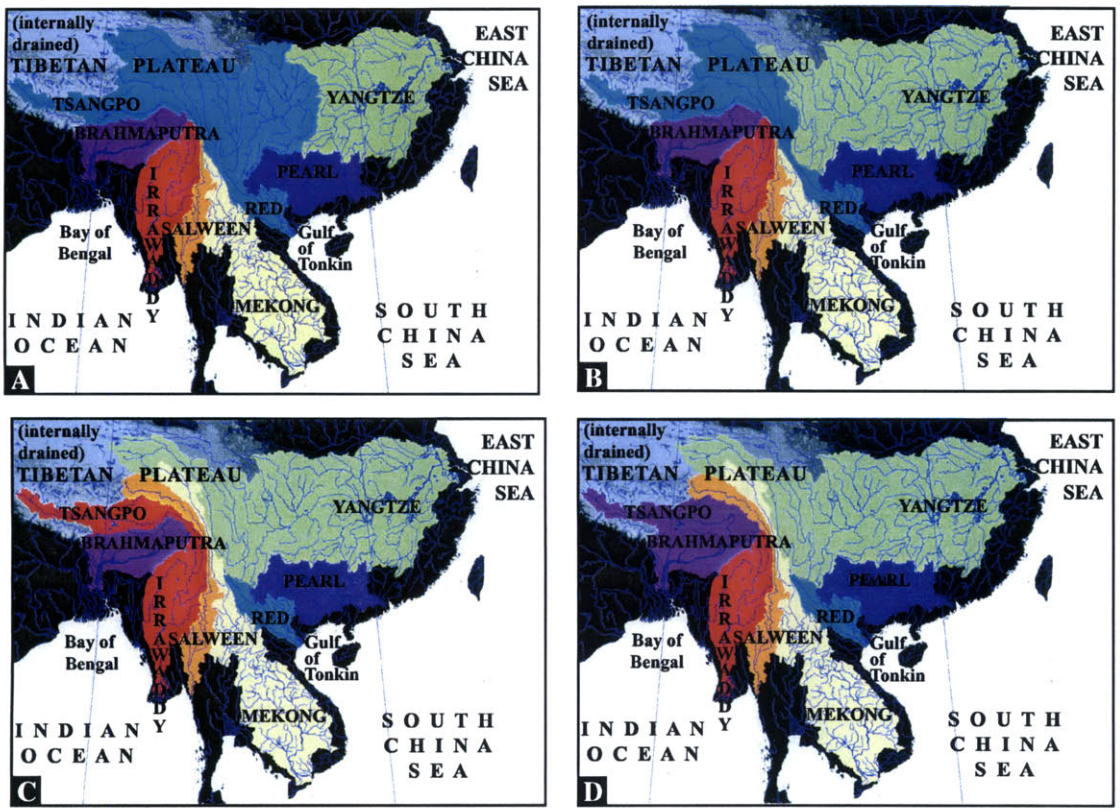

Figure 3.14: Changes in drainage basin morphology by reconstruction of drainage lines due to river capture/reversals of major rivers in Eastern Tibet. Colors represent individual drainage basins drawn on top of grayscale topography (topography and drainage basin outlines are derived from publicly available HYDRO1K digital topography data [*U.S.G.S.*, 1993]). a) Interpreted pattern prior to the major captures, where the Upper Yangtze, Middle Yangtze, Upper Mekong, Upper Salween and the Tsangpo rivers drained together to the South China Sea through the paleo- Red River (blue). b) Capture/reversal of the middle Yangtze River redirects drainage away from Red River and into the East China Sea through the Lower Yangtze River (green). c) Capture of the Upper Yangtze River to the east into the Lower Yangtze River, and the Upper Mekong and Upper Salween rivers into their modern drainage positions (green, yellow and orange respectively). Also, capture of the Tsangpo River to the south through the Irrawaddy River (red). d) Capture of the Tsangpo River through the Brahmaputra River into its modern course (pink). This final configuration is the modern drainage basin pattern.

estimates based on published geologic and thermochronometric data.

3.4.1 Dadu/Anning River capture

The sediments preserved in the wind gap between the Dadu and Anning rivers are assigned a Pliocene age [1:200,000 map, *Bureau of Geology and Mineral Resources of Sichuan*, 1991], but these sediments do not have direct paleontologic control. Their age has been tentatively assigned by correlation with similar lithologies of the Xigada Formation that are dated 300 km to the south on the Yangtze River (X. Zhang, personal communication). The Dadu-Anning capture point is associated with an area of anomalously high topography of sub-regional extent (the Daxue Shan and adjacent areas), and the local, uplifted areas of the Gonga Shan massif (Figure 3.4). Low-temperature thermochronometric ages from this area suggest rapid uplift of Gonga Shan and the Daxue Shan compared to the surrounding region since at least late-Miocene time [*Xu and Kamp*, 2000; *Clark et al.*, 2000; *Clark et al., 2001*].

The location of the capture point with respect to the region of anomalously high topography and to the proximity of the Sichuan Basin, suggests that the river capture event is likely related to the aggressive headwater retreat of a small transverse river draining the steep Longman Shan/Sichuan Basin plateau margin and the defeat of the paleo Dadu-Anning river course due to the uplift of the Daxue Shan/Gonga Shan region. Timing of the initiation of uplift of these areas may approximate or provide a lower bound on the timing of river capture. Recent elevation transects of low-temperature thermo-chronometric data (U-Th)/He and apatite/zircon fission track) along the Dadu River suggest a period of slow exhumation that continues from at least 25 Ma to ~8 Ma, followed by rapid exhumation that continues to the present time [*Xu and Kamp*, 2000; *Clark et al.*, 2000]. We interpret the change in exhumation rates to reflect initiation of rapid river incision. Development of the high relief, steep Sichuan Basin margin is interpreted from thermochronometric data that indicate rapid cooling at the basin margin beginning at ~5-12 Ma [*Kirby et al.*, 2002]. High bedrock terraces located along the Dadu River upstream of the capture point (Figure 3.4c and 5c) are interpreted as remnants of the fluvial channel of the paleo Dadu-Anning prior to

capture. These terraces are located approximently 1 - 2.5 km below the average elevation of nearby plateau surface, indicating significant incision of the paleo Dadu-Anning River prior to capture and an additional 800 meters of incision following capture (Figure 3.4c). We expect that capture may be coeval or postdate the initiation of river incision and the uplift interpreted for the Longman Shan plateau margin, therefore, we suggest that capture of the Dadu/Anning is probably younger than ~12-5 Ma.

3.4.2 Brahmaputra/Tsangpo capture

Wind gaps and capture points associated with the paleo- Tsangpo-Irrawaddy, and the Parlung-Irrawaddy courses occur in an area of both sub-regional anomalously high topography (Nyainqentanglha Shan *senso-stricto*), as well as localized rapid uplift (Nambshebarwa massif), both of which disrupt a regional low-relief relict landscape (Figure 3.2c, 12 and 13a). The location of the capture points within the broad high area of the Nyainqentanglha Shan and the proximity of the capture point to the Himalaya topographic front suggest that both aggressive headwater retreat of trans-Himalayan rivers (i.e. the Brahmaputra and the Lhuit rivers) and the uplift of the Nyainqentanglha Shan contributed to river capture (Figure 3.13a). However, the post-capture river course of the Tsangpo-Brahmaputra rivers cross-cuts an area of localized, structural uplift of the Nambshebarwa massif, located just to the south of the sub-regional topographic high of the Nyainqentanglha Shan [e.g. *Zeitler et al.*, 2001]. The cross-cutting relationship suggests that the river course is antecedent to the local uplift associated with the Nambshebarwa massif itself (Figure 3.13a), allowing us to suggest that the capture of the Tsangpo by either the Lhuit River or the Brahmaputra River was prior to ~4 Ma, based on the suggested age of the uplift of the massif [*Burg et al.*, 1998]. River capture prior to the development of the Nambshebarwa massif involving the paleo-Tsangpo would have allowed this river to become sufficiently entrenched in its course so that subsequent uplift would not alter the present river course across the massif.

3.4.3 Middle Yangtze River reversal and capture of Upper Yangtze River

The successive capture events associated with the Middle Yangtze River reversal, terminating in the capture of the Upper Yangtze River, offer an excellent opportunity to correlate the timing of river capture with initiation of major plateau development. It is critical to recognize that reversal of drainage flow direction is thought to occur when a river has a very low longitudinal gradient and is typically not deeply incised into a bedrock gorge [i.e. *Ollier and Pain*, 1997; *Summerfield*, 1991]. In the specific case of the Upper Yangtze and Yangtze tributaries, the wind gaps associated with capture are in broad valleys with elevations not far below the elevation of the regional relict landscape that defines the plateau surface across the southeastern margin. Therefore we infer that the drainage reversals and associated captures along the Yangtze and its tributaries must have occurred when the rivers were flowing in valleys close to the regional low-relief erosion surface, most likely as alluvial rivers, and not in the deeply incised bedrock gorges in which they now flow. Thus the timing of drainage reversal/capture offers the opportunity to establish a lower bound on the timing of the development of significant regional relief and the crustal thickening that is associated with the development of the eastern plateau margin. We can estimate the amount of surface uplift along a section of reversed drainage by using the paleo-course of the river as a horizontal datum. This datum allows us to estimate the total surface uplift since the time of capture.

In the previous section, we discussed our interpretation that drainage flow-direction reversal of a major segment of the Yangtze River consisted of a sequence of river reversals and westward headward erosion over small segments of the river, leading to successive capture tributary basins (Figure 3.7). In this manner, the timing and initial reversal at the Three Gorges area, the capture of the Jialing River, and the capture of the upper Yangtze River at the "First Bend" bound the time period in which the Middle Yangtze River and its tributaries underwent significant reorganization. We can estimate the magnitude of surface uplift along the Middle Yangtze River since reversal and subsequent captures by comparing the elevation of the river valley in the Sichuan Basin (average elevation $\sim$500 m), which does

not appear to have experienced significant surface uplift in Cenozoic time, with the current elevation of wind-gaps and abandoned channels that formed along the south-flowing Middle Yangtze River. The Yangpai gap and all of the other wind gaps that would be related to the southerly course of the Yangtze and its tributaries (Yalong, Dadu/Anning), are currently at ~2500 m elevation. This suggests that ~2000m of surface uplift in the location of the southeastern plateau margin, along strike of the wind gaps, has occurred since the capture of the Upper Yangtze River.

It will be critical to understand better the timing of the capture of the Upper Yangtze, since it is the last capture that takes place along the reversal of the Middle Yangtze River, therefore offering the tightest constraint on the timing of plateau uplift in this area.

The eastward captures of both the Upper Yangtze and Yalong rivers appear to be associated with portions of the rivers that reversed their flow direction, giving rise to "hairpin" loops in the modern river courses (Figure 3.10). The northeastern of these two loops, the Yalong loop, is spatially correlated with the Yalong Thrust Belt, which has been interpreted as the southward continuation of the Longmen Shan Thrust Belt [*Burchfiel et al.*, 1995; *Wang et al.*, 1998]. The thrust faults are parallel to the two river "limbs" that make up the Yalong loop, and the thrust belt projects along strike to the Yangtze loop, although it does not outcrop there [*Burchfiel et al.*, 1995; *Wang et al.*, 1998] (Figure 3.10). We propose that Tertiary activity along these structures may have back-tilted the rivers, inducing or aiding reversal and capture. Assuming that the reversal of a segment of river is associated with the capture, we suggest that the capture event occurred prior to regional uplift of the plateau margin, and also prior to or coeval with the local uplift along the Yalong Thrust Belt. By correlation with the Longmen Shan Thrust Belt, the Yalong Thrust Belt experienced a few tens of kilometers of shortening during Oligo-Miocene time [*Burchfiel et al.*, 1995]. Therefore, an Oligocene to mid-Miocene estimate for the timing of activity on the Yalong Thrust Belt (30-10 Ma), and an estimate of ~2 km of surface uplift along the reversed segment of the Middle Yangtze River, allows us to assign a very speculative range of *averaged* surface uplift rates of ~0.1 mm/yr (0.07-.2 mm/yr).

3.5 Tectonic implications of reconstructed drainage patterns

Capture events affecting major rivers of southeastern Tibet have been proposed in disparate works by many authors for nearly a century [e.g. *Abendanon*, 1907; *Burrard and Hayden*, 1907; *Gregory and Gregory*, 1925; *Lee*, 1933; *Barbour*, 1936; *Tregar*, 1965; *Koons*, 1995; *Brookfield*, 1998; *Metivier et al.*, 1999]. Compilation of these observations in a regional tectonic context, combined with new field work and DEM analyses, yields a salient first order pattern to the drainage history of the southeastern Tibetan Plateau. We suggest that the modern drainage pattern can most easily be understood with the restoration of individual capture events as proposed for the major rivers of southeastern Tibet. Thus reorganization of drainage lines by capture and reversal events can explain most of the peculiar shapes of the drainage basins of these rivers, without having to appeal to large magnitude tectonic shear [*e.g. Hallet and Molnar*, 2001].

We stress that this interpretation does not preclude some amount of horizontal shear affecting the shapes of the drainage basins (e.g. dextral shear strain accommodating the relative northward movement of India with respect to Eurasia, especially in the "Three Rivers" area). However, we propose that surface uplift, rather than horizontal shear strain, has been the primary control on the drainage basin morphology, as uplift has induced changes in drainage lines due to river capture and reversal of flow along major river segments. Disruption of the drainage pattern due to local deformation around the eastern Himalayan syntaxis appears mainly limited to the Tsangpo-Irrawaddy and Salween drainage basins where they curve westward around the syntaxis. A smaller amount of distributed shear strain could have modified the shape of the uppermost Salween, Mekong and Yangtze rivers. We do not agree that the drainage lines as they exist today were in place prior to the onset of the Indo-Asian collision (i.e. prior to $\sim$55 Ma) because of the abundant geomorphic evidence of river capture and reversal. We also favor the interpretation that the Tsangpo-Irrawaddy and the Salween were originally major tributaries to the paleo-Red River system and have been subsequently captured by headward erosion of the Irrawaddy and Lower Salween Rivers, not originally individual major drainage basins that have been deformed into their present

morphology.

The observations presented here underscore the importance of the reorganization of drainage lines during uplift and erosion of eastern Tibet, and demonstrate how the development of major drainage patterns are related to the uplift history of the plateau margin. The capture events described here for the major rivers in eastern Tibet are related to uplift at local, sub-regional and regional scales- thus offering the possibility of understanding and relating tectonic phenomenon over a broad range of scales.

The Dadu-Anning and the Tsangpo-Brahmaputra River captures have similar geometries and appear to be related to sub-regional uplift of the plateau adjacent to steep plateau margins. Both involve the capture of a relatively long, large drainage line of moderate to low gradient by a short, steep transverse river that drains a steep plateau margin. Both captures are spatially correlated with sub-regional areas of extreme relief and anomalously high topography that also disrupt the erosion surface which defines the eastern plateau, and are associated with very young low-temperature thermochronometric ages. We observe a spatial correlation of these areas of high relief and high topography with concave-indentations (in plan view) of steep plateau margins (Figure 3.13a). These indentations develop in areas where we interpret weak lower crustal material from beneath the plateau to be flowing around areas in the foreland where lower crustal flow is essentially absent. Geodynamic modeling suggests that these topographic, thermochronometric, and structural observations may be consistent with dynamic topography produced by lower crustal flow [*Clark et al.*, 2001].

In contrast, the reversal of the Middle Yangtze River and capture of its major tributaries to the East China Sea appear to have resulted from the large scale initiation of plateau uplift along the entire southeastern Tibetan plateau margin. The proposed piecewise reversal of the Middle Yangtze is not associated with any single structure nor set of related structures along the Middle Yangtze. Broad scale tectonic uplift or tilting of the plateau margin would likely be a candidate for the cause of such a regional scale reversal. However, the more local scale reversed segments of river at the capture points of the Yalong and Yangtze bends may be related to activity on local structures.

The reconstruction of drainage lines in this paper suggests that the paleo-drainage net-

work of southeastern Tibet resembles the large scale dendritic patterns observed in continental interiors commonly developed in areas of low regional relief (i.e. the Mississippi, the Amazon, the Zaire (Congo) Rivers) (Figure 3.13c, Figure 3.14 [color]). We propose that the initial drainage patterns of eastern Tibet were formed on a regional low-relief landscape (i.e. low paleo-topographic gradients), on the order of what is observed in continental interior basins. We suggest that the timing of river capture/reversals and the onset of reorganization of regional drainage patterns predate, or are coeval with, initiation of plateau uplift in eastern Tibet.

Understanding the paleo-courses of these rivers and the changes in drainage pattern not only yields information about surface uplift and surface uplift rates, but also about the lengthscale of surface uplift. Comparison of modern and reconstructed drainage patterns suggest that, with the exception of border between the high, flat plateau and the gently sloping plateau margin, where the Yalong and Yangtze loops have formed, we do not observe evidence for drainage pattern disruption as might be expected by formation of a steep plateau margin propagating through the eastern foreland in time. Therefore, we suggest that the uplift of eastern Tibet most likely occurred over long wavelengths.

Acknowledgments

This research was supported by the Continental Dynamics program at the National Science Foundation (EAR-961497 and EAR-0003571), NASA (NAG5-6062), and by a National Science Foundation Graduate Fellowship (MKC). We thank David Mohrig, Peter Clift, Eric Kirby, and Simon Brocklehurst for helpful discussions on various aspects of this work. Simon Brocklehurst contributed to preparation of this material for Spring AGU 2000, which I greatly appreciate (MKC). Historical research on many early geomorphic studies of eastern Tibet could not have been achieved without the skilled efforts of Joe Hankins and Katherine Keefe at Lindgren Library at MIT, and Jim O'Donnell at the Geological and Planetary Sciences Library at Caltech. We especially thank Peng Dong, drivers, and staff at the Chengdu Institute of Geology and Mineral Resources, drivers and staff from the Yunnan Institute of Geology and Mineral Resources, Katra Andreini, Martha House, and Michael Stewart for

their assistance and expertise during our field work.

3.6 References

Abendanon, E. C., Structural geology of the middle Yang-Tzï-Kiang gorges, *J. Geol., 16*, 587–616, 1908.

Barbour, G. B., Physiographic history of the Yangtze, *Geogr. J., 87*, 17–34, 1936.

Brookfield, M. E., The evolution of the great river systems of southern Asia during the Cenozoic India-Asia collision: rivers draining southwards, *Geomorphology, 22*, 285–312, 1998.

Burchfiel, B. C., Z. Chen, Y. Liu, and L. H. Royden, Tectonics of the Longman Shan and adjacent regions, central China, *Int. Geol. Rev., 37*, 661–735, 1995.

Burchfiel, B. C., M. K. Clark, E. Wang, Z. Chen, Y. Liu, and G. Pan, Tectonic framework of the Namche Barwa region, eastern Himalayan syntaxis, SE Tibet, *Geol. Soc. Am. Abstr. Programs, 32*(7), A–33, 2000.

Bureau of Geology and Mineral Resources of Sichuan Province, *Regional Geology of Sichuan Province*, Geological Publishing House, Beijing, 1991.

Bureau of Geology and Mineral Resources of Yunnan Province, *Regional Geology of Yunnan Province*, Geological Publishing House, Beijing, 1990.

Burg, J-P., P. Nievergelt, F. Oberli, D. Seward, P. Davy, J-C. Maurin, Z. Diao, and M. Meier, The Nambshe-Barwa syntaxis: evidence for exhumation related to compressional crustal folding, *J. Asian Earth Sci., 16*, 239–252, 1998.

Burrard, S. G., and H. H. Hayden, *Geography and geology of Himalayan Mountains and Tibet, part 3: the rivers of Himalaya and Tibet*, 119–230, Government of India Press, Calcutta, 1907.

Chen, Z., B. C. Burchfiel, Y. Liu, R. W. King, L. H. Royden, W. Tang, E. Wang, J. Zhao, and X. Zhang, GPS measurements from eastern Tibet and their implications for India/Eurasia intercontinental deformation, *J. Geophys. Res., 105*, 16,215–16,227, 2000.

Clark, M. K., and L. H. Royden, Topographic ooze: building the eastern margin of Tibet

by lower crustal flow, *Geology, 28*, 703–706, 2000.

Clark, M. K., L. H. Royden, J. Bush, B. C. Burchfiel, and X. Zhang, Sub-regional dynamic topography and deformation of the lower crust by decoupled channel flow in Tibet, *Eos Trans. AGU, (82)* Fall Meet. Suppl., Abstract T11H-06, 2001.

Clark, M. K., M. A. House, L. H. Royden, B. C. Burchfiel, X. Zhang, W. Tang, and Z. Chen, River incision and tectonic uplift in eastern Tibet from low-temperature apatite U-Th/He thermochronology, *Eos Trans. AGU, 81*(48), Fall Meet. Suppl., 1102, 2000.

Cox, K. G., The role of mantle plumes in the development of continental drainage patterns, *Nature, 342*, 873–877, 1989.

Cox, R. T., Analysis of drainage-basin symmetry as a rapid technique to identify areas of possible Quaternary tilt-block tectonics: an example from the Mississippi Embayment, *Geol. Soc. Am. Bull., 106*, 571–581, 1994.

Dirks, P. H. G. M., C. J. L. Wilson, S. Chen, Z. Luo, S. Liu, Tectonic evolution of the NE margin of the Tibetan Plateau; evidence from the central Longman Mountains, Sichuan Province, China, *J. Southeast Asian Earth Sci., 9(1-2)*, 181–192, 1994.

Gregory, J. W., and C. J. Gregory, The geology and physical geography of Chinese Tibet, and its relations to the mountain system of south-eastern Asia, from observations made during the Percy Sladen Expedition 1922, *Philos. Trans. R. Soc. London Ser. B, 213*, 171–298, 1925.

Gregory, J. W., *The structure of Asia*, 227 p., Methuen and Co. Ltd., London, 1929.

Hack, J. T., Stream profile analysis and stream-gradient index, *J. Res. U. S. Geol. Surv., 1*, 421–429, 1973.

Hallet, B. and P. Molnar, Distorted drainage basins as markers of crustal strain east of the Himalaya, *J. Geophys. Res., 106*, 13,697–13,709, 2001.

Houvius, N., Macroscale process systems of mountain belt erosion, in *Geomorphology and Global Tectonics*, eds. M. A. Summerfield, pp. 77–105, John Wiley and Sons, Ltd., 2000.

Howard, A. D., Drainage analysis in geologic interpretation: a summation, *AAPG Bull., 51*, 2246–2259, 1967.

Howard, A. D., Long-profile development of bedrock channels: Interaction of weathering,

mass wasting, bed erosion, and sediment transport, *in Rivers Over Rock: Fluvial Proesses in Bedrock Channels*, Tinkler, K. J., and Wohl, E. E., eds., Volume 107: Geophysical Monograph: Washington, D. C., Amerian Geophysical Union, pp. 297–319, 1998.

Howard, A. D., and G. Kerby, Channel changes in badlands, *Geol. Soc. of Am. Bull., 94*, 739–752, 1983.

Jackson, J., and M. Leeder, Drainage systems and the development of normal faults: an example from Pleasant Valley, Nevada, *J. Struct. Geol., 16*, 1041–1059, 1994.

King, R. W., F. Shen, B. C. Burchfiel, L. H. Royden, E. Wang, Z. Chen, Y. Liu, X. Zhang, J. Zhao, and Y. Li, Geodetic measurement of crustal motion in southwest China, *Geology, 25*, 179–182, 1997.

Kirby, E., P. W. Reiners, M. A. Krol, K. X. Whipple, K. V. Hodges, K. A. Farley, W. Tang, and Z. Chen, Late Cenozoic evolution of the eastern margin of the Tibetan Plateau: Inferences from $^{40}Ar/^{39}Ar$ and (U-Th)/He thermochronology, *Tectonics, 21, 10.1029/2000TC001246*, 2002.

Kirby, E. and K. X. Whipple, Quantifying differential rock-uplift rates via stream profile analysis, *Geology, 29*, 415–418, 2001.

Kirby, E., K. X. Whipple, W. Tang, and Z. Chen, Distribution of active rock uplift along the eastern margin of the Tibetan Plateau: inferences from bedrock channel longitudinal profiles, *J. Geophys. Res.*, in press.

Koons, P. O., Modeling the topographic evolution of collisional belts, *Annu. Rev. Earth Planet. Sci., 23*, 375–408, 1995.

Lave, J. and Avouac, J. P., Active folding of fluvial terraces across the Siwaliks Hills, Himalayas of central Nepal, *J. Geophys. Res., 105*, 5,735–5,770, 2000.

Lee, C. Y., The development of the upper Yangtze Valley, *Bull. Geol. Soc. China, 13*, 107–117, 1933.

Leloup, P. H., T. M. Harrison, F. J. Ryerson,, W. Chen, Q. Li, P. Tapponnier, R. Lacassin, Structural, petrological and thermal evolution of a Tertiary ductile strike-slip shear zone, Diancang Shan, Yunnan, *J. Geophys. Res, 98*, 6,715–6,743, 1993.

Leloup, P. H., R. Lacassin, P. Tapponnier, U. Schäerer, D. Zhong, S. Lui, L. Zhang, S.

Ji, and P. T. Trinh, The Ailao Shan-Red River shear zone (Yunnan, China), Tertiary transform boundary of Indochina, *Tectonophysics, 251*, 3–84, 1995.

Li, S., and W. D. Mooney, Crustal structure of China from deep seismic sounding profiles, *Tectonophysics, 288*, 105–113, 1998.

Metivier, F., Y. Gaudemer, P. Tapponnier, and M. Klein, Mass accumulation rates in Asia during the Cenozoic, *Geophys. J. Int., 137*, 280–318, 1999.

Merrits, D., and K. R. Vincent, Geomorphic response of coastal streams to low, intermediate, and high rates of uplift, Mendocino junction region, northern California, *Geol. Soc. Am. Bull., 101*, 1373–1388, 1989.

Oberlander, T. M., Origin of drainage transverse to structures in orogens, in *Tectonic geomorphology*, Proceedings of the 15^{th} annual Binghampton Symposia in Geomorphology, 155–182, 1985.

Ollier, C. D., *Tectonics and landforms*, 324 p., Longman, New York, 1981.

Ollier, C. D., and C. F. Pain, Equating the basal unconformity with the paleoplain: a model for passive margins, *Geomorphology, 19*, 1–15, 1997.

Paola, C., and D. Mohrig, Palaeohydraulics revisited: palaeoslope estimation in coarse-grained braided rivers, *Basin Res., 8*, 243–254, 1996.

Potter, P. E., Significance and origin of big rivers, *J. Geol., 86*, 13–33, 1978.

Royden, L., B. C. Burchfiel, R. W. King, E. Wang, Z. Chen, F. Shen, and Y. Liu, Surface deformation and lower crustal flow in eastern Tibet, *Science, 276*, 788–790, 1997.

Seeber, L., and V. Gornitz, River profiles along the Himalayan arc as indicators of active tectonics, *Tectonophysics, 92*, 335–367, 1983.

Schäerer, U., P. Tapponnier, R. Lacassin, P. H. Leloup, D. Zhong, and S. Ji, Intraplate tectonics in Asia: a precise age for large-scale Miocene movement along the Aliao Shan-Red River shear zone, China, *Earth Planet. Sci. Lett., 97*, 65–77, 1990.

Schäerer, U., Z. Lian-Sheng, and P. Tapponnier, Duration of strike-slip movements in large shear zones: the Red River belt, China, *Earth Planet. Sci. Lett., 126*, 379–397, 1994.

Shen, F., L. H. Royden, and B. C. Burchfiel, Large-scale crustal deformation of the Tibetan Plateau, *J. Geophys. Res., 106*, 6793–6816, 2001.

Snyder, N. P., Whipple, K. X., Tucker, G. E., and Merritts, D. J., Landscape response to

tectonic forcing: Digital elevation model analysis of stream profiles i the Mendocino triple junction region, northern California, Geol. Soc. Am. Bull., 112, 1,250–1,263, 2000.

Summerfield, M., it Global geomorphology, 537 p., Longman Group Ltd., Essex, England, 1991.

Ting, V. K., Notes of a geological traveller, *Independent Review, 48*, 11–12, 1933.

Tregar, T. R., *A geography of China*, 342 p., University of London Press, London, 1965.

U.S. Geological Survey, *Digital elevation models, data user guide, 5*, pp. 1-50, U.S. Geological Survey, Reston, Virginia, 1993.

Wang, E., B. C. Burchfiel, L. H. Royden, L. Chen, J. Chen, and W. Li, Late Cenozoic Xianshuihe-Xiaojiang, Red River, and Dali fault systems of southwestern Sichuan and central Yunnan, China, *Geol. Soc. Am. Spec. Paper, 327*, 1998.

Wang, E., and B. C. Burchfiel, Late Cenozoic to Holocene deformation in southwest Sichuan and adjacent Yunnan, China, and its role in formation of the southeastern part of the Tibetan plateau, *Geol. Soc. Am. Bull., 112*, 413–423, 2000.

Whipple, K. X. and G. E. Tucker, Dynamics of the stream-power river incision model: Implications for height limits of mountain ranges, landscape response timescales, and research needs, *J. Geophys. Res., 104*, 17,661–17,674, 1999.

Xu, G., and P. Kamp, Tectonics and denudation adjacent to the Xianshuihe Fault, eastern Tibetan Plateau; constraints from fission track thermochronology, *J. Geophys. Res., 105*, 19,231–19,251, 2000.

Zeitler, P., A. S. Meltzer, P. O. Koons, D. Craw, B. Hallet, C. P. Chamberlain, W. S. F. Kidd, S. K. Park, L. Seeber, M. Bishop, and J. Shroder, Erosion, Himalayan geodynamics, and the geomorphology of metamorphism, *GSA Today, 11*(1), 4–9, 2001.

Zernitz, E. R., Drainage patterns and their significance, *J. Geol., 40*, 498–521, 1932.

Zhao, C., R. Xu, and S. Wang, The special long reversed river section in the Yangtze River reaches, *Geology and Mineral Resources of South China, 3*, 37–38, 1997.

Chapter 4

Incipient bedrock river incision in southeastern Tibet constrained by low-temperature thermochronology

Abstract

The timing of bedrock river incision initiation offers a powerful constraint on the age of plateau uplift in eastern Tibet. The topographically high eastern plateau and southeastern plateau margin are defined by an uplifted, low-relief "relict" landscape representing a time of slow erosion governed by low elevation and low uplift conditions that dominated prior to uplift of the modern plateau. Preservation of this "relict" landscape allows us to relate the initiation of rapid erosion by incipient bedrock river incision to the development of high topography in eastern Tibet. Apatite (U-Th)/He and apatite fission-track thermochronology from elevation transects beneath the plateau surface (defined by the "relict" landscape) and in the major river gorges suggest rapid erosion along the southeastern Tibetan plateau margin commenced by ~7-13 Ma. These ages are broadly contemporaneous with the reported timing of uplift in the Longmen Shan, initiation of clockwise rotation of crustal fragments around the eastern Himalayan syntaxis, and intensification of the southeast Asian monsoon. The superposition of these events may suggest a relationship between the onset of

crustal thickening and the establishment of the modern-day strain pattern, as well, underscore the potential synergy between surface uplift and climate.

4.1 Introduction

The Tibetan Plateau is an extensive, topographically high plateau with average elevations of ~5 km over an area approximately equal to that of the eastern United States (Figure 4.1). Models of the tectonic evolution of orogenic plateaus, such as Tibet, depend critically on knowledge of the patterns of plateau growth, for example: Did the plateau grow progressively or episodically? How rapidly did the plateau attain its present-day elevation? When did plateau uplift initiate and has it reached a maximum elevation? The first two questions bear on rheologic models of continental deformation and the control of rheologic or structural heterogeneity in the distribution of deformation. The latter is critical for relating plateau growth to far-field tectonic events, mantle dynamics and changes in regional or global climate. It is generally agreed that the elevated region of the plateau is related to the early Eocene Indo-Asian continent-continent collision [e.g. *Rowley et al.*, 1996], however the spatial and temporal patterns of topographic development remain intensely debated.

The development of such an expansive region of high topography has also generated arguments about the feedback systems between tectonics and climate, suggesting for example that intense erosion of the Himalaya is responsible for the drawdown of atmospheric CO_2 leading to Cenozoic global cooling [*Raymo et al.*, 1988] and that plateau uplift is linked to intensification of the Asian monsoon [*Ruddiman and Kutzbach*, 1989; *Prell and Kutzbach*, 1992; *Prell and Kutzbach*, 1997]. Thus, the study of spatial and temporal variations in plateau development offers an opportunity to address the interaction between tectonics, surface uplift, and climate.

The topographic evolution of Tibet is difficult to directly measure. Paleo-elevation has therefore been inferred by a variety of means including by upper crustal shortening [e.g. *Kapp et al.*, in press], the onset of east-west extension in the central plateau [e.g. *Harrison et al.*, 1992; *Pan and Kidd*, 1992; *Williams et al.*, 2001], the appearance of potassic volcanism [e.g. *Chung et al.*, 1998], paleobotany [e.g. *An et al.*, 2000], and the oxygen isotopic

composition of paleo-waters [*Rowley et al.*, 2001]. While the differences in uplift ages produced by these different studies may reflect real spatial variation in surface uplift, each method suffers from the limitation that it relies on first-order assumptions about the relationship of crustal deformation, climate conditions or mantle dynamics to the development of high topographic relief. In this paper we use a more direct approach to dating of uplift of eastern Tibet by dating the initiation and rates of incision of major river systems into the eastern Tibetan Plateau using (U-Th)/He and fission-track dating on apatites collected from the walls deeply incised river gorges that cross the southeastern plateau margin. This should offer a straightforward estimate of the age of surface uplift because the initiation of river incision into the relict landscape of the plateau margin reflects a major change in erosional conditions that can be directly related to the development of high topography. These unique landscape relationships that allow us to relate river incision to surface uplift are described in the next section.

4.2 Geomorphology of southeastern Tibet: Relict landscapes and incised river gorges

Recent field work and DEM analysis show that remnant, local areas of a low-relief landscape (< 600m) are geographically continuous across long distances (>1000 km) and define the maximum elevation of the gently dipping southeastern plateau margin [*Clark et al.*, submitted A] (Figure 4.2). Regional continuity of this landscape and reconstruction of paleo-river patterns [*Clark et al.*, in press], suggest that a relict (pre-modern plateau) landscape of low regional relief (less than 1 km) near sea level existed across southeastern Tibet prior to uplift of the modern plateau margin. The continuity of these remnants suggests that the landscape probably experienced a protracted period of slow erosion over a regional extent. Surface remnants are geographically continuous from plateau elevations of near 5 km to low elevations near 1 km, dipping to the southeast, where they merge with the present-day low-elevation, low-relief landscape along the coastal margins of southern Asia. This implies that the relict low-relief landscape, which mantles southeastern Tibet,

was at low-elevations prior to uplift and long wavelength tilt of the southeastern plateau. Glacial modification of this landscape is minor and has occurred only locally in areas of high elevation (generally > 5000 m). We use the modern altitude of the relict landscape can be used as a datum to measure surface uplift related to plateau development.

The major rivers that cross the southeastern plateau margin have cut substantial gorges up to 3.5 km deep (Figure 4.3). This deep fluvial dissection has not yet progressed entirely through the landscape and large perched (elevated) remnants of the relict, pre-uplift landscape are still preserved. This relict landscape is locally mantled by early Tertiary sediment, indicating that little exhumation of this landscape surface has occurred since early Tertiary time. The preservation of remnants of this older landscape is of great importance in constraining the uplift history of Tibet because it not only provides a datum for measuring surface uplift, but also establishes a datum by which to measure the total amount of fluvial incision that has occurred since uplift of the modern plateau margin. River gorges that are entrenched into an elevated remnant landscape require that uplift occurred prior to or coeval with the initiation of major river incision because elevated topography is necessary in order to create the deep river canyons observed in eastern Tibet today. Thus the approximate time of initiation of rapid fluvial incision in eastern Tibet probably indicates the initiation of uplift of the eastern Tibetan Plateau although intensification of regional precipitation during and/or after could potentially contribute to the acceleration of erosion rates. Low-temperature age dating techniques used to estimate exhumation rate through time offer the opportunity to determine or limit the age of river incision in eastern Tibet.

4.3 Apatite (U-Th)/He and fission-track data

Apatite (U-Th)/He thermochronology (reflecting time since sample passed through the "partial retention zone" ~40-80 ° C; [*Wolf et al.*, 1996; *Farley*, 2000]) and apatite fission-track thermochronology (reflecting the time in which a sample passed through the "partial annealing zone" 60 - 110 ° C; [e.g. *Laslett et al.*, 1987]) yield ages which reflect the residence time of samples in the shallow crust. These two thermochronometric systems are well-suited to studying the Cenozoic development of the eastern Tibetan Plateau margin

because of the extreme depth of the river gorges that have excised up to 3.5 km of crustal section beneath the mantling relict landscape that defines the plateau and plateau margin. This exposure potentially has exhumed rocks with apatite (U-Th)/He or fission-track ages directly related the bedrock river incision.

Analysis of samples collected along elevation transects using low-temperature thermochronology allows one to determine (or estimate) exhumation rate [e.g. *Wagner and Reimer*, 1972] and changes in the exhumation rate can be used to identify tectonic or erosional exhumation events. Along such transects, elevation is usually taken as a proxy for depth beneath a surface held at constant temperature (usually the surface of the earth, assumed to be at 5 - 10 $^{\circ}$C). The rate at which closure ages change downward along an age-elevation transect yields an exhumation rate, assuming that the regional geothermal gradient and surface temperature remain constant through time. In general, gentle age-elevation gradients indicate slow exhumation and steep gradients imply rapid exhumation and inflection points on age/elevation diagrams are used to determine the timing of tectonic or erosional events.

We analyzed 42 samples from granitoids over a region of the high eastern plateau and the topographically highest portions of the southeastern plateau margin for apatite (U-Th)/He dating. A subset of 8 samples was used for apatite fission-track analysis [analyses performed by Raymond A. Donelick at Apatite to Zircon, Inc., Viola, Idaho, U.S.A.]. Samples were collected from several elevation transects above the Yangtze River and its major tributaries, the Yalong and Dadu rivers and others were collected from various parts of the high relict landscape (Figure 4.4 and 4.5; Table 4.1). Rugged terrain, limited accessibility, and exposure of appropriate lithologies for helium dating prohibited collection of a complete $\sim$3 km vertical transect from the plateau surface to the bottom of the valley gorge in any single locality. Consequently, we collected individual elevation transects covering as great an elevation range as possible in multiple localities. Below we discuss the samples collected and analyzed within each of the individual elevation transects (river gorges) or local portions of the high relict landscape.

4.3.1 Apatite (U-Th)/He ages: Sample preparation and analytical techniques

Apatite separates for (U-Th)/He analyses were produced from eastern Tibet granitoids collected during field campaigns in 1998 and 2001 (Table 4.1). Grains were initially selected for euhedral morphology and scanned for visible inclusions of potentially high U or Th-rich phases under a $\sim$190 power binocular microscope using cross-polars. Prior to analysis, grains were measured for the α-ejection correction [*Farley et al.*, 1996; *Farley*, 2000].

Helium outgassing was performed by both furnace heating and laser heating procedures outlined in *House et al.* [1999] and *House et al.* [2000] respectively. Furnace samples are denoted as such in Table 4.1. Additional single-grain laser replicate analyses were performed on a subset of the furnace samples in order to demonstrate consistency between the two techniques used for this survey. In so far as possible, we attempted to two or more single grain analyses (or two or more multiple grain aliquot analyses) for each sample, although not all samples yielded sufficient quality material (Table 4.2). Replicate data for multi-grain aliquot furnace samples represent an averaging of many grains compared to the replicate data of sample transects which were performed on single grains. For multiple-grain aliquots a mass-weighted average was used for the F_t correction.

While lithology of a particular sample played the primary role in grainsize and quality of available grains, the lower blanks, and the single-grain analyses afforded by laser analysis resulted in overall lower analytical uncertainties, smaller F_t corrections, and a higher number of replicate analyses. Analyses that were performed with furnace heating techniques required multi-grain aliquots of uniform grainsize. Because apatite yields were generally low from these samples, small-grainsizes were necessary to obtain uniform multi-grain aliquots. Laser techniques that were developed in 1999, afforded single-grain analyses and allowed us to use a larger grainsize (because fewer uniformly-sized grains were needed), which resulted in smaller F_t corrections for alpha-ejection. Because of age variation with grainsize, and because large α-emission corrections are required for small grains, we limited our dataset to include grains of radii 34 - 80 m, resulting in typical α-ejection corrections of 18-35% (F_t = 0.65 - 0.83; Table 4.2). Analyses with F_t corrections

of less than 0.65 were excluded (Table 4.2).

Following initial outgassing of ^{4}He, samples were heated a second time in order to potentially identify excess He in the sample that may indicate the presence of undetected, problematic U or Th rich phases which introduce "parentless He" and result in erroneously old ages [*House et al.*, 1997]. Samples producing He during this "re-extract" step were excluded (Table 4.2). After outgassing, grains were retrieved, dissolved and spiked with ^{235}U and ^{230}Th and analyzed in a Finnigan Element inductively couple plasma mass spectrometer (ICPMS). Anomalously high ratios of Th/U possibly indicate the presence of Th rich phases (such as monazite) which can be undetected under microscope inspection prior to analysis and unidentified in the re-extraction step following He outgassing [*Farley*, 2002]. We have excluded these anomalous analyses (Table 4.2). Low He yields (near blank level) are susceptible to implantation from surrounding phases, and are also excluded from our final results (Table 4.2). Other analyses were excluded due to the loss of the apatite grain during the analysis or due to incomplete helium outgassing (Table 4.2).

The number of replicate analyses varied with the amount and quality of sample material. Some samples simply did not yield sufficient quality material to obtain a meaningful age, or in some cases to obtain more than one replicate analysis. We averaged 3.5 analyses for all samples with multiple replicates (33 samples), and were only able to obtain single replicate analyses on 5 samples. 4 of our 42 analyzed samples did not yield any reliable ages (i.e. all attempted analyses were excluded for reasons identified in Table 4.2 and discussed above) and 13 samples collected during this survey (mostly granitoids and a few metamorphic rocks) did not yield sufficient quality apatite for analysis.

Propagated errors on He ages based on the analytical uncertainty in U, Th, and He measurements are 4% (2σ) for laser samples and 6% (2σ) for furnace samples [*Farley*, 2002], however we report a 6% (2σ) uncertainty for individual analyses (Table 4.2) based on the reproducibility of laboratory standards [*Farley*, 2002]. Our data, which was collected from a range of geographic localities and different rock units that vary in composition and age, display considerably more scatter (a larger spread) in replicate ages from single samples than consistent with lab standard reproducibility. Thus we use the standard deviation of the spread of the replicate analyses reported at 1σ and 2σ (Table 4.3) for each sample as

our uncertainty estimate, which is a more conservative approach than citing the analytical uncertainty or reproducibility of laboratory standards [e.g. *House et al.*, 2001; *Bevington and Robinson*, 1992; *Davis*, 2002; *Lyons*, 1991]. This error estimate is larger than the analytical error alone and is intended to reflect the age uncertainty due to differences in grain size, minor crystal defects, zoning of parent material and other factors which may contribute to grain to grain differences in He age and uncertainties in the α-ejection correction [i.e. *House et al.*, 2001]. For samples with accompanying apatite fission-track data (AFT), age/elevation data are shown in adjacent plots (Figure 4.6). AFT data are plotted as pooled (mean) ages (large open symbols) with reported 1σ and 2σ uncertainty (Table 4.4).

4.3.2 Sample description and ages

In the following section, we describe results from four transects that were collected in river gorges (Danba, Yalong, Anning, Dadu, Kanding and Gonga) and two transects that were collected near or across the plateau surface (Daocheng and Pamai). Age/elevation plots for individual sample transects show individual replicate analyses (small open symbols) and calculated mean ages for samples with more than one replicate analysis (large solid symbols) for (U-Th)/He data with reported uncertainties at 1σ and 2σ (Table 4.2 and 4.3; Figure 4.6). Where applicable, apatite fission-track data is also plotted with large open symbols (pooled (mean) age) with reported errors at 1σ and 2σ (Table 4.4; Figure 4.6.

Danba transect

Five Mesozoic granite samples in the Danba transect were collected from the north-central Dadu River [*Bureau of Geology and Mineral Resources, Sichuan,* 1991](Table 4.1; Figure 4.4 and 4.5) which is a tributary to the Yangtze River. These samples were collected over an elevation range of between 2100 - 3000 m and across a horizontal distance of a few km. These samples yield uniformly high quality apatite (glassy, euhedral, inclusion-free grains) for (U-Th)/He thermochronology with an average grain radius of 56 μm which resulted in typical F_t corrections of $\sim$0.75 (Table 4.2). Three to six single-grain replicate

analyses were performed on each sample by laser methods. Mean ages were calculated for the entire transect and range from 9.35 - 5.50 Ma, defining a steep, positive correlation with elevation (Table 4.3; Figure 4.6A). Across this entire transect, ages on individual replicate analyses vary on average 13% from the calculated mean age for that sample.

We performed apatite fission-track analyses (AFT) on all five samples in the Danba transect (Table 4.4). Pooled AFT ages range from 8.43 to 10.5 Ma and define a steep positive age/elevation gradient similar to the (U-Th)/He analyses (Figure 4.6B). Mean track lengths for these samples range from 13.44 - 13.96 μm. The highest three samples are within error of the (U-Th)/He data. The average difference between the pooled AFT and mean (U-Th)/He ages is 2.7 Myr, and 3.6 Myr for the lowest three samples only.

Yalong transect

Six samples from the Yalong transect were collected from three small Mesozoic granite plutons which outcrop in the main trunk stream of the Yalong River, which is also a tributary to the Yangtze River, and a deeply incised major tributary to the Yalong River [*Bureau of Geology and Mineral Resources, Sichuan*, 1991] (Figure 4.4 and 4.5). These samples were collected over an elevation range of 1620 - 2750 m (Table 4.1). The three lowest elevation samples were collected from the same pluton over a narrow horizontal distance (< a few km in the horizontal direction) directly in the main Yalong river gorge and the lowest two samples are within 200 m of each other. Because of lack of access to the cliff face directly above the three lowest samples, and the scarcity of exposed of granitoids in this region, the three highest samples were collected from a major, deeply incised tributary valley over a horizontal distance of 40 km.

Sample quality was variable and samples MC-01-(25 - 29) had particularly low apatite yield. We were able to obtain between 3 - 5 single grain replicate analyses, performed by laser methods, in all but one sample (MC-01-29) (Table 4.2). Average grain radius of these samples is 57 μm, resulting in an average F_t correction of 0.75. Across this entire transect, individual replicate analyses vary on average 31% from the calculated mean age. Mean ages were calculated for samples with more than one replicate analysis, and range from

4.6 - 10.78 Ma (Table 4.3). These ages define a steep, positive correlation with elevation, except for the lowest elevation sample in the transect (Figure 4.6C). This lowest elevation sample is significantly older than would be predicted from the age/elevation trend of the higher elevation samples.

The three lowest elevation samples were analyzed for apatite fission-track thermochronology. These pooled AFT ages range from 4.73 - 6.38 Ma (Table 4.4). Mean track lengths for these samples range from 13.47 - 13.93 μm. All three samples are within error of the (U-Th)/He data, and samples MC-01-26 and 27 have pooled AFT ages that are older than the mean (U-Th)/He ages. The Yalong fission-track data define a steep, slightly negative age/elevation gradient (Figure 4.6D).

Dadu transect

Six samples of Proterozoic granite that make up the Dadu transect were collected from the bottom of the lower Dadu River and up a small tributary valley which leads to a low-elevation divide that separates the Dadu and Anning rivers [*Bureau of Geology and Mineral Resources, Sichuan*, 1991](Figure 4.4 and 4.5). These samples were collected from elevations of 800 - 1450 m (Table 4.1). Quality of individual grains varied from fair to poor and sufficiently large grains were scarce. We were unable to obtain reliable analyses from samples MC-98-2 and MC-98-4 and because many of the Dadu transect samples were analyzed by multi-grain aliquots for furnace heating techniques, only one or two replicate analyses were possible for most of the samples on this transect because many analyses were excluded due to small grainsizes (Table 4.2). The average grain radius is 51 μm with an average F_t correction of 0.72. To compare the consistency between multi-grain and single grain analyses, we performed additional single-grain analyses on samples MC-98-12.

Across this entire transect, individual replicate analyses vary on average 34% from the calculated mean age. These samples show a moderate to low gradient, positive correlation between age and elevation with mean ages that range from 5.09 to 21.03 Ma (Table 4.3; Figure 4.6E).

Anning Transect

Five samples were collected from above the Anning River, a tributary to the Yangtze River (Figure 4.4 and 4.5). Samples Y-98-5 and MC-98-(18-20) are closely spaced over a horizontal distance of a few km and collected from Proterozoic granite [*Bureau of Geology and Mineral Resources, Sichuan*, 1991]. The lowest elevation sample, MC-98-17, was collected from a Mesozoic granodiorite located 55 km north from the other samples in the transect [*Bureau of Geology and Mineral Resources, Sichuan*, 1991]. These samples were collected over an elevation range of 1650 - 2350 m.

Sample quality of these samples was fair to poor for these samples and apatite yield was low. A combination of single-grain laser analyses and multi-grain aliquots furnace analyses were performed on these samples (Table 4.2). Many analyses from this transect have been excluded on the basis of grainsize (Table 4.2). The average grain radius is 52 μm with an average F_t correction of 0.75. Across this entire transect, individual replicate analyses vary on average 15% from the calculated mean. Mean ages for samples with 2 or more replicate analyses range from 16.98 to 18.18 Ma (Table 4.3). The ages on the Anning transect overlap with the Dadu transect, however the mean ages define a steeper age/elevation gradient than the Dadu transect (Figure 4.6F).

Daocheng transect

The ten samples analyzed for the Daocheng transect were collected from a single Mesozoic granitic pluton [*Bureau of Geology and Mineral Resources, Sichuan*, 1991](Figure 4.4 and 4.5). Samples were collected over an elevation range of 4620 - 3860 m. Samples MC-01-(37:42) were collected on the north side of the pluton across a distance of 20 km, and samples MC-01-(43:48) were collected on the south side of the pluton over a distance of 30 km.

Sample quality was variable. All samples in this transect were analyzed with single-grain laser techniques. Many individual analyses were excluded on the basis of extremely old ages in excess of the crystallization age of the granite or anomalous Th that may in-

dicate the presence of monazite inclusions not observed during ocular screening prior to analysis. Two of the ten samples did not yield sufficient quality material to obtain more than one replicate analysis (despite single-grain laser methods), and one sample did not yield any reliable analyses (Table 4.2). Many other samples collected in this area did not yield sufficient quality apatite to even attempt an analysis. Between 2 - 4 replicates were performed on all other samples. The average grain radius of these samples is 53 μm with an average F_t correction of 0.72.

Mean ages in the Daocheng transect are range from 50.04 - 112.30 Ma (Table 4.3). Across this entire transect, individual replicate analyses vary on average 19% from the calculated mean age. These ages are older and have a greater variance in the absolute ages of replicate analyses than do younger samples. However, the average percent spread of replicate analyses from the mean ages is not significantly different than other transects. The age/elevation gradient of the mean ages generally define a low-gradient trend indicating slow exhumation (Figure 4.6G), however there is more significant variation in mean ages about that trend than what is observed in other transects.

Pamai Transect

The Pamai transect contains only one sample collected from a Mesozoic granite [*Bureau of Geology and Mineral Resources, Sichuan*, 1991](Figure 4.4 and 4.5), at an elevation of 4000 m (Table 4.1). This sample was of good quality. Six replicate analyses (single-grain) were performed (Table 4.2). Replicate ages ranging from 52.90 - 69.19 Ma, with a mean age of 57.63 Ma (Table 4.3). Average grainsize for this sample is 59 μm with an average F_t correction of 0.76. Individual replicate analyses vary on average 7% from the calculated mean age. The low percent spread of replicate ages reflects good results on a single sample. The age of this sample is within the age range of samples on the Daocheng Transect which were also collected at or near the elevation of the relict landscape (Figure 4.6H).

Gonga Transect

Three samples were collected in the vicinity of Gonga Shan (7756 m), a region of anomalously high topography, intense fluvial and glacial dissection and extensional exhumation (Figure 4.4 and 4.5). These samples were not collected on a vertical transect, but rather from an area of over 100 km horizontal distance in a region defined by the anomalously high topography surrounding Gonga Shan. Samples were collected over an elevation range of 1150 - 3000 m (Table 4.1). Sample K1 comes from a granite batholith that appears on Chinese geologic maps as Mesozoic, but dates as young as Late Miocene have been reported for granites in this terrane 20 km south of our sample site (ca. 12.4±1.4 Ma; *Roger et al.*, [1995]). The rest of the samples come from a Proterozoic granite [*Bureau of Geology and Mineral Resources, Sichuan*, 1991].

Sample quality was variable. Analyses of samples from this transect were performed using both multi-grain aliquots as well as single-grain analyses (Table 4.2). Multiple replicates were possible on all samples and ranged from 2 - 6 replicates each. The average grainsize for this sample group is 42 μm, with an average F_t correction of 0.69. Mean sample ages range from 0.42 - 2.5 Ma and define a steep age/elevation gradient, steeper than the Dadu and Yalong transect data (Table 4.3; Figure 4.7A). Individual replicate analyses vary on average 28% from the calculated mean age.

Kanding Transect

Four samples were collected on the Kanding Transect from a Proterozoic granite [*Bureau of Geology and Mineral Resources, Sichuan*, 1991] (Figure 4.4 and 4.5), also in the vicinity of the high topography and intense erosion/uplift region associated with Gonga Shan. These samples were collected over an elevation of 1420 - 2520 m (depth of -1780 to -2880) and over a horizontal distance of 20 km in a small tributary valley to the Dadu River (Table 4.1). Sample quality was good. Three of these samples yielded multiple replicate analyses (3-4 replicate analyses per sample), while one sample failed to produce a reliable age (Table 4.2). Average grain radius for replicates in this transect is 53 μm and an average

F_t correction is 0.74. The mean ages range from 1.8 - 3.35 Ma (Table 4.3). These data define a steep age/elevation trend, similar to the Gonga transect. Individual replicate analyses vary on average 19% from the calculated mean age (Figure 4.7B).

4.3.3 Discussion of error and uncertainty in measured (U-Th)/He ages

The spread of ages between replicate analyses within single samples observed in this dataset could be due to many factors. For example, the correction for ejection of alpha particles from the apatite grain during radioactive decay of U and Th (F_t correction) assumes a homogeneous distribution of parent material. Extreme zoning of parent material may produce as much as $\pm$33% error in this correction [*Farley*, 2000]. Usually, for an order of magnitude variation in the concentration of parent material across the grain, errors produce in applying this correction should produce only a $\sim$10% error in the corrected age. Because this correction is based on an assumed ideal crystal geometry and is a function of the grain size and geometry, variable or irregular grain geometries within a samples population will also introduce error, and smaller grains (less than 0.85 F_t correction) are more sensitive to errors in this correction [*Farley*, 2000].

Other sources of error include undetected high U or Th mineral inclusions. Every effort is made to select inclusion-free grains for analysis by scanning each grain with a $\sim$ 190 power binocular microscope under plain and polarized light. However, inclusions may be parallel to the c-axis (possibly due to the exsolution of monazite) or extremely small [*House et al.*, 1999; *Farley*, 2002]. Many of these cases can be identified during a second heating procedure where helium produced from the grain is indicative of high U or Th phases and the sample replicate age is discarded (denoted as a re-extract, or "excess helium" on Table 4.2). Several individual replicate analyses in the Daocheng transect, as well as one sample on the Kanding transect, yield ages that are greater than the crystallization age or reported higher temperature thermochronology of the host rock and may be attributed to the presence of undetected inclusions (Table 4.2).

Grain to grain variation in diffusive properties coupled with long residence times in the partial retention zone for helium in apatite, may also be a source of scatter among

single-grain replicate ages within individual samples. Experimentally determined diffusivity values for helium vary little for most apatites [*Wolf et al.*, 1996; *Farley*, 2000], but at long residence times even slight grain to grain variability (zoning of parent distribution, cracks/defects, grainsize, etc.) will affect He loss from the crystal to a much greater extent than for samples that have rapidly cooled through the partial retention zone, leading to a significantly greater spread between replicate analyses [e.g. *House et al.*, 1999; *Reiners and Farley*, 2001]. Slow cooling through the PRZ could potentially contribute to the variability in the mean ages of the Daocheng samples because their age/elevation gradient suggests that these samples have been slowly exhumed (or slowly cooled) for at least 50 Myr. However, we do not observe a systematic correlation between grainsize and age in these samples, indicating that other factors (i.e. zoning, defects, etc.) contribute more significantly to the age variability within individual samples than grainsize. While there is more variability in the mean ages with respect to elevation than on other transects, the percent variability of individual replicates about the mean age is within the range observed on other transects.

4.3.4 Relationship of sample transects relative to relict, low-relief landscape of southeastern Tibet

Comparison of ages along our individual transects over a region of more than 300 km^2 requires that we consider our samples relative to a common surface datum beneath which the samples cooled (Figure 4.2 and 4.5). Exhumation rate and the timing of exhumation rate changes are most accurately determined when samples are plotted relative to a datum beneath which the shallow isotherms are horizontal. The regional low-gradient and low-relief surface of the relict landscape suggests that low-temperature isotherms may be parallel to this surface. Thus, for individual elevation transects, we determine the depth of each sample beneath local areas of preserved surface remnants (Table 4.1). This allows us to consider the elevation of individual transects in context with the uplift and deep river incision into the pre-modern plateau low-relief, low-elevation landscape.

The depth of each sample transect beneath the regional, relict landscape can be de-

termined by subtracting each sample elevation from the elevation of the nearest surface remnant. In most cases this yields a depth estimation that is within the local relief observed across the surface itself (< 600 m). Therefore, unless otherwise noted, the uncertainty of the depth estimate is ± 300 m. Some transects are in regions where there surface remnants are not preserved (due to intense fluvial/glacial dissection and/or localized uplift) and the depth determination for these transects can not be made. Other transects were collected in areas where the local surface remnants had less than average relief. Below we summarize the depth calculations for all transects.

The Danba and Yalong transects represent the deepest exposure beneath the relict landscape. The Danba transect was collected beneath a preserved surface remnant at an elevation of 4800 m. This surface has some indication of glacial modification. However, surfaces just to the west have not experienced glaciation and are at few hundred meters lower elevation. Glacial modification of this surface since incision of the Dadu River was probably limited to a few hundred meters, and not more than 500 meters.

The immediate area of the Yalong transect has experienced intense fluvial dissection, however remnant surfaces occur 50 km west of the transect and also occur extensively to the north and the south. Based on elevations of these nearby surface remnants we estimate the surface elevation for the Yalong transect to be 4500 m.

The Dadu and Anning transects represent an intermediate range of depth beneath the plateau surface. In the vicinity of the Dadu transect, a rare vertical offset of $\sim$1 km of the remnant surface occurs across the Xianshuihe Fault. Surface elevations are 4 km to the west and 3 km to the east of the sample transect. Therefore the depth determination of this transect has a greater uncertainty associated with it, than the other sample transects where samples can be tied to a single elevation datum (i.e. tied to a single surface with the uncertainty associated with the local relief). The Dadu samples lie to the west of the main strand of the Xianshuihe fault [*Wang et al.*, 1998], so we use the elevation of the surface remnants east of the Xianshuihe fault (3 km), within 30 km horizontal distance from sample transect, to calculate the depth of the Dadu transect samples.

The estimation of depth for the Anning transect suffers from the same complexity as the Dadu transect, although the offset in adjacent surface is less (500 - 1000 m). Since these

samples are east of the Xianshuihe fault, we elect to use a surface elevation of 3800 m.

The high elevation samples of the Daocheng transect were collected across the Daocheng surface, a planar erosional feature with elevations concordant with surrounding low-relief relict landscape surfaces [*Clark et al.*, in prep.]. Samples were also collected in river valleys that have incised up to 840 m beneath the average surface elevation. We estimate the average elevation of the pediment surface to be at 4700 m elevation. This surface remnant has less than average local relief, therefore the depth determination has smaller associated uncertainty ($\pm$150 m). This The Pamai transect contains only one sample and was also collected in a small river valley near the elevation of the relict landscape surface (4300 m). This area also has less than average local relief ($\pm$200 m. Samples from the Daocheng and Pamai transects represent a shallow range of depth beneath the relict landscape.

The Gonga and Kanding samples lie in an area of anomalously high topography and active uplift [e.g. *Roger et al.*, 1995; *Wang et al.*, 1998]. A depth determination from an original surface is difficult to estimate and assign uncertainty on because of the lack of preserved plateau surfaces and localized rapid uplift. Any estimation of a surface elevation can only be considered a minimum. We propose to simply consider these samples in their elevation context alone, because the relationship to the relict low-relief plateau surface is unknown.

4.3.5 Summary of age data

Sample transects in this survey can be divided into two groups. The first group consists of samples collected across remnant surfaces or in river gorges near areas where remnant surfaces are well preserved or can be reasonably estimated (i.e. Anning, Dadu, Danba, Daocheng, Pamai, and Yalong transects). The second group consists of samples that were collected from the Gonga Shan region (i.e. Gonga and Kanding transects), an area that is characterized by high relief, anomalously high topography, rapid erosion, and extensional faulting. The localized rapid uplift and erosion has erased the surface remnants in the immediate vicinity and these samples need to be evaluated separately from the first group.

Samples collected across remnants of the relict landscape up to a depth of $\sim$1 km below

the surface are from the Daocheng transect and a single sample from Pamai. Together, the mean ages from these samples generally define a positive low-gradient depth/age slope with ages that range from ~100 to 50 Ma. There is a gap between these samples collected near the plateau surface and samples collected from ~1500 - 3000 m below the relict landscape surface.

Samples from the Dadu transect were collected ~1500 - 2000 m below the plateau surface, and define a positive low-gradient age/elevation relationship that indicates slow exhumation from ~21 - 5 Ma. The Anning transect also overlaps the intermediate depth range of exposed crustal section in the river gorges of eastern Tibet, but the mean ages on the Anning transect define a steeper age/elevation gradient, indicating a greater exhumation rate from ~17 - 18 Ma than the Dadu samples.

Ages from depths of more than 2 km beneath the plateau surface come from the Yalong and Danba transects. These data define a steep depth/age trend that ranges from ~11 - 4.5 Ma suggesting that these samples experienced rapid exhumation. AFT track-lengths also suggest rapid cooling of these samples (Table 4.4). This gradient is well defined except for the lowest most sample on the Yalong transect (MC-01-25), which is anomalously old compared to the other samples at slightly higher elevations. Because this sample was collected within 200 m of sample MC-01-25 and within a few kilometers of sample MC-01-27, and because the apatite fission-track age on this sample does not show the age relationship with nearby samples, variations in geothermal gradient, lithology, or spatial variability in erosion rate are not likely to be the cause of the anomalous (U-Th)/He age. Thus we do not consider the results for sample MC-01-25 when constraining exhumation rates for eastern Tibet.

4.4 Thermal and erosional history of eastern Tibet

The age data presented in this study can be used to constrain the timing and rate of rapid river incision in southeastern Tibet. We first consider samples from the Danba transect, which represent some of the deepest exposures of crustal section beneath the relict landscape of eastern Tibet and therefore offer the best opportunity to determine thermochrono-

logic ages related to recent major river incision. The Danba samples were collected over a short horizontal distance and contain abundant, high-quality apatite. The resulting ages on all five samples display reproducible replicate data for (U-Th)/He analyses and yield consistent (U-Th)/He and apatite fission-track (AFT) age pairs for individual samples on the transect.

In order to determine the range of acceptable erosion histories compatible with the Danba data, we forward model the (U-Th)/He and AFT ages using a simple 1-D thermal model constrained by: 1) the (U-Th)/He age/ elevation data, 2) the AFT age/elevation data, and 3) the elevation of the relict landscape as a stable (non-eroding) surface since the initiation of rapid river incision.

We use a finite-difference algorithm to solve the partial differential equation governing heat conduction:

$$\frac{\partial T}{\partial t} = \kappa \left(\frac{\partial^2 T}{\partial z^2} \right) + u(t) \left(\frac{\partial T}{\partial z} \right) + \frac{A}{K} \tag{4.1}$$

where T is temperature, κ is the thermal diffusivity, u is the material velocity with respect to the surface (e.g. erosion rate), A is the heat production per unit volume per unit time, and K is the thermal conductivity. For reasonable values of crustal heat production, the effect of including the production term ($\frac{A}{K}$) is small, therefore for simplicity we set this term to zero [e.g. *Moore and England*, 2001]. We use a constant surface temperature of 10 ° C, a uniform thermal diffusivity of κ = 10^6 $m^2 s^{-1}$ and a nodal spacing of δz = 0.1 km with time steps of δt = 0.1 Ma. The initial geotherm was assumed to be linear and the lower boundary at the base of the lithosphere was maintained at 100 km depth. The temperature structure below ~20 km depth will not significantly affect results over the timescales considered here (10 - 20 Myr). The time-temperature history is computed by allowing the upper surface (held at constant temperature) to move downward through the grid at a rate equal to the exhumation rate (u). (U-Th)/He cooling ages were computed from nominal closure temperatures for grain radii of 45 μm as a function of cooling rate (62 - 72 ° C) [e.g. *Farley*, 2000]. AFT cooling ages were determined using a nominal closure temperature of 105 ° C [e.g. *Fowler*, 1993].

The elevation of the relict plateau landscape (i.e. the depth of the sample transect beneath the surface datum) places a strong constraint on the initial geothermal gradient by establishing the initial depth of the closure isotherm for each system. The steep age/elevation gradients observed in both datasets and the track-lengths determined in the AFT data suggest that these ages are the result of young and rapid incision, so these samples must have resided at or above the closure temperature for apatite fission-track prior to initiation of young incision. If we assume that the position of the east Tibetan relict landscape represents the surface prior to young river incision, then an initial geothermal gradient greater than $\sim$50 ° C/km is required for the AFT samples to have been above their closure temperature at the initiation of rapid river erosion. If the geothermal gradient was lower, we would expect the AFT ages to be much older than the (U-Th)/He ages. If the geothermal gradient was less than $\sim$30 ° C/km, we would expect the (U-Th)/He ages to reflect slow cooling beneath the relict landscape, and thus have a much lower age/elevation gradient.

Fitting only the (U-Th)/He data, we examine a range of erosion rates for an initial geothermal gradient of between 50 - 60 ° C/km (we consider geotherms in excess of 60 ° C/km to be unrealistically high). The three lowest samples on the Danba transect can be fit with an erosion rate $\geq$0.25 mm/yr, although erosion rates fit through all five samples require a range between 0.25 - 1.0 mm/yr. We then consider which of these models are also consistent with the AFT data. Acceptable fits produced in this manner correspond to an initial geothermal gradient between 50 - 60 ° C/km, exhumation rates of 0.25 - 0.5 mm/yr, and an age of initiation of rapid erosion of 8 - 13 Ma (Figure 4.8). If erosion rates are less than 0.25 mm/yr, then the slope of the age/elevation data cannot be matched for either the (U-Th)/He or the AFT data. Erosion rates in excess of 0.5 mm/yr cannot fit the (U-Th)/He and AFT ages simultaneously, and produce model AFT ages that are much younger than observed.

If some erosion of the relict landscape remnants has occurred since river incision began, then the current elevation of the relict landscape gives an underestimate of the position of the sample with respect to the surface datum. The presence of glaciers on the surface remnant west of the Danba transect suggests that some differential erosion of the surface may have occurred since initiation of the river incision; however, in our opinion, it is unlikely to

be > 200 m. Even if 500 m had been eroded from the surface since the beginning of *rapid* river initiation, results of the thermochronologic modeling would be unaffected except that the initiation of river incision may be as old as 15 M.a.

A two-phase model of river erosion was also considered, where a rapid phase of erosion is preceded by a somewhat slower rate of erosion. For example, the highest two (U-Th)/He ages on the transect may be fit with an erosion rate of 0.25 mm/yr, while the lowest three samples can be fit with an erosion rate of 0.5 mm/yr (Figure 4.9). Thus this two-step erosion model for Danba produces results within the range for river initiation produced by single step model. However, this model provides a poor fit to the AFT data. Of course, the presence of very slow erosion rates, with small magnitudes of total erosion occurring prior to the cooling of our highest samples through the closure temperature for (U-Th)/He cannot be ruled out. Because we aim to establish the timing of rapid river incision in eastern Tibet, we do not consider these very low erosion rates.

Samples from the Yalong transect cover a depth range beneath the relict landscape that is similar to the Danba samples, but in our opinion these data are not sufficiently consistent to warrant the detailed thermal modeling that was done for the Danba data. Nevertheless, because the Yalong data show a trend similar to the Danba data, we can apply the results of our Danba model to the Yalong data. This yields a sense of the regional applicability of the model results. Figure 4.10 shows good general agreement between the thermal/erosional history determined for the Danba region and the Yalong transect ages, indicating that these two areas, which are more than 200 km apart, may have experienced similar exhumation histories tied to a regional onset of rapid incision between 8 and 13 Ma.

These results are consistent with the depth of the major river gorges in eastern Tibet, which are a maximum of 3.5 km depth below the relict landscape surface. Using the elevation of the relict landscape as an erosional datum we can calculate the average exhumation rate by dividing the total amount of erosion observed in the river gorges by the duration of rapid erosion as determined from our modeling (8 - 13 Ma). This yields an estimate of average river incision rates from the initiation of incision to the present of 0.27 - 0.44 mm/yr. Thus the rates determined from the thermochronology data with ages between 11.4 - 4.5 Ma (the Danba and Yalong transects), are consistent also with the average rate at which the

deep river gorges were incised, an estimate that includes erosion up to the present. Thus, the rapid cooling observed in the thermochronology data is consistent with rapid erosion due to river incision because the rates and duration of erosion determined from the data are consistent with the depth of the major river gorges in eastern Tibet.

4.5 Composite plot: General age/depth relationships for samples beneath the eastern Tibet relict landscape (erosion surface)

Another approach to interpreting these (U-Th)/He data from eastern Tibet is to combine the individual transects into a composite plot. This combined dataset offers the opportunity to assess and quantify the concept that regional exhumation of a long-lived, slowly eroding low-relief landscape was affected by Late Miocene onset of rapid river erosion of regional extent. Because erosion occurred relative to the pre-existing landscape surface, we must plot data from multiple transects relative to this common surface datum. Thus data from all six transect locations are plotted as a function of depth beneath the regional low-relief relict landscape which, as before, is assumed to be an approximated the surface at the beginning of rapid river incision (Figure 4.11). These transects contain samples collected across remnant surfaces and in river gorges near areas where the elevation of the remnant surface can be reasonably estimated (i.e. Anning, Dadu, Danba, Daocheng, Pamai, and Yalong transects). Although we do not know if the geothermal gradient or timing and rate of rapid incision are uniform across this large area, plotting the data in this fashion will show whether, within the constraints of our data, there has been a regionally consistent young erosion history in this part of eastern Tibet.

Samples collected across remnants of the relict landscape surface up to a depth of $\sim$1 km below the surface are from the Daocheng Transect and a single sample from the Pamai Transect. The mean ages ($\sim$100 to 50 Ma) display an ill-defined positive low-gradient depth/age trend with shallower samples generally yielding older ages. Beneath these samples there is a spatial gap in depth from $\sim$1 - 1.5 km below the relict landscape. Samples

from the Dadu transect were collected from depths of ~1500 - 2000 m below the plateau surface, and the mean ages also define a positive low-gradient depth-age relationship, although there is considerable spread in individual replicate ages. Anning transect samples overlap the depth range of the Dadu transect but, considered independently, the mean ages would define a steeper depth-age relationship. Together the Daocheng and Pamai samples give a reasonably well-defined trend that is similar to the age/depth trend of the mean ages within the Daocheng and Dadu transects. This trend includes data at elevations from the plateau surface to $\sim$ 2000 m depth below the plateau surface with ages as old as $\sim$ 100 Ma for samples close to the surface to as young as $\sim$ 8-10 Ma for samples 2 km below the surface. Data collected at depths of 2 km or more below the plateau surface come from only the Yalong and Dadu transects, with a steep depth/age trend from $\sim$ 11 Ma to 4.5 Ma.

To first order, the cooling pattern observed from this composite dataset is consistent with a protracted period of slow erosion or slow cooling beneath the east Tibetan relict landscape beginning at or before 50 - 100 Ma and lasting until 7 - 10 Ma. The large scatter in data collected within 1 km elevation of the remnant landscape surface (Daocheng and Pamai transects) precludes direct quantitative estimation of exhumation rate. However the positive gradient defined by the mean ages and the high degree of scatter in replicate ages suggest slow erosional exhumation ($\leq$0.02 mm/yr?) or slow conductive cooling ($\leq 1\,^{\circ}$ C/My) beneath a relatively uneroded surface since >100 Ma. These alternatives are indistinguishable on the basis of our data.

The timing of the transition from slow cooling conditions beneath the low-relief relict landscape to rapid incision is not well constrained by our data because we lack elevation transects that cross the entire depth range from the slowly to quickly cooled samples. However, the timing of this transition can be inferred tentatively from the projected intersection of the steep portion of the depth/age curve and the shallow, low-slope portion of depth/age curve (as well as from modeling of the Danba data alone). By inspection, these data considered together are consistent with a scenario of slow exhumation since 100 Ma followed by the inception of rapid erosion at 7 - 10 Ma. The interval of rapid exhumation is largely defined by the data on the Danba and Yalong transects, although, its upper bound is determined by the intersection with the Dadu transect.

The geothermal gradient present at the time that rapid incision began can be computed from the depth of the transition zone (where steep/gentle age/elevation trends intersect) beneath the relict landscape surface (by inspection). If, as seems likely, little erosion has occurred across the surface remnants since initiation of river incision, the depth of this transition zone ($\leq$2000 m) should correspond to the base of the partial retention zone for (U-Th)/He ($\sim$80 ° C) and indicate a geothermal gradient of $\sim$35 ° C/km, assuming a surface temperature of 10 ° C. This estimate produced an initiation age for river incision that is consistent with the modeling of the Danba data, however the difference in geothermal gradient determined from these two approaches may reflect real regional variability of the geotherm and/or uncertainty in the position of the relict landscape with respect to the Dadu transect samples (Section 4.3.4).

4.6 Relationship of thermochronology to landscape history in eastern Tibet

From the geomorphic record, we have established a relative chronology of landscape evolution in eastern Tibet [*Clark et al.*, in prep.] where prior to the Cenozoic evolution of the Tibetan plateau, the region of the modern eastern plateau was characterized by a long-lived low-elevation, low-relief landscape. This region experience uplift due to the initiation of crustal thickening in eastern Tibet, and was followed by incipient rapid erosion into the elevated relict landscape. The thermochronology results presented here help to provide an absolute chronology of landscape evolution in eastern Tibet and its relationship to the tectonic history of the region.

4.6.1 Age of low-relief relict landscape

An upper bound on the age of the pre-modern plateau relict landscape is important for constraining the degree of exhumation that the landscape in eastern Tibet experienced prior to rapid uplift in Miocene time. The presence of this surface is used to determine the total amount of erosion in river gorges and for constraining the depth of the thermochronology

samples prior to initiation of river incision.

The shallow emplacement depth of the Songpan-Garze plutons at 2.5 to 3 kbars and preservation of Triassic shallow-water basin sediments in the western Songpan-Garze terrane, limit the total post-Triassic - Jurassic erosion to less than about 10 km [*Mattauer et al.*, 1992; *Roger*, 1994; *Burchfiel et al.*, 1995; *Kirby et al.*, 2002]. Stratigraphic constraints from coarse clastic sediment that mantles the surface in some areas suggest that the relict landscape surface in these regions is at least as old as early Tertiary in age.

In some regions, anomalously high topography disrupts the continuity of the relict landscape. The elevation (depth) invariant age data from Gonga Shan indicate that rapid, localized exhumation has occurred in the Gonga Shan region, in excess of the exhumation related to bedrock river incision into the relict landscape observed elsewhere in the region since at least ~11 Ma. The Gonga Shan region is a local area of rapid uplift [*Wang et al.*, 1998] which locally exposes late-middle Miocene age granites [e.g. *Roger et al.*, 1995]. Rapid exhumation expressed in the (U-Th)/He data likely reflects increased erosion rates due to glaciation, mass wasting and river capture related to higher local uplift rates in the Gonga Shan region [*Clark et al.*, in press], as well as exhumation by extensional faulting in this region [*Clark et al.*, 2001]. These data, along with the geomorphic evidence for rapid exhumation and the lack of preserved remnant surfaces argue for a greater degree of exhumation than is observed elsewhere in eastern Tibet.

(U-Th)/He ages from samples at elevations within 1 km of the relict landscape surface indicate that this landscape surface has experienced limited exhumation (<2 km) since ~50 - 100 Ma. The mean cooling ages of these samples suggest slow exhumation or cooling during this time interval, on the order of ~0.02 mm/yr. Mean AFT ages for this area and depth interval, as reported by *Xu and Kamp* [2000], are within 1 km of the surface range generally range from (65 - 85 Ma), with a few outliers at ~20 Ma.

Estimates for pre- late Miocene cooling rates can be determined for samples from the Pamai region, using our (U-Th)/He age (58 Ma) and other reported cooling ages from the same locality (75 Ma (AFT) and 120 Ma (ZFT) [*Xu and Kamp*, 2000]; biotite K/Ar ages of 113 - 136 Ma [*Bureau of Geology and Mineral Resources, Sichuan*, 1991]). These ages yield an approximate cooling rate of 2.7C/m.y. which suggests an exhumation rate of 0.05

- 0.08 mm/yr for geothermal gradients between 35 - 50 ° C. This cooling/exhumation estimate is higher than the estimate determined from the (U-Th)/He age/elevation data alone (~1 ° C/m.y. and 0.02 mm/yr). However, more reliable 40Ar/39Ar thermochronology and (U-Th)/He ages reported by *Kirby et al.*, [2002] show similar cooling rates for samples beneath the plateau several hundred kilometers to the east of our samples (~3 ° C/Ma) and lower rates for samples collected at the Longmen Shan margin (<1 ° C/My), prior to the initiation of rapid exhumation at the Longmen Shan margin in late Miocene time.

Taken together, all of these data from a broad range of areas across the eastern plateau suggest that the relict landscape that mantles the high eastern plateau is a long-lived, slowly eroding landscape that has experienced limited exhumation since Late-Jurassic - Early Cretaceous time and long-term slow cooling (exhumation) rates. Slow cooling and characteristically low exhumation rates continue to the present day beneath preserved remnant surfaces not yet affected by fluvial incision related to the rapid entrenchment of major river gorges in eastern Tibet.

4.6.2 Timing of major river incision

Forward modeling of the Danba transect data yields estimates of the initiation of rapid river incision at ~8 - 13 Ma, incision rates of 0.25 - 0.5 mm/yr and a geothermal gradient of 50 - 60 ° C/km. These results are also consistent with data from the Yalong transect collected from a similar depth range from beneath the relict landscape surface. The transects are located in different tributaries to the Yangtze River, suggesting that the initiation of rapid incision on these rivers was broadly contemporaneous (i.e. within 1-2 Myr). Combining the forward modeling results of the Danba data with a regional composite dataset suggests that river incision probably occurred on the younger end of this age range between 7 - 10 Ma. Estimates of averaged erosion rates based on the present depth of the river gorges are consistent with the exhumation rates determined from the thermochronology results. These ages are also consistent with reported rapid cooling at the Longmen Shan plateau margin between ~ 5 - 12 Ma [*Kirby et al.*, 2002]. We conclude that the major phase of rapid river incision (i.e. reflecting erosion rates in excess of 0.25 mm/yr) begins by late

mid-Miocene time and continues to the present, actively destroying elevated remnants of the relict, slowly-eroding landscape.

4.7 Discussion

Establishing the age of the relict landscape (in the region covered by our sample transects), the timing of river incision and the timing of local, rapid uplift at Gonga Shan allows us to link the geomorphic and tectonic records for a more complete view of uplift and erosion in eastern Tibet, as well as to address larger scale problems that relate plateau uplift to crustal dynamics and climate change.

The timing of uplift in eastern Tibet is critical for understanding the lateral growth of the plateau. The total surface area of eastern Tibet is significant, comprising approximately one third of the total area of high topography in Tibet and adjacent regions. Eastern Tibet is unusual in that it has a remarkable surface datum (the relict landscape) by which to measure surface uplift and total bedrock river erosion into that landscape. Therefore we can relate the initiation of bedrock incision into that relict landscape to the generation of high topography of the Tibetan Plateau.

High topography is a pre-requisite for formation of deep bedrock canyons. However, the thermochronologic data, by themselves, cannot specify if the commencement of bedrock incision was coeval with surface uplift in eastern Tibet. Bedrock river incision requires that a critical shear stress acting on the base of the river be exceeded, which is a function of river discharge and slope [e.g. *Howard and Kerby*, 1983; *Howard et al.*, 1994; *Whipple and Tucker*, 1999]. A river crossing a region of long-wavelength uplift, such as the southeastern plateau, under arid climate conditions could remain at or near sub-critical shear stress levels and therefore not begin to incise into the uplifting landscape for some period of time (probably not more than 1-2 Myr). Thus if the climate were particularly arid when uplift began, major bedrock incision in eastern Tibet may have occurred after surface uplift began, when precipitation increased sufficiently to allow rivers to exceed the required critical shear stress for erosion.

Uplift and increased precipitation may have had important synergistic effects that are re-

sponsible for the overlap in age estimates for plateau development, monsoon strengthening, and rapid river incision in eastern Tibet. Topographic development of the eastern Tibetan Plateau bears strongly on climate studies that suggest wind circulation patterns are sensitive to a laterally extensive, topographically high landmass [e.g. *Hahn and Manabe*, 1975]. This perturbation of wind patterns may have led to regional patterns of humidification and aridification, introducing the strong seasonality associated with the modern-day monsoonal climate observed in southeast Asia [*Ruddiman and Kutzbach*, 1989; *Prell and Kutzbach*, 1992; *Prell and Kutzbach*, 1997]. Initial uplift of eastern Tibet may have strengthened precipitation (by strengthening the monsoon) and thus may have produced a very dramatic increase in fluvial incision reflecting the linked increase in elevation and precipitation. This scenario is consistent with many present estimates for the timing of monsoon strengthening (8.5 Ma [*Kroon et al.*, 1991; *Prell et al.*, 1992; *An*, 2000]) and the suggestion of a Late Miocene age for uplift followed by rapid erosion of major rivers in eastern Tibet.

A Late Miocene initiation age for major river incision in eastern Tibet is broadly contemporaneous with the development of high topographic gradients at the steep Longmen Shan plateau margin, located to the east and northeast of our study area. Thermochronology results reported by *Kirby et al.* [2002] suggest that slow cooling occurred across the Longmen Shan escarpment from Jurassic time to at least 12 Ma, followed by initiation of rapid cooling (exhumation) between $\sim$ 12 - 5 Ma [*Kirby et al.*, 2002]. These data likely represent the initiation of rapid erosion due to increased topographic relief in response to developing high elevations at the steep plateau margin [*Kirby et al.*, 2002]. The age of river incision from this study, and the rapid cooling event at the Longmen Shan are also broadly contemporaneous with the 8 - 4 Ma initiation of the modern pattern of strike-slip and normal faults that accommodate clock-wise rotation of crustal fragments around the eastern Himalayan syntaxis [*Wang et al.*, 1998; *Wang and Burchfiel*, 1997; *King et al.*, 1997; *Chen et al.*, 2000]. The superposition of these events suggest that major regional tectonic changes took place in eastern Tibet in late mid Miocene to late Miocene time, related to the establishment of the modern day strain pattern and the onset of crustal thickening.

4.8 References

An, Z. 2000, The history and variability of the East Asian paleomonsoon climate, Quat. Sci. Rev. 19, p. 171 - 187.

Bevington, P. R., and Robinson, D. K., 1992, Data Reduction and error analysis for the physical sciences, 2nd ed., Mc Graw Hill, Boston, 328 p.

Burchfiel, B. C., Chen, Z., Liu, Y., Royden, L. H., 1995, Tectonics of the Longmen Shan and adjacent regions, Central China, International Geology Review, v. 37, pp. 661 - 735.

Bureau of Geology and Mineral Resources of Sichuan Province, 1991, in Regional Geology of Sichuan Province, Beijing, Geological Publishing House, 730 p.

Chen, Z., Burchfiel, B. C., Liu, Y., King, R. W., Royden, L. H., Tang, W., Wang, E., Zhao, J., and Zhang, X., 2000, GPS measurements from eastern Tibet and their implications for India/Eurasia intercontinental deformation, J. Geophysics Research, v. 105, p. 16,215 - 16, 227.

Chung, S., Lo, C., Lee, T., Zhang, Y., Xie, Y., Li, X., Wang, K., Wang, P., 1998, Diachronous uplift of the Tibetan plateau starting 40 Myr ago, Nature, v. 394, p. 769 - 773.

Clark, M. K., Royden, L. H., Bush, J., Burchfiel, B. C., X. Zhang, 2001, Sub-regional dynamic topography and deformation of the lower crust by decoupled channel flow in Tibet, EOS, Transactions, American Geophysical Union, Fall Meeting Suppl., Abstract T11H-06.

Clark, M. K., Royden, L. H., Whipple, K. X., Burchfiel, B. C., Schoenbohm, L., X. Zhang, W. Tang, E. Wang, L. Chen, in press, Surface uplift, tectonics, and erosion of eastern Tibet as inferred from large-scale drainage patterns, Tectonics.

Clark, M. K., House, M. A., Royden, L. H., Burchfiel, B. C., Whipple, K. X., Zhang, X., Tang, W., in prep. for submission to J. Geophys. Res., Late Cenozoic uplift in eastern Tibet, Part 1: Deformation of a regional low-relief relict landscape (erosion surface).

Davis, J. C., 2002, Statistics and Data Analysis in Geology, 3rd ed., John Wiley and Sons, New York, 638 p.

Farley, K. A., Wolf, R. W., Silver, L. T., 1996, The effects of long-stopping distances on (U-Th)/He ages, Geochim. Cosmochim. Acta, v. 60, p. 4223-4229.

Farley, K. A., 2000, Helium diffusion from apatite; general behavior as illustrated by Durango fluorapatite, J. of Geophys. Res., 105, p. 2903-2914.

Farley, K. A., 2002, (U-Th)/He Dating: Techniques, Calibrations, and Applications, Noble gases in geochemistry and cosmochemistry, Reviews in Mineralogy and Geochemistry, v. 47, p. 819-843.

Fowler, C. M. R., 1993, The Solid Earth, An introduction to global geophysics, Cambridge University Press, 472 p.

Hahn, D. G. and Manabe, S., 1975, The Role of Mountains in the South Asian Monsoon Circulation, J. Atmos. Sci., v. 32, n. 8, p. 1515-1541.

Harrison, T. M., Copeland, P., Kidd, W. S. F., Yin, A., 1992, Raising Tibet, Science, v. 255, p. 1663-1670.

House, M. A., Wernicke, B. P., Farley, K. A., and Dumitru, T. A., 1997, Cenozoic thermal evolution of the central Sierra Nevada, California, from (U-Th)/He thermochronometry, Earth and Planetary Science Letters, v. 151, p. 167-179.

House, M. A., Farley, K. A., Kohn, B. P., 1999, An empirical test of helium diffusion in apatite: borehole data from the Otway basin, Australia, Ear. Plan. Sci. Lett., 170, p. 463-474.

House, M. A., Farley, K. A., Stockli, D., 2000, Helium chronometry of apatite and titanite using Nd-YAG laser heating, Ear. Plan. Sci. Lett., 183 (3-4), p. 365-368.

House, M. A., Wernicke, B. P., Farley, K. A., 2001, Paleo-geomorphology of the Sierra Nevada, California, from (U-Th)/He ages in apatite, Am. J. Sci, v. 301, p. 77-102.

Howard, A. D. and Kerby, G., 1983, Channel changes in badlands, Geol. Soc. Am. Bull., v. 94, p. 739 - 752.

Howard, A. D., Seidl, M. A., Dietrich, W. E., 1994, Modeling fluvial erosion on regional to continental scales, J. Geophs. Res., v. 99, p. 13,971 - 13,986.

Kapp, P. , Murphy, M. A., Yin, A., Harrison, T. M., Ding, L., Guo, J., in press, Mesozoic and Cenozoic tectonic evolution of the Shiquanhe area of western Tibet.

King, R. W., Shen, F., Burchfiel, B. C., Royden, L. H., Wang, E., Chen, Z., Liu, Y., Zhang,

X., Xhao, J., Li, Y., 1997, Geodetic measurement of crustal motion in Southwest China, Geology, v. 25, n. 2, pp. 179 - 182.

Kirby, E., Reiners, P. W., Krol, M. A., Whipple, K. X., Hodges, K. V., Farley, K. A., Tang, W., Chen, Z., 2002, Late Cenozoic evolution of the eastern margin of the Tibetan Plateau: Inferences from 40Ar/39Ar and (U-Th)/He thermochronology, Tectonics, 10.1029/2000TC001246.

Kroon, D., Steens, T., Troelstra, S. R., 1991, Onset of monsoonal related upwelling in the western Arabian Sea as revealed by planktonic foraminifers, in Prell, W. L., Niitsuma, N., et al., (Eds.), Proc. ODP Sci. Results 117, p. 257 - 263.

Laslett, G. M., Green. P. F., Dudy, I. R., and Gleadow, A. J. W., 1987, Thermal annealing of fission tracks in apatite, 2, A quantitative analysis, Chem. Geo. (Isot. Geosci. Section), v. 65, p. 1 - 13.

Lyons, L., 1991, A Practical Guide to Data Analysis for Physical Science Students, Cambridge Univ. Press, Cambridge, U. K., 95 p.

Mattauer, M., Malavieille, J., Calassou, S., Lancelot, J., Roger, F., Hao, Z., Xu, Z., and Hou, L., 1992, La chane Triasique de Songpan-Garze (Ouest Sichuan et Est Tibet): une chane de plissement-dcollement sur marge passive, C. R. Acad. Sci. Paris, 314, p. 619 - 626.

Moore, M. A. and England, P. C., 2001, On the inference of denudation rates from cooling ages minerals, Earth Planet. Sci. Lett., v. 185, p. 265 - 284.

Prell, W. L., Murray, D. W., Clemens, S. C., Anderson, D. M., 1992, Evolution and variability of the Indian Ocean summer monsoon: evidence from the western Arabian Sea drilling program, in Duncan, R. A., Rea, D. K., Kidd, R. B., von Rad, U., Weissel, J. K. (Eds.), Synthesis of Results from Scientific Drilling in the Indian Ocean, Am. Geophys. Union Monogr., 70, p. 447 - 469.

Pan, Y., and Kidd, W. S. F., 1992, Nyainqentanglha shear zone; a late Miocene extensional detachment in the southern Tibetan Plateau, Geology (Boulder), v. 20, p. 775-778.

Prell, W. L. and Kutzbach, J. E., 1992, Sensitivity of the Indian monsoon to forcing parameters and implications for its evolution, Nature, 360, p. 647 - 652.

Prell, W. L. and Kutzbach, J. E., 1997, The impact of tibet-Himalayan Elevation on the

sensitivity of the monsoon climate system to changes in solar radiation, in Tectonic Uplift and Climate Change, p. 171 - 201, Plenum Press, New York.

Raymo, M. E., Ruddiman, W. F., and Froelich, P. N., 1988, Influence of late Cenozoic mountain building on ocean geochemical cycles, Geology, V. 16, p 649 - 653.

Reiners, P. W. and Farley, K. A., 2001, Influence of crystal size on apatite (U-Th)/He thermochronology: an example from the Bighorn Mountains, Wyoming, Earth Planet Sci. Lett., v. 188, p. 413-420.

Roger, F., 1994, Datation et tracage des granitodes associes a la chaine de Songpan-Garze (W Sichuan, Chine) par les methodes: U-Pb, Rb-Sr et Sm-Nd [PhD thesis], Universite Montpellier II, France.

Roger, F., Calassou, S., Lancelot, J., Malavieille, J., Mattauer, M., Xu, Z., Hao, Z., and Hou, L., 1995, Miocene emplacement and deformation of the Konga Shan granite (Xianshui He fault zone, west Sichuan, China): Geodynamic implications, Earth Plan. Sci. Lett., v. 130, p. 201 - 216.

Rowley, D. B., 1996, Age of initiation of collision between India and Asia: A review of stratigraphic data: Earth Planet. Sci. Lett., v. 145, p. 1 - 13.

Rowley, D. B., Raymond, T. P., and Currie, B. S. , 2001, A new approach to stable isotope-based paleoaltimetry: implications for paleoaltimetry and paleohypsometry of the High Himalaya since the Late Miocene, Earth Planet. Sci. Lett., v. 188, p. 253 - 268.

Ruddiman, W. F. and Kutzbach, J. E., 1989, Forcing of late Cenozoic Northern Hemisphere climate by plateau uplift in southern Asia and the American West, J. Geophys. Res., 94, p. 18,409 - 18,427.

U.S. Geological Survey, 1993, Digital elevation models, data user guide, 5: Reston, Virginia, U.S. Geological Survey, p. 1-50.

Wang, E. and Burchfiel, B. C., 1997, Interpretation of Cenozoic tectonics in the right-lateral accommodation zone between the Ailao Shan Shear Zone and the eastern Himalayan syntaxis: Int. Geol. Rev., v. 39, p. 191 - 219.

Wang, E., Burchfiel, B. C., Royden, L. H., Chen, L., Chen, J., Li, W., Chen, Z., 1998, Late Cenozoic Xianshuihe-Xiaojiang, Red River, and Dali fault systems of southwestern Sichuan and central Yunnan, China, Geological Society of America Special Paper, v.

327, 108 p.

Wagner, G. A. and Reimer, G. M., 1972, Fission-track tectonics: the tectonic interpretation of fission-track apatite ages, Earth Planet. Sci. Lett., v. 14, pp. 263 - 268.

Whipple, K. X. and Tucker, G. E., 1999, Dynamics of the stream-power river incision model: Implications for height limits of mountain ranges, landscape response timescales and research needs, J. Geophs. Res, v. 104, p. 17,661 - 17,674.

Williams, H., Turner, S., Kelley, S., Harris, N. B. W., 2001, Age and composition of dikes in southern Tibet; new constraints on the timing of east-west extension and its relationship to postcollisional volcanism, Geology, v. 29, p. 339-342.

Wolf, R. A., Farley, K. A., Silver, L. T., 1996, Helium diffusion and low-temperature thermochronology of apatite, Geochim. Cosmochim. Acta, v. 60, p. 4231-4240.

Xu, G. and Kamp, P., 2000, Tectonics and denudation adjacent to the Xianshuihe Fault, eastern Tibetan Plateau: Constraints from fission-track thermochronology, J. Geophys. Res., v. 105, p. 19,231 - 19,251.

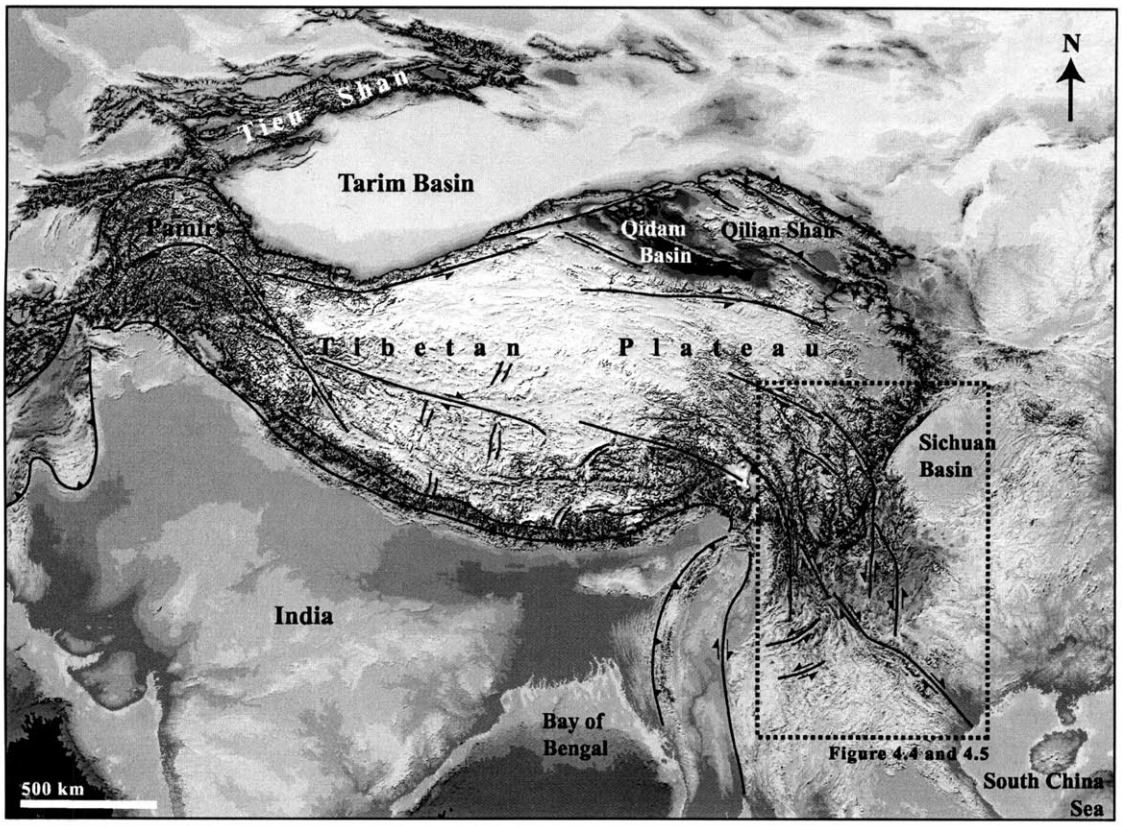

Figure 4.1: Topographic map of Tibet and major geologic structures of Cenozoic age. Topography derived from publicly available $\sim$1 km resolution GTOPO30 topography data [*U.S.G.S.*, 1993]. Inset box shows location of Figure 4.4 and 4.5

Figure 4.2: Low-relief relict landscape of eastern Tibet, elevation 4800 m. View south across Daocheng surface. Site of Daocheng sample transect.

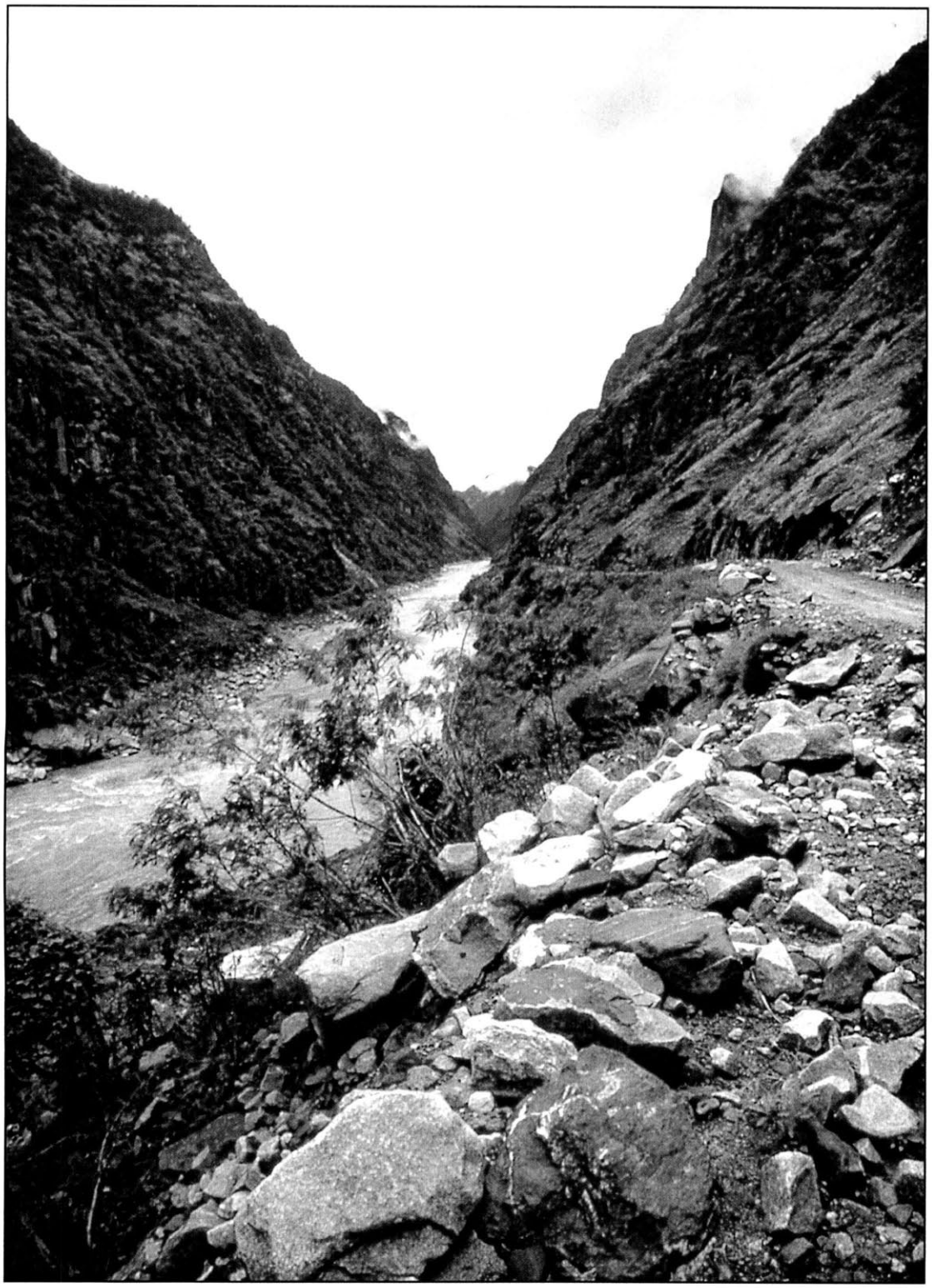

Figure 4.3: Yalong River gorge, elevation 1600 m. Site of Yalong River sample transect.

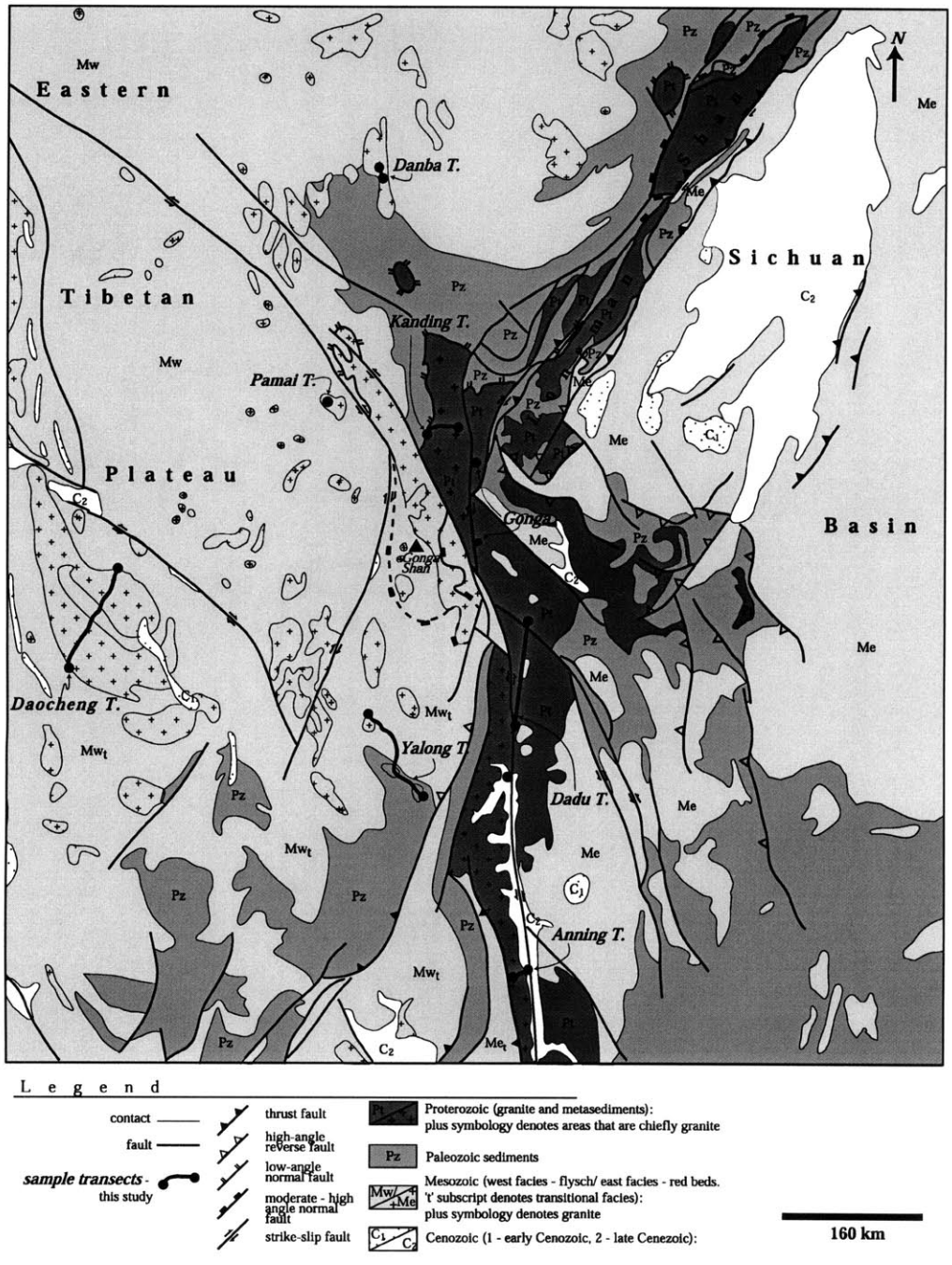

Figure 4.4: Generalized geologic map with sample transect locations [*Bureau of Geology and Mineral Resources, Sichuan* [1991] 1:200,000 and 1:1,500,000 maps; *Burchfiel et al.*, 1995; and our own mapping].

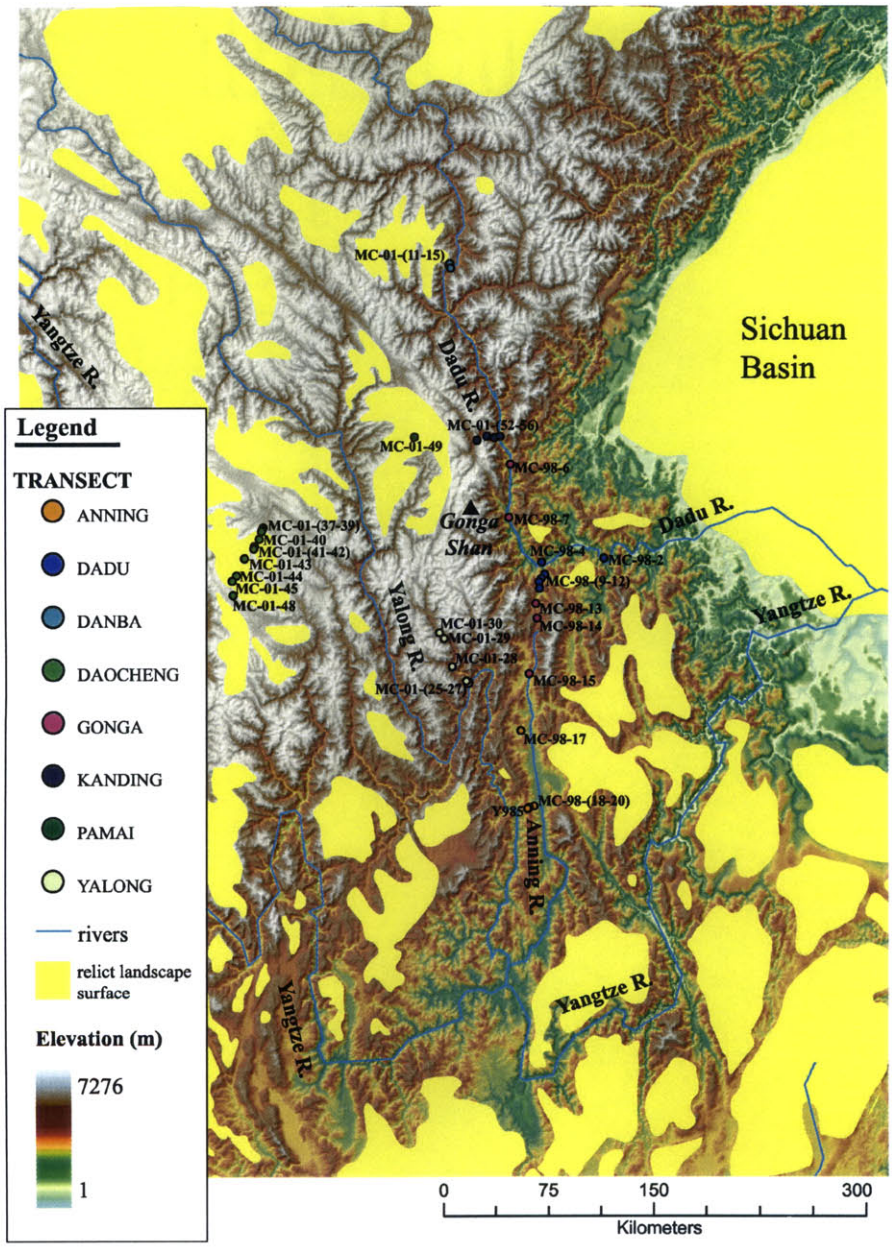

Figure 4.5: Geomorphic map with sample locations. Yellow polygons denote low-relief, relict landscape remnants *Clark et al.*, [in prep.].

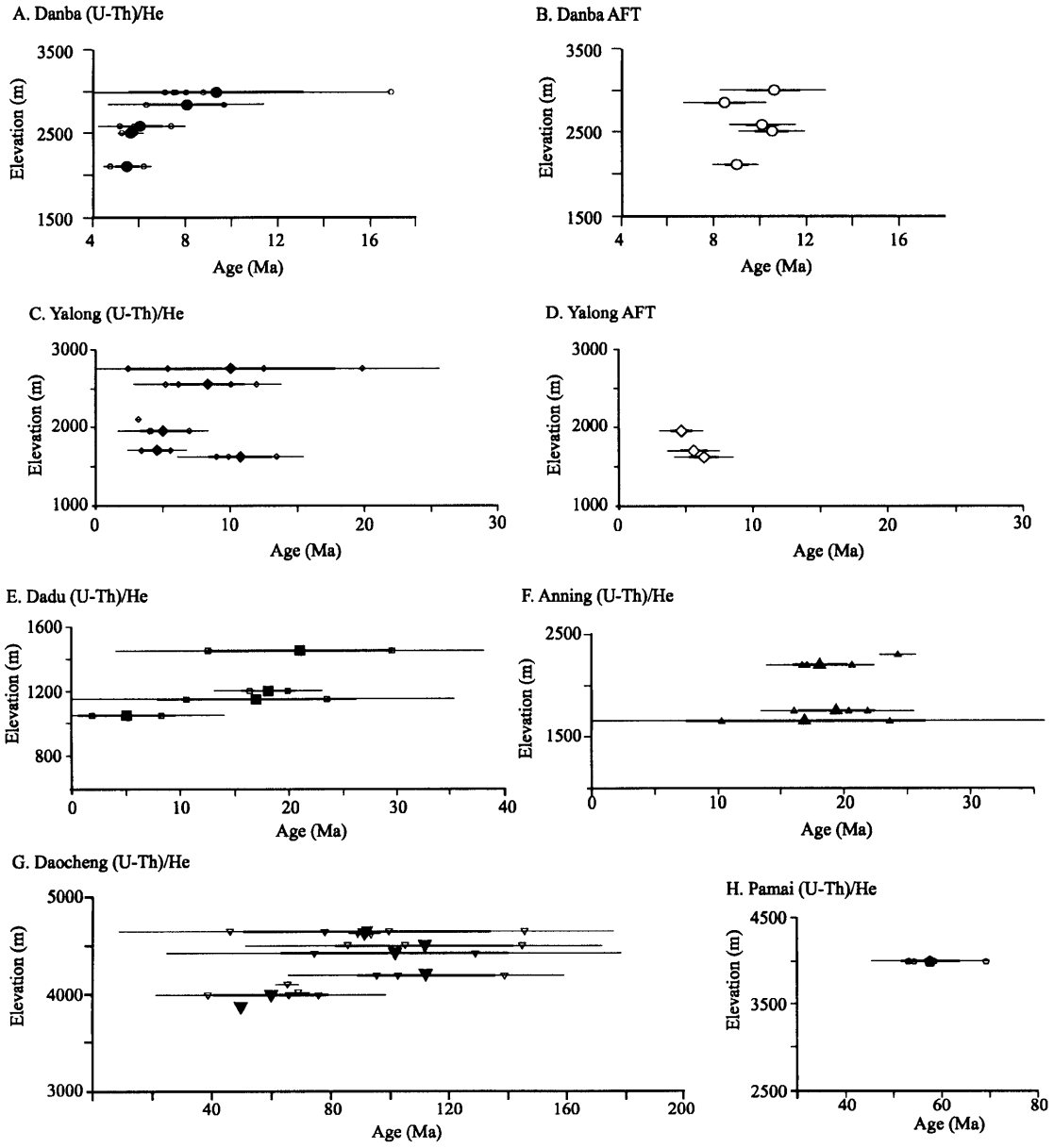

Figure 4.6: Apatite (U-Th)/He and fission-track age/elevation data for individual sample transects. Small open symbols represent individual replicate data for (U-Th)/He analyses. Large solid symbols represent mean ages based on replicate data for samples with two or more replicate analyses. Uncertainty estimates are plotted for the standard deviation based on the spread of replicate analyses for mean ages or 6% uncertainty for individual replicates based on laboratory standards [*Farley,* 2002]. Uncertainties for both the (U-Th)/He and AFT data are plotted at 1σ (thick error bar) and 2σ (thin error bar). A) (U-Th)/He data, Danba transect. B) AFT data, Danba transect. C) (U-Th)/He data, Yalong transect. D) AFT data, Yalong transect. E) (U-Th)/He data, Dadu transect. F) (U-Th)/He data, Anning transect. G) (U-Th)/He data, Daocheng transect. H) (U-Th)/He data, Pamai transect.

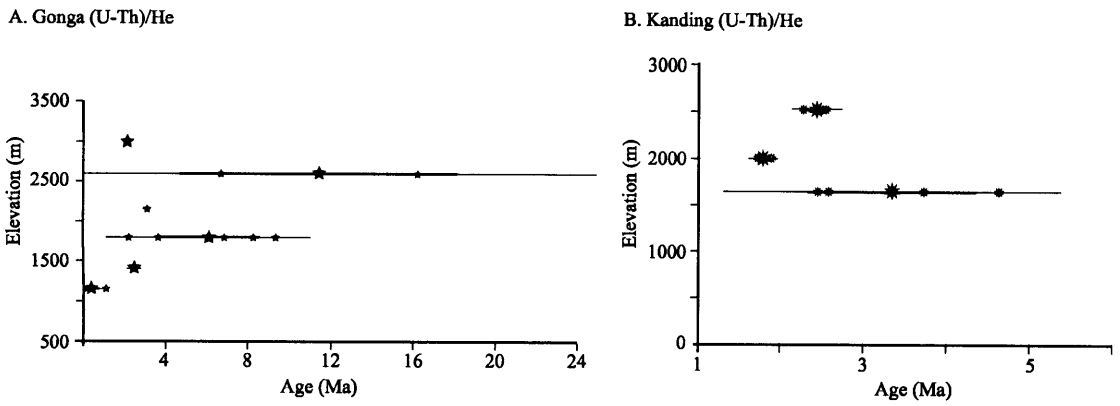

Figure 4.7: Apatite (U-Th)/He age/elevation data for individual sample transects (continued). Symbols and uncertainty estimates are described in Figure 4.6. A) (U-Th)/He data, Gonga transect. B) (U-Th)/He data, Kanding transect.

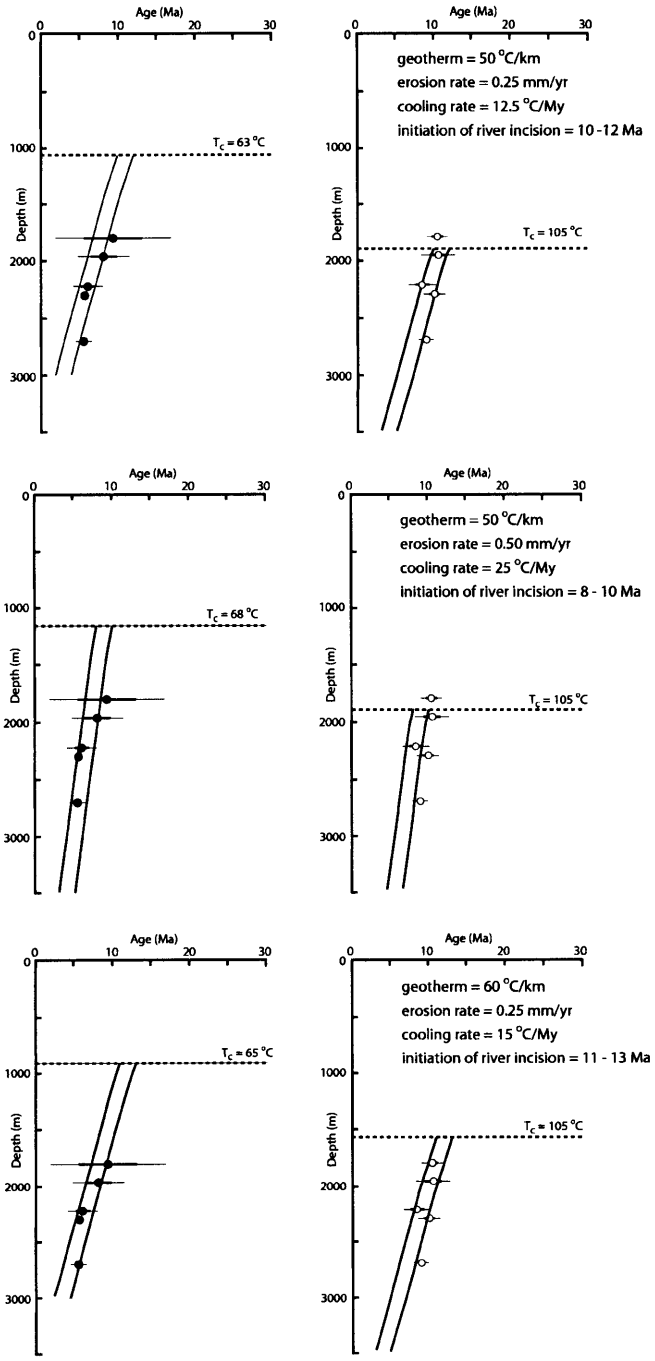

Figure 4.8: Forward modeling results (single erosion rate) compared to the Danba (U-Th)/He and AFT data. Samples are plotted as depth beneath the relict landscape surface (plateau surface). The depth position of the closure isotherm for each system is shown by the dotted line. Solid lines represent the range of acceptable model fits to the data for varying initiation ages of rapid erosion. Model fits are shown for a range of geothermal gradients (50-60 ° C) and erosion rates (0.25 - 0.5 mm/yr). Geothermal gradients and erosion rates outside these limits produce unacceptable simultaneous fits to both the (U-Th)/He and AFT data.

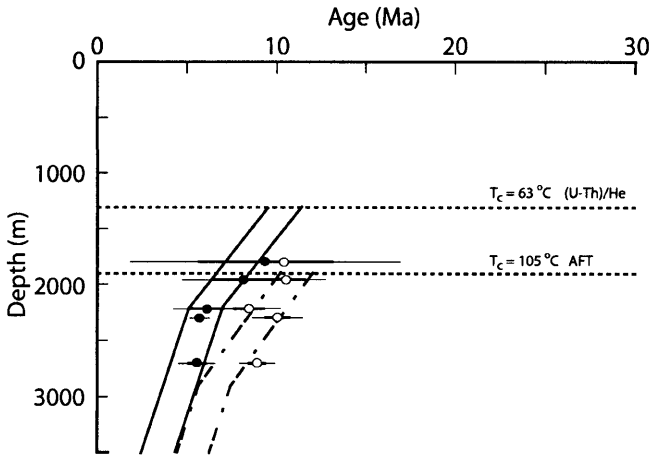

Figure 4.9: Forward modeling results (two-phase erosion rate) compared to the Danba (U-Th)/He and AFT data. Samples are plotted as depth beneath the relict landscape surface (plateau surface). The depth position of the closure isotherm for each system is shown by the dotted line (for an initial geothermal gradient of 50 ° C/km and initial erosion rate of 0.25 mm/yr). Solid lines represent the range of acceptable model fits to the (U-Th)/He data for an initial erosion rate of 0.25 mm/yr beginning between 9.5 - 11.5 Ma, and increasing the erosion rate to 0.5 mm/yr at 5 - 7 Ma. The dash-dot lines represent the range of acceptable model fits to the AFT data for an initial erosion rate of 0.25 mm/yr beginning between 10 - 12 Ma, and increasing the erosion rate to 0.5 mm/yr at 5.5 - 7.5 Ma.

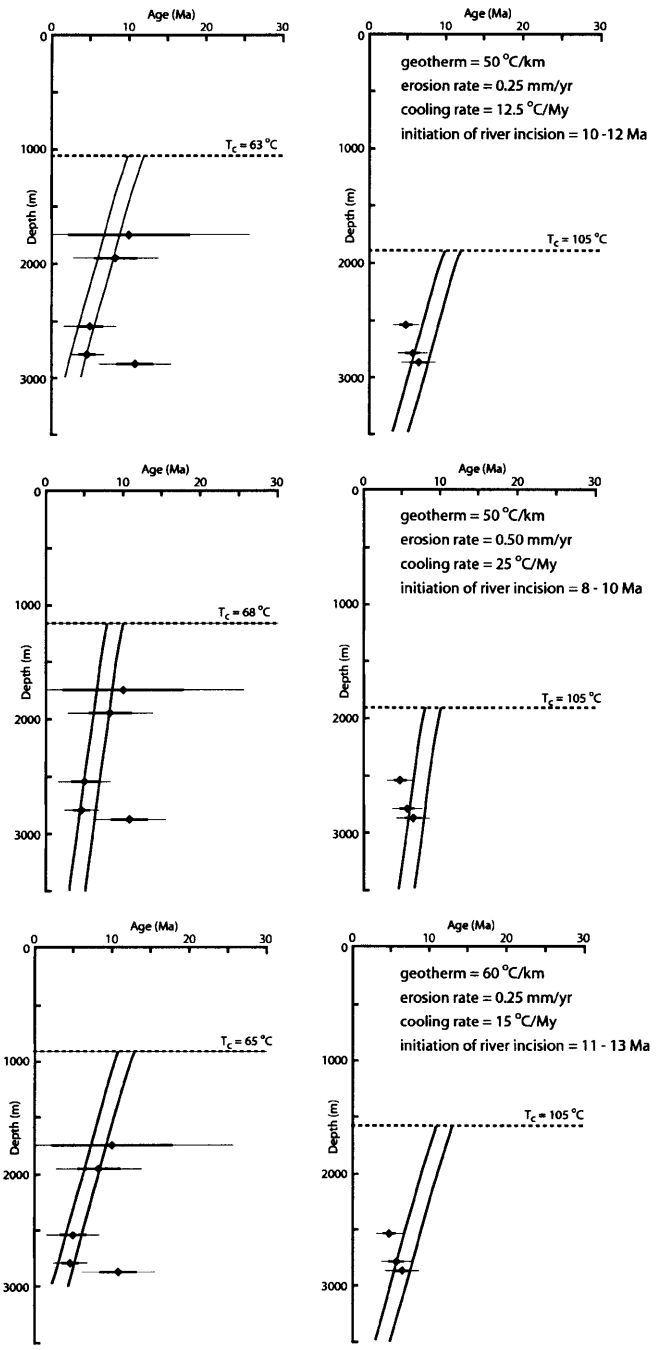

Figure 4.10: Forward modeling results (single erosion rate) compared to the Yalong (U-Th)/He and AFT data. Samples are plotted as depth beneath the relict landscape surface (plateau surface). The depth position of the closure isotherm for each system is shown by the dotted line. Solid lines represent the range of acceptable model fits to the data (determined from the Danba transect) for varying initiation ages of rapid erosion. Model fits are shown for a range of geothermal gradients (50-60 ° C) and erosion rates (0.25 - 0.5 mm/yr).

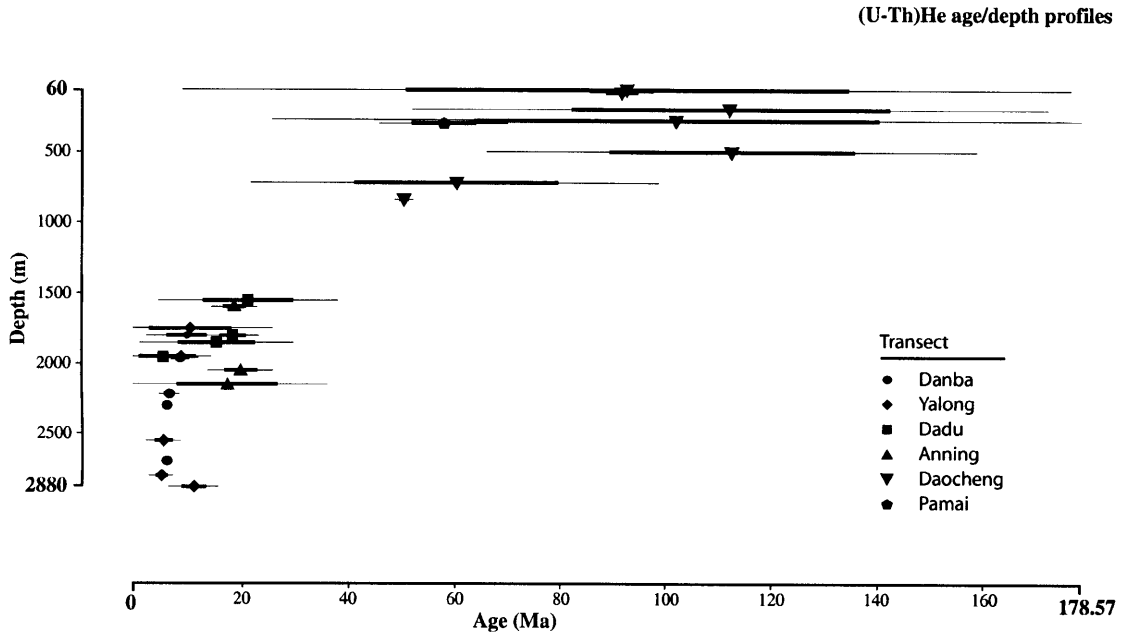

Figure 4.11: Composite plot for apatite (U-Th)/He age data versus depth beneath the regional relict landscape surface. Individual transects are plotted as depth beneath the local elevation of the relict landscape (erosion surface) of the eastern plateau. Mean ages and uncertainty estimates are described in Figure 4.6.

Table 1: Sample Descriptions

Transect	Sample ID	Rock type/age	Long (N)	Lat (E)	Elev (m)	Depth (m)†
ANNING	MC-98-17	granodiorite/Mesozoic	102.0933	28.1985	1650	-2150
	MC-98-18	granite/Proterozoic	102.1322	27.7119	1750	-2050
	MC-98-19	granite/Proterozoic	102.0964	27.7059	2200	-1600
	MC-98-20	granite/Proterozoic	102.0856	27.6999	2300	-1500
	Y985	granite/Proterozoic	102.0840	27.7005	2350	-1450
DADU	MC-98-2	granite/Proterozoic	102.8334	29.2321	800	-2200
	MC-98-4	granite/Proterozoic	102.3763	29.2504	900	-2100
	MC-98-9	granite/Proterozoic	102.3871	29.1724	1050	-1950
	MC-98-10	granite/Proterozoic	102.3602	29.1474	1150	-1850
	MC-98-11	granite/Proterozoic	102.3408	29.1282	1200	-1800
	MC-98-12	granite/Proterozoic	102.3396	29.0886	1450	-1550
DANBA	MC-01-11	granite/Mesozoic	101.9297	31.1980	2840	-1960
	MC-01-12	granite/Mesozoic	101.9262	31.1951	2580	-2220
	MC-01-13	granite/Mesozoic	101.9241	31.1937	2500	-2300
	MC-01-14	granite/Mesozoic	101.9290	31.2042	3000	-1800
	MC-01-15	granite/Mesozoic	101.9320	31.1733	2100	-2700
DAOCHENG	MC-01-37	granite/Mesozoic	100.3529	29.6446	3860	-840
	MC-01-38	granite/Mesozoic	100.3447	29.6346	3980	-720
	MC-01-39	granite/Mesozoic	100.3385	29.6218	4100	-600
	MC-01-40	granite/Mesozoic	100.3165	29.5741	4200	-500
	MC-01-41	granite/Mesozoic	100.2764	29.5322	4500	-200
	MC-01-42	granite/Mesozoic	100.2695	29.5162	4640	-60
	MC-01-43	granite/Mesozoic	100.1955	29.4605	4620	-80
	MC-01-44	granite/Mesozoic	100.1261	29.3575	4420	-280
	MC-01-45	granite/Mesozoic	100.0905	29.3259	4300	-400
	MC-01-48	granite/Mesozoic	100.0878	29.2360	4020	-680
GONGA	MC-98-6	granite/Proterozoic	102.2227	29.8886	1400	-3200
	MC-98-7	granite/Proterozoic	102.1703	29.5543	1150	-3450
	MC-98-13	granite/Proterozoic	102.3000	28.9951	1800	-2000
	MC-98-14	granite/Proterozoic	102.2979	28.9011	2600	-1200
	MC-98-15	granite/Proterozoic	102.1977	28.5558	2150	-1650
	K1	granite/Miocene(?)			3000	-1600
KANDING	MC-01-52	granite/Proterozoic	101.9947	30.0615	2520	-1780
	MC-01-54	granite/Proterozoic	102.0716	30.0815	2000	-2300
	MC-01-55	granite/Proterozoic	102.1255	30.0672	1640	-2660
	MC-01-56	granite/Proterozoic	102.1672	30.0724	1420	-2880
PAMAI	MC-01-49	granite/Mesozoic	101.5319	30.1241	4000	-300
YALONG	MC-01-25	granodiorite/Mesozoic	101.7510	28.5425	1700	-2800
	MC-01-26	granite/Mesozoic	101.7480	28.5342	1620	-2880
	MC-01-27	granite/Mesozoic	101.7335	28.5520	1950	-2550
	MC-01-28	granite/Mesozoic	101.6400	28.6533	2100	-2400
	MC-01-29	granite/Mesozoic	101.6034	28.8347	2550	-1950
	MC-01-30	granite/Mesozoic	101.5734	28.8742	2750	-1750

† Measured from local remnant surface elevation, positive downward.

Table 2: (U-Th)/He replicate analyses

Transect	Sample replicate	[U] (ppm)	[Th] (ppm)	U/Th	[4He] (nmol/g)	radius (μm)	length (μm)	FT	Raw Age (Ma)	Corr Age[†] (Ma)	error[‡] 2σ
ANNING	MC9817A[f,2]	5.8826	13.9998	0.42	1.7765	48.60	187.20	0.74	35.54	48.22	2.89
ANNING	MC9817B[f,1]	3.8955	3.2305	1.21	0.3100	33.00	158.40	0.64	12.24	19.19	1.15
ANNING	MC9817LA[1]	11.7807	11.4834	1.03	0.2279	29.28	169.28	0.61	2.90	4.77	0.29
ANNING	MC9817LB[1]	11.4529	13.2076	0.87	0.3563	30.71	162.85	0.62	4.50	7.27	0.44
ANNING	MC9817LC	4.4675	3.6608	1.22	0.2289	55.94	193.71	0.77	7.90	10.30	0.62
ANNING	MC9817LD	5.2998	3.0108	1.76	0.6322	70.28	284.56	0.82	19.33	23.66	1.42
ANNING	MC9818[f]	10.7888	24.2697	0.44	0.9550	33.60	199.80	0.66	10.65	16.08	0.96
ANNING	Mc9818LA	15.5962	28.1200	0.55	2.1991	77.14	251.42	0.83	18.20	21.93	1.32
ANNING	MC9818LB[6]	9.8642	21.2714	0.46	0.6123	62.85	239.99	0.80	7.58	9.53	0.57
ANNING	MC9818LC	20.7470	29.7400	0.70	2.3896	57.14	222.85	0.78	15.83	20.41	1.22
ANNING	MC9819[f]	12.4197	9.4239	1.32	1.1978	45.00	181.13	0.73	15.04	20.66	1.24
ANNING	MC9819LA	9.9653	4.7428	2.10	0.7899	53.33	245.70	0.77	13.11	17.13	1.03
ANNING	MC9819LB	15.5671	15.7997	0.99	1.2308	40.24	199.99	0.70	11.74	16.74	1.00
ANNING	MC9820[f]	8.9909	17.3340	0.52	1.1274	36.00	135.00	0.65	15.86	24.32	1.46
ANNING	MC9820B[f,1]	6.1008	9.3656	0.65	0.5706	27.90	144.90	0.59	12.63	21.52	1.29
ANNING	Y985[f,1]	6.1633	8.6476	0.71	1.1322	31.50	151.20	0.64	25.37	39.95	2.40
DADU	MC9802B[f,1]	12.7298	74.5115	0.17	1.0056	25.71	107.75	0.53	6.11	11.51	0.69
DADU	MC9804[f,1]	11.4547	55.1178	0.21	0.7333	27.21	127.29	0.57	5.52	9.67	0.58
DADU	MC9804L1[1]	23.2885	35.0751	0.66	0.1678	29.52	142.85	0.61	0.98	1.61	0.10
DADU	MC9804L2[1]	49.2948	80.7577	0.61	0.6622	31.43	148.56	0.62	1.78	2.89	0.17
DADU	mc9804aa[5]	1.4080	0.6880	2.05	0.1162	57.14	188.56	0.75	13.61	18.12	1.09
DADU	MC9809[f]	10.4325	51.9791	0.42	0.6865	38.14	142.71	0.67	5.57	8.27	0.50
DADU	MC9809B[f,2]	7.7382	42.2680	0.18	2.3441	44.14	200.57	0.73	24.36	33.28	2.00
DADU	MC9809L1[1]	11.0000	47.0000	0.23	0.1496	33.64	137.14	0.64	1.20	1.87	0.11
DADU	MC9809BMH	3.5347	16.3266	0.22	0.0572	60.00	179.99	0.74	1.43	1.92	0.12
DADU	MC9810A[f]	9.7943	50.5702	0.19	1.9135	39.75	148.50	0.69	16.22	23.50	1.41
DADU	MC9810B[f,1]	9.6999	56.0797	0.17	0.9030	33.56	153.00	0.64	7.26	11.28	0.68
DADU	MC9810C[f]	6.1207	34.4450	0.18	0.5385	35.44	163.13	0.66	6.96	10.57	0.63
DADU	MC9811[f]	5.9244	25.3099	0.23	0.7614	45.00	174.00	0.72	11.79	16.37	0.98
DADU	MC9811B[f]	5.2509	18.2645	0.29	0.6872	34.88	167.63	0.67	13.24	19.90	1.19
DADU	MC9812[f,1]	7.6235	31.5680	0.24	1.1353	27.90	128.70	0.58	13.87	24.12	1.45

Table 2: (U-Th)/He replicate analyses (continued)

Transect	Sample replicate	[U] (ppm)	[Th] (ppm)	U/Th	[4He] (nmol/g)	radius (μm)	length (μm)	FT	Raw Age (Ma)	Corr Age[†] (Ma)	error[‡] 2σ
DADU	MC9812[f,1]	13.1204	52.5371	0.25	1.1986	26.33	115.00	0.55	8.65	15.65	0.94
DADU	mc9812aa	6.1909	35.7002	0.17	1.7984	68.57	188.56	0.77	22.65	29.50	1.77
DADU	MC9812BMH	16.5845	59.7495	0.28	1.6784	74.28	282.84	0.80	10.08	12.57	0.75
DADU	mc9812cc	3.5852	16.5794	0.22	0.6551	62.85	239.99	0.77	16.09	21.01	1.26
DANBA	MC0111A	30.1291	17.1642	1.76	1.3362	54.28	188.56	0.74	7.19	9.71	0.58
DANBA	MC0111B	27.3484	16.1807	1.69	0.8393	62.85	265.70	0.78	4.96	6.34	0.38
DANBA	MC0111D	27.5736	15.4220	1.79	1.0048	45.71	265.70	0.72	5.93	8.24	0.50
DANBA	MC0112A	242.5972	164.3851	1.48	6.3616	42.86	274.27	0.70	4.16	5.91	0.35
DANBA	MC0112B	105.3082	63.9108	1.65	2.6874	48.57	154.28	0.71	4.11	5.81	0.35
DANBA	MC0112C	53.9249	24.4732	2.20	1.8977	62.85	325.70	0.79	5.85	7.42	0.45
DANBA	MC0112D	77.9043	115.5803	0.67	2.0823	48.57	154.28	0.70	3.65	5.19	0.31
DANBA	MC0113A	167.8283	81.3861	2.06	4.5538	68.57	308.56	0.80	4.48	5.59	0.34
DANBA	MC0113B	96.9987	49.8358	1.95	2.7172	62.85	299.99	0.79	4.60	5.85	0.35
DANBA	MC0113C	97.3014	44.4243	2.19	2.4059	45.71	162.85	0.70	4.11	5.87	0.35
DANBA	MC0113D	129.1798	72.0500	1.79	3.0925	48.57	325.70	0.74	3.89	5.27	0.32
DANBA	MC0114B	20.5177	21.6374	0.95	1.7038	51.43	171.42	0.72	12.23	16.93	1.02
DANBA	MC0114C	16.5021	19.5777	0.84	0.7367	51.43	205.70	0.73	6.42	8.79	0.53
DANBA	MC0114D	28.1196	31.9762	0.88	1.1307	62.85	231.42	0.77	5.84	7.54	0.45
DANBA	MC0114E	36.1871	40.7568	0.89	1.3768	51.43	188.56	0.73	5.53	7.61	0.46
DANBA	MC0114F	18.5550	17.7740	1.04	0.7240	51.43	179.99	0.73	5.86	8.07	0.48
DANBA	MC0114G	12.9094	10.2987	1.25	0.4302	54.28	137.14	0.72	5.16	7.15	0.43
DANBA	MC0115A	201.8482	162.1951	1.24	4.6411	54.28	222.85	0.75	3.56	4.76	0.29
DANBA	MC0115B	60.6838	25.3059	2.40	1.5666	62.85	222.85	0.78	4.33	5.57	0.33
DANBA	MC0115C	81.2040	36.8953	2.20	2.0748	57.14	334.27	0.77	4.25	5.50	0.33
DANBA	MC0115D	69.9776	33.3677	2.10	1.9388	48.57	282.84	0.74	4.58	6.24	0.37
DANBA	MC0115E	139.3074	75.9523	1.83	3.4533	51.43	274.27	0.75	4.04	5.42	0.33
DAOCHENG	MC0137A[1]	25.9567	56.4382	0.46	8.2352	34.28	171.42	0.62	38.52	62.17	3.73
DAOCHENG	MC0137B	9.2613	13.9203	0.67	2.6554	62.85	222.85	0.77	38.87	50.42	3.03
DAOCHENG	MC0137C	6.0328	11.2204	0.54	1.6594	48.57	137.14	0.69	35.12	50.62	3.04
DAOCHENG	MC0137D	7.9246	13.2491	0.60	2.2602	74.28	128.57	0.77	37.57	49.09	2.95
DAOCHENG	MC0137F[4]	12.7994	10.6365	1.20	0.5136	62.85	171.42	0.76	6.17	8.11	0.49
DAOCHENG	MC0138a	46.4884	49.4490	0.94	8.2958	42.86	159.99	0.68	26.21	38.59	2.32

Table 2: (U-Th)/He replicate analyses (continued)

Transect	Sample replicate	[U] (ppm)	[Th] (ppm)	U/Th	[4He] (nmol/g)	radius (μm)	length (μm)	FT	Raw Age (Ma)	Corr Age[†] (Ma)	error[‡] 2σ
DAOCHENG	MC0138b[2]	31.4667	71.0083	0.44	40.0489	40.00	188.56	0.67	151.24	227.38	13.64
DAOCHENG	MC0138c	27.6008	82.7297	0.33	12.7016	42.86	119.99	0.65	49.50	75.86	4.55
DAOCHENG	MC0138d	9.6608	23.0216	0.42	3.7091	45.71	154.28	0.69	45.13	65.75	3.95
DAOCHENG	MC0139a[2]										0.00
DAOCHENG	MC0139b[2]	33.9906	93.4136	0.36	43.2543	45.71	188.56	0.70	140.79	202.42	12.15
DAOCHENG	MC0139c	11.5503	30.0908	0.38	4.8169	51.43	205.70	0.73	47.43	65.40	3.92
DAOCHENG	MC0140A	14.5865	23.0803	0.63	10.2853	40.00	231.42	0.68	93.85	138.73	8.32
DAOCHENG	MC0140B[2]	25.3405	57.9910	0.44	42.4041	34.28	257.13	0.64	197.15	310.24	18.61
DAOCHENG	MC0140C	11.9056	33.4183	0.36	7.5712	51.43	257.13	0.73	70.14	95.63	5.74
DAOCHENG	MC0140D[2]	6.1157	7.6107	0.80	5.4200	48.57	137.14	0.70	124.81	179.12	10.75
DAOCHENG	MC0140E	16.0150	49.2790	0.32	11.2457	51.43	222.85	0.73	74.58	102.54	6.15
DAOCHENG	MC0141a	24.5035	68.7974	0.36	23.7157	54.28	205.70	0.74	106.46	144.74	8.68
DAOCHENG	MC0141b[2]	32.5831	78.6878	0.41	59.9619	60.00	154.28	0.74	212.48	286.88	17.21
DAOCHENG	MC0141c	25.1852	62.1728	0.41	16.2782	51.43	154.28	0.71	74.84	105.22	6.31
DAOCHENG	MC0141d	25.3300	68.9352	0.37	13.1782	45.71	137.14	0.68	58.14	85.77	5.15
DAOCHENG	MC0142A	8.5611	16.0411	0.53	5.3266	74.28	205.70	0.79	78.99	99.67	5.98
DAOCHENG	MC0142B	11.8765	27.1849	0.44	10.8302	57.14	188.56	0.74	108.20	145.62	8.74
DAOCHENG	MC0142C	40.0365	93.7098	0.43	12.2011	68.57	228.56	0.78	36.08	46.06	2.76
DAOCHENG	MC0142D	12.6068	23.2967	0.54	5.7540	57.14	205.70	0.75	58.29	77.83	4.67
DAOCHENG	MC0142E[2]	16.7871	19.4741	0.86	28.0726	51.43	274.27	0.74	236.64	318.80	19.13
DAOCHENG	MC0142F[2]	76.3435	72.2682	1.06	246.0973	48.57	148.56	0.70	463.07	658.22	39.49
DAOCHENG	MC0143A	11.2951	24.4606	0.46	6.1269	54.28	205.70	0.74	65.81	89.24	5.35
DAOCHENG	MC0143B	14.4713	40.0709	0.36	8.4868	45.71	188.56	0.70	65.06	93.55	5.61
DAOCHENG	MC0144A	24.1648	50.1674	0.48	18.1791	48.57	214.28	0.72	92.37	128.88	7.73
DAOCHENG	MC0144B	17.3602	87.0130	0.20	11.2024	54.28	197.13	0.73	54.32	74.53	4.47
DAOCHENG	MC0144C[1]	31.2443	39.4173	0.79	12.6372	34.28	154.28	0.62	57.13	92.24	5.53
DAOCHENG	MC0145a[2]	13.7482	38.5883	0.36	13.3785	40.00	154.28	0.65	107.04	164.02	9.84
DAOCHENG	MC0145b[1,2]	5.6540	17.9071	0.32	10.0808	40.00	114.28	0.63	185.58	293.86	17.63
DAOCHENG	MC0148A	62.2723	71.4717	0.87	20.9347	45.71	188.56	0.70	48.52	69.08	4.14
DAOCHENG	MC0148b[1]	51.4475	87.6067	0.59	19.8616	31.43	77.14	0.54	50.53	93.67	5.62

Table 2: (U-Th)/He replicate analyses (continued)

Transect	Sample replicate	[U] (ppm)	[Th] (ppm)	U/Th	[4He] (nmol/g)	radius (μm)	length (μm)	FT	Raw Age (Ma)	Corr Age[†] (Ma)	error[‡] 2σ
GONGA	K1[f,1]	41.2075	32.2088	1.28	0.5510	31.80	175.95	0.64	2.08	3.26	0.20
GONGA	MC-K1A	32.4857	30.2885	1.07	0.3326	48.57	308.56	0.74	1.55	2.10	0.13
GONGA	MC-K1B	30.2403	20.7996	1.45	0.2975	48.57	137.14	0.70	1.56	2.23	0.13
GONGA	MCk1cc	37.2700	23.7136	1.57	0.3451	45.71	291.41	0.72	1.48	2.05	0.12
GONGA	MCk1dd	30.7546	18.3721	1.67	0.2950	48.57	148.56	0.71	1.55	2.19	0.13
GONGA	MC9806A[f]	11.3017	49.2867	0.23	0.1976	37.80	143.10	0.67	1.59	2.38	0.14
GONGA	MC9806B[f]	10.7606	34.8899	0.31	0.1909	40.50	205.20	0.71	1.85	2.62	0.16
GONGA	MC9807[f]	17.3096	38.1793	0.45	0.0339	38.00	154.00	0.67	0.24	0.35	0.02
GONGA	MC987B[2]	14.3035	32.4375	0.44	0.3392	45.71	171.42	0.69	2.85	4.11	0.25
GONGA	MC987C	10.3118	16.7850	0.61	0.0258	37.14	205.70	0.65	0.33	0.51	0.03
GONGA	MC987dd	7.5072	10.5022	0.71	0.0067	68.57	222.85	0.79	0.12	0.16	0.01
GONGA	MC987ee	17.8571	37.4275	0.48	0.0343	40.00	188.56	0.67	0.24	0.36	0.02
GONGA	MC987ff	17.0200	38.7079	0.44	0.1104	45.71	171.42	0.69	0.78	1.12	0.07
GONGA	MC987gg	19.2915	45.5823	0.42	0.0024	40.00	188.56	0.66	0.01	0.02	0.00
GONGA	MC9813A[f]	5.1399	21.9287	0.23	0.2591	50.63	183.38	0.75	4.63	6.19	0.37
GONGA	MC9813A[5]	1.3268	37.4264	0.04	0.3796	32.38	131.42	0.62	6.89	11.07	0.66
GONGA	MC9813B[f]	6.0698	29.1563	0.21	0.2948	40.13	174.38	0.70	4.20	6.04	0.36
GONGA	MC9813B[5]	0.4995	17.9615	0.03	0.2423	36.19	162.85	0.66	9.43	14.22	0.85
GONGA	MC9813C[f]	5.5852	28.2388	0.20	0.4041	34.67	163.00	0.65	6.08	9.34	0.56
GONGA	MC9813C[5]	0.4407	16.8680	0.03	0.1438	40.00	174.28	0.69	6.00	8.68	0.52
GONGA	MC9813D	4.3330	31.7843	0.14	0.3167	42.86	197.13	0.72	4.93	6.86	0.41
GONGA	MC9813LA	16.6498	48.0795	0.35	0.3738	35.24	245.70	0.68	2.46	3.62	0.22
GONGA	MC9813LB	17.1216	36.5123	0.47	0.2042	34.28	171.42	0.65	1.46	2.25	0.14
GONGA	MC9813LC	10.6470	35.4547	0.30	0.6420	50.71	216.42	0.75	6.22	8.26	0.50
GONGA	MC9813LD[1]	16.6117	38.7766	0.43	0.2786	29.71	119.99	0.59	1.99	3.39	0.20
GONGA	MC9814[f,1]	7.2570	38.3891	0.19	0.4090	33.75	119.25	0.63	4.62	7.39	0.44
GONGA	mc9814aa[5]	0.0886	0.3226	0.27	0.0209	42.86	205.70	0.68	23.34	34.24	2.05
GONGA	mc9814bb	8.2656	51.8585	0.16	0.5175	45.71	222.85	0.70	4.65	6.69	0.40
GONGA	mc9814cc	3.8562	18.6011	0.21	0.4982	42.86	257.13	0.69	11.13	16.19	0.97
GONGA	MC9815[f]	7.7438	13.2793	0.58	0.1227	36.43	136.29	0.67	2.08	3.12	0.19

Table 2: (U-Th)/He replicate analyses (continued)

Transect	Sample replicate	[U] (ppm)	[Th] (ppm)	U/Th	[4He] (nmol/g)	radius (μm)	length (μm)	FT	Raw Age (Ma)	Corr Age[†] (Ma)	error[‡] 2σ
KANDING	MC0152A	13.5552	6.2114	2.18	0.1343	51.25	154.28	0.72	1.65	2.28	0.14
KANDING	MC0152B	8.4497	6.8372	1.24	0.1049	60.00	205.70	0.76	1.92	2.52	0.15
KANDING	MC0152C	27.2456	6.3307	4.30	0.3033	57.14	231.42	0.76	1.94	2.55	0.15
KANDING	MC0154B	50.3721	27.5380	1.83	0.4172	45.71	222.85	0.71	1.35	1.89	0.11
KANDING	MC0154C	73.6928	40.4109	1.82	0.5527	51.43	137.14	0.71	1.22	1.71	0.10
KANDING	MC0154D	71.5257	29.2338	2.45	0.5884	57.14	239.99	0.76	1.38	1.81	0.11
KANDING	MC0154E	94.0450	48.9577	1.92	0.7802	62.85	171.42	0.76	1.36	1.78	0.11
KANDING	MC0155A	9.2760	3.7726	2.46	0.1045	48.57	239.99	0.73	1.89	2.59	0.16
KANDING	MC0155B	4.9093	3.5161	1.40	0.0883	60.00	197.13	0.76	2.83	3.73	0.22
KANDING	MC0155C	18.3474	3.5607	5.15	0.1784	42.86	205.70	0.70	1.71	2.45	0.14
KANDING	MC0155D	48.1811	4.7236	10.20	0.9096	51.43	188.56	0.73	3.40	4.63	0.28
KANDING	MC0156A[2,3]	40.4172	230.3554	0.18	69.0586	40.00	205.70	0.66	133.28	201.95	12.12
KANDING	MC0156BMH[1,2]	1.6271	3.7339	0.44	20.4705	28.57	171.42	0.56	1300.08	2308.54	138.51
KANDING	mc0156cc[1,2]	11.3783	55.3123	0.21	1.3570	34.28	111.42	0.58	10.23	17.52	1.05
PAMEI	MC0149a	34.3195	38.9909	0.88	9.9084	60.00	265.70	0.77	41.78	54.24	3.25
PAMEI	MC0149b	31.8870	54.4310	0.59	12.9244	62.85	205.70	0.77	53.00	69.19	4.15
PAMEI	MC0149c	26.7199	28.7860	0.93	7.2268	54.28	239.99	0.75	39.58	52.90	3.17
PAMEI	MC0149e	23.7932	27.4183	0.87	7.3646	57.14	274.27	0.76	44.65	58.52	3.51
PAMEI	MC0149f	17.7622	42.8296	0.41	6.4375	54.28	205.70	0.74	42.43	57.60	3.46
PAMEI	MC0149g	44.4106	58.3869	0.76	13.0064	62.85	214.28	0.77	41.03	53.31	3.20
YALONG	MC0125A	5.2504	2.1084	2.49	0.0853	74.28	214.28	0.80	2.73	3.41	0.20
YALONG	MC0125B	27.8077	6.6682	4.17	0.6714	57.14	188.56	0.75	4.21	5.59	0.34
YALONG	MC0125C[3]	27.7804	101.6324	0.27	1.4546	48.57	245.13	0.72	5.18	7.22	0.43
YALONG	MC0125D	19.5992	17.1913	1.14	0.4665	56.00	257.13	0.76	3.63	4.79	0.29
YALONG	MC0126A	10.7639	18.3445	0.59	0.6000	57.14	171.42	0.74	7.32	9.89	0.59
YALONG	MC0126B	24.9910	146.0244	0.17	2.3549	80.00	291.41	0.81	7.30	9.01	0.54
YALONG	MC0126C[4]	0.1178	0.7166	0.16	0.0005	60.00	205.70	0.75	0.34	0.45	0.03
YALONG	MC0126D	11.4838	16.9510	0.68	0.8311	57.14	154.28	0.74	9.88	13.44	0.81
YALONG	MC0127A	17.2433	21.6004	0.80	0.3614	54.28	274.27	0.75	2.98	3.96	0.24
YALONG	MC0127B	8.1270	6.3074	1.29	0.1666	62.85	205.70	0.77	3.19	4.14	0.25
YALONG	MC0127C[3]	13.4471	31.7027	0.42	1.4350	57.14	171.42	0.74	12.62	17.11	1.03
YALONG	MC0127D	17.6511	17.1318	1.03	0.6265	57.14	274.27	0.76	5.32	6.96	0.40

Table 2: (U-Th)/He replicate analyses (continued)

Transect	Sample replicate	[U] (ppm)	[Th] (ppm)	U/Th	[4He] (nmol/g)	radius (μm)	length (μm)	FT	Raw Age (Ma)	Corr Age† (Ma)	error‡ 2σ
YALONG	MC0128A	14.3972	4.8389	2.98	0.1905	45.71	222.85	0.71	2.26	3.16	0.19
YALONG	MC0128B[1]	47.7478	108.5203	0.44	0.6890	31.43	179.99	0.60	1.73	2.91	0.17
YALONG	MC0129A[5]	0.1295	0.2735	0.47	0.0034	54.28	239.99	0.74	3.25	4.36	0.26
YALONG	MC0129bb[5]	0.0492	0.1707	0.29	0.0089	51.43	308.56	0.74	18.30	24.80	1.48
YALONG	MC0129cc	17.4385	1.9751	8.83	0.7368	57.14	179.99	0.75	7.57	10.07	0.60
YALONG	MC0129dd	9.1919	1.3530	6.79	0.3189	57.14	179.99	0.75	6.17	8.21	0.49
YALONG	MC0129ee	12.5308	2.2676	5.53	0.6018	45.71	188.56	0.71	8.47	11.95	0.72
YALONG	MC0129ff	14.3686	2.9833	4.82	0.3098	45.71	291.41	0.72	3.78	5.22	0.31
YALONG	MC0129gg	35.3152	1.5604	22.63	0.8725	45.71	325.70	0.73	4.50	6.17	0.37
YALONG	MC0130A	3.2529	5.4604	0.60	0.2343	62.85	171.42	0.76	9.50	12.54	0.75
YALONG	MC0130B	11.2158	30.3959	0.37	0.1737	48.57	205.70	0.71	1.74	2.44	0.15
YALONG	MC01-30A	7.9567	19.8513	0.40	1.0630	62.85	308.56	0.78	15.48	19.86	1.19
YALONG	MC0130bb[2]	2.8967	5.0629	0.57	0.5376	85.71	257.13	0.82	24.16	29.38	1.76
YALONG	MC0130cc	3.6311	3.7775	0.96	0.0987	57.14	197.13	0.75	4.02	5.36	0.32

^{f} furnace sample

† Corrected for alpha-ejection after *Farley et al.*, [1996].

‡ errors on single replicate analyses are 6 percent (2σ) and represent uncertainty on reproducibility of laboratory standards [*Farley*, 2002].

Analysis excluded on the basis of:

[1] small grainsize (FT < 0.65)

[2] excess He (on the basis of crystalization age or higher temp thermochronology data (K-Ar, Ar/Ar)) or re-extracts

[3] anomalous Th

[4] grain or grain fragment lost

[5] U, Th, or He near blank levels.

[6] Incomplete outgassing.

Table 3: Apatite (U-Th)/He mean ages

Transect	Sample ID	number of reps	mean age†	stdev‡
ANNING	MC-98-17	2	16.98	9.45(18.9)
	MC-98-18	3	19.47	3.03(6.06)
	MC-98-19	3	18.18	2.16(4.32)
DADU	MC-98-9	2	5.09	4.49(8.98)
	MC-98-10	2	17.04	9.15(18.3)
	MC-98-11	2	18.14	2.50(5.0)
	MC-98-12	3	21.03	8.46(16.92)
DANBA	MC-01-11	3	8.10	1.69(3.38)
	MC-01-12	4	6.08	0.95(1.9)
	MC-01-13	4	5.65	0.28(0.56)
	MC-01-14	6	9.35	3.76(7.52)
	MC-01-15	5	5.50	0.52(1.04)
DAOCHENG	MC-01-37	3	50.04	0.83(1.66)
	MC-01-38	3	60.07	19.28(38.56)
	MC-01-40	3	112.30	23.14(46.28)
	MC-01-41	3	111.91	30.05(60.1)
	MC-01-42	4	92.29	41.81(83.62)
	MC-01-43	2	91.39	3.04(6.08)
	MC-01-44	2	101.71	38.43(76.86)
GONGA	K1	4	2.14	0.08(0.16)
	MC-98-06	2	2.50	0.17(0.34)
	MC-98-07	6	0.42	0.38(0.76)
	MC-98-13	7	6.08	2.47(4.94)
	MC-98-14	2	11.44	6.72(13.44)
KANDING	MC-01-52	3	2.45	0.15(0.3)
	MC-01-54	4	1.80	0.07(0.14)
	MC-01-55	4	3.35	1.02(2.04)
PAMAI	MC-01-49	6	57.63	6.11(12.22)
YALONG	MC-01-25	3	4.60	1.10(2.2)
	MC-01-26	3	10.78	2.35(4.7)
	MC-01-27	3	5.02	1.68(3.36)
	MC-01-29	5	8.32	2.76(5.52)
	MC-01-30	4	10.05	7.80(15.6)

† 5 individual samples yielded only one replicate analysis and are not included with the mean ages. See Table 2.

‡ The standard deviation (stdev) was computed for the *spread of replicate values* for each sample at 1σ and 2σ (in parentheses).

Table 4: Apatite Fission-track data

Transect	Sample ID	$\rho_s^{\dagger}$	$\rho_i^{\dagger}$	$\rho_d^{\dagger}$	Grains (dmnls)	Q (dmnls)	Dpar (μm)	Dper (μm)	Mean length (μm)	Std dev (μm)	Pooled FT age (Ma)
DANBA	MC-01-11	0.179 (106)	4.841 (2863)	4.004 (4115)	21	0.487	1.74	0.48	13.55 ± 0.32 (111)	1.64	8.43 ± 0.87 (1.74)
	MC-01-12	0.641 (272)	14.52 (6161)	4.002 (4115)	24	0.395	1.90	0.44	13.63 ± 0.30 (114)	1.64	10 ± 0.7 (1.40)
	MC-01-13	0.764 (303)	16.731 (6639)	4.006 (4115)	18	0.234	1.97	0.45	13.44 ± 0.40 (110)	2.07	10.4 ± 0.7 (1.40)
	MC-01-14	0.153 (96)	3.311 (2083)	4.007 (4115)	21	0.353	1.82	0.40	13.67 ± 0.36 (100)	1.82	10.5 ± 1.1 (2.20)
	MC-01-15	0.957 (470)	24.574 (12063)	4.003 (4115)	22	0.026	2.01	0.45	13.96 ± 0.34 (110)	1.74	8.87 ± 0.49 (0.98)
YALONG	MC-01-25	0.064 (34)	2.598 (1372)	3.997 (4115)	22	0.769	1.77	0.47	13.93 ± 0.46 (53)	1.68	5.63 ± 0.99 (1.98)
	MC-01-26	0.058 (35)	2.068 (1247)	3.999 (4115)	23	0.618	1.66	0.42	13.71 ± 0.60 (32)	1.69	6.38 ± 1.11 (2.22)
	MC-01-27	0.042 (35)	2.023 (1682)	4.000 (4115)	24	0.488	1.63	0.43	13.47 ± 1.02 (13)	1.76	4.73 ± 1.32 (1.64)

† track densities are 10^6 tracks cm^{-2}. Abbreviations used are: ρ_s = spontaneous track densities; ρ_i = induced track densities; ρ_d = induced track densities in mica detector over standard glass.

Number of tracks counted or measured is shown in parentheses. Uncertainties are quoted at 1σ and 2σ (in parentheses).

Chapter 5

Topographic ooze: Building the eastern margin of Tibet by lower crustal flow[1]

Marin Kristen Clark and Leigh Handy Royden

Department of Earth, Atmospheric, and Planetary Sciences, Massachusetts Institute of Technology
77 Massachusetts Avenue, Cambridge, Massachusetts 02139, *USA*

Abstract

Topography extracted from swath profiles along the northern, southern, and eastern margins of the Tibetan Plateau show two end-member morphologies: steep, abrupt margins and long-wavelength, low-gradient margins. Because the lack of significant upper crustal shortening across much of the eastern plateau margin implies that the crustal thickening occurs mainly in the deep crust, we compare regional topographic gradients surrounding the plateau to model results for flux of a Newtonian fluid through a lower crustal channel of uniform thickness. For an assumed 15-km-thick channel, we estimate a viscosity for the lower crust of 10^{18} Pa·s beneath the low-gradient margins, 10^{21} Pa·s beneath the steep margins, and an upper bound of 10^{16} Pa·s beneath the plateau. These results indicate that the large-scale morphology of the eastern plateau reflects fluid flow within the underlying crust; crustal material flows around the strong crust of the Sichuan and Tarim Basins, creating broad, gentle margins, and "piles up" behind the basins creating narrow, steep margins. These results imply that this portion of the Eurasian crust was heterogeneous, but largely

[1]From Geology, Clark, M. K. and Royden, L. H. Modified with permission of the publisher, the Geological Society of America, Boulder, Colorado, USA.

weak, even prior to construction of the Tibetan Plateau.

Keywords: Tibet, topography, regional tectonics, lower crustal flow, viscosity.

5.1 Introduction

The behavior of the lower continental crust is an integral element of many recent tectonic models of intracontinental deformation, but the basic physical parameters that govern the mechanics of the lower crust remain poorly understood. Many authors have proposed that in regions where the continental crust is hot, the middle or lower crust acts as a weak viscous layer capable of flow on geologic time scales (e.g., Block and Royden, 1990; Wernicke, 1990; Kruse et al., 1991; Bird, 1991; Wdowinski and Axen, 1992). Thus, lower-crustal flow has been proposed as a mechanism by which lateral pressure gradients within the crust are equilibrated, reducing variations in topography and crustal thickness (e.g., Bird, 1991).

Lateral variations in topography, crustal thickness, and style of deformation suggest differences in strain distribution within active orogens and underscore the important role of the rheology of the lower continental crust in governing crustal deformation. Most studies aimed at constraining physical parameters of the lower crust have concentrated on the Basin and Range extensional province of the western United States and have yielded estimates of effective viscosity of the lower crust of 10^{17}-10^{19} Pa·s for assumed channel thicknesses of 10-15 km (e.g., Kruse et al., 1991; Wdowinski and Axen, 1992; Kaufman and Royden, 1994). However, estimates of lower-crustal viscosity beneath active convergent orogens are largely lacking. In this regard, the Tibetan Plateau and its associated mountain belts offer an excellent natural laboratory in which to explore the relationship of tectonics and topography in order to estimate rheologic parameters for the lower crust.

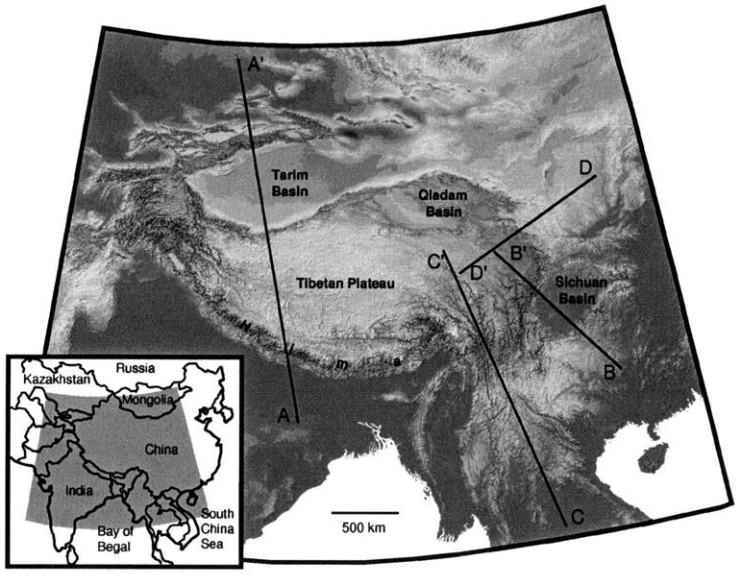

Figure 5.1: Topographic relief of Tibetan Plateau and surrounding regions. Lines represent axes of swath profiles for different margins of plateau. A–A′, Tibetan Plateau–Tarim Basin profile; B–B′, Sichuan Basin profile; C–C′, southeast margin profile; D–D′, northeast profile.

5.2 Tibet

The Tibetan Plateau has been created by the continent-continent collision of India with Eurasia since 45 Ma, and is an example of extreme regional topography over scales of hundreds to thousands of kilometers (e.g., Molnar and Tapponnier, 1975; Le Fort, 1975) (Fig. 2.1). The low-relief, but topo-graphically high, central plateau that has persisted despite continuing Cenozoic shortening has provoked explanations ranging from continental under-plating (Barazangi and Ni, 1982) and thermal uplift by delamination of the mantle lithosphere (e.g., England and Houseman, 1989) to deformation within a weak, fluid layer in the middle to lower crust (e.g., Bird, 1991; Zhao and Morgan, 1987).

Rock-mechanics laboratory experiments predict that for moderately high geothermal gradients or for thick crust, the middle or lower crust could contain a weak ductile zone, separating the more competent layers of the brittle upper crust from the rheologically strong upper mantle (e.g., Goetze and Evans, 1979; Brace and Kohlstedt, 1980; Kirby, 1983). Many geophysical observations from Tibet suggest the presence of a weak crustal zone;

e.g., short-wavelength gravity anomalies imply compensation of topography within the crust (Jin et al., 1994), and the Project INDEPTH observation of coincident mid-crustal low velocities, high electrical conductivity, and reflection bright spots in Tibet indicate that the middle crust in Tibet contains fluids and may be partially molten (Nelson et al., 1996; Makovsky et al., 1996; Chen et al., 1996).

In contrast to the flat central plateau, most of the marginal mountain belts bordering the plateau are characterized by steep topographic gradients, such as along the southern margin of the Himalaya (e.g., Le Fort, 1975) (Fig. 2.2A). Previous topographic studies have concentrated on these steep margins of the plateau but have ignored low-gradient margins of the plateau (e.g. Fielding et al., 1994). For example, excluding the areas adjacent to the Sichuan Basin (Fig. 2.2B), the eastern margin exhibits low topographic gradients with a gradual change in topographic elevation and crustal thickness from the plateau to the outer foreland (Li and Mooney, 1998) (Fig. 2.2C and 2D). Unlike the southern plateau margin, where crustal thickening can be explained by shortening of the upper crust through faulting and folding, most of the eastern margin has been uplifted without significant shortening of the upper crust along large-magnitude thrust faults (Burchfiel et al., 1995; Wang et al., 1998). The presence of such long-wavelength, regional topographic gradients in the absence of upper-crustal shortening suggests deformation within the lower crust by ductile flow. Therefore the elevated topography along the eastern plateau margin may be the direct result of thickening of the deep crust in concert with evacuation of the lower crust from beneath the central plateau (Royden, 1996; Royden et al., 1997).

5.3 Topographic Profiles

Several topographic swath profiles were taken from the northern, eastern, and southern margins of the Tibetan Plateau (Fig. 2.1). Topographic data are from the publicly available GTOPO30 digital elevation model (DEM) data set, which has $\sim$ 1 km horizontal resolution (U.S. Geological Survey, 1993). Swath topography was selected by extracting a narrow rectangular patch of topography with the long axis perpendicular to the plateau margin. The topographic values of the swath are projected onto a vertical plane parallel to the long

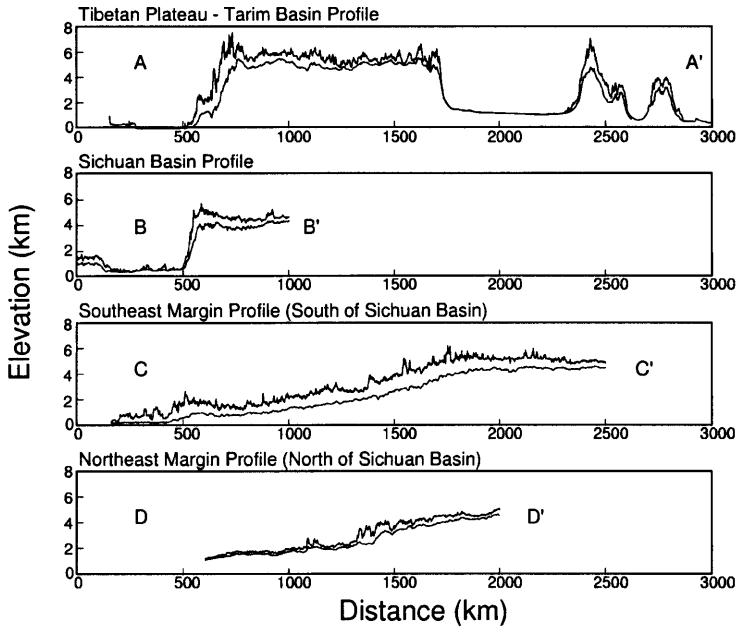

Figure 5.2: Topographic swath profiles for margins of Tibetan Plateau (width of swath is 100–300km). Profile curves represent maximum and mean profiles projected onto axis of swath profile. Locations of profiles are shown in Figure 2.1.

axis of the swath rectangle, and maximum, mean, and minimum topographic curves are calculated. The width of our swath profiles was 100-300 km, a range that was narrow enough to avoid averaging in the large-scale along-strike variations in geologic structure or crustal rheology. The envelope of maximum topography can be considered a proxy for the current elevated position of the pre-uplift surface, on the basis of previous studies by Wang et al. (1998), DEM analysis, and our own field observations along the eastern plateau margin, where large remnants of an old erosion surface are preserved between major drainage systems.

The topographic profiles fall into two end-member categories. The first group, located along the eastern margin but excluding the area adjacent to the Sichuan Basin, shows similar low topographic gradients despite very different climates and erosional histories (Fig. 2.2C and 2D). Topography along the southeastern margin decreases from 5.2 km to sea level over a distance of ~2500 km (Fig. 2.2C). Profiles north of the Sichuan Basin decrease from 4.5 km to 1 km over nearly the same distance (Fig. 2.2D). Steep regional topographic gradients characterize the second group of profiles along the northern (Tarim

Basin) and southern (Himalaya) borders of the plateau and along portions of the eastern border (Sichuan Basin) (Fig. 2.2A and 2B). The drop from plateau height (4.5-5 km) to <1 km elevation over only 50-200 km produces an average regional slope for these profiles that is more than an order of magnitude greater than along the low-gradient margins.

5.4 Model for Ductile Flow in the Lower Crust

In a simplified model of ductile flow in the lower crust, we consider the region of the lower crust to be a channel of uniform thickness in which crustal material is allowed to flow in response to lateral pressure gradients. In a two-dimensional model, we calculate the flux of a Newtonian fluid crust through a channel of thickness (h). For Poiseuille flow with zero velocity at the top and bottom of the channel, the velocity (u) of crustal material in the channel as a function of viscosity (μ), lateral pressure gradient (dp/dx), and depth (z) is

$$u = \frac{1}{2\mu}\frac{dp}{dx}\left(z^2 - hz\right) \tag{5.1}$$

(e.g. Turcotte and Schubert, 1982). The flux (U) of material in the channel can be expressed by integrating the velocity of the material over the channel height (h),

$$U = \int_0^h u(z)dz, \tag{5.2}$$

and can be related to changes in crustal thickness (c) over time by

$$\frac{dc}{dt} = \frac{-dU}{dx} = \frac{1}{12}h^3\frac{d}{dx}\left(\frac{1}{\mu}\frac{dp}{dx}\right). \tag{5.3}$$

We assume that the lateral pressure gradient in the channel is a function of topography only, with pressure given by $p = \rho_c g T(x)$, where ρ_c is the density of the crust (2600 kg/m^3, g is the acceleration due to gravity, and $T(x)$ is the topographic elevation. By considering only topographic wavelengths that are long compared to the flexural wavelength of the crust (Airy isostatic equilibrium), changes in topographic relief can be linearly related to

changes in crustal thickness. Thus, the change in topographic elevations over time as a result of flux of crustal material in the lower crust can be expressed by

$$\frac{dT}{dt} = \frac{(\rho_m - \rho_c)}{\rho_m}\left[\frac{1}{12}h^3\rho_c g\frac{d}{dx}\left(\frac{1}{\mu}\frac{dT}{dx}\right)\right], \tag{5.4}$$

where ρ_m is mantle density (3300 kg/m^3).

Topography is built by specifying a constant flux of material into the lower crustal channel from beneath the thick part of the plateau (Fig. 2.3). For the sake of simplicity, we require the channel thickness to be uniform and constant. Excess crustal material that does not participate in flow is accreted to the top and bottom of the channel; this material thickens the crust (Fig. 2.3). The flux rate into the channel from beneath the central plateau was chosen to allow a plateau margin of ~5 km elevation to develop over 20 m.y. (We chose 20 m.y. as an average time for plateau evolution on the basis of estimates of plateau uplift from geologic data; e.g., Harrison et al., 1992. Although the timing of the uplift is not precisely known, varying the model run time between 10 and 30 m.y. did not significantly alter results.) Crustal channel thicknesses have been estimated to be between 5 and 25 km (e.g., Wernicke, 1990). We chose a channel thickness of 15 km, although this approach provides nonunique results for viscosity because results scale with the variable (h^3/μ) (equation 5.4).

5.5 Results

Topographic profiles were computed for a range of spatially uniform lower crustal viscosities within a 15-km-thick channel, and were compared with observed topographic swath profiles. Model profile results for the southeastern margin of the plateau yield an excellent fit to the observed topography for a lower crustal viscosity of 10^{18} Pa·s (Fig. 2.4A); for the northeast profile an acceptable fit is also obtained for a viscosity of 10^{18} Pa·s (Fig. 2.4B). The topography across the steep margins of the Sichuan Basin (Fig. 2.4C) and the southern Tarim Basin (Fig. 2.4D) are fit with a much higher channel viscosity of 10^{21} Pa·s. However, there must be a viscosity contrast between the flat central plateau and the mar-

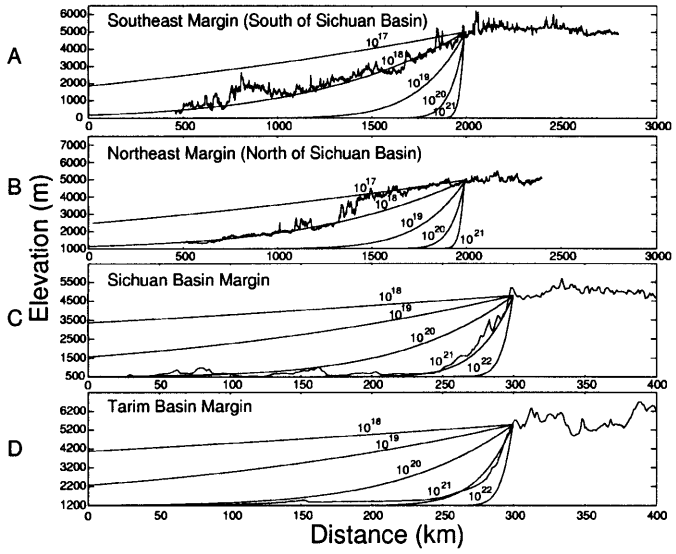

Figure 5.3: (1) Schematic drawing of viscous flow model. Viscous lower crustal material flows through crustal channel of uniform height (h) with specified viscosity. (2) Material is allowed to flux into channel for model run time of 20 m.y. so that elevation of 5 km is reached at edge of plateau. Parabolic channel flow is represented by velocity (u), and material that does not participate in channel flow is accreted to top and bottom of channel and thereby thickens crust (light gray areas). Viscosity of channel material in foreland determines regional topographic slope.

gins of the plateau, because the central plateau must have sufficiently low viscosity so that no significant regional topographic slope can be maintained. Because viscosity estimates vary approximately linearly with topographic slope, we estimate an upper bound on the viscosity beneath the flat central plateau of 10^{16} Pa·s.

If channel viscosity is varied with crustal thickness (i.e., is less under higher parts of the margin), then compared to the uniform case described here the model curves would be steeper at low elevations and flatter at high elevations. This yields a poor fit to the topography of the southeast and northeast margins.The very long wavelength relief that is observed along these margins requires a very low channel viscosity beneath all parts of the margin. Model results yielded the best agreement with observations when viscosity in the channel was uniformly weak at the initiation of flux into the channel, suggesting that the low-gradient margins of Tibet were already weak before the onset of crustal thickening. (Qualitatively similar results would be obtained if a power-law rheology for the channel

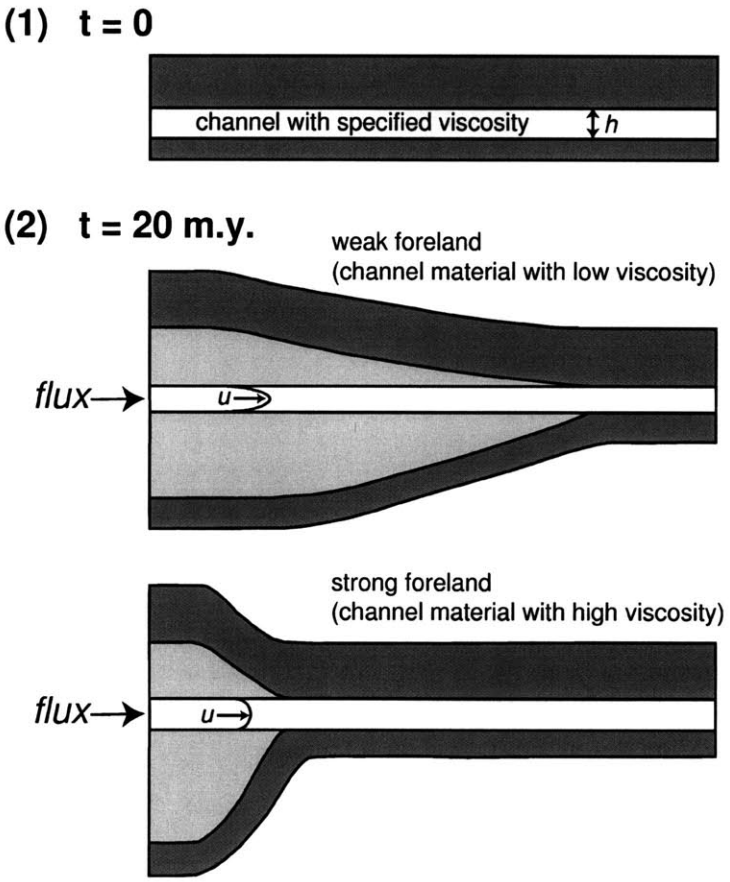

Figure 5.4: Model results vs. maximum topographic profiles. Model profiles represent runs for uniform lower crustal channel of thickness $h = 15$ km and variable viscosity (labeled in Pa·s).

material were assumed, such as n = 3, although the upward concavity of the profiles would be less pronounced.)

5.6 Discussion

The margins of the Tibetan Plateau fall naturally into two end-member categories (Fig. 2.2). Where the lower crust beneath the margin and adjacent foreland is weak, the lower crust of the central plateau escapes and flows over distances of 1000-2000 km; the result is the lack of a distinct edge to the plateau margin and little shortening deformation in the upper crust. By contrast, where the margins are strong, regional flow of lower-crustal material

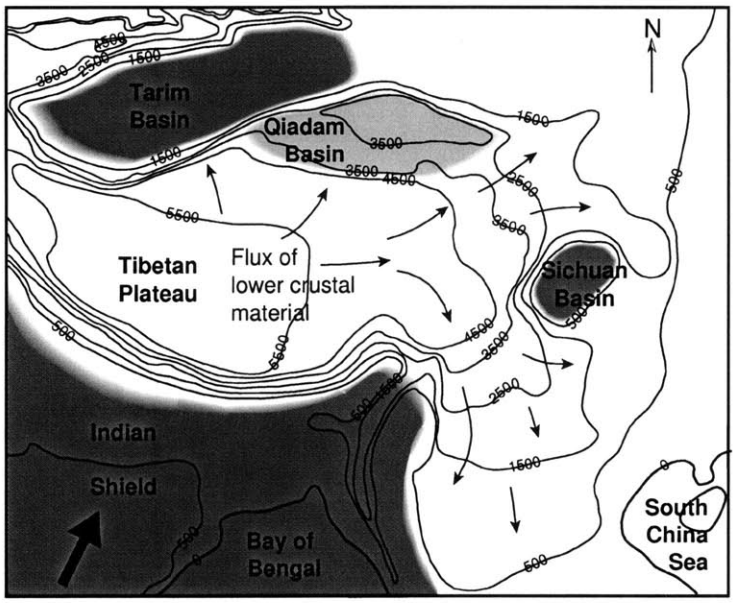

Figure 5.5: Contour plot of smoothed elevations of Tibetan Plateau and surrounding regions. Contour interval is 1000 m. Areas shaded in dark gray represent regions of cold, strong, continental material; light gray area represents intermediate strength; and white areas represent weak crustal regions. Thus, lower crust escapes from beneath thickened, elevated plateau through regions where crust is weak

from the weak central plateau is inhibited, and a steep topographic margin develops. These end-member cases are exemplified by changes in along-strike morphology of the eastern plateau margin. A smoothed-contour elevation map shows topography flowing or oozing around the Sichuan Basin (Fig. 2.5), reflecting the strength heterogeneity of the crust along the eastern plateau margin.

The Sichuan Basin is an old, intact craton that has remained relatively undeformed despite orogenic events at its margins in Mesozoic and Cenozoic time (see also England and Houseman [1985] for discussion of crustal heterogeneities). We propose that the strength of the crust beneath the Sichuan Basin inhibits flow of lower crustal material from central Tibet and therefore builds a steep topographic margin that is steeper than that of the Himalayan front, despite the lack of large-magnitude thrust faulting.

Similarly, the Tarim Basin is a relatively strong crustal region that has undergone little internal deformation during Mesozoic and Cenozoic orogenies (e.g., Molnar and Tapponnier, 1981). Crustal material also appears to be flowing eastward around the Tarim Basin

through areas of intermediate crustal strength in the Qaidam region and low crustal strength in the northeast corner region of the plateau. This analysis suggests that the greater part of the lower crust of Eurasia surrounding the eastern margin of the plateau was weak prior to building of the Tibetan Plateau.

Acknowledgments

We thank Clark Burchfiel, Kelin Whipple, John Southard, and Eric Kirby for insights and comments on the manuscript, and Chen Zhiliang and other colleagues the Chengdu Institute of Geology and Mineral Resources, China. R. Bürgmann D. Kohlstedt provided constructive reviews. Many thanks to Jeffery Nighbert providing his algorithm for "painted relief" used to produce the shaded relief map. work was supported by National Science Foundation (NSF) grant EAR-9614970 Royden, Burchfiel, and Whipple and by an NSF graduate fellowship to Clark.

5.7 References

Barazangi, M., and Ni, J., 1982, Velocities and propagation characteristics of P_n and S_n beneath the Himalayan arc and Tibetan Plateau: Possible evidence for underthrusting of Indian continental lithosphere beneath Tibet: Geology, v. 10, p. 179-185.

Bird, P., 1991, Lateral extrusion of lower crust from under high topography, in the isostatic limit: Journal of Geophysical Research, v. 96, p. 10,275-10,286.

Block, L., and Royden, L.H., 1990, Core complex geometries and regional scale flow in the lower crust: Tectonics, v. 9, p. 557-567.

Brace, W.F., and Kohlstedt, D.L., 1980, Limits on lithospheric stress imposed by laboratory experiments: Journal of Geophysical Research, v. 85, p. 6248-6252.

Burchfiel, B.C., Chen Zhiliang, Liu Yuping, and Royden, L.H., 1995, Tectonics of the Longmen Shan and adjacent regions, Central China: International Geology Review, v. 37, p. 661-735.

Chen Leshou, Booker, J.R., Jones, A.G., Nong Wu, Unsworth, M.J., Wenbo Wei, and

Handong Tan, 1996, Electrically conductive crust in southern Tibet from INDEPTH magnetotelluric surveying: Science, v. 274, p. 1694-1696.

England, P.C., and Houseman, G., 1985, Role of lithospheric strength heterogeneities in the tectonics of Tibet and neighbouring regions: Nature, v. 315, p. 297-301.

England, P.C., and Houseman, G., 1989, Extension during continental convergence, with application to the Tibet Plateau: Journal of Geophysical Research, v. 94, p. 17,561-17,579.

Fielding, E., Isacks, B., Barazangi, M., and Duncan, C.C., 1994, How flat is Tibet?: Geology, v. 22, p. 163-167.

Goetze, C., and Evans, B., 1979, Stress and temperature in the bending lithosphere as constrained by experimental rock mechanics: Royal Astronomical Society Geophysical Journal, v. 59, p. 463-478.

Harrison, T.M., Copeland, P., Kidd, W.S.F., and Yin, A., 1992, Raising Tibet: Science, v. 255, p. 1663-1670.

Jin, Y., McNutt, M.K., and Zhu Yongshen, 1994, Evidence from gravity and topography data for folding of Tibet: Nature, v. 371, p. 669-674.

Kaufman, P.S., and Royden, L.H., 1994, Lower crustal flow in an extensional setting: Constraints from the Halloran Hills region, eastern Mojave Desert, California: Journal of Geophysical Research, v. 99, p. 15,723-15,739.

Kirby, S.H., 1983, Rheology of the lithosphere: Reviews of Geophysics and Space Physics, v. 21, p. 1458-1487.

Kruse, S., McNutt, M.K., Phipps-Morgan, J., Royden, L., and Wernicke, B.P., 1991, Lithospheric extension near Lake Mead, Nevada: A model for ductile flow in the lower crust: Journal of Geophysical Research, v. 96, p. 4435-4456.

Le Fort, P., 1975, Himalayas: The collided range. Present knowledge of the continental arc: American Journal of Science, v. 275-A, p. 1-44.

Li, S., and Mooney, W.D., 1998, Crustal structure of China from deep seismic sounding profiles: Tectonophysics, v. 288, p. 105-113.

Makovsky, Y., Klemperer, S.L., Ratschbacher, L., Brown, L., Li Ming, Zhao Wenjin, and Meng Fanle, 1996, INDEPTH wide-angle reflection observation of P-wave-to-S-wave

conversion from crustal bright spots in Tibet: Science, v. 274, p. 1690-1691.

Molnar, P., and Tapponnier, P., 1975, Cenozoic tectonics of Asia: Effects of a continental collision: Science, v. 189, p. 419-426.

Molnar, P., and Tapponnier, P., 1981, A possible dependence of tectonic strength on the age of the crust in Asia: Earth and Planetary Science Letters, v. 52, p. 107-114.

Nelson, K.D., Zhao Wenjin, Brown, L.D., Kuo, J., Che Jinkai, Lui Xianwen, Klemper, S.L., Makovsky, Y., Meissner, R., Mechie, J., Kind, R., Wenzel, F., Ni, J., Nabelek, J., Chen Leshou, Tan Handong, Wei Wenbo, Jones, A.G., Booker, J., Unsworth, M., Kidd, W.S.F., Hauck, M., Alsdorf, D., Ross, A., Cogan, M., Wu Changde, Sandvol, E., and Edwards, M., 1996, Partially molten middle crust beneath southern Tibet: Synthesis of Project INDEPTH initial results: Science, v. 274, p. 1684-1688.

Royden, L., 1996, Coupling and decoupling of crust and mantle in convergent orogens: Implications for strain partitioning in the crust: Journal of Geophysical Research, v. 101, p. 17,679-17,705.

Royden, L.H., Burchfiel, B.C., King, R.W., Wang, E., Chen Zhiliang, Shen Feng, and Liu Yuping, 1997, Surface deformation and lower crustal flow in eastern Tibet: Science, v. 276, p. 788-790.

Turcotte, D., and Schubert, G., 1982, Geodynamics; applications of continuum physics to geological problems: New York, John Wiley & Sons, 450 p.

U.S. Geological Survey, 1993, Digital elevation models, data user guide, 5: Reston, Virginia, U.S. Geological Survey, p. 1-50.

Wang, E., Burchfiel, B.C., Royden, L.H., Chen Liangzhong, Chen Jishen, Li Wenxin, and Chen Zhiliang, 1998, Late Cenozoic Xianshuihe-Xiaojiang, Red River, and Dali fault systems of southwestern Sichuan and central Yunnan, China: Geological Society of America Special Paper 327, 108 p.

Wdowinski, S., and Axen, G.J., 1992, Isostatic rebound due to tectonic denudation: A viscous flow model of a layered lithosphere: Tectonics, v. 11, p. 303-315.

Wernicke, B.P., 1990, The fluid crustal layer and its implications for continental dynamics, *in* Salisbury, M.H., and Fountain, D.M., eds., Exposed cross sections of the continental crust: Dordrecht, Netherlands, Kluwer Academic Publishers, p. 509-544.

Zhao, W., and Morgan, W.J.P., 1987, Injection of Indian crust into Tibetan lower crust; a two-dimensional finite element model study: Tectonics, v. 6, p. 489-504.

Chapter 6

Dynamic topography produced by lower crustal flow against rheologic strength heterogeneities bordering the Tibetan Plateau[1]

Marin K. Clark,[a] John W. M. Bush,[b] and Leigh H. Royden[a]

[a] *Department of Earth, Atmospheric, and Planetary Sciences, Massachusetts Institute of Technology 77 Massachusetts Avenue, Cambridge, Massachusetts* 02139, *USA.*
[b] *Department of Applied Mathematics, Massachusetts Institute of Technology, Cambridge, Massachusetts* 02139, *USA.*

Abstract

We propose that dynamic topography may be a consequence of weak lower crustal flow against high-strength heterogeneities in the continental crust. Thus, resultant dynamic pressures developed in the deep crust may explain anomalously high topography and extensional structural features localized at orogenic plateau margins. In Tibet, we observe patterns of anomalously high topography (in excess of plateau elevations) adjacent to regions thought to be characterized by sharp contrasts in crustal strength. We construct a model of lower crustal channel flow based on the lubrication equations commonly used in fluid dynamics for studies of viscous flows in a thin-gap geometry. Dynamic pressures are produced where channel flow is inhibited by the presence of an obstruction, specifically,

[1] in preparation for submission to Geophysical Journal International

a rigid cylindrical block through which flow is absent. Dynamic topography is calculated by modeling the upper crust as an elastic layer loaded by the dynamic (non-lithostatic) pressures originating in the channel. Plan-view geometries of dynamic topography depend on the direction of lower crustal flow and the shape of the rigid crustal block. As much as 1500 meters of dynamic topography can be produced for lower crustal material with a viscosity of $2x10^{18}$ Pa s flowing in a 15 km thick channel around a rigid (infinite viscosity) cylindrical block at a rate of 8 cm/yr. Model results depend on the velocity(v), viscosity(μ) and channel thickness(h), uniquely through the term $\left(\frac{\mu v}{h^2}\right)$. Cross-sectional profiles of dynamic topography are concave-up for low flexural rigidities for the upper crust and resemble damped asymmetric antiforms for high flexural rigidities. Model dynamic topographic profiles are in good agreement with observed topographic profiles for eastern Tibet where model low values of flexural rigidity for the upper crust and low viscosity values for the lower crust are consistent with previously cited values for Tibet.

6.1 Background: Lower crustal flow

The strength and mechanical behavior of the lower continental crust is critical to the tectonic evolution and crustal dynamics of active orogens. A lower crust that is strong relative to the upper crust produces deformation that is plate-like, where strain is largely concentrated in narrow zones that are interpreted to root into the lithospheric mantle, and crustal motions are directly coupled to mantle motions over very short lengthscales (tens of kilometers) [*Royden*, 1996]. However, in regions where the crust is hot or excessively thick, laboratory experiments predict that the middle or lower crust could contain a weak ductile zone, separating the more competent layers of the brittle upper crust from the rheologically strong upper mantle [e.g. *Goetze and Evans*, 1979; *Brace and Kohlstedt*, 1980; *Kirby*, 1983]. Many authors have proposed that where the lower crust is sufficiently weak, it will deform by channelized flow in response to lateral pressure gradients arising from differential crustal thicknesses or density contrasts within the crust [*Bird*, 1991; *Royden*, 1996; *Bott*, 1999; *Beaumont et al.*, 2001].

A general model of viscous channel flow is supported by the static properties of the

lower crust delineated by geophysical and geological observations. Seismic data of ancient and active orogens shows that the deep crust is often highly reflective [e.g. *White et al.*, 2000; *Rabbel and Lueschen*, 1996; *Allmendinger et al.*, 1987] suggesting that it has experienced high differential strains. Geophysical evidence beneath active orogens, such as Tibet, suggest that wide-spread fluids (partial melt or aqueous fluids) at mid-crustal levels are present [e.g. *Makovsky and Klemperer*, 1999; *Alsdorf and Nelson*, 1999; *Ross et al.*, in press; *Wei et al.*, 2001], indicating a mechanism by which substantial weakening of the mid to lower crust may have taken place [*Nelson et al.*, 1996]. Recent rock mechanics experiments concur that introduction of even small amounts of partial melts may greatly reduce the bulk strength of the crust [*Rushmir*, 2001]. Geologic exposures of the deep crust show rocks that have experienced extreme ductile deformation and anatexis [*Klepeis et al.*, 1999; *Khazanehdari et al.*, 2000; *Kullerud et al.*, 2001]. The rheologic strength of the lower crust has also been proposed to be time-transgressive, where the transition from strong to weak lower crust may occur as a product of crustal thickening [e.g. *Royden*, 1996; *Vanderhaaeghe and Teyssier*, 2001].

Insights gained directly from geophysical observations, and from exhumation of the deep crust, are limited because they offer only a "snapshot" of the behavior of the lower crust and therefore are a step removed from studying the dynamics of active processes controlling lower crustal behavior. Key parameters governing flow of weak lower crustal material are not yet well established, and are paramount to our understanding of crustal deformation. Outstanding questions include: Over what wavelength does flow occur? What is the flow velocity? What is the effective viscosity of the material in the channel? We must establish or link temporal processes we can measure (i.e. surface uplift, exhumation rates, crustal thickening rates, etc.) to lower crustal dynamics in order to constrain parameters like fluid viscosity, flow velocity and the distance over flow occurs.

Modeling studies which relate lower crustal dynamics to observations and processes in active tectonic settings offer a direction in which to investigate the dynamic behavior of the lower crust during orogenesis. A depth-dependent rheology of the crust, which is a result of developing a weak zone, drastically changes predicted patterns of surface deformation [e.g. *Royden*, 1996; *Roy and Royden*, 2000]. Pressure-driven lower crustal flow

would allow for differential thickening of the upper and lower crust, potentially causing crustal thickening and upper crustal deformation to occur disproportionately during active orogenesis [*Marquart*, 1991; *Schmeling and Marquart*, 1990; *Royden et al.*, 1997; *Clark and Royden*, 2000] in both compressional [*Synder and Barazangi*, 1986] and extensional settings [*Kruse et al.*, 1991; *Block and Royden*, 1990]. Long-wavelength transfer of crustal material [*Clark and Royden*, 2000; *Mc Quarrie and Chase*, 2000] and "crustal isostasy" where upper crustal loads may be accommodated within a weak ductile lower crust, are also proposed consequences of development of a weak lower crust [*Bird*, 1991; *Bott*, 1999; *Mc Quarrie and Rodgers*, 1998].

In this paper we explore the dynamics of actively deforming continental areas where there is a contrast between crustal regions with and without a weak ductile layer. We propose that non-lithostatic pressure gradients, which result in dynamically-maintained (non-isostatic) excess topography, are a consequence of the interaction of weak flowing crust with static regions of strong crust.

6.2 Motivation: Crustal dynamics and Topography in Tibet

Strength contrasts in the continental crust may play an important role in the spatial distribution of crustal thickening and strain partitioning within the crust. Created by the ongoing continent-continent collision of India with Eurasia since ~45 Ma, the Tibetan Plateau is an example of extreme regional topography over scales of hundreds to thousands of kilometers [e.g. *Molnar and Tapponnier*, 1975; *Le Fort*, 1975]. The collision has resulted in the development of a low-relief but topographically high central plateau where the thickness of the crust has roughly doubled to about ~70 km. The flatness of the central plateau has been attributed to the low strength of the lithosphere prohibiting support of lateral pressure gradients produced by large topographic gradients [e.g. *England and Houseman*, 1988].

Throughout the Alpine-Himalaya region, it has also been recognized that there are regions of the continental crust that virtually escape deformation and crustal thickening dur-

ing active orogenesis. These blocks behave as rigid obstacles to ongoing deformation, often with concentrated deformation at their margins [e.g. *England and Houseman*, 1985]. In the region surrounding Tibet, these areas include the Tarim and Sichuan Basin, as well as the Indian Shield. It has been proposed that these high-strength heterogeneities can be partly attributed to their "tectonic age" [e.g. *Molnar and Tapponnier*, 1981; *Hsu*, 1993] but may also be related to low lithospheric temperatures, lack of aqueous fluids, underplating of strong mafic material or thermal insulation by cold mantle lithosphere.

It has subsequently been proposed that the weakness of the lithosphere can be attributed to the development of a low-viscosity layer in the middle or lower crust [e.g. *Bird*, 1991; *Royden*, 1996]. The hypothesis of a weak layer developed in the deep crust is supported by regional high heat flow beneath the plateau [*Hu et al.*, 2000], a highly reflective and conductive middle crust observed in central Tibet [*Nelson et al.*, 1996; *Wei et al.*, 2001], and gravity data consistent with a model of a rheologically layered lithosphere beneath Tibet consisting of a mechanically competent upper crustal and mantle layers separated by a weak low-viscosity zone in the lower crust [*Jin et al.*, 1996].

The elevated topography of the eastern plateau margin has been proposed to be the direct result of crustal thickening by weak, lower crustal material evacuated from beneath the central plateau [*Royden et al.*, 1997]. Flux of this weak lower crustal material from beneath the central plateau into eastern Tibet explains how crustal thickening along the eastern plateau and its margins has occurred despite a lack of significant shortening structures observed in the upper crust along the Longmen Shan/Sichuan Basin and southeastern plateau margins [*Dirks et al.*, 1994; *Burchfiel et al.*, 1995; *Wang et al.*, 1998]. Gradients in crustal thickness extending from the 60-70 km thick central plateau out into the 35 km thick eastern foreland [*Li and Mooney*, 1998] are interpreted to be the driving force for crustal flow. By relating the topographic gradient of the eastern plateau margin to the strength of the channel material, quantitative analysis of regional topographic slopes across the eastern plateau margin indicate that the strength of the mid-lower crust beneath the southeastern and northeastern low-gradient margins of the plateau is very low (10^{18} Pa s if one assumes a 15 km channel) [*Clark and Royden*, 2000]. By contrast, the mid-lower crust beneath the eastern steep margin bordering the Sichuan Basin is strong ($\geq 10^{21}$ Pa s for a 15 km

channel). The regional topographic gradients as displayed on a smoothed elevation contour map and from 3-dimensional digital topography perspectives show the continental crust "flowing" from the high central plateau around the low-elevation Sichuan Basin, reflecting the flow of weak lower crustal material around a strength heterogeneity of the crust along the eastern margin of Tibet (Figure 6.1).

6.3 Model: Viscous channel flow within the lower crust around cylindrical obstacles

Effective lower crustal channel thicknesses have been estimated to be between 5 –25 km [e.g. *Wernicke*, 1990], though the behavior of the system is characterized the inverse relationship between channel thickness and viscosity as (h^2/μ) for simple Poiseuille (channel) flow. For channel thicknesses between 10-15 km estimates of channel viscosities range from 10^{17} – 10^{20} Pa s and flow in the channel has been proposed to occur over lengthscales of 10's - 100's of kilometers [e.g. *Block and Royden*, 1990; *Kauffman and Royden*, 1994; and *Mc Quarrie and Chase*, 2000], and possibly over more than 1000 kilometers [*Clark and Royden*, 2000], with flow durations on the order of a few to a few tens of millions of years. Flow within the channel is driven by horizontal pressure gradients, due to topographic gradients and variations in crustal thickness or density. In reality, flowing lower crustal material is likely not to have sharp, well-defined channel boundaries, but most geodynamic models approximate flow behavior as Poiseuille flow [*Bird*, 1991].

We model the lower crust as a viscous fluid bound within a channel with fixed rigid horizontal boundaries which is overlain by an elastic layer that is free to deform under the influence of the dynamic pressures generated within the channel. We assume that the total deflection of the upper surface is small relative to the total channel thickness, and that the channel thickness is small relative to the characteristic horizontal scale of the flow. Flow within the channel is presumed to be driven by horizontal pressure gradients associated with topographic gradients across the plateau.

Flow is governed by the Stokes equation:

$$0 = -\nabla p - \rho g \mathbf{z} + \mu \nabla^2 \mathbf{u}, \qquad \nabla \cdot \mathbf{u} = 0, \tag{6.1}$$

where $-gz$ is the gravitational acceleration.

In the thin gap geometry, the dominant viscous stresses are those associated with the vertical velocity gradients, and the flow $\mathbf{u}$ reduces to parabolic channel flow:

$$\mathbf{u} = -\frac{b^2}{2\mu} \nabla P \left(1 - (\frac{z}{b})^2\right) \tag{6.2}$$

where $z = \pm b$ defines the upper and lower boundaries of the channel (h), μ is the viscosity(Newtonian) of the channel material, and ∇P is the horizontal pressure gradient driving flow. Our model for the weak, ductile channel layer corresponds to a Hele-Shaw cell bound above by a deformable elastic solid. The Hele-Shaw cell is commonly used to model flow in porous media and inviscid flows because of the peculiar feature that the depth averaged flow across the gap, $\overline{\mathbf{u}} = \frac{1}{h} \int_0^h \mathbf{u} dz$, is a pure potential flow satisfying Darcy's Law:

$$\overline{\mathbf{u}} = -\kappa \nabla P \tag{6.3}$$

where $\kappa = b^2/(3\mu)$ is the effective permeability of the medium [*Batchelor*, 1967; *Acheson*, 1990; *Furbish*, 1997].

We proceed by exploring the interaction between flow in our model lower crust and an "impermeable" region (infinite μ) corresponding to an area of high crustal strength. We prescribe a unidirectional far-field flow $\overline{U}$ within the channel and examine the effect of an impermeable rigid obstacle corresponding to a rigid block or subregional crustal fragment (Figure 6.2A). One anticipates that the flow will be diverted around such obstacles. The appropriate potential solution for potential flow around a cylinder is given by:

$$\overline{u_r} = \overline{U}(1 - \frac{a^2}{r^2}) cos\theta \tag{6.4}$$

$$\overline{u_\theta} = -\overline{U}(1 + \frac{a^2}{r^2})sin\theta \tag{6.5}$$

where a is the radius of the cylindrical obstacle, r is the radial distance and θ is the angle made with the direction of far-field flow (Figure 6.2). The corresponding pressure field (excluding lithostatic pressure) is

$$P = -\frac{1}{\kappa}\overline{U}(r + \frac{a^2}{r})cos\theta. \tag{6.6}$$

This pressure field is composed of two parts: a pressure relating to the background (far-field) flow, and a local pressure field developed due to flow being diverted around the rigid obstacle. The latter can be thought of as a dynamic pressure or the dynamic load applied at the base of the overlying elastic crust where the dynamic pressure in dimensional form is equal to: $P_{dyn} = \frac{1}{\kappa}\overline{U}r\cos(\theta)\left(\frac{a^2}{r^2}\right)$. In order to calculate the dynamic topography, we compute the flexural response of the upper crust in cross-section by applying a dynamic load to an elastic upper crustal layer and calculating the resulting deflection $w(x)$ [e.g. *Turcotte and Schubert*, 1982] (Figure 6.2B):

$$Dw_{xxxx}(x) + \rho g w(x) = P_{dyn}(x). \tag{6.7}$$

This model relies on several important assumptions. For simplicity, we assume that the channel walls are rigid and parallel. In reality, it is likely that the "channel" (defined as the spatial domain over which the flow is active) is deflected or thickened near the boundary with the rigid block, and possibly elsewhere. The background pressure gradient driving regional, uniform velocity flow is not explicitly modeled as a regional topographic slope here and instead, a flow velocity is imposed on the channel material. Finally, the no-slip upper and lower boundary conditions are expected to be valid provided that pressure-driven channel flow is significantly faster than flow associated with differential motion of under- or overlying plates. Relative motion of these boundaries would impart an additional shear that would act to either enhance or retard flow and so influence the magnitude of dynamic topography [*Beaumont, et al.*, 2001].

6.4 Model parameters and general results

Qualitatively, the dynamic pressure produced by the flow results in a first order pattern of symmetric highs and lows oriented "upstream" and "downstream" of the obstacle respectively (Figure 6.3). The region of significant dynamic pressure are roughly crescent-shaped, with the highest magnitude dynamic pressure located at the stagnation points of the flow adjacent to the boundary with the obstacle. The magnitude of the dynamic pressure decreases away from the obstacle as the inverse of the radial distance from the center of the obstacle, resulting in concave-up cross-sectional profiles (Figure 6.4). The maximum dynamic pressure is highest along a section oriented parallel to the flow direction (stagnation point), and decreases as a cosine function to zero at an orientation perpendicular to the regional flow (Eq. 4).

The dynamic pressure acts as a non-lithostatic load on the base of the upper crust and produces dynamic topography modified by the flexural strength of the upper crust. We express the flexural strength of the crust in terms of the effective elastic thickness (Te), which is related to the flexural rigidity D by $Te = (12D(1-\nu^2)/E)^{-3}$, where E and ν are Young's modulus and Poisson's ratio, respectively (e.g. Burov and Diament, 1995). For low flexural rigidities, the topography closely mirrors the dynamic pressure field. For increasing flexural strength, the cross-sectional shape of the predicted dynamic topography changes from a concave-up form that mirrors the calculated dynamic pressures to a damped, asymmetric antiform with increasing wavelength and decreasing amplitude (Figure 6.4). The mechanical behavior of the system is a function of the ratio (h^2/μ) of the channel thickness and the viscosity of the channel material, therefore we cannot independently determine both quantities. For example, the same dynamic topography profile would result from a thin channel with a very low viscosity as would from a much thicker channel with a higher viscosity.

6.5 Comparison of model results to topography along the eastern Tibetan plateau margin

6.5.1 General map view pattern compared to model results

Across the Tibetan Plateau, we observe a spatial correlation between regions of anomalously high topography (in excess of surrounding plateau elevations) and areas of contrasting crustal strength (Figure 6.5). In particular, these topographic anomalies occur adjacent to convexities (curvature of the plateau margin in plan view) to regions of strong foreland material that appears to "indent" the weaker plateau. From digital topography analyses these areas of anomalously high topography are roughly crescent shaped in plan view and are deeply dissected by fluvial and glacial erosion, especially compared to the adjacent relatively uneroded plateau surface (Figure 6.3). These areas are also associated with high rates of exhumation, and in some areas, detachment-style extensional faulting [*Burg et al.*, 1998; *Hubbard et al.*, 1995; *Clark et al.*, 2001].

We find a good correlation between position of the crustal "obstacle", regional lower crustal flow direction (interpreted to be down the regional topographic gradient), and the geographical extent of anomalously high topography (Figure 6.2). For example, in the eastern syntaxial region, flow is interpreted to be moving southeastward past the eastern syntaxis, and this geometry can be approximated as flow past the top half of a cylindrical obstacle (Figure 6.7). Thus our model predicts dynamic highs on the "upstream" side, in this case, west of the syntaxial corner. Near the Sichuan Basin, regional flow is interpreted to be flowing east directly against the southwest corner of the basin. This geometry is approximated as flow against the "upstream" side of the cylindrical obstacle. In this case, positive dynamic topography is predicted to occur as a symmetric crescent located directly about the cylindrical axis (Figure 6.7). We also observe a symmetry between the topographic patterns in eastern Tibet and those in the western plateau, where topographic highs at the western Himalayan syntaxis (Karakorum) and south of the Tarim Basin (W. Kunlun Shan) are observed (Figure 6.5).

6.5.2 Topographic analysis of the Sichuan Basin plateau margin

The topography surrounding the Sichuan Basin in eastern Tibet has been suggested to be the product of active lower crustal flow from central Tibet toward the east [*Royden et al.*, 1997; *Clark and Royden*, 2000; *Kirby et al.*, 2000] and most closely resembles the model geometry of flow around a cylindrical obstacle (Figure 6.1). River profiles and thermochronologic data along the steep plateau margin (Longmen Shan) bordering the Sichuan Basin support localized, young and active uplift concentrated at the plateau margin front [*Kirby et al.*, in press; *Kirby et al.*, 2002], despite a lack of evidence for significant horizontal motion (> 3 mm/yr) by surface shortening [*Chen et al.*, 2000; *King et al.*, 1997]. We propose that focused vertical uplift in the Longmen Shan may be a manifestation of dynamic topography produced by the diversion of lower crustal flow around the rigid Sichuan Basin.

The highest mountain peaks are concentrated at the margin front and profiles of maximum topography define smooth, concave up profiles (Figure 6.8) that can be considered as a minimum measure of surface uplift relative to the adjacent, modestly eroded plateau surface to the west. Localized peak uplift at the margin front suggests that lower crustal flow, coupled with erosion and extensional exhumation (observed in the Gonga Shan region and along strike of the Longmen Shan), may be responsible for creating and maintaining the Longmen Shan topographic escarpment. However, the predicted dynamic pressure arising from flow at depth should be reflected in the **mean** topography, not the maximum, which does not show deflection (except locally) at the Sichuan Basin plateau margin (Figure 6.8).

First we must be able to calculate this far-field topographic gradient driving flow and subtract it from the observed topography in order to quantify any "excess" topographic loads related to dynamic pressure within the lower crustal channel at depth. We present the following analysis which calculates a baseline, or predicted mean topographic slope, from regions north and south of the Sichuan Basin, beneath which lower crustal material is predicted to be flowing. We assume this slope is the far-field pressure gradient driving lower crustal material from central Tibet to the east.

We compare the "baseline mean profiles" to topographic profiles across the areas of anomalously high elevation and high local relief along the Longmen Shan (Sichuan Basin)

plateau margin. We use publically-available GTOPO30 digital topography (~1 km resolution) [*U.S.G.S.*, 1993] to calculate a mean elevation grid using a "focal-mean" calculation, which determines the mean value for each cell in the topographic grid based on a surrounding circular neighborhood domain. Figure 6.9 shows examples of three such focal mean grids for neighborhood domain radii of 10, 20 and 30 grid cells (with the map projection used here, this equates to radii of ~9, 17, and 26 km respectively). A focal mean of 10 cells retains much of the local variability and higher wavelength topographic signature, which is likely to be supported by the flexural strength of the upper crust. A focal mean of 30 cells begins to average out salient features such as the steep plateau margin adjacent to the Sichuan Basin (wavelength 50-100 km). Thus, we propose that the focal mean grid with radius of 20 cells represents the average crustal loads of interest. We calculate the baseline slope from the average of profiles taken from the focal mean grid across the southeastern and northeastern plateau margins Figure 6.10.

Mean topographic profiles that cross areas of anomalously high topography (peak heights well in excess of plateau elevations) are mapped onto the baseline slope using segments of the profile that fall outside the areas of excess topography (red) (Figure 6.11). In the region of Gonga Shan, low-sloping plateau segments flank either side of the anomalous topography (profiles D and E). These low-slope segments (red) were mapped onto the background profile. Profiles from farther north along the Longmen Shan and Min Shan (profiles G, H, I, and K) front do not have flanking low-slope plateau segments on either side of the anomalously high topography. These profiles were aligned to the baseline profile by aligning the high plateau, low-sloping segment (red) to the background profile and by matching the steep margin front (blue) to the steep front on the Gonga profiles (profiles D and E). All profiles show additional steep segments that are topographically lower than the projection of the baseline profile (green).

Topographic profiles from the Longmen Shan/Sichuan Basin plateau margin are subtracted from the baseline profile in order to calculate the topography in excess of the far-field topographic slope driving flow (Figure 6.12). We compare the result, referred to as "deflection profile" to model predictions for dynamic topography produced by flow past a rigid, cylindrical obstacle.

6.5.3 Comparison of topography to model results

The profiles shown here from the Gonga Shan region in the south, through the Longmen Shan, and north into the Min Shan, represent cross-sectional views of the topography oriented from 0 through 60 ° with respect to the flow direction, around a cylindrical obstacle of 200 km radius (Figure 6.13). Profile D (oriented parallel to flow direction, theta = 0 °), is fit with model parameters of viscosity = 2×10^{18} Pa s, velocity = 8 cm/yr, and channel thickness of h = 15 km Figure 6.13. It is important to bear in mind that we do not independently know the value of any one of these parameters and that the dependence of the model profiles on viscosity, velocity and channel thickness enters exclusively through the group $\frac{\mu v}{h^2}$. Using the parameters that best fit the amplitude for profile D, a best fit for the elastic strength of the upper crust is determined (Te) (Figure 6.13). The observed profiles very clearly show a best fit to very low values of the effective elastic thickness of the upper crust (Te). The closest fits are for Te between 1 and 5 km, suggesting that the upper crust is quite weak. Finally, using the parameters for velocity, viscosity, channel thickness and effective elastic thickness from the model fits in (Figure 6.13), we compare variations in model azimuth with respect to the flow direction, for profiles along the Sichuan Basin plateau margin (Figure 6.14). These profiles show a gross overall pattern which matches the prediction of lower amplitudes and shorter wavelengths predicted by the model for cross-sectional profiles oriented between 0 – 60 ° with respect to the flow direction. Deviation from this pattern is seen in the topography of profile H which is in excess of the predicted model profile, and in profile I which is less than the predicted topography for the orientation with respect to the flow. Also, the wavelength predicted for profiles I and K are greater than that observed in the topography.

6.5.4 Model assumptions

Our model of channel flow interacting with rigid obstacles relies on several simplifying assumptions: 1) We have assumed that the channel walls (defined as the area over which flow is occurring in the crust) remain rigid and parallel and have also only considered the effect of the pressure field created in the channel acting on the top of the channel. Pre-

sumably there is an equal, and symmetric, pressure acting on the base of the channel and it is likely that the channel thickens directly at the boundary with the obstacle. Since the flow behavior in our model is dependent on the ratio of the velocity and channel thickness squared to the viscosity, thickening of the channel would increase the viscosity or velocity required to fit observations compared estimates made for a uniform channel; 2) Symmetric dynamic "lows", or areas of subsidence, are also predicted by the general model to occur downstream of the obstacle (Figure 6.3) but are not observed in Tibet. On the basis of the topographic gradients in Tibet, we only observe flow interacting with the 'upstream' side of the rigid foreland regions, and do not observe flow completely encompassing foreland obstacles as illustrated in the model geometry. Therefore, a more specific treatment of the geometry in Tibet and its foreland regions might consider a time-dependent model describing the initiation of flow against the foreland obstacles instead of the steady uniform flow model described here. 3) Our model also assumes unidirectional flow and rheologic homogeneity at depth. The regional topographic gradients around the Sichuan Basin (and elsewhere in Tibet) indicate that the flow-field is more arcuate than unidirectional. Variability in flow direction, as well as expected geologic heterogeneity, most likely explains the variability in the detailed topographic profiles around the Sichuan Basin as compared to our model predictions (Figure 6.14). Thus, modeling a time-dependent flow within flexible boundaries warrants further study and may alter estimates of flow velocity, viscosity and channel thickness.

6.6 Discussion

Because it occurs tens of kilometers deep in the crust, active lower crustal flow cannot be directly observed. Understanding how lower crustal flow dynamics may be expressed in surface morphology and geology is one avenue for investigating the role of lower crustal behavior during orogenesis. The model presented here makes specific predictions about what may be observed in the topography, and by inference, the exhumation and structural history of an elevated region where a significant portion of the observed topography is dynamically maintained by stresses due to flow of weak material in the mid to lower crust.

By exploiting the simple equations that govern Hele-Shaw flow, we are able to propose a simple analytical, first-order surface expression of these flow dynamics.

The large scale over which crustal flow has been proposed to occur in Tibet (particularly in eastern Tibet) makes it an ideal locality for the application of such models [e.g. *Royden et al.*, 1997; *Clark and Royden*, 2000; *Shen et al.*, 2001]. The spatial distribution of areas of anomalously high topography in Tibet is consistent with our simple model of weak flowing material interacting with high-strength obstacles that inhibit flow and cause the dynamically maintained 'excess' topography. Model parameters used to match real topographic profiles from the eastern plateau margin adjacent to the Sichuan Basin are in good agreement with previously cited viscosity and channel thickness values reported for Tibet and the Basin and Range Province [*Block and Royden*, 1990; *Kruse et al.*, 1991; *Kaufman and Royden*, 1994; *Clark and Royden*, 2000].

Thin-sheet models of lithospheric deformation that have previously examined the effect of rigid obstacles located within an otherwise weak, deforming lithosphere predict thickening to occur at the boundary between the rigid block and the weak surrounding lithosphere [*England and Houseman*, 1985; *Hsui et al.*, 1990]. However, using a depth-dependent (or layered) rheology for the crust, drastically alters the predicted geologic and geophysical observations from those proposed by lithospheric thin-sheet models. Thin-sheet models predict thickening of the viscous layer at a rigid boundary with deformation distributed uniformly between upper crust, lower crust and mantle lithosphere. Only surface shortening structures are predicted in the geologic record. A model with a depth-dependent rheology and weak lower crustal layer predicts that this weak layer will experience rapid, differential motion compared to the upper crust and mantle lithosphere. The upwelling or thickening of lower crustal material, induced by dynamic pressure gradients created by flow against a rigid obstacle, may be expected to induce extensional strain in the upper crust and lead to the exhumation of mid-crustal rocks [*Royden*, 1996; *Shen et al.*, 2001]. This phenomenon could explain the juxtaposition of anomalously high standing topography, rapid surface uplift and exhumation, and in particular, the presence of extensional faulting and exposure of young, anatectic mid-crustal rocks concentrated at rheologic boundaries in Tibet (Figure 6.15) [e.g. *Shen et al.*, 2001; *Royden et al.*, 1996; *Hubbard et al.*, 1995; *Roger et al.*, 1995;

Burg et al., 1998; *Clark et al.*, 2001].

6.7 Conclusion

The Hele-Shaw geometry provides a simple way to model viscous channel flow in the lower crust. Rigid cylindrical obstacles represent plan-view convexities commonly observed along strike of orogenic belts. By presenting a geometry of flow past a cylindrical obstacle, we attempt to explore a general relationship between predicted dynamic topography and the presence of weak lower crustal flow in the vicinity of crustal strength heterogeneities, predicting first order geometric patterns in map view and cross-sectional topography.

Comparison of model results to observations in Tibet suggests that areas of anomalously high topography, extensional faulting, and young magmatism, may be related to the dynamics of the lower crust as it flows out from beneath the high plateau and against high strength heterogeneities in the surrounding foreland. In particular, this geometry works well for the Sichuan Basin in eastern Tibet, because its geometry most closely resembles the cylindrical geometry used in our model. Also, the contribution of upper crustal thickening to the development of high topography in eastern Tibet has been relatively minor and has likely been produced by preferential thickening of the lower crust. Model results show that anomalously high topography at the Sichuan Basin margin is consistent with flow of weak lower crust (viscosity = 2×10^{18} Pa s) within a 15 kilometer channel at 8 mm/yr.

Other margins of the Tibetan plateau are undoubtedly more complex. Modeling more complicated geometries, which may correspond to a specific geographical area, and considering the contribution of crustal thickening by upper crustal structures certainly warrants further study. Results for Tibet may also be applicable to other regions, particularly along the Alpine-Himalaya orogenic system, adjacent to the Black Sea, the Caspian Sea, and along the region of the Lut block in Iran, where strength contrasts in the deforming continental lithosphere have been described. Additional observations about the structural patterns, development of high topography and rates of exhumation in these regions could provide more insight into the parameters governing lower crustal flow.

6.8 References

Acheson, D. J., 1990, *Elementary Fluid Dynamics*, Clarendon Press, New York, 397 p.

Allmendinger, R., Nelson, K. D., Potter, C. J., Barazangi, M., Brown, L. D., Oliver, J. E., 1987, Deep seismic characteristics of the continental crust, *Geology*, v. 15, n. 4, pp. 304 – 310.

Alsdorf, D. and Nelson, K. D., 1999, Tibetan satellite magnetic low; evidence for widespread melt in the Tibetan crust?, *Geology*, v. 27, n. 10, pp. 943 – 946.

Batchelor, G. K., 1967, *An Introduction to Fluid Dynamics*, Cambridge University Press, Cambridge, 615 p.

Beaumont, C., Jamieson, R. A., Nguyen, M. H., Lee, B., 2001, Himalayan tectonics explained by extrusion of a low-viscosity crustal channel coupled to focused surface denudation, *Nature*, v. 414, p. 738 – 742.

Bird, P., 1991, Lateral extrusion of lower crust from under high topography, in the isostatic limit, *J. Geophys. Res.*, v. 96, n. B6, pp. 10,275 - 10,286.

Block, L. and Royden, L. H., 1990, Core complex geometries and regional scale flow in the lower crust, *Tectonics*, v. 9, pp. 557 – 567.

Bott, M., 1999, Modeling local crustal isostasy caused by ductile flow in the lower crust, *J. Geophys. Res.*, v. 104, n. B9, pp. 20,349 – 20,359.

Brace, W. F. and Kohlstedt, D. L., 1980, Limits on lithospheric stress imposed by laboratory experiments, *J. of Geophys. Res.*, v. 85, pp. 6,248 – 6,252.

Burchfiel, B. C., Chen, Z., Liu, Y., Royden, L. H., 1995, Tectonics of the Longmen Shan and adjacent regions, Central China, *Int. Geol. Rev.*, v. 37, pp. 661 – 735.

Burg, J-P., P. Nievergelt, F. Oberli, D. Seward, P. Davy, J-C. Maurin, Z. Diao, and M. Meier, 1998, The Nambshe-Barwa syntaxis: evidence for exhumation related to compressional crustal folding, *J. Asian Earth Sci., 16*, 239–252.

Burov, E. and Diament, M., 1995, The effective elastic thickness (Te) of continental lithosphere: What does it really mean?, *J. of Geophys. Res.*, v. 100, n. B3, pp. 3,905 – 3,927.

Chen, Z., Burchfiel, B. C., Liu, Y., King, R. W., Royden, L. H., Tang, W., Wang, E., Zhao,

J., and Zhang, X., 2000, GPS measurements from eastern Tibet and their implications for India/Eurasia intercontinental deformation, *J. Geophys. Res.*, v. 105, p. 16,215 – 16, 227.

Clark, M. K., House, M. A., Royden, L. H., Burchfiel, B. C., Zhang, X., Tang, W., and Chen, Z., 2000, River incision and tectonic uplift in eastern Tibet from low-temperature apatite U-Th/He thermochronology, *EOS Trans. AGU*, v. 81, no. 48, Fall Meet. Suppl., 1102.

Clark, M. K. and Royden, L. H., 2000, Topographic ooze: Building the eastern margin of Tibet by lower crustal flow, *Geology*, v. 28, n. 8, pp. 703 – 706.

Clark, M. K., L. H. Royden, J. Bush, B. C. Burchfiel, and X. Zhang, 2001, Sub-regional dynamic topography and deformation of the lower crust by decoupled channel flow in Tibet, *Eos Trans. AGU, (82)* Fall Meet. Suppl., Abstract T11H-06.

Dirks, P. H. G. M., Wilson, C. J. L., Chen, S., Luo, Z. L., and Liu, S.,1994, Tectonic evolution of the NE margin of the Tibetan Plateau; evidence from the central Longmen Mountains, Sichuan Province, China, *J. of Southeast Asian Earth Sci.*, v. 9, no. 1-2, pp. 181 – 192.

England, P. C. and Houseman, G. A., 1988, The mechanics of the Tibetan Plateau, *Phil. Trans. Royal Soc. of London A*, v. 326, pp. 301 - 320.

England, P. C. and Houseman, G., 1985, Role of lithospheric strength heterogeneities in the tectonics of Tibet and neigbouring regions, *Nature*, v. 315, pp. 297 – 301.

Furbish, D. J., 1997, *Fluid Physics in Geology*, Oxford University Press, New York, 476 p.

Goetze, C. and Evans, B., 1979, Stress and temperature in the bending lithosphere as constrained by experimental rock mechanics, *Royal Astro. Soc. Geophys. J.*, v. 59, p. 463 – 478.

Heim, A., ETH-library, Zürich, Call no. Hs 494b:25 ♯290.

Hu, S., He, L., Wang, J., 2000, Heat flow in the continental area of China: a new data set, *Earth Planet. Sci. Lett.*, v. 179, pp. 407 – 419.

Hubbard, M. S., Spencer, D. A., and West, D. P., 1995, Tectonic exhumation of the Nanga Parbat massif, northern Pakistan, *Earth and Planet. Sci. Lett.*, v. 133, p. 213 – 225.

Hsui, A. T., Wilkerson, M. S., and Marshak, S., 1990, Topographically driven crustal flow

and its implication to the development of pinned oroclines, *Geophys. Res. Lett.*, v. 17, n. 12, pp. 2421 - 2424.

Hsu, K. J., 1993, Relict back-arc basins; principles of recognition and possible new examples from China, *Acta Petrolei Sinica*, v. 14, n. 1, pp. 1 – 13.

Jin, Y., Mc Nutt, M. K., Zhu, Y., 1996, Mapping the descent of Indian and Eurasian plates beneath the Tibetan Plateau from gravity anomalies, *J. of Geophys. Res.*, v. 101, n. B5, pp. 11,275 – 11,290.

Kaufman, P. S. and Royden, L. H., 1994, Lower crustal flow in an extensional setting: Constraints from the Halloran Hills region, eastern Mojave Desert, California, *J. of Geophys. Res.*, v. 99, pp. 15,723 – 15,739.

Khazanehdari, J., Rutter, E. H., Brodie, K. H., 2000, High-pressure-high-temperature seismic velocity structure of the midcrustal and lower crustal rocks of the Ivrea-Verbano Zone and Serie dei Laghi, NW Italy, *J. of Geophys. Res.*, v. 105, n. 6, pp. 13,843 – 13, 858.

King, R. W., Shen, F., Burchfiel, B. C., Royden, L. H., Wang, E., Chen, Z., Liu, Y., Zhang, X., Xhao, J., Li, Y., 1997, Geodetic measurement of crustal motion in Southwest China, *Geology*, v. 25, n. 2, pp. 179 – 182.

Kirby, E., Whipple, K. X., Burchfiel, B. C., Tang, W., Berger, G., Sun, Z., 2000, Neotectonics of the Min Shan China; implications for mechanisms driving Quaternary deformation along the eastern margin of the Tibetan Plateau, *Geol. Soc. of Am. Bull.*, v. 112, n. 3, pp. 375 – 393.

Kirby, E., Reiners, P. W., Krol, M. A., Whipple, K. X., Hodges, K. V., Farley, K. A., Tang, W., Chen, Z., 2002, Late Cenozoic evolution of the eastern margin of the Tibetan Plateau: Inferences from 40Ar/39Ar and (U-Th)/He thermochronology, *Tectonics*, 10.1029/2000TC001246.

Kirby, E., Whipple, K. X., Tang, W., Chen, Z., in press, Distribution of active rock uplift along the eastern margin of the Tibetan Plateau: inferences from bedrock channel longitudinal profiles, *J. of Geophys. Res.*.

Kirby, S. H., 1983, Rheology of the lithosphere, *Rev. of Geophys. and Space Phys.*, v. 21, pp. 1,458 – 1,487.

Klepeis, K., Daczko, N. R., Clarke, G. L., 1999, Kinematic vorticity and tectonic significance of superposed mylonites in a major lower crustal shear zone, northern Fiordland, New Zealand, *J. of Struct. Geol.*, v. 21, n. 10, pp. 1,385 – 1,405.

Kruse, S., Mc Nutt, M. K., Phipps-Morgan, J., Royden, L., and Wernicke, B. P., 1991, Lithospheric extension near Lake Mead, Nevada: A model for ductile flow in the lower crust, *J. of Geophys. Res.*, v. 96, pp. 4,435 – 4,456.

Kullerud, K., Flaat, K., Davidsen, B., 2001, High-pressure fluid-rock reactions involving Cl-bearing fluids in lower-crustal ductile shear zones of the Flakstadoy basic complex, Lofoten, Norway, *J. of Petrology*, v. 42, n. 7, pp. 1,349 – 1,372.

Le Fort, P., 1975, Himalayas: The collided range. Present knowledge of the continental arc, *Am. J. Sci.*, v. 275-A, pp. 1 – 44.

Lebedev, S. and Nolet, G., 2003, The upper mantle beneath SE Asia from S-velocity tomography, Journal of Geophysical Research, v. 108, 10.1029/2000JB000073.

Li, S. and Mooney, W. D., 1998, Crustal structure of China from deep sounding profiles, *Tectonophysics*, v. 288, pp. 105 – 113.

Makovsky, Y. and Klemperer, S., 1999, Measuring the seismic properties of Tibetan bright spots; evidence for free aqueous fluids in the Tibetan middle crust, *J. Geophys. Res.*, v. 104, n. 5, pp. 10,795 – 10,825.

Marquart, G., 1991, Finite element modeling of lower crustal flow: A model for crustal thinning variations, *J. Geophys. Res.*, v. 96, n. B12, pp. 20,331 – 20,335.

Masek, J. G., Isacks, B. L., Fielding, E. J., Browaeys, J.,1994, Rift flank uplift in Tibet; evidence for a viscous lower crust, *Tectonics*, v. 13, n. 3, pp. 659 – 667.

Mc Quarrie, N. and Chase, C., 2000, Raising the Colorado Plateau, *Geology*, v. 28, n. 1, pp. 91 – 94.

Mc Quarrie, N. and Rodgers, D. W., 1998, Subsidence of a volcanic basin by flexure and lower crustal flow: The eastern Snake River Plain, Idaho, *Tectonics*, v. 17, n. 2, pp. 203 – 230.

Molnar, P. and Tapponnier, P., 1975, Cenozoic tectonics of Asia: Effects of a continental collision, *Science*, v. 189, pp. 419 – 426.

Molnar, P. and Tapponnier, P., 1981, A possible dependence of tectonic strength on the age

of the crust in Asia, *Earth Planet. Sci. Lett.*, v. 52, pp. 197 - 114.

Nelson, K. D., Zhao, W., Brown, L. D., Kuo, J., Che, J., Lui, X., Klemper, S. L., Makovsky, Y., Meissner, R., Mechie, J., Kind, R., Wenzel, F., Ni, J., Nablek, J., Chen, L., Tan, H., Wei, W., Jones, A., Booker, J., Unsworth, M., Kidd, W. S. F., Hauck, M., Alsdorf, D., Ross, A., Cogan, M., Wu, C., Sandvol, E., Edwards, M., 1996, Partially molten middle crust beneath southern Tibet: Synthesis of Project INDEPTH initial results, *Science*, v. 274, pp. 1,684 – 1688.

Rabbel, W. and Lueschen, E., 1996, Shear wave anisotropy of laminated lower crust at the Urach geothermal anomaly, *in* Seismic reflection probing of the continents and their margins, Ansorge, J., Bodoky, T. J., Hajnal, Z., eds., *Tectonophysics*, v. 264, n. 1 – 4, pp. 219 – 233.

Roger, F., Calassou, S., Lancelot, J., Malavieille, J., Mattauer, M., Xu, Z., Hao, Z., and Hou, L., 1995, Miocene emplacement and deformation of the Konga Shan granite (Xianshui He fault zone, west Sichuan, China): Geodynamic implications, *Earth Planet. Sci., Lett.*, v. 130 p. 201 – 216.

Ross, A., Brown, L. D., Nelson, K. D., in press, Deep Seismic Bright Spots and Magmatism in Southern Tibet, *J. Geophys. Res.*.

Roy, M. and Royden, L. H., 2000, Crustal rheology and faulting at strike-slip plate boundaries; 2, Effects of lower crustal flow, *J. Geophys. Res.*, v. 105, n. 3, pp. 5, 599 – 5,613.

Royden, L. H., 1996, Coupling and decoupling of crust and mantle in convergent orogens: Implications for strain partitioning in the crust, *J. Geophys. Res.*, v. 101, n. B8, pp. 17,679 - 17,705.

Royden, L. H., Burchfiel, B. C., King, R. W., Wang, E., Chen, Z., Shen, F., and Yuping, L., 1997, Surface deformation and lower crustal flow in eastern Tibet, *Science*, v. 276, pp. 788 – 790.

Rushmer, T., 2001, Volume change during partial melting reactions; implications for melt extraction, melt geochemistry and crustal rheology, in Partial melting of the crust and flow of orogens, C. Teyssier and O. Vanderhaeghe, eds., *Tectonophysics*, v. 342, n. 3 – 4, pp. 389 – 405.

Shen, F., Royden, L. H., and Burchfiel, B. C., 2001, Large-scale crustal deformation of the Tibetan Plateau, *J. Geophys. Res.*, v. 106, n. 4, pp. 6,793 – 6,816.

Schmeling, H. and Marquart, G., 1990, A mechanism for crustal thinning without lateral extension, *Geophys. Res. Lett.*, v. 17, n. 12, pp. 2417 - 2420.

Synder, D. and Barazangi, M., 1986, Deep crustal structure and flexure of the Arabian Plate beneath the Zagros collisional mountain belt as inferred from gravity observations, *Tectonics*, v. 5, n. 3, pp. 361 – 373.

Turcotte, D. L. and Schubert, G., 1982, *Geodynamics: Applications of Continuum Physics to Geological Problems*, John Wiley and Sons, Inc., New York, 450 p.

U.S. Geological Survey, *Digital elevation models, data user guide, 5*, pp. 1-50, U.S. Geological Survey, Reston, Virginia, 1993.

Vanderhaeghe, O. and Teyssier, C., 2001, Crustal-scale rheological transitions during late-orogenic collapse, *in* Deformation processes in the earth's crust, Boland, J. and Ord, A., eds, *Tectonophysics*, v. 335, n. 1 – 2, pp. 211 – 228.

Wang, E., Burchfiel, B. C., Royden, L. H., Chen, L., Chen, J., Li, W., Chen, Z., 1998, Late Cenozoic Xianshuihe-Xiaojiang, Red River, and Dali fault systems of southwestern Sichuan and central Yunnan, China, *Geol. Soc. Am. Spec. Paper*, v. 327, 108 p.

Wei, W., Unsworth, M. J., Jones, A. G., Booker, J. R., Tan, H., Nelson, K. D., Chen, L., Li, S., Solon, K., Bedrosian, P. A., Jin, S., Deng, M., Ledo, J., Kay, D., Roberts, B., 2001, Detection of widespread fluids in the Tibetan crust by magnetotelluric studies, *Science*, v. 292, pp. 716 – 718.

Wernicke, B. P., 1990, The fluid crustal layer and its implications for continental dynamics, in Salisbury, M. H. and Fountain, D. M., eds. Exposed cross-sections of the continental crust, Dordrecht, Netherlands, Kluwer Academic Publishers, pp. 509 – 544.

White, D. J., Forsyth, D. A., Asudeh, I., Carr, S. D., Wu, H., Easton, R. M., and Mereu, R. F., 2000, A seismic-based cross-section of the Greenville Orogen in southern Ontario and western Quebec, *Canadian J. Earth Sci.*, v. 37, pp. 183 – 192.

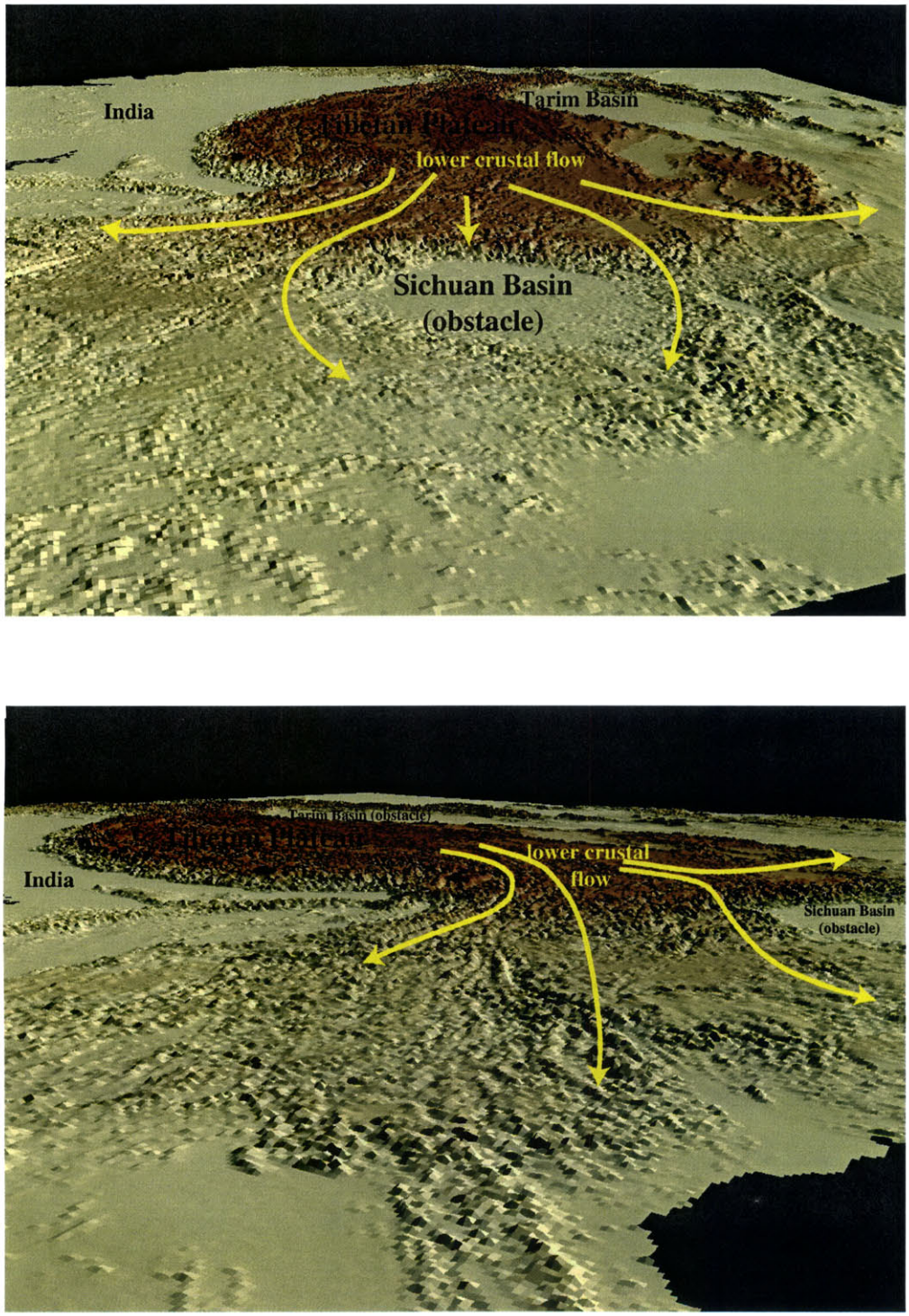

Figure 6.1: 3D perspective of digital topography, view to the west. Topography mimics flow of weak, lower crustal material around the rheologically strong Sichuan Basin, shown by yellow arrows.

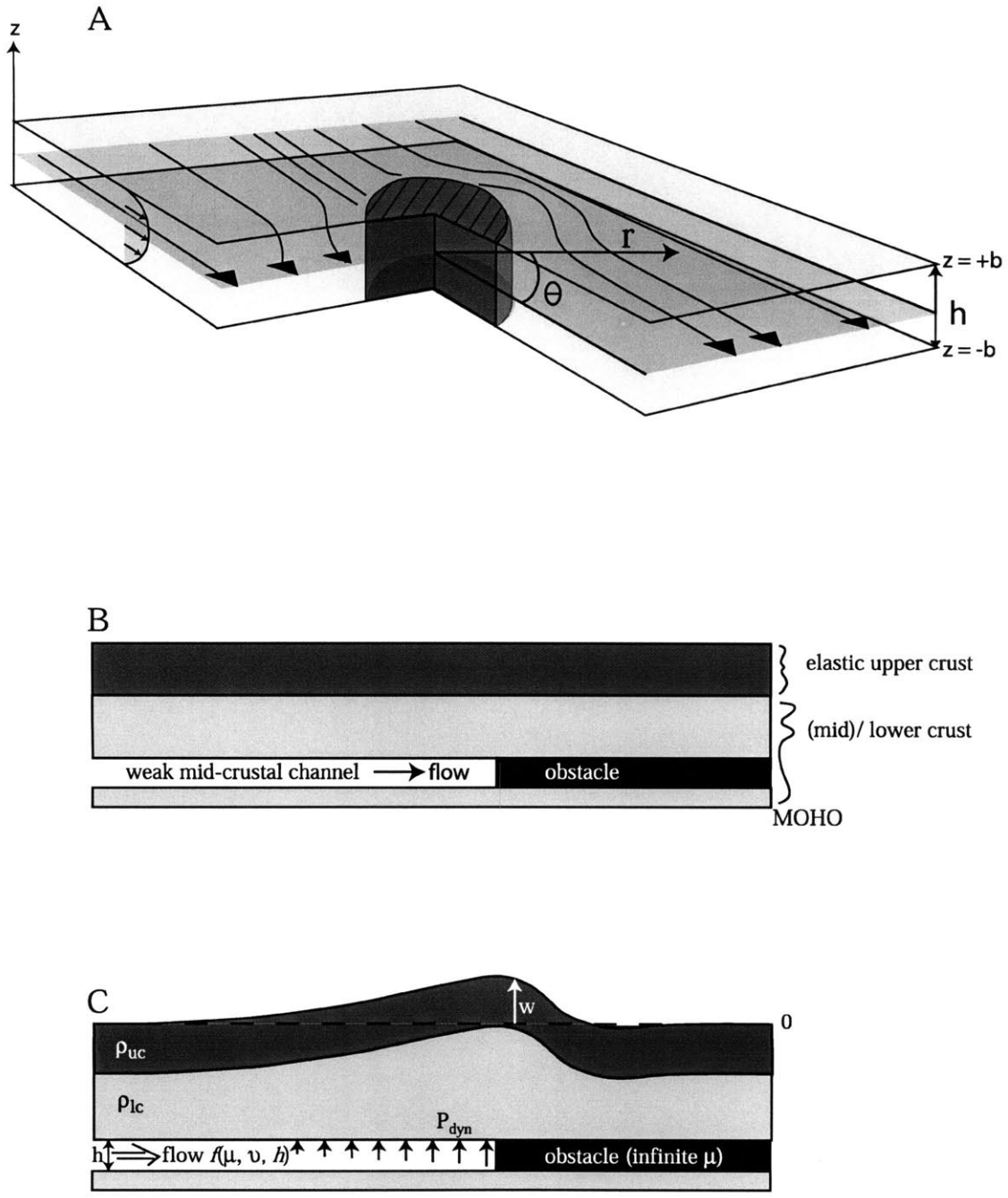

Figure 6.2: (A) Model geometry of Hele-Shaw cell flow (channel flow within a thin-gap geometry) past a rigid cylindrical obstacle. (B) Cross-sectional model geometry. Dynamic pressure calculated for the flow layer adjacent to the obstacle acts as a load on the elastic upper crust. Deflection of the upper crust is observed as dynamic topography, which is damped by the elastic strength of the upper crust.

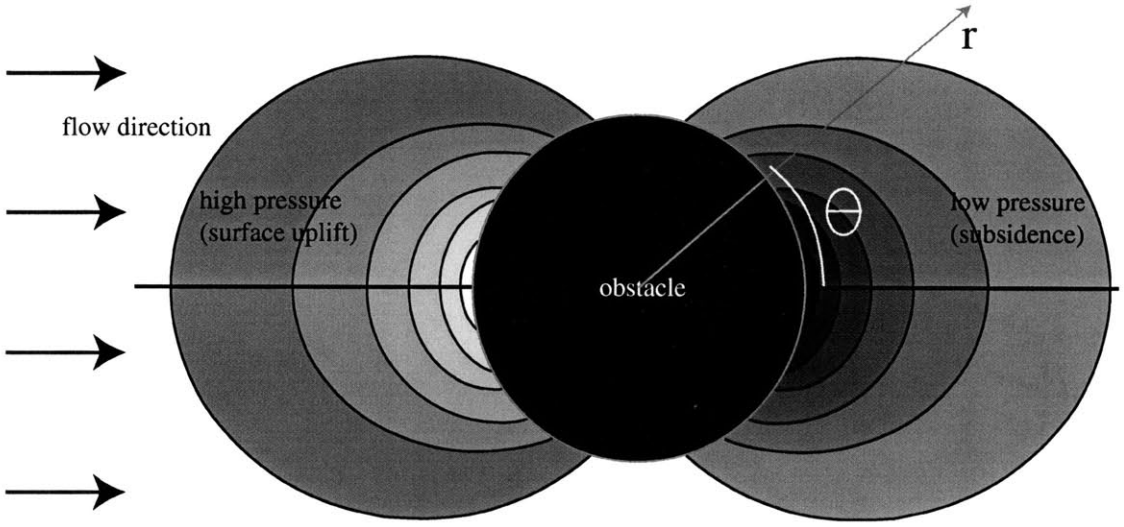

Figure 6.3: General model results showing map-view patterns of high and low dynamic pressures. Background flow is from the left. Dynamic high pressure is observed "upstream" the flow direction, and dynamic low pressure is observed "downstream".

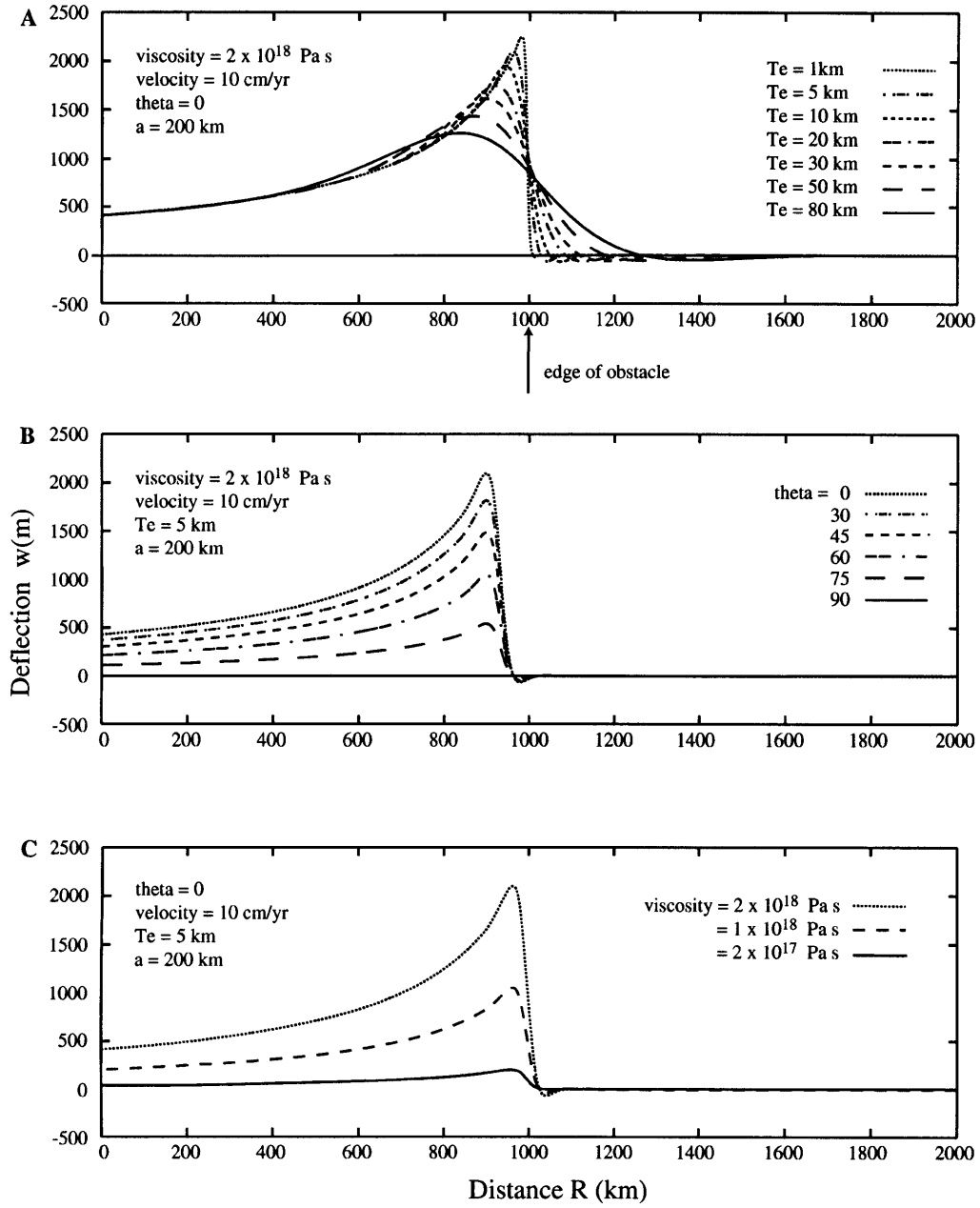

Figure 6.4: Example of dimensional cross-sectional deflection profiles (dynamic topography). A) Model deflection profiles for varying elastic strengths of the upper crust. Low flexural rigidities closely mirror the pressure distribution in the lower crustal layer. High flexural rigidities result in damped antiformal profiles. B) Deflection profiles for varying profile azimuth with respect to flow direction. For example, $\theta = 0^\circ$ represents a profile oriented parallel to the flow direction and $\theta = 90^\circ$ is oriented perpendicular to the flow direction. C) The influence of viscosity of the channel material on the deflection profiles. Acceptable deflection amplitudes obtained with viscosity in the range of $2\text{x}10^{17}$ to $2\text{x}10^{18}$ Pa s, however viscosity scales with flow velocity and channel thickness as $\frac{\mu v}{h^2}$.

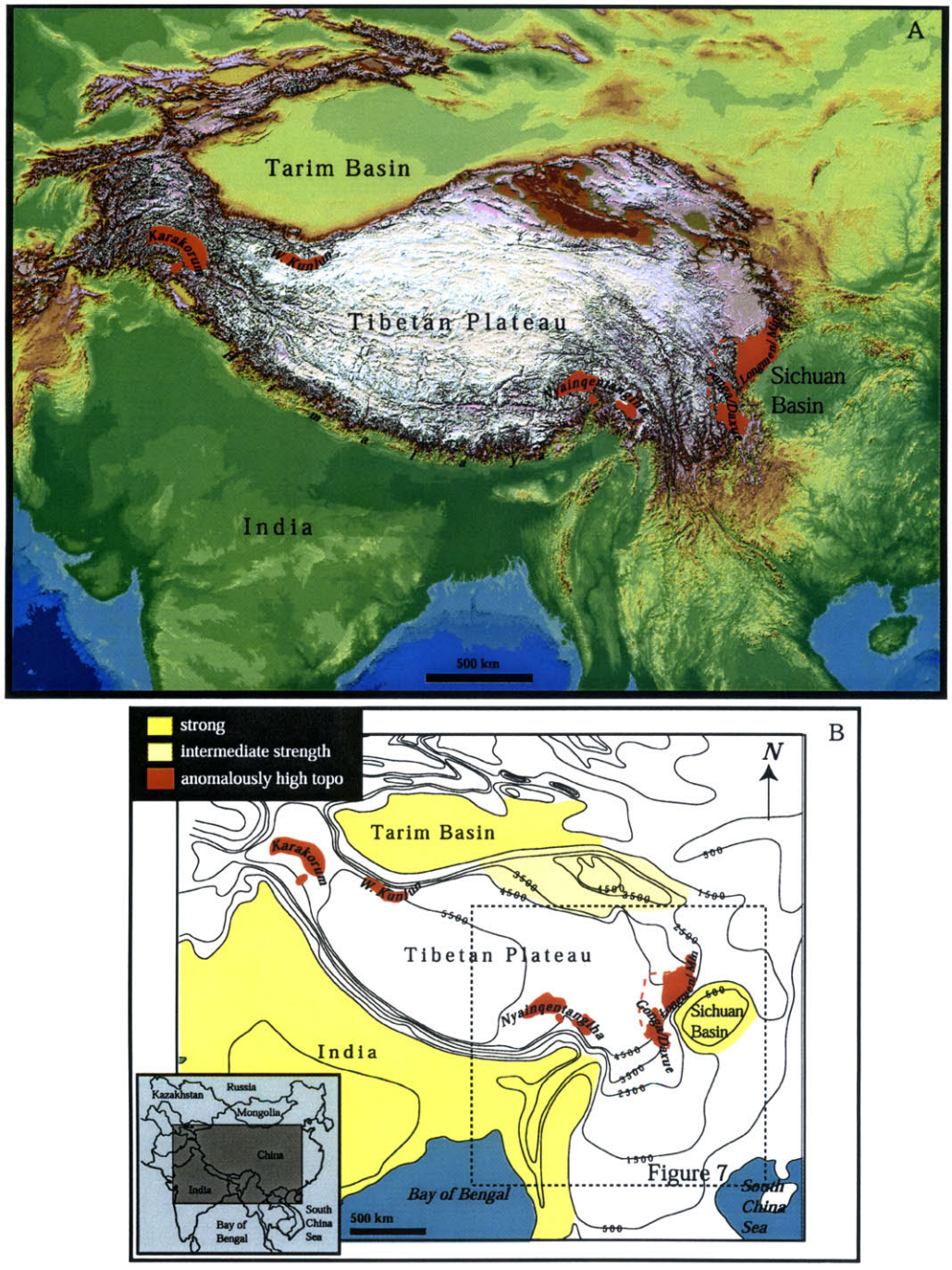

Figure 6.5: Color digital topography map of Tibet highlighting areas of anomalously high topography (top panel). Smoothed contour elevation map derived from digital topography (bottom panel). Areas highlighted in dark yellow and light yellow indicate rheologically strong, and intermediate strength crustal blocks. Regions in red indicate areas of anomalously high topography with respect to background plateau elevations.

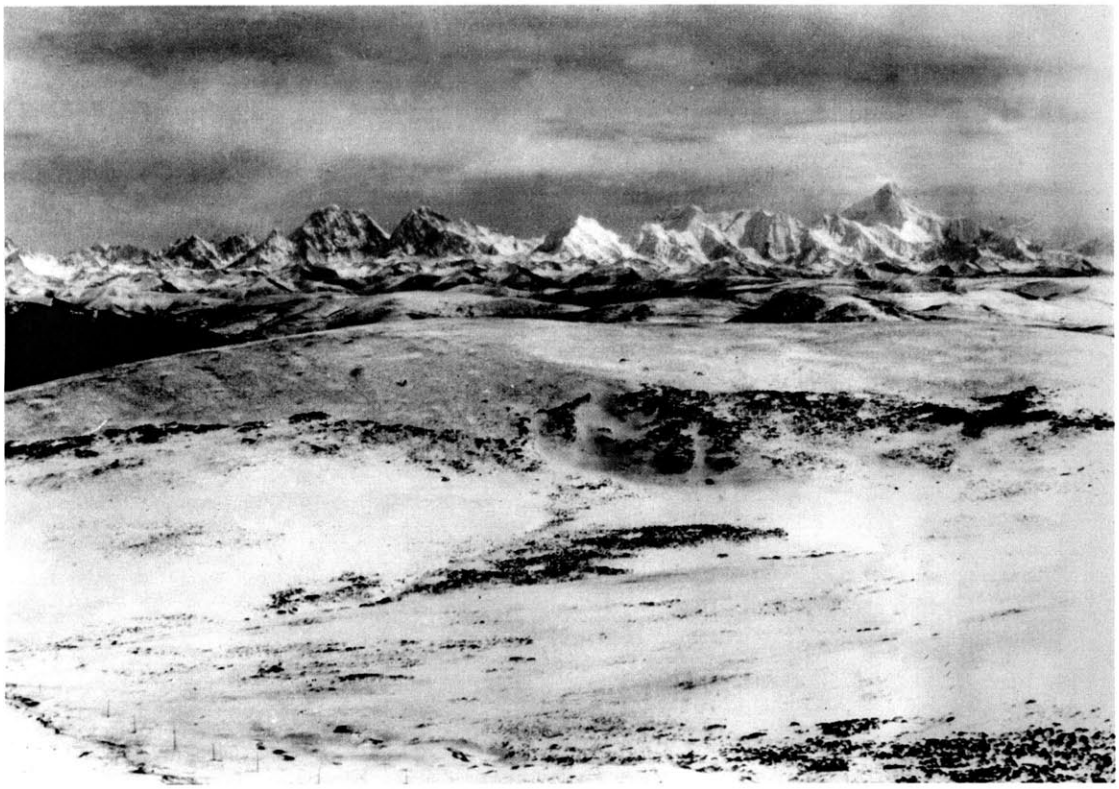

Figure 6.6: View east of the plateau surface at 4 km elevation (foreground) interrupted by the high elevations which define the Gonga massif at elevations of 5500-7556 m (background). Further east from the horizon, elevations decrease dramatically from the peak height of Gonga Shan (7756 m) into the Sichuan Basin (~500 m). Photo courtesy of ETH Library, archive of Prof. Arnold Heim, 1930-1.

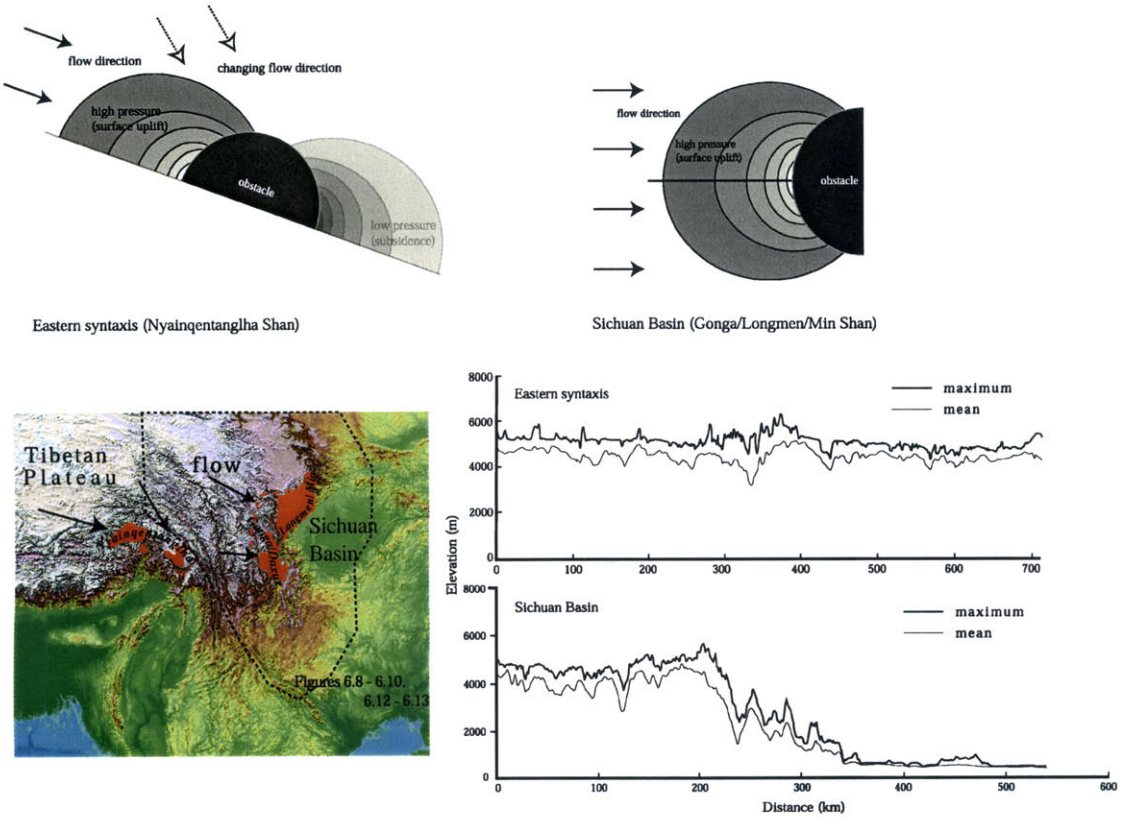

Figure 6.7: Model results compared to Tibet topographic observations in plan-view and in cross-section.

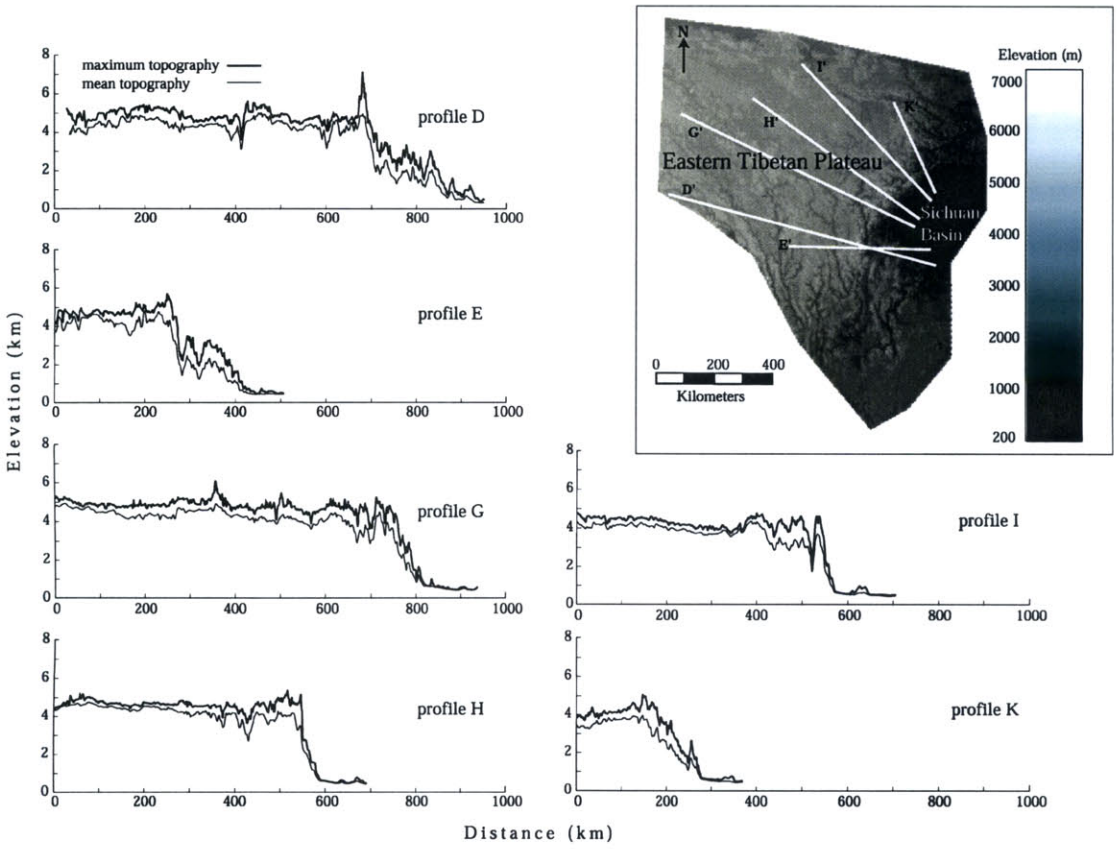

Figure 6.8: Maximum and mean swath profiles for the eastern plateau margin, with swath width equal to 30 km. This swath width is comparable to the focal mean grid used in Figure 6.9. Max/mean swath profiles are taken in the same location as the focal mean profiles in Figure 6.10.

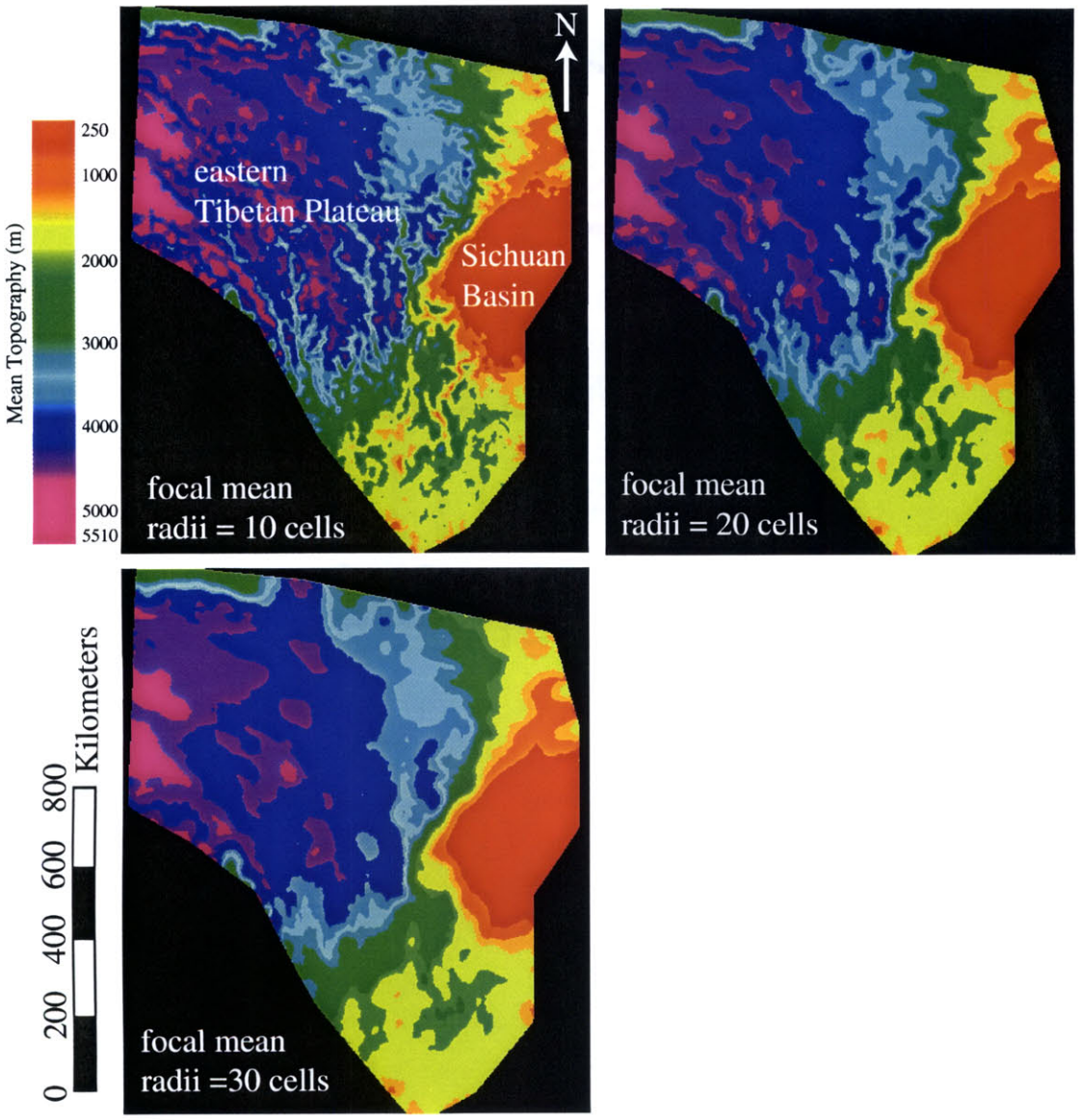

Figure 6.9: Three examples of mean topographic grids calculated from GTOPO30 digital topography [*U.S.G.S.*, 1993]. Mean topography was calculated using a focal-mean which averaged neighborhood topographic values over a circular neighborhood domain. These plots show the effect of varying the radius of the neighborhood domain.

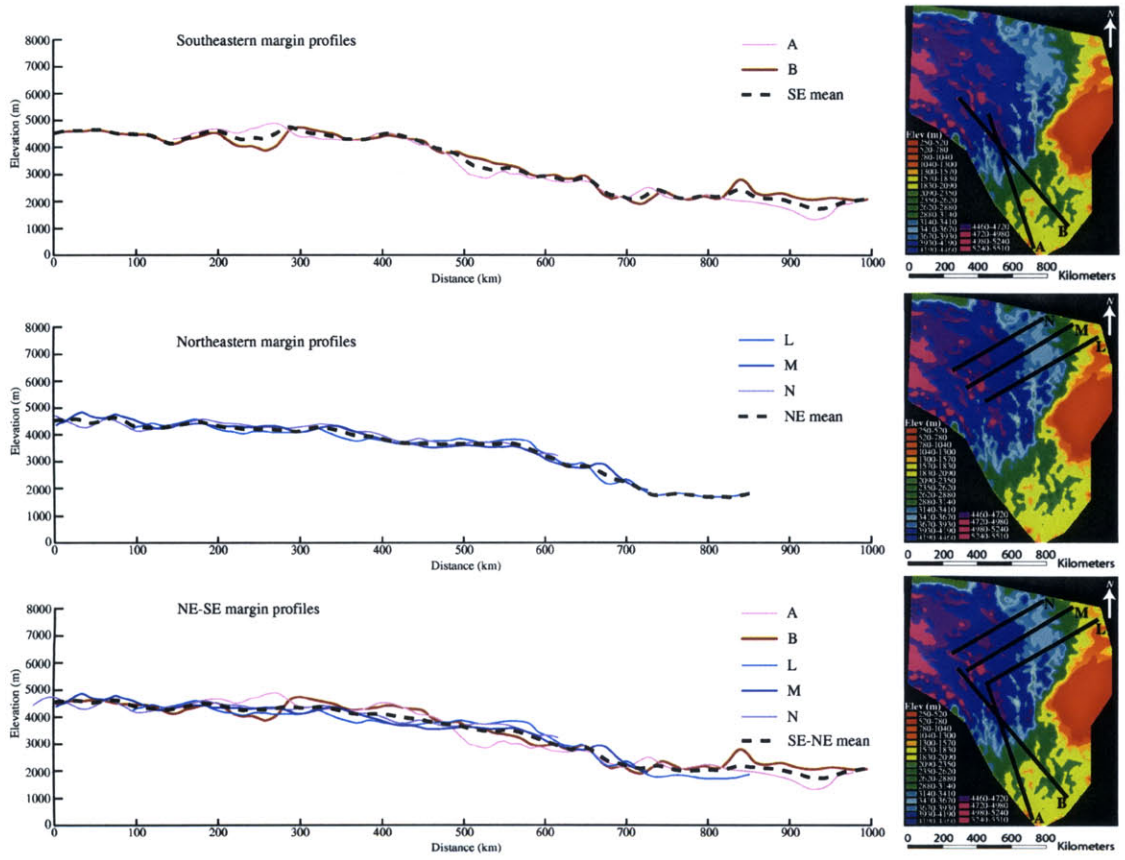

Figure 6.10: Averaged focal mean topographic profiles for the southeast, northeast and both margins combined.

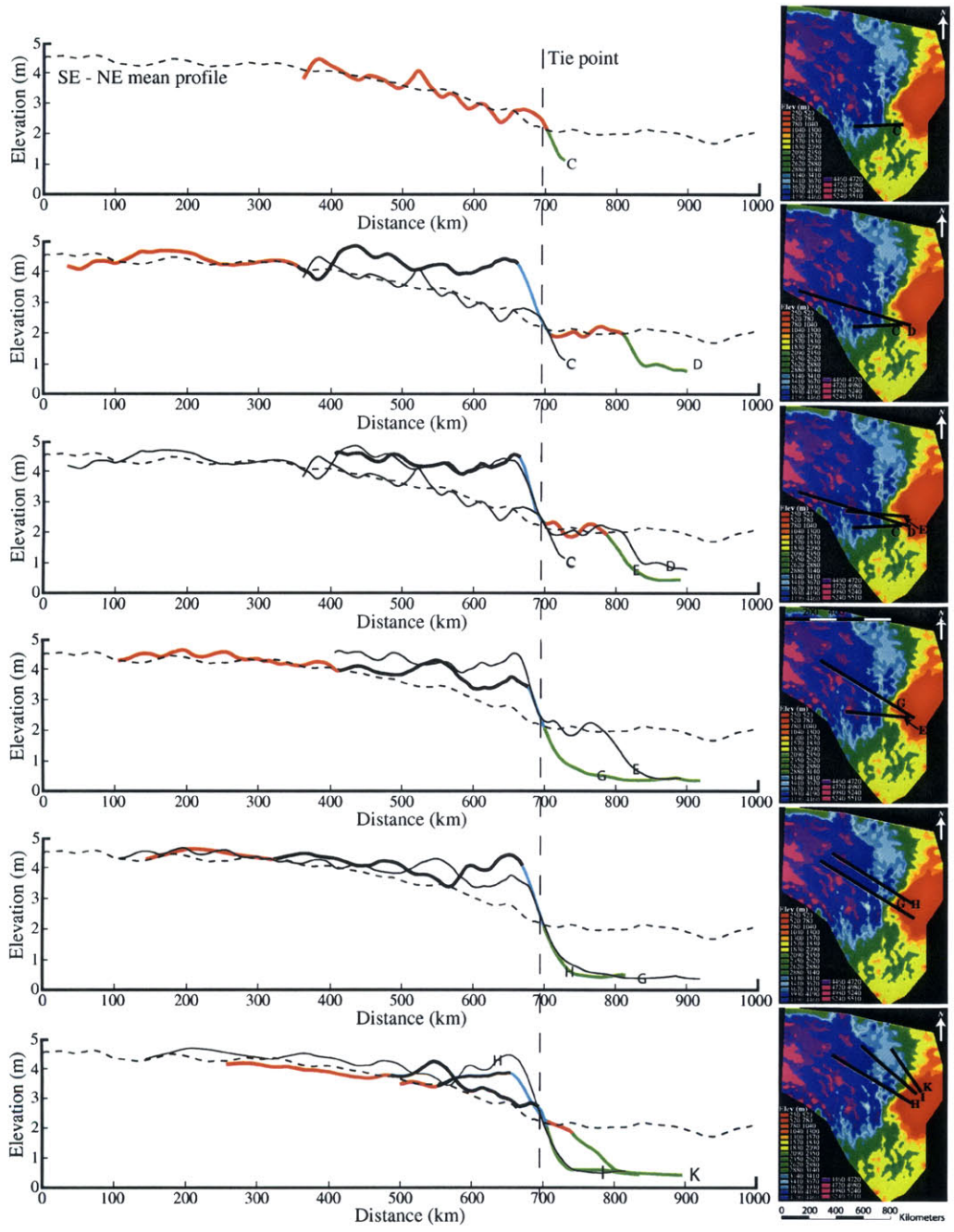

Figure 6.11: Comparison of individual focal mean profiles with respect to the background averaged SE-NE mean profile for the gently sloping margins that surround the Sichuan Basin (dashed line). Segments highlighted in red represent portions of profiles that match on to the background SE-NE profile. Profiles were aligned with the background slope by matching both low-slope segments (red) to the background and by matching up steep segments (blue). Profile segments in green represent crustal thickening at the Sichuan Basin margin front in the absence of dynamic (or excess) topography due to lower crustal flow.

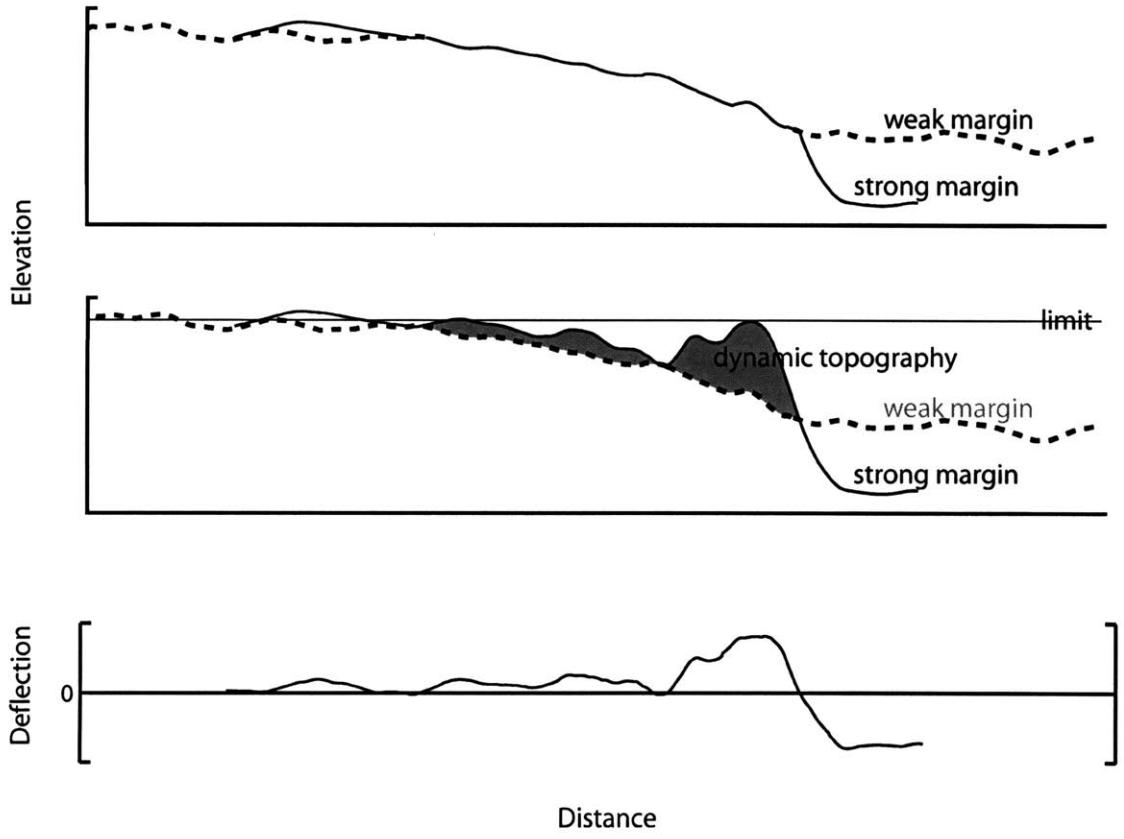

Figure 6.12: Example of dynamic topography calculation. In the absence of dynamic topography or preferential thickening of the lower crust at the boundary of strong crustal margins, this background topographic slope reflects the strength of the underlying material (upper panel). Flow against the strong margin results in elevated topographic profiles localized at the basin margin. Subtraction of the elevated profile from the background profile yields the excess topography ("deflection profile" - lower panel).

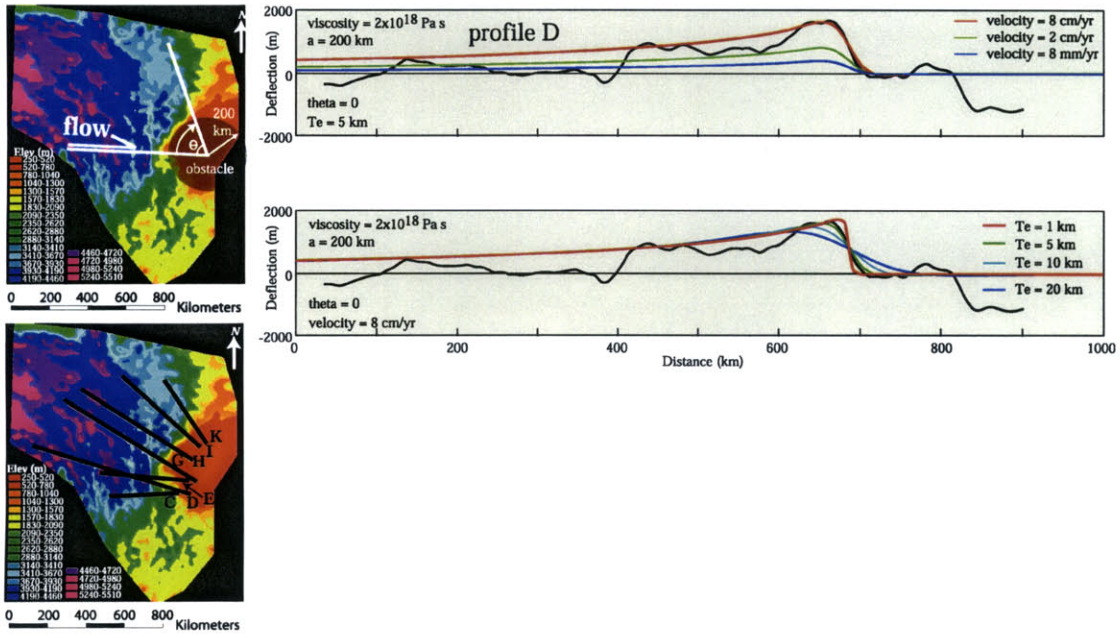

Figure 6.13: Comparison of model results to deflection profiles calculated for the eastern plateau margin.

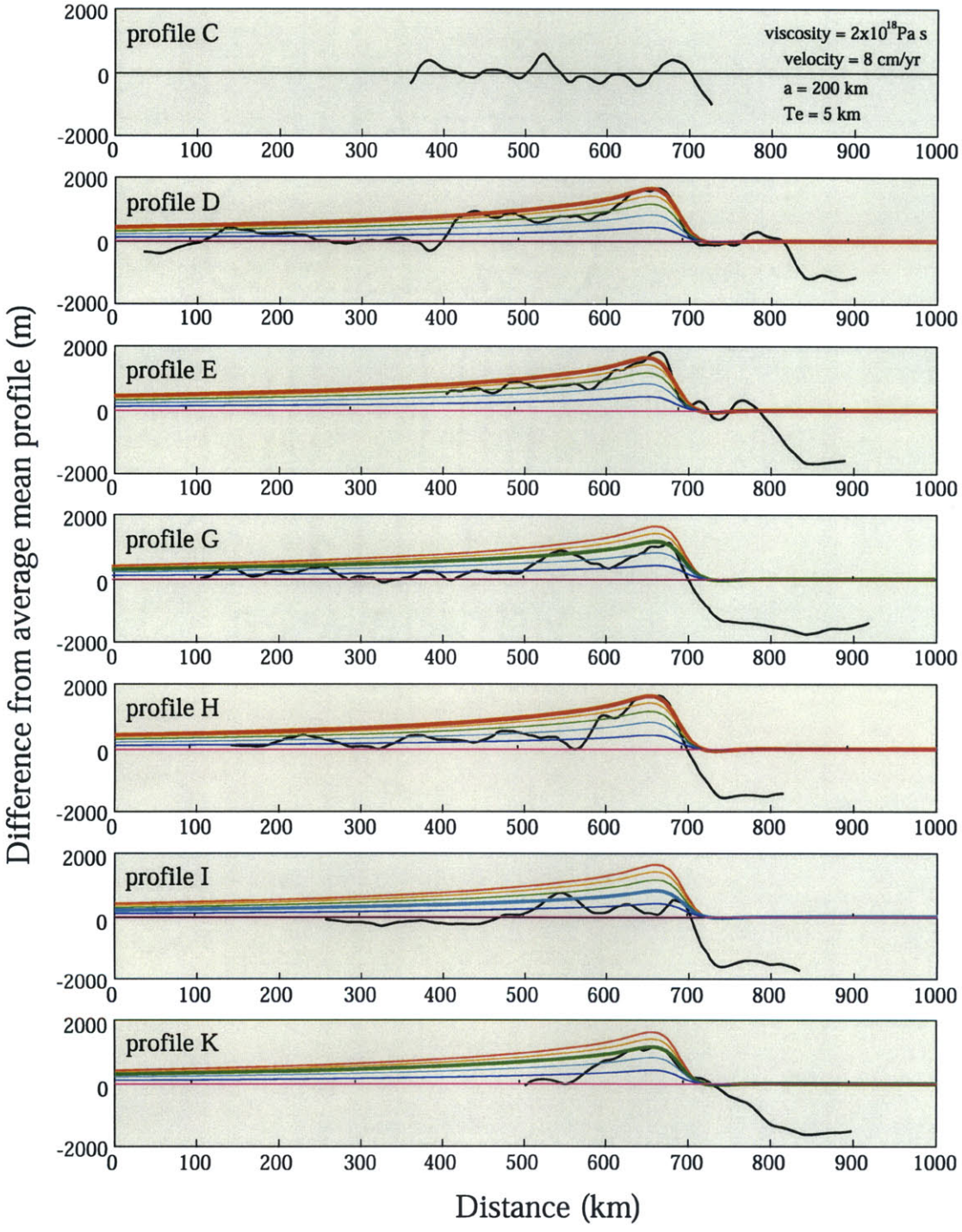

Figure 6.14: Comparison of model results to deflection profiles calculated for the eastern plateau margin.

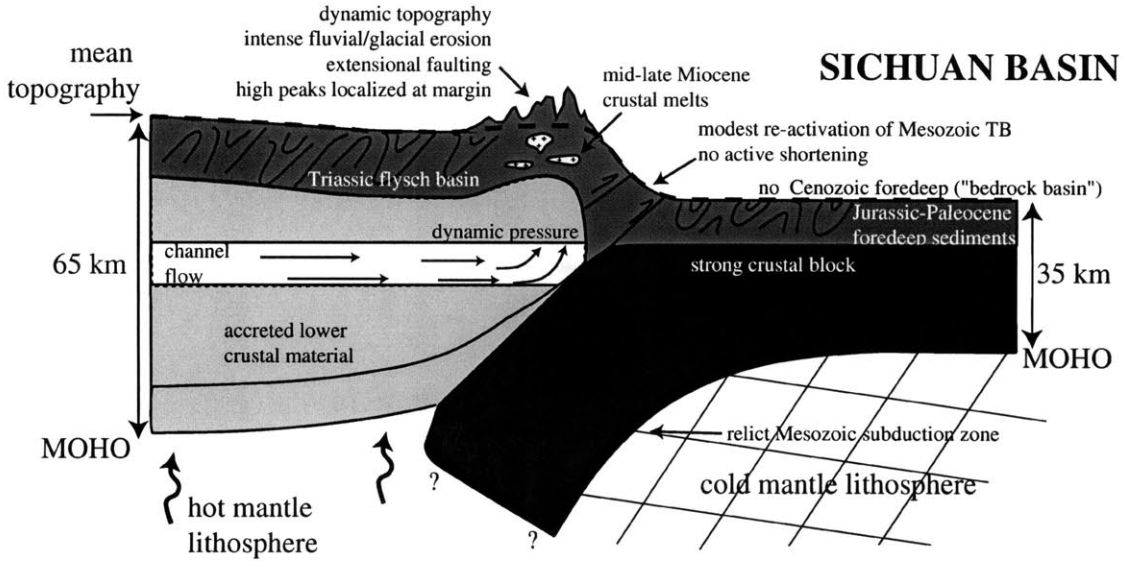

Figure 6.15: Schematic cross-sectional interpretation of the eastern plateau margin, at the latitude of the Gonga Shan massif.

Chapter 7

Conclusion

Despite the complex surface geology in eastern Tibet the magnitude and orientation of much of the late Cenozoic deformation in the upper crust [*Burchfiel et al.*, 1995; *Dirks et al.*, 1994; *Leloup et al.*, 1995; *Wang and Burchfiel*, 1997; *Wang et al.*, 1998] does not correlate with the pattern of surface uplift (i.e. crustal thickening) across the plateau margin. We delineate a history of landscape evolution in southeastern Tibet that suggests that the pattern of crustal thickening occurred independently of the complex evolution of the upper crust, and that the deep crust played a principle role in thickening and elevating the eastern plateau by viscous flow of weak crustal material evacuated from central Tibet and transported toward the eastern foreland. Decoupling of upper crustal structures from crustal thickening suggests that the best record of deep crustal deformation comes from understanding the topographic evolution of the eastern plateau reflected in the topography and the geomorphic and sedimentary records.

Surface uplift of the southeastern plateau margin is defined by the regional scale, long-wavelength tilt of a relict low-relief landscape (erosion surface), suggesting that plateau uplift has occurred over wavelengths greater than 1000 km. The transition from this low-gradient plateau margin in the southeast to the steep plateau margin that borders the Sichuan Basin may directly reflect the rheologic strength of the deep crust in the plateau foreland.

Fluvial systems are highly sensitive to surface uplift, and we propose that measured changes in drainage pattern evolution and river erosion rates reflect important tectonic events related to the initiation of plateau uplift. Reconstruction of paleo-river patterns on

the basis of geomorphology, sedimentology and structural data suggests that an originally south-directed, continental-scale drainage pattern, similar to the Mississippi or Amazon rivers, may have existed prior to uplift. We relate the unusual modern drainage patterns to river capture and river reversals affecting the paleo-dendritic network. Evidence for reversals in river drainage direction along a major section of the Yangtze River suggests that more than 2 km of surface uplift of the lower plateau margin has occurred since capture. These observations concur with the interpretation of long-wavelength surface uplift across the plateau margin of a relict, low-relief and initially low-elevation ($<$ 1 km) landscape.

The timing of uplift is a critical constraint for placing the uplift history in context with the structural history, as well as for determining the physical parameters (such as viscosity and velocity) that control the deformation in the ductile lower crust. Based on the initiation of major river incision into the relict landscape of southeastern Tibet, our apatite (U-Th)/He and fission-track thermochronologic data indicate that uplift along the highest portions of the southeastern margin began by 7 - 13 Ma. This is in good agreement with rapid cooling ages and proposed uplift of the Longmen Shan plateau margin between $\sim$ 5 - 12 Ma [*Kirby et al.*, 2002]. We expect uplift more proximal to the plateau interior to be older and more distal portions of the margin to be younger. Future work determining how uplift varies across the eastern plateau offers the best avenue for constraining the rates of plateau growth.

Based on topographic profiles across southeastern Tibet, long wavelength uplift of the southeastern plateau margin is consistent with a simple 2D model of pressure-driven channel flux of weak mid-lower crustal rocks from beneath elevated regions in central Tibet into the low elevation eastern foreland for a channel thickness of 15 km and viscosities of $\sim 10^{18}$ Pa s (using t = 20 Ma as the initiation of uplift). Assuming that prior to uplift eastern Tibet was underlain by average thickness crust (30 km) and that the present topography reflects crustal thickening in approximate Airy isostatic equilibrium, we can determine a rough estimate for total volume flux of lower crustal material from beneath central Tibet into the eastern foreland of 2.25×10^7 km^3. If we consider that the flux of material occurs through a crustal channel 15 km thick, this requires a viscosity of $\mu \sim 7\times 10^{17}$ Pa s (for t = 20 Ma) or $\mu \sim 5\times 10^{17}$ Pa s (for t = 15 Ma). These parameters are in good general agreement with our 2D topographic profile models cited above. This amount of "extruded"

lower crustal material is similar to the crustal component of the lateral extrusion of lithospheric blocks proposed by *Leloup et. al.*, [1995] assuming an extruded area of 830,000 km^2 and a crustal thickness of 30 km ($\sim 2.49 \times 10^7$ km^2).

We propose that dynamic topography focused at the steep Sichuan Basin margin offers an additional opportunity to determine the physical parameters of the deep crust and provides a means with which we can evaluate the consistency of estimates of physical parameters of the deep crust from different geologic observations. Viscous flow modeling for a Hele-Shaw cell geometry around a rigid cylindrical obstacle suggests that channel viscosities of 2×10^{18} Pa s and mean flow velocities of $\overline{v} = 80$ mm/yr (for a channel thickness of 15 km) are required to explain geologic and geomorphic observations at the plateau margin adjacent to the Sichuan Basin. These estimates can be compared to the mean velocity of the channel calculated from the averaged mean topographic gradient of the northeastern and southeastern plateau margins driving mid-crustal channel flow of $\overline{v} = \sim 20$ mm/yr for a 15 km thick channel and $\mu = 2 \times 10^{18}$ Pa s. These estimates are also in reasonable agreement with the modelling of dynamic topography at the Sichuan Basin plateau margin.

The wavelength and magnitude of material flux through the lower crust of southeastern Tibet is probably very unusual and it is likely that many factors have contributed to this phenomenon. The rheologic strength of the deep crust is largely a function of lithology, temperature and the presence of aqueous fluids [*Brace and Kohlstedt*, 1980; *Kirby*, 1983]. Thermochronology data from apatite (U-Th)/He and apatite fission-track suggest that eastern Tibet has a high geothermal gradient of ~ 40 - 60 $^\circ$C/km. Potassic volcanism since the Oligocene in eastern Tibet and slow seismic velocities in the mantle lithosphere beneath southeastern Tibet also suggest the presence of a hot mantle lithosphere beneath eastern Tibet that may be partially responsible for the elevated crustal geotherms. The crustal composition in southeastern Tibet is dominated by thick sedimentary sequences from Paleozoic to Cenozoic in age. These thick sedimentary sequences likely have high heat production due to the concentration of radioactive heat producing elements. The introduction of fluids, by the dehydration of muscovite in metasedimentary rocks, may introduce partial melt at elevated temperatures in the mid-crust, resulting in melt-induced weakening of the deep crust [e.g. *Rushmer*, 2001]. All of these factors may have contributed to the development

of a weak crustal layer beneath southeastern Tibet.

Surface geology and GPS data suggest that southeastern Tibet is undergoing rotation around the eastern Himalayan syntaxis with little net translation toward the foreland since about 4-8 Ma (Wang, et al., 1998; Chen et al., 2000) while the pattern of surface uplift suggests the mobilization of deep crustal material to the southeast, independent of the pattern of strain recorded in the upper crust, since 7-13 Ma. The lack of correlation between the orientation, style and magnitude of structure in the upper crust and the pattern of crustal thickening determined from the topography suggests that the upper and lower crust in southeastern Tibet are decoupled. Therefore we propose that the strike-slip faults which dominate the surface strain record must sole into mid-crustal detachments since at least middle-late Miocene time and precludes any major tectonic extrusion of lithospheric fragments during this time. We suggest that a model of viscous deformation concentrated in the deep crust may explain the distributed pattern of surface uplift and crustal thickening in southeastern Tibet, which has occurred independently of the structural history of the upper crust in Late Cenozoic time.

7.1 References

Brace, W.F., and Kohlstedt, D.L., 1980, Limits on lithospheric stress imposed by laboratory experiments: Journal of Geophysical Research, v. 85, p. 6248-6252.

Burchfiel, B. C., Z. Chen, Y. Liu, and L. H. Royden, Tectonics of the Longman Shan and adjacent regions, central China, *Int. Geol. Rev., 37*, 661–735, 1995.

Chen, Z., B. C. Burchfiel, Y. Liu, R. W. King, L. H. Royden, W. Tang, E. Wang, J. Zhao, and X. Zhang, GPS measurements from eastern Tibet and their implications for India/Eurasia intercontinental deformation, *J. Geophys. Res., 105*, 16,215–16,227, 2000.

Dirks, P. H. G. M., C. J. L. Wilson, S. Chen, Z. Luo, S. Liu, Tectonic evolution of the NE margin of the Tibetan Plateau; evidence from the central Longman Mountains, Sichuan Province, China, *J. Southeast Asian Earth Sci., 9(1-2)*, 181–192, 1994.

Kirby, E., P. W. Reiners, M. A. Krol, K. X. Whipple, K. V. Hodges, K. A. Farley,

W. Tang, Z. Chen, Late Cenozoic evolution of the eastern margin of the Tibetan Plateau: Inferences from $^{40}Ar/^{39}Ar$ and (U-Th)/He thermochronology, *Tectonics, 10.1029/2000TC001246.*

Kirby, S.H., 1983, Rheology of the lithosphere: Reviews of Geophysics and Space Physics, v. 21, p. 1458-1487.

Leloup, P. H., R. Lacassin, P. Tapponnier, U. Schäerer, D. Zhong, S. Lui, L. Zhang, S. Ji, and P. T. Trinh, The Ailao Shan-Red River shear zone (Yunnan, China), Tertiary transform boundary of Indochina, *Tectonophysics, 251*, 3–84, 1995.

Rushmer, T., 2001, Volume change during partial melting reactions; implications for melt extraction, melt geochemistry and crustal rheology, *in Partial melting of the crust and flow of orogens, C. Teyssier and O. Vanderhaeghe, eds., Tectonophysics, 342*, 389–405.

Wang, E., and B. C. Burchfiel, 1997, Interpretation of Cenozoic tectonics in the right-lateral accommodation zone between the Ailao Shan Shear Zone and the eastern Himalayan syntaxis, *Int. Geol. Rev., 39*, 191–219.

Wang, E., B. C. Burchfiel, L. H. Royden, L. Chen, J. Chen, and W. Li, Late Cenozoic Xianshuihe-Xiaojiang, Red River, and Dali fault systems of southwestern Sichuan and central Yunnan, China, *Geol. Soc. Am. Spec. Paper, 327*, 1998.